POLITECNICO DI MILANO

Department of Structural Engineering

Doctoral School in Structural, Earthquake and Geotechnical Engineering

XXIV cycle

Advanced cementitious composites for structural retrofitting

Supervisor

Prof. Marco di Prisco

Coordinator

Prof. Roberto Paolucci

Phd Candidate

Anna Magri 738616

09 November 2012

Anna Magri 738616
Advanced cementitious composites for structural retrofitting

e-mail:
anna.magri@mail.polimi.it

Advanced cementitious composites for structural retrofitting

A Thesis
Presented to
The Academic Faculty

by

Anna Magri 738616

In Partial Fulfillment
of the Requirements for the Degree
Doctor of Philosophy
in
Structural, Earthquake and Geotechnical Engineering
XXIV cycle

09 November 2012

Doctoral School in Structural, Earthquake and Geotechnical Engineering
XXIV cycle
Department of Structural Engineering
Politecnico di Milano

XXIV cycle

Faculty Members

Prof. Roberto Paolucci (Co-ordinator)
Prof. Fabio Biondini
Prof. Gabriella Bolzon
Prof. Claudia Comi
Prof. Alberto Corigliano
Prof. Maria Laura Costantino
Prof. Claudio di Prisco
Prof. Marco di Prisco
Prof. Roberto Felicetti
Prof. Attilio Frangi
Prof. Pietro Gambarova
Prof. Federico Perotti
Prof. Alberto Taliercio
Prof. Pasquale Vena

Preface

Strengthening of existing traditional concrete structures is becoming one of the most important issue for the structural engineering. The necessity to make safe old buildings comes mainly from that they were not designed for earthquake loads. This performance can be obtained either by adding new lateral load resisting members or by strengthening the existing structure. This is the most common and feasible alternative. A large number of techniques have been developed such as RC or steel jacketing, advanced material such fibre reinforced concrete and textile reinforced concrete: the last solution has been investigated from only few years. Traditional methods of seismic retrofitting fall for two main causes: the request for an increase of strength and stiffness on one hand and on the other hand a mass reduction. This problem has encouraged researchers to develop new materials and new retrofitting techniques. The traditional solutions include the Reinforced Concrete (RC) jacketing or externally glued steel. These techniques have some limits. In particular the use of RC jacket implies thickness greater than 60 or 70 mm that can increase too much the section and the mass of the element. The use of glued steel may have some problem in the case of fire resistance. New solutions are called for. One of these is textile reinforced concrete (TRC). It is a good combination of high compressive and tensile strength that can lead to suitable load carrying capacity. This strengthening material allows the design of thin structure elements. Another solution is the use of Ultra High Performance Fiber Reinforced Concrete (UHPFRC). In this case the high tensile strength and ductility are due to the presence of steel fibres that can be oriented during the casting procedure to improve its performance. In both alternative proposals thin layer of retrofitting material can be used also due to the absence of a concrete cover requirement. This research aims to investigate the contribution offered by retrofitting materials applied on damage concrete element. The tensile strength contribution makes the concrete behaviour ductile. The improved performance of traditional concrete occurs due to the transmission of tangential stresses through the contact surface which should be treated to increase bond mechanism. Shrinkage problem can be lead to detachment of the materials. The mechanical properties of fiber reinforced concrete are determined for both stress strain states in tension and compression. A lot of time was spend to the design of textile reinforced concrete to find a proper combination between the fabric and the cement matrix. The parameters that influence the behavior of the cementitious composite are multiple. The fabric can be varied for the geometry, the tensile strength, the warp and weft, the nature of the fibre and the way that they can be woven. The matrix must have a good workability to penetrate in the mesh of the fabric as well as a high tensile strength. The thesis is aimed of suggesting the best possible solution in terms of performances, cost, casting procedure. To reach this goal, several parameters have been analyzed by means of experimental investigations. The mechanical characterization of TRC and UHPFRC was carried out by traditional test in compression and in tension while the coupling behavior of retrofitting materials with weakly reinforced concrete was investigated through a technique called Double Edge Wedge Splitting (DEWS) that usually is adopted to investigate the post-peak tensile strength of fiber reinforced concrete.

Acknowledgements

I would like to thank all those who contributed to the development of this thesis.

I would like to gratefully acknowledge my supervisor Professor Marco di Prisco for his comprehensive guidance and encouragement during the study. He created the opportunity to carried out this PhD research project and he contributed with critical comments and suggestions to the outcome of this research project. His support was really appreciated.

I want to thank Dr. Matteo Colombo whose suggestions were fundamental in performing the experimental investigations.

A special thanks to my dear friend and colleague Giulio Zani who more than anyone has always supported and helped me with his valuable advice.

An essential part of this research project was to carry out experimental tests and a special word to thanks goes to Isabella Colombo for the specimen preparation and execution of the tests and also to Andrea Stefanoni and Marco Perego, the technicians of the laboratory of Politecnico di Milano for their support in carrying out all the experimental program.

I want to thank all my colleagues Dr. Alessio Caverzan, Dr. Pamela Bonalumi and Dr. Paolo Martinelli for their helping and support.

A thank goes to Dr. Liberato Ferrara for his precious help in analyzing fresh state properties.

I want to thank my parents, sisters, friends and in particular my nephews Federica and Alessandro for their joy and liveliness.

Last, but not least, my boyfriend Michael for his love, support and patience.

Anna Magri

Contents

List of Figures

List of Tables

Chapter 1

Introduction

There are a lot of situations in which a civil structure would require strengthening due to the lack of shear resistance. Some structures need strengthening during their lifespan to satisfy current code requirements or damage caused horizontal loads. The aim of concrete rehabilitation is to extend the service life of an existing structure or to reestablish its load-bearing capacity or to improve it by taking into account the new requirements imposed by seismic loadings. Ultra High Performance Fiber Reinforced Concrete (UHPFRC) and Textile Reinforced Mortar (TRM) have a good durability and optimum mechanical properties; for these reasons they are suitable materials for rehabilitation of reinforced concrete (RC) structures. This thesis presents investigation on the mechanical properties of UHPFRC and TRM and also bond problems between the repairing layers and the existing substrate.

1.1 Research Significance

Light-weight materials and on site installing easiness are considered the most favored solutions in many strengthening applications. The theoretical and experimental research carried out in this thesis provides a contribution to understand the structural behavior of fiber-reinforced concrete elements and textile reinforced mortar applied on traditional damaged concrete. The thesis is aimed at analyzing two principal solutions compared in terms of tensile performance, redistribution of stresses in a cracked zone, of costs and installation easiness. The properties to be exploited in structural applications are the mechanical characterization of tensile behavior of retrofitting layers and the bond between the existing substrate and the new materials. After the mechanical characterization of the two solutions, the advantages of the retrofitting layers were studied through a new experimental technique called Double Edge Wedge Splitting. This kind of test was inspired by the Wedge Splitting test but the main advantage was to reproduce a tensile state of stress without any compressive disturb. This made possible by introducing two 45° V-shaped notch. The load was transmitted through two compressive arches outside the central zone, that is characterized by a state of stress of pure tension. This is a very innovative technique because it allows the tensile strength measure in indirect way and also the prevention of the complications typically introduced by tensile test. The purpose of the thesis is to analyze the effectiveness of the retrofitting layers under tensile load in terms of strength and ductility both measured by the same type of test. The treatment of the interface surface and the bond slip laws are fundamental aspects to understand the ductility contribution of the new layers.

1.2 Outline of the thesis

The thesis is divided into eight chapters. After the introduction (Chapter 1), in Chapter 2 an overview of the traditional retrofitting techniques is presented. The last few earthquakes have shown that many buildings are seismically vulnerable and retrofitting interventions are required. Different traditional repair techniques are suitable to increase the strength and ductility of traditional structural concrete elements.

Chapter 3 presents the reviewing literature about the mechanical characterization of textile reinforced mortar and ultra high performance fiber reinforced concrete.

Chapter 4 reports the extensive experimental programme carried out to investigate the mechanical properties of the innovative cementitious composite materials (UHPFRC and TRC). The main advantages of these two materials are the thin layers used to repair from 6 mm for the TRC to 2 cm for fiber reinforced concrete. This is possible due to the high performance and for the absence of cover concrete requirement. A lot of direct tensile tests were performed to analyze the behavior of TRC and to understand the bond mechanism between the matrix and the AR Glass fabric. A series of fabrics were taken into account to investigate the influence of different parameters like the geometry, the coating, the reinforcement ratio, the temperature, the curing condition. Ultra High Performance Fiber Reinforced Concrete was investigated by three point bending test. The compressive capacity of the matrices were studied by standard compressive tests.

Chapter 5 shows a rather new technique, DEWS test to investigate the coupling behavior of the retrofitting layer and existing reinforced concrete. The aim is the uncoupling compressive stresses from tensile stresses by using an indirect tensile test, contrary to what occurs in Bending and Brazilian tests, where compressive and tensile stresses act on the bending/splitting plane at the same time. To reproduce the stress distribution on the sections of a notched specimen loaded in pure tension, the compressive load was applied by two steel cylinders acting on 45°-shaped notches with steel plates, in this way two compressive stress arches were established and and uniaxial tensile state of stress in the mid-span section occurred. Square concrete plates 30 cm long and 10 cm thick were retrofitted with TRC 6 mm thick and UHPFRC 2 cm thick. The interface problems between the retrofitting layers and traditional concrete were studied through compression tests.

Chapter 6 summarizes the experimental test results obtained by DEWS and compressive tests. The traditional concrete plates were precracked at three different levels of crack opening displacement to consider different conditions, serviceability and ultimate limit states. The results show the improvement in the performances due to the retrofitting layer in terms of maximum load and ductility behavior.

Chapter 7 reports a simplified model to understand mechanisms involved in tensile experiments. The tensile tests performed in the experimental programme presented two very important aspects to be take into account: the geometry and the presence of different materials with which the specimen was made of. In particular, the model considers the delamination problems that involves both the steel bars and the retrofitting layer.

The last chapter compares the different alternatives and discusses the best application in terms of performances, cost and kind of application, thus provide future perspectives concerning the best solution for retrofitting structures.

Chapter 2

Retrofitting methods

Strengthening of existing reinforced concrete elements is becoming a key issue in civil engineering. This may derive from the necessity of retrofitting existing building to meet safety requirements in seismic zone where most buildings have been not designed to earthquake load or peak ground acceleration proposed by codes has been upgrade in later year. In such situation walls are prone to failure during earthquakes or high wind pressure and they represent a significant hazard. The imminent need for upgrading existing structures has been taken into account by the development of different techniques including metallic grid reinforced surface coatings, shotcrete overlay, externally bonded fiber reinforced polymers (FRP), textile reinforced concrete (TRC), ultra high fiber reinforced concrete (HPFRC). A lot of attention has been paid in the literature both to Unreinforced masonry (URM) and reinforced concrete (R/C) elements. In this chapter some principal retrofitting cases, taken from the literature, were analyzed: unreinforced masonry walls, beams subjected to bending or shear failure, and the confinement on columns. Several techniques (FRP, TRC, HPFRC and ferrocement) were taken into account in order to compare the effectiveness of the strengthening layer.

2.1 Unreinforced masonry walls

Considering studies, that can be found in literature on unreinforced masonry wall, two kind of loads are here considered: in plane and out of plane load. In particular walls subjected to in-plane cyclic shear load combined with axial force or to out of plane bending are width discussed in the literature [21]. Some tests are here reported with different strengthening materials that were considered as possible solutions.

2.1.1 In-plane loading: TRM and FRP

According to studies performed by Papanicolaou [26], Textile Reinforced Mortar (TRM) was investigated as a new method for seismic retrofitting of URM walls and then it was compared with identical structures strengthened with FRP. An experimental program was performed on retrofitting wall subjected to cycling loading in-plane. The authors studied masonry wall reinforced on both sides with TRM layer and their efficiency with FRP counterparts. Two major parameters were considered, the use of inorganic mortar instead of resin material and the number of textile layers (one or two on both sides). Specimen was 1300 mm high and 800 mm wide and made of perforated bricks. The retrofitting layer was made by a commercial textile with equal quantity of high strength carbon fiber in the two directions and a weight of 168 kg/m^2 with a

nominal thickness of 0.047 mm. Tensile strength and elastic modulus were equal 3350 MPa and 225 GPa respectively. Two binder materials were used: mortar, characterized by flexural and compressive strength equal to 5.77 MPa and 31.36 MPa respectively, and adhesive bonding epoxy resin characterized by tensile strength of 30 MPa and elastic modulus of 3.8 GPa. A standard wet lay up procedure was adopted to apply the bonding agent on the wall surface by hand and roller pressure. The mortar layer was approximately 2 mm thick.

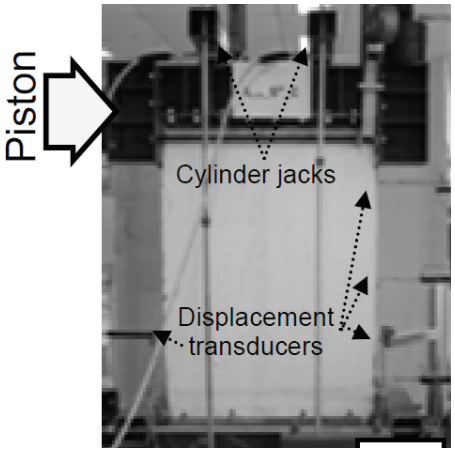

Figure 2.1: Experimental setup of in-plane loading

The specimen were tested as a shear wall with a localized load acting in the plane of the wall at distance of 1.10 m from the base. Five displacement transducers were adopted to measure the horizontal displacements (fig. 2.1). During the cyclic loading an axial load was applied. The results are collected in table 2.1 where specimen had this notation $I_X\_S^W\_YN$. The subscript X denoted the axial compressive load level as a percentage of the compressive strength of the wall, Y the binder (M mortar and R resin) and N the number of layer. The results are normalized with reference unstrengthened specimen called C.

Specimen	$P_{max}/P_{max,C}$	$\delta_u/\delta_{u,C}$
$I_{10\%}\_S^W\_C$	1.00	1.00
$I_{10\%}\_S^W\_R1$	7.00	12.49
$I_{10\%}\_S^W\_R2$	6.98	10.90
$I_{10\%}\_S^W\_M1$	5.08	13.46
$I_{10\%}\_S^W\_M2$	6.17	13.57

Table 2.1: Summary of the results

Comparing TRM with FRP, in all the cases presented FRP solutions seems to be most effective in terms of load, but TRM solution shows larger ultimate displacement and therefore a higher ductility.

2.1.2 Out of plane behavior: FRC and ferrocement

The out of plane behavior of masonry wall strengthened with an overlay (FRC or ferrocement) was studied by Tan [21]. The strengthening materials were (a) ferrocement and (b) steel fiber reinforced ferrocement. The wall specimen had dimension of 1 x 1 m and 115 mm thick. 13

series I	material overlay
F11-F12	ferrocement
FS10-FS11	fiber reinforced ferrocement
REF	none
series II	
S1-S4	steel fiber reinforced mortar (2.5-0.5% fiber volume)

Table 2.2: Types of specimens

specimen designation	reinf. ratio (%)	tensile capacity (kN/m)	ultimate capacity (kN)	ultimate deflection (mm)
F11	0.20	164.3	277.4	17.52
F12	0.27	200.5	660.9	13.05
FS10	0.19	153.6	348.1	11.69
FS11	0.25	189.6	372.2	10.54
S1	0.10	50.7	154.3	3.95
S2	0.16	76.2	214.6	4.47
S3	0.21	101.7	237.1	4.42
S4	0.26	127.2	290.9	4.18

Table 2.3: Reinforcement ratio details, [21]

specimens were reinforced and one unreinforced was taken as a reference. The strengthening layer was equal to 30 mm on tension face. The walls were divided in two series as described in table 2.2. All walls were made by clay bricks 72 x 95 x 215 mm. The steel fiber were hooked-end (35 mm long, 0.75 mm diameter) and two steel welded mesh were adopted: skeletal steel mesh 6 mm diameter with 150 mm square openings, galvanized wire mesh 1.25 mm wire and 12.5 mm square openings. Details of the reinforcement ratio (fiber and steel) in the retrofitting layer are shown in table 2.3.

Each specimens were tested as a simply supported along the four edges, the effective span was 900 mm and the load was applied using an airbag over a 750 x 750 mm square area in the center of the wall. The displacement was measured in the centre of the bottom side . The results are expressed in terms of load-displacement curves for each series (fig.2.2)

Considering series I the stiffness, load capacity and the ductility of the reinforced wall were significantly increased compared to the reference wall. The volume increasing of fraction of the reinforcement (fine wire mesh) brings to a higher peak load and lower ductility (F12-F11). The addition of steel fiber (FS11) led higher initial stiffness but lower ductility compared to F11 with no fiber. For higher volume fraction, it appeared that fine wire mesh had best performances compared to fiber. According to the authors this results was associated to mixing problem with steel fiber. Considering specimen with steel fiber reinforced mortar (series II), the failure was ductile due to the pull out of fiber from the matrix. The load capacity enhanced according to the volume fraction (S4 Vf=2.5%) but it was not the same for the ductility since any variation in the ultimate deflection is evident. These value was smaller than the displacement obtained with ferrocement specimen reinforced. The authors concluded that using reinforced cement composite overlay contributes significantly to the flexural performance in terms of stiffness, strength and ductility. A higher percentage of fine wire mesh gave a higher strength but lower ductility. Considering the total volume fraction, fine wire mesh is preferred over steel fiber.

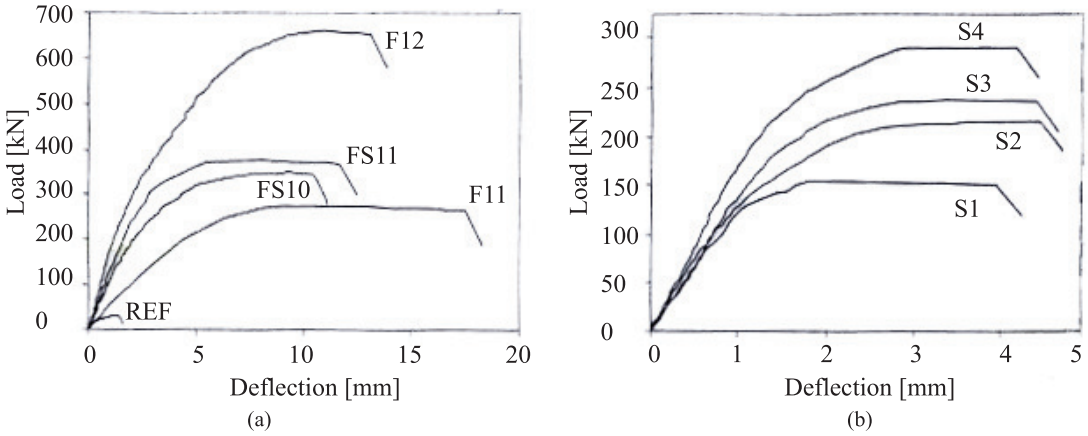

Figure 2.2: Results in terms of load-displacement (a) series I (b) series II

2.2 Bending behavior of beams

In this paragraph some results taken from the literature are summarized in order to compare the performance of different retrofitting solutions on the bending behavior of beams.

2.2.1 TRC and FRP jacketing

Studies on the use of textiles for flexural strengthening beam were conducted by Papanicolaou [27]. TRM layer and FRP was chosen to reinforce R/C beams. The beams considered had a cross section of 150 x 250 mm and were reinforced with $2\phi 12$ longitudinal rebar on top and bottom and shear reinforcement made by stirrups 8 mm diameter with a spacing of 100 mm. The compressive strength of the concrete was 34 MPa. The specimens were reinforced with four layers of textile bonded in one case with cement based matrix ($M4\_fl$) and the second case with epoxy resin based matrix ($R4\_fl$). Four point bending tests were performed and the load was monotonically applied. The displacement were measured at mid-span and the results were reported by load-displacement curves (fig.2.3). The reference specimen (C_fl) showed the

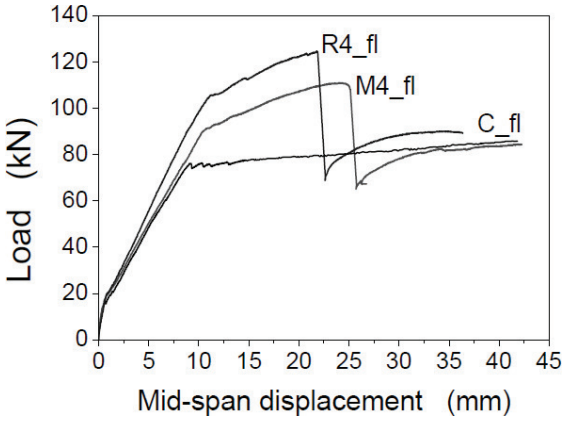

Figure 2.3: Load-displacement results

typical response of reinforced beam. The specimen with epoxy resin (R4_fl) quite double the strength and experience an increased stiffness. The failure was associated to the tensile fracture of the externally bonded layer in the mid span zone. The TRM specimen (M4_fl) had a similar response to R4_fl but with a little more ductile behavior, a lower ultimate load mainly related to a failure due to debonding at the end anchorage. The TRM effectiveness was around 30% less in terms of strength compared to FRP specimen.

2.2.2 HPFRC strengthening layer

An other retrofitting application was investigated by Martinola [28], [29].

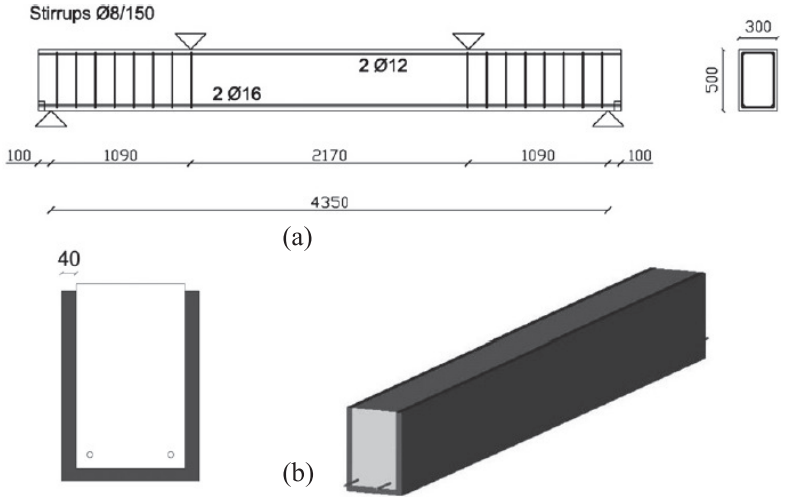

Figure 2.4: (a) Geometry of support specimen and (b) strengthening scheme

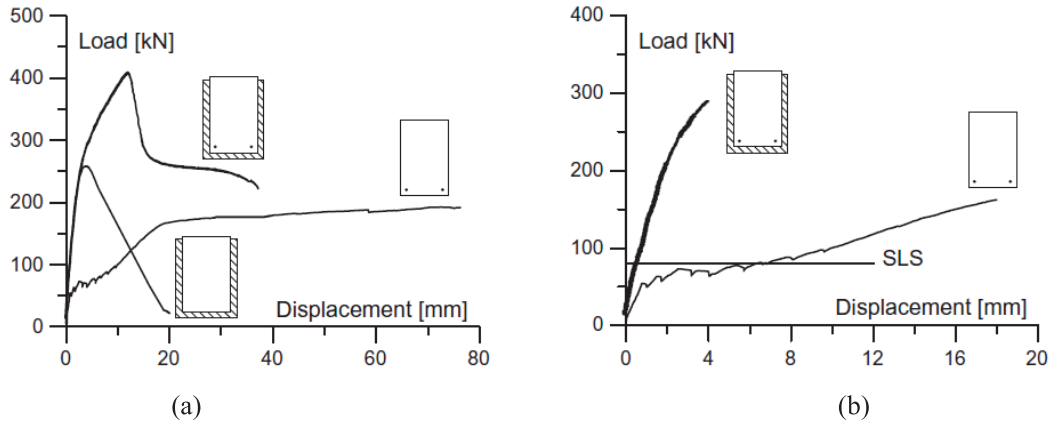

Figure 2.5: Comparison of the experimental results

The strengthening technique provided the use of High Performance Fiber Reinforced Concrete (HPFRC) jacketing on existing beams. The effectiveness of this application was shown on beam

specimen (4.55 m long, 0.50 m depth) with a retrofitting layer thickness layer of 40 mm and the results were compared with reference specimen without retrofitting layer. One beam was cast without any longitudinal reinforcement while the other two beams were characterized by a longitudinal reinforcement of two bottom rebars (ϕ16 mm) and two top rebars (ϕ12 mm). In order to avoid shear failure, stirrups (ϕ 8 mm) were placed at a distance of 150 mm at the beam ends (fig. 2.4a). The concrete beam was characterized by a class of compressive strength C20/25 in order to simulate a real case of a weak beam. The strengthening layer, made by FRC with 2.5% of microsteel fiber (12 mm length and 0.18 mm diameter) and compressive strength of 176.8 MPa, was placed on three side of the concrete specimen (fig. 2.4b). Before applying the reinforcement, the surface was treated by a sandblasting procedure in order to make the surface rough (depth 1-2 mm). A four point bendind tests were performed in order to evaluate the effectiveness of the solutions. The results (fig. 2.5a) shows that the HPFRC layer increased the bearing capacity of 2.15 times. The post peak response was determined by a softening branch followed by a plate with a higher value than maximum bearing capacity of the unstrengthened R/C specimen. It is worth notice that this technique produced a significant increase in stiffness in the uncracked stage in the specimen without longitudinal reinforcement. Considering the service load (fig.2.5b) the decrease in midspan displacement was 12 times less.

2.3 Shear behavior of beam: TRM and FRP retrofitting layer

The effectiveness of TRM jackets compared to FRP as shear strengthening reinforcement of RC element was investigated by Triantafillou [30], [27]. The studies was carried out on beams with a large space of the stirrups and subjected to four point bending tests. The length of the beams was 2.60 m with a cross section of 150 x 300 mm. The details of the geometry are shown in fig. 2.6. Concrete used had a compressive strength of 30.5 MPa. Textile used for retrofitting was

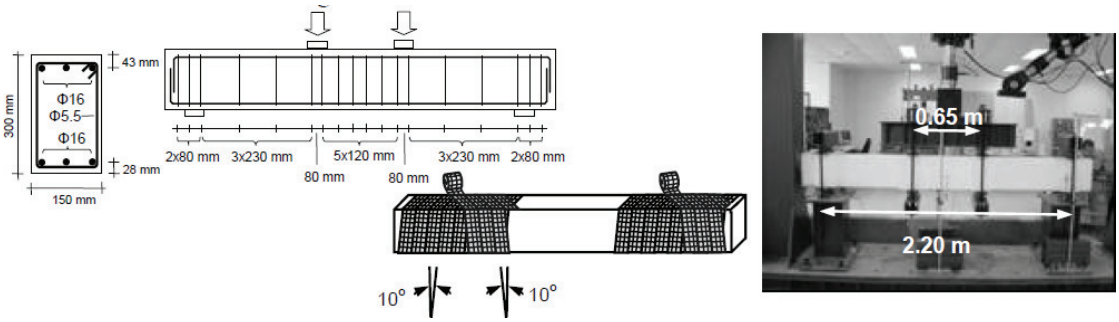

Figure 2.6: Geometry of the beams, detail of the reinforcement and test setup

made by high strength carbon fiber with $168 g/m^2$ and a layer 0.047 mm thick. The variables considered were the different bonding agent (mortar or epoxy resin), number of layer and the conventional wrapping versus spirally applied textile. Four beams were tested monotonically in particular the following situations were considered: a control specimen (C), specimen with two textiles layers of mortar (M2), two layer with epoxy resin (R2) and specimen with 2 layer applied with spirally method with mortar (M2-s). The results are shown in fig. 2.7 as load vs. mid-span displacement curve. The control specimen had a shear collapse with diagonal cracks and an ultimate load of 116.5 kN. The response of the other specimens indicated that the failure was

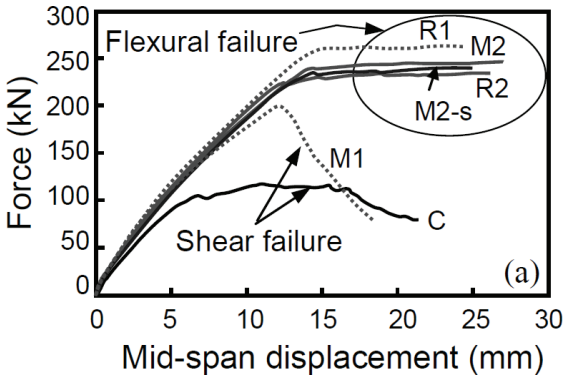

Figure 2.7: Force-mid span results

due to bending with cracks in the region with constant bending moment. The maximum loads for all retrofitting solutions are very similar as can be seen in table 2.4.

specimen	maximum load [kN]
R2	233.4
M2	243.8
M2-s	237.7

Table 2.4: Maximum peak load

The increase in shear resistance was significant for all the solutions with two textile layer. Specimen with R1 had a flexural failure load greater than the specimen with two layer. According to the authors it could be due to a larger concrete cover at the top of each beam compared to the one available at the bottom. Specimen M1 experienced a shear failure at maximum load of 200 kN and increased the shear capacity of 70% compared to control specimen .

2.4 Columns retrofitting

In this section the effectiveness of retrofitting materials are considered when applied to columns subjected to axial force. TRM, FRP and HPFRC were analyzed and for the case of HPFRC also the combination of axial force and bending moment was taken into account.

2.4.1 HPFRC compared to concrete jacketing

The possibility of strengthening existing columns with the application of High Performance Fiber Reinforced Concrete (HPFRC) jacket has been investigated by Meda [31]. The authors showed the effectiveness of HPFRC jacketing applied on columns subjected both to axial load and bending moment and the results were compared with traditional R/C jacket. Since columns are subjected to horizontal and vertical actions, axial force (N) and bending moment (M) the effectiveness of the retrofitting solution was evaluated by the analytical definition of the M-N interaction envelops. Square section of 300 x 300 mm reinforced with $8\phi16$ mm bars was adopted. The compressive stress of the concrete was equal to 15 MPa and yield value of steel bar was equal to 400 MPa. The jacket of HPFRC, equal to 30 mm with tensile strength of 11 MPa and compression strength of 170 MPa, was applied. The results obtained by the authors

are reported in fig. 2.8a and they were compared with unreinforced specimen. Look at the M-N envelope is possible to observe that the retrofitting solution guaranteed a bearing capacity that is 4 times the one of the reference structure in the case of simply compressed column and double of the reference both in the case of pure bending and tensile load.

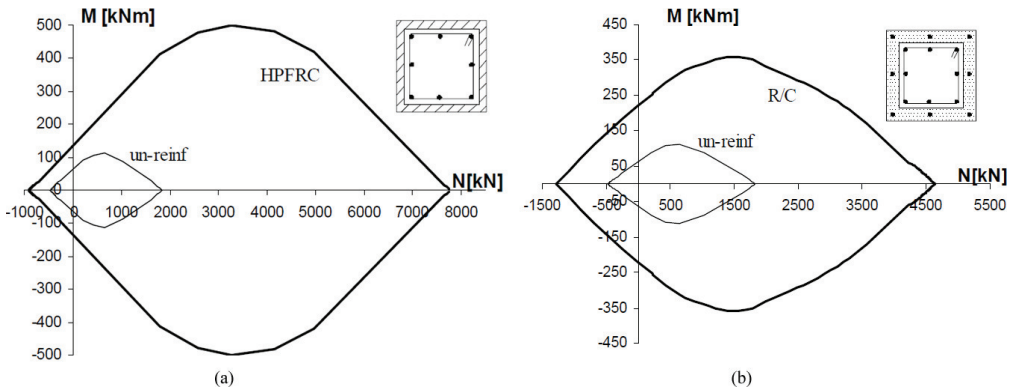

Figure 2.8: M-N envelops for (a) UHPFRC and (b) traditional concrete jacketing solution

The effectiveness of this technique was evaluated by a comparison with classic R/C jacket (fig. 2.8b). The thickness layer was a range between 60 and 100 mm with a consequent increase of section and mass. The M-N envelope obtained is reported in fig. 2.8b and it is possible to notice that the maximum compressive load was 2.5 higher than unreinforced solution. The bending strength was four times and the maximum tensile force was 3.5 times higher respect to the reference section.

2.4.2 TRM and FRP jacketing

The confinement effect of axially loaded concrete specimen was also evaluated by Papanicolaou [27]. The authors used TRM jackets and FRP to increase the resistance of RC members. The experimental program included unreinforced specimen as a reference and considered the following specimens:

- cylindrical specimens with 150 mm diameter and 300 mm height defined as the notation (A, B);
- rectangular cross section 250 x 250 mm and 700 mm height (C).

All specimens were reinforced with textile sheets of high strength carbon fiber (168 g/m^2 with a thickness of 0.047 mm) and using both (mortar and epoxy resin) bonding agents. The response in uniaxial compression was obtained by monotonically loading. The results are normalized with to control specimen for peak load and ultimate strain (table 2.5). The notation were given in terms of Y_XN where Y denoted the series (A, B, C), X the type of jacketing (C control specimen, MI mortar lower strength, MII mortar with higher strength, R resin based jacket) and N indicated the number of textile layer (1 or 2). TRM jacketing provided a significant increase in compressive strength and deformability significantly. This depended on the number of the layer and on the tensile strength of the mortar. Compared with their resin counterparts (FRP), TRM seems to be less effective both in strength and durability. The failure of mortar specimen was less abrupt due to the slowly progressing fracture of fiber compared to FRP that exhibited an

Specimen	f_{cc}/f_{co}	$\epsilon_{cc}/\epsilon co$
A_C	1.00	1.00
A_MI2	1.36	4.80
A_MII2	1.57	5.40
A_MI3	1.74	5.65
A_MII3	1.77	6.10
B_C	1.00	1.00
B_R2	1.53	8.35
B_MII2	1.25	4.90
B_R3	1.92	12.75
B_MII3	1.49	5.40
C_C	1.00	1.00
C_R2	1.29	6.20
C_MII2	1.40	5.90
C_R4	1.47	10.15
C_MII4	1.51	8.80

Table 2.5: Strength and deformability results

explosive failure without any kind of visible jacket damage. This failure was due to the release of a large amount of strain energy.

2.5 Final considerations

The aim of overlay layer was to extend the useful service life of an existing structure, to restore the load-carrying capacity and stiffness, and to strengthen its element. A prerequisite to obtain a suitable composite action is lasting bond between the existing substrate and retrofitting layer. In fact, regardless of the repair material and application method employed, the quality of the surface preparation prior to repair is a key issue. In some research studies [32] it was demonstrated that a sandblasting giving a roughness of about 1-2 mm leads to a good bond between the old concrete and the new jacket. Despite this consideration common to all jacketing applications, the effectiveness of the materials here considered was compared in terms of load bearing capacity and ductility in these different research studies. In table 2.6 and 2.7 the increment in the performances and the layer thickness for different materials and loads discussed in this chapter are summarized.

All these techniques can be successfully used even if some limits. The use of traditional concrete jacket is possible by adding layers of concrete with thickness greater than 60-70 mm that can excessively increase the cross section geometry. The FRP seems to be the best solution in terms of strength, high stiffness, good durability and minimal change of cross section dimension due to thin thickness layer. Despite these advantages, this technique entails a number of drawbacks which are mainly attributed to the organic resin used to bind the fibers. The disadvantages are:

- poor behavior at temperatures above the glass transition temperature;
- the high cost of resin;
- lack of vapor permeability;
- potential hazards for the worker;

wall in plane loading			
	increment load	max disp. increment	thick [mm]
TRM	5.08	13.36	≈ 4
FRP	7.00	12.49	≈0.94+resin
out of plane			
FRC	3	2	30
Flexural strengthened beam			
TRM	1.58	1	4
FRP	1.78	1	0.094+ resin
HPFRC	2.15	0.083	40
Shear strengthened beam			
TRM	2.09		4
FRP	2.01		0.094+resin

Table 2.6: Performances of the materials and thickness layer

confinement	pure bending	axial compression	tensile	thickness [mm]
HPFRC	2.3	4	2	30
concrete	2.5	2.5	3.5	60-100
	loading	deformability	thickness [mm]	
TRM	1.2-1.5	4-8	4	
FRP	1.3-1.9	6-12	0.094+epoxy resin	

Table 2.7: Confinement effectiveness

- no application at low temperature;
- difficult to conduct an evaluation of damage after earthquake.

Furthermore the main problem is the costs that is several time more than steel and concrete. FRP can be more suitable as complementary material and not to replace concrete or steel in every single applications. The replacement of organic binders with inorganic ones seems the best choice. The substitution of FRP with fiber reinforced mortars would be prevented by the poor bond between matrix and fiber sheets due to the granularity of the mortar. So for enhancing bond between fiber and matrix could be obtained by using textile fabric that are made by meshes where rovings can be woven, knitted or unwoven in at least two orthogonal directions. The mechanical properties can be affected by the quantity and the spacing of rovings for each direction. Only few studies on the use of TRM in strengthening concrete structures are available in the literature and focused on flexural or shear strengthening beams and bond between concrete and cement based textile composites [4]. In this thesis two materials jacketing has been investigated: HPFRC and TRM reinforced with AR glass fabric. The effectiveness of these overlays was investigated by indirect tensile and compressive tests on traditional concrete plates. Furthermore a part of the experimental program was dedicated to the mechanical characterization of the TRM under direct tensile load.

Chapter 3

Advanced cementitious composites

3.1 Introduction

Cement-based composites materials offer a wide field of structural applications and they are the most economical building materials able to bring compressive loads. By the use of fiber or fabric as reinforcement, the possible range where adopting concrete for structural design, is enlarged. The use of fiber to improve the mechanical properties of brittle materials such as concrete is a well known concept since long time. A combination of these properties allow designers to produce thinner elements, lighter and innovative in geometry, impermeable against corrosion with improved durability. Ultra High Performance Fiber Reinforced Concrete (UHPFRC) and Textile Reinforced Mortar (TRM) offer an optimum combination of high strength and ductility in a highly moldable product with a good surface aspect. These properties make these materials a promising solution for reinforcement and protection of existing concrete members. These materials are being employed because of their easy on-site casting combined with their good strength and durability properties. These materials show a high performance in compression due to the features of the matrix and a good behavior in tension due to the presence of fibers and non metallic fabrics. The tensile performances depend on various parameters such as the kind of the mortar, the reinforcement ratio, the characteristic of the reinforcement, depending on sample orientation fiber distribution and fabric geometry.

3.2 Historical background

High Performance Concretes (HPC) are characterized by a compressive strength from 60 to about 150 MPa and with the recent developments, it is also possible to increase the compressive resistance over 200 MPa, Reactive Powder Concrete (RPC). HPC has been developed since the eighties, but the technological premises go back many decades before. The principal theories that lead to reach high performance started in the '50 years where the Powers's theory studied the influence of water to cement ratio on compressive strength [33]. Also according to Powers, for enhancing the mechanical behavior reducing water-cement ratio bring to a decrease of capillary porosity. He studied a physical model to quantify the influence of capillary pores on the mechanical resistance without stone aggregate. This theory remained an utopia for two reasons: the impossibility to realize concrete with the water-cement ratio lower than 0.36 for the poor workability and the consequent difficult casting procedure; and also the Powers's theory has been thought out neglecting the presence of aggregates leading to the formation of an interstitial

Figure 3.1: Seonyu Footbridge, Seoul, Korea, 2002

area more porous and therefore weaker. Afterwards in the seventies the invention of admixtures superplasticizers allowed to reduce the water-cement ratio without penalize the workability and to obtain a compressive strength about 60-80 MPa. The superplasticizers modify the rheology of fresh concrete. Workability of fresh concrete depends on its rheological properties. They are defined by two features: yield stress and plastic viscosity. The first is correlated with the slump and the second can be determined by various rheometers. Admixtures are made by polymers that are able to be absorbed on the surface of the cement grains. Cement particles tend to thicken in the absence of superplasticizers for the presence of electrostatic charges. Because the absence of flocculation of the cement, the matrix results to be more workable and then it is possible to adopt a lower water-cement ratio. The effectiveness of the additives, in terms of reduction of the water-cement ratio and the enhancement of the compressive strength, increases with the dosage up to a limit of 3% cement by weight. High contents cause the formation of water (bleeding) between the cement matrix and the aggregates. The compressive strength was limited to values of about 80 MPa. To overcome this strength, it was necessary to introduce very fine particles such as fly ash and silica fume in the mortar. The silica fume is a waste product of the industry of silicon and metal alloys. Excellent performance has been obtained thanks to the coupling of this material with superplasticizers. The size of the particles are dimensions between 0.01 and 1 mm and this allowed the particles to fit within the interstitial voids thus obtaining a more dense matrix and therefore more strength and difficult for the agressive elements to penetrate. The large specific surface of these materials leads to increase the quantity of required water, thereby reducing the resistance. For this reason the use of superplasticizer combined with the silica fume was an optimum solution. It was possible to reach the water-cement ratio less than 0.25. The major applications have been devoted to engineering infrastructure works such as offshore platforms, span bridges,pavements, tunnels. In 1993, Federal Highway Administration (FHWA) of Washington initiated a national program to increment the use of HPC in bridges structures. The bridges were located in different climatic regions of the United States. The elements made by HPC were the superstructure such as (deck and girders) and substructure (piers and abutments). In the bridges both strength and durability are important characteristics. Several bridges made of HPC have been built, some example are reported in Figs. 3.1, 3.2 and 3.3. Besides bridges this type of concrete was also used for columns, walls in high-rise buildings. One of the first applications in high-rise buildings in the USA was "Two-Union Square" in Seattle, [34]. Columns with 3 m and 1 m of diameter were constructed by using a concrete with 140 MPa compressive strength. This concrete was cast in steel pipes that were used as a formwork. The fresh concrete was pumped from the button to ensure the completely filling of the pipes. In Germany a concrete with C85 class was used for the first time in the 1990 for a "Trianon" building high 180 m in Frankfurt (Fig. 3.4). This concrete was not regulated in German standards and so a special

Figure 3.2: Sakata-Mirai Footbridge, Japan, 2004

Figure 3.3: Gärtnerplatz Footbridge, Kassel, Germany, 2007

permission was required for the structural applications. Meanwhile HPC with C115 class was adopted for other building such as "Taunustor" in Frankfurt for the first time for the flexural and shear stressed elements (Fig. 3.4). For this reasons one again extensive investigations were done to obtain a permit. The fibers content can be mixed into the fresh concrete in homogeneously way without segregation problems. The durability of concrete is compromised by the chemical attack but in the UPC matrix the resistance against such effects was improved due to the dense microstructure characterized by few or no capillary pores. For this feature the material was used also in industrial buildings or in structural elements in sewage treatment. In recent decades, numerous researches have been focused on fiber reinforced materials, in particular the use of steel fibers. The idea of using short fibers randomly distributed to reinforce brittle materials with the aim to improve physical properties is very old. Fibers had been used to reinforce brittle materials from the Egyptian and Babylonian eras. Straws were used to reinforce sun-baked bricks and horse hair for the plaster and asbestos fibers for the portland cement. Despite this the first studies devoting to the use of fiber composite concrete, as we know nowadays, it went back to 1950s and early 1960s when Romualdi and Batson [35] and Romualdi and Mandel [36] studied the effectiveness of short steel fiber in reducing the brittleness concrete. In 1964 Krenchel in Denmark [37] published studies about fiber reinforced concrete. In U.K. Majumdan and Ryder analyzed the use of glass fiber as reinforcement. During the 1970s numerous researches were led by Shah and Rangan, Swamy, Kelly [38], Neville and Naaman [39]. Other developments were obtained by studying different fibers such as glass, carbon, natural and synthetics. The Romualdi and Mandel's approach was based on fracture mechanics to explain the tensile strength of fiber reinforced concrete. Naaman in 1972 [39, 40, 41, 42] analyzed the stress elongation curves and he explained a method to classify the kind of concrete. Several papers about the tensile response of FRC were presented at 1978 RILEM symposium and in the same year Naaman and Shah investigated multiple cracking behavior through tensile and bending experiments. In the 1970s

Figure 3.4: Trianon and Taunustor building, Frankfurt

the idea to use continuous aligned fibers for obtaining high tensile ductility developed, Aveston (1971), Krechel and Stang (1989). Actually the concept of continuous aligned fiber reinforcement is represented by the textile reinforced mortar.
Nowadays fiber reinforced concrete has numerous applications [43], [44]. Stan alone cases are slabs on grades, pavements, electrical poles and pipes. It can be used to support other structural elements such as prestressed concrete element and concrete reinforced with steel bar and as jacketing for repair beams and columns damaged by fire or seismic loads. Other particular example are offshore platforms, high rise structures and blast resistance structures. Sometimes the use of UHPFRC can be done only in a selected zone of the structures for strengthening. Some example are punching shear zones, anchorage zone in prestressed concrete beam, beam to column connections in seismic frames, coupling beams and compression zone of beam and column for improving ductility.

3.3 UHPFRC

The mechanical properties of fiber reinforced concrete depend on the features of the components, their dosages and in particular by the geometry, the volumetric percentage and the characteristics of the fibers such as mechanical properties and adherence fiber matrix. The fibers dispersed in the matrix improve the tensile strength and ductility by counteracting the progressive opening of cracks and increases the energy absorbed in the fracture process. Other contributions are referred to structural performance in general such as enhancing bonding between the bar and the matrix, preserving the concrete cover during large deformation and restraining spalling.
The fiber must be selected such that the microcracking length is reduced and no large deformations develop during the macro crack stage. The mechanical behavior of concrete under tensile load can be subdivided into four phases according to Van Mier [45]:
(O) elastic stage

(A) microcraking phase
(B) macrocrak un-stable branch
(C) bridging effect.

The first branch is the elastic contribution (O) and after the microcraking stable phase oc-

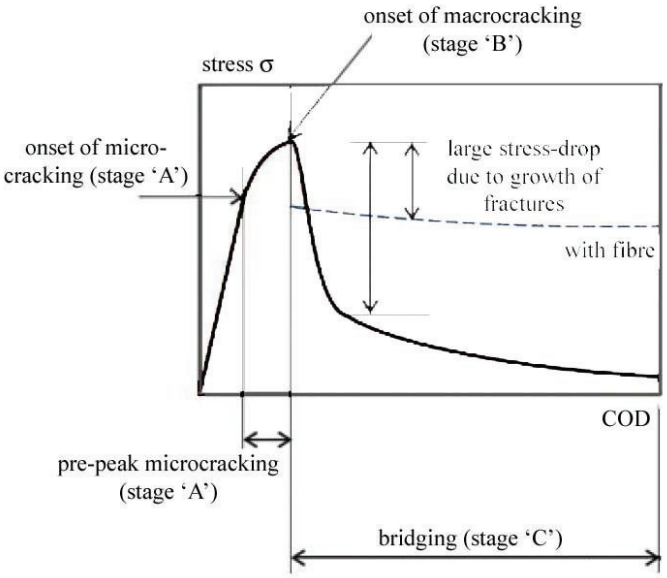

Figure 3.5: Different stages during the fracture process

curs (stage A). This stage influences the material strength. After that the maximum capacity is reached and fiber debonding begins. The effect of fiber is to stabilize the stage (B) with the bridging effect. Stages (B) and (C) characterize the post peak behavior and the ductility. They depend on the fiber volume, the adherence in the interface, the orientation and distribution of fiber. For small fiber volumes (less than 1%) the post peak behavior decreases (softening branch), on the other hands for higher volumes the branch can increase due to the appereance of multi-cracking. Best performances are obtained aligning the fiber, Fig. 3.6. Cementitious composite reinforced with discontinuous fibers can be classified according to their tensile behavior.

3.3.1 Strain and hardening behavior

Tensile response of fiber reinforced concrete can be classified in two categories depending on their behavior after first crack, namely strain softening and strain hardening. In the category of strain softening, Naaman [40] defines deflection hardening and deflection softening, Fig. 3.7. The classification is related to the volume content of fiber and it depends on the typology of tensile test (uniaxial or flexural). The strain hardening concrete is considered mechanically more powerful and it is used in structural applications where bending prevails, while deflection softening materials are adopted in concrete pavements and slab. Naaman and Reinhardt [41] classified the fiber reinforced concrete as it indicates in Fig. 3.8 where it illustrates the different response and the transition from quasi brittle FRC to ductile HPFRC. After reaching the crack strength (A), FRC shows a softening behavior and a localized crack. In the softening branch only a localized fracture plane occurred controversely during the hardening behavior multiple cracks are generated, Fig. 3.8b (under area II). Before cracking the elongation can be transformed into strain

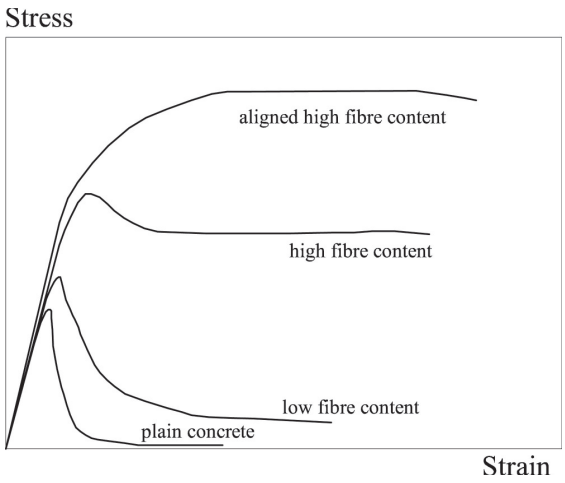

Figure 3.6: Comparison plain concrete with fiber reinforced concrete

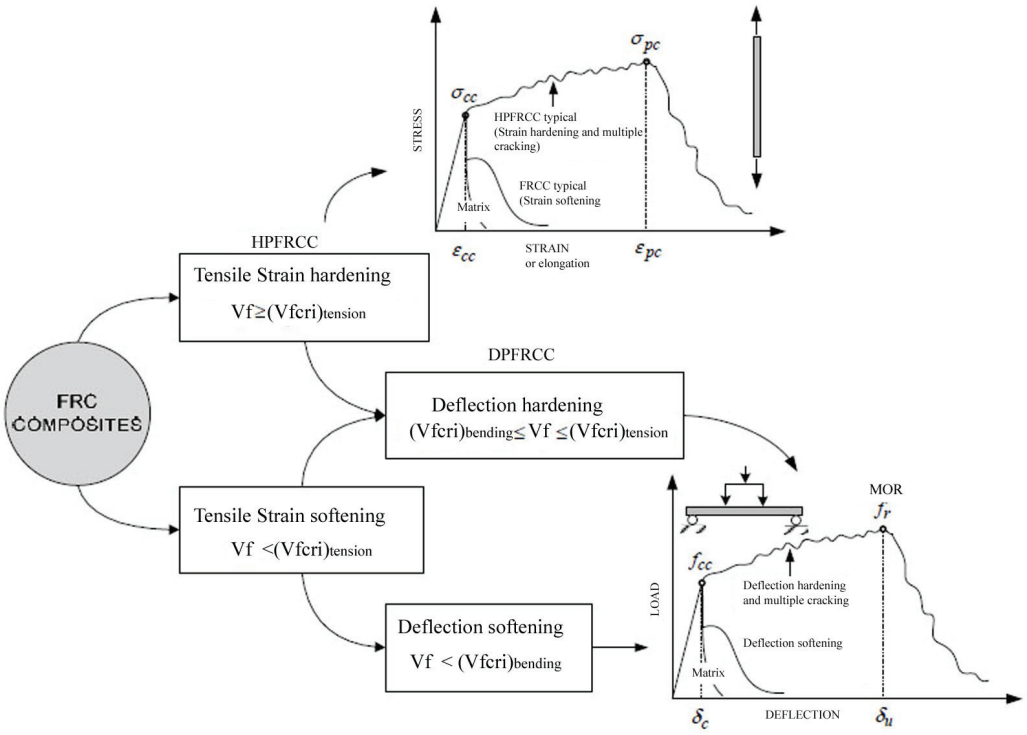

Figure 3.7: Classification of stress strain response for tensile and bending case

while after that the deformation is measured within the gage length of the instrument. In the case of strain hardening the elongation can be translated into equivalent strain because the crack width can be considered as smeared. The stress strain hardening curve is characterized by the

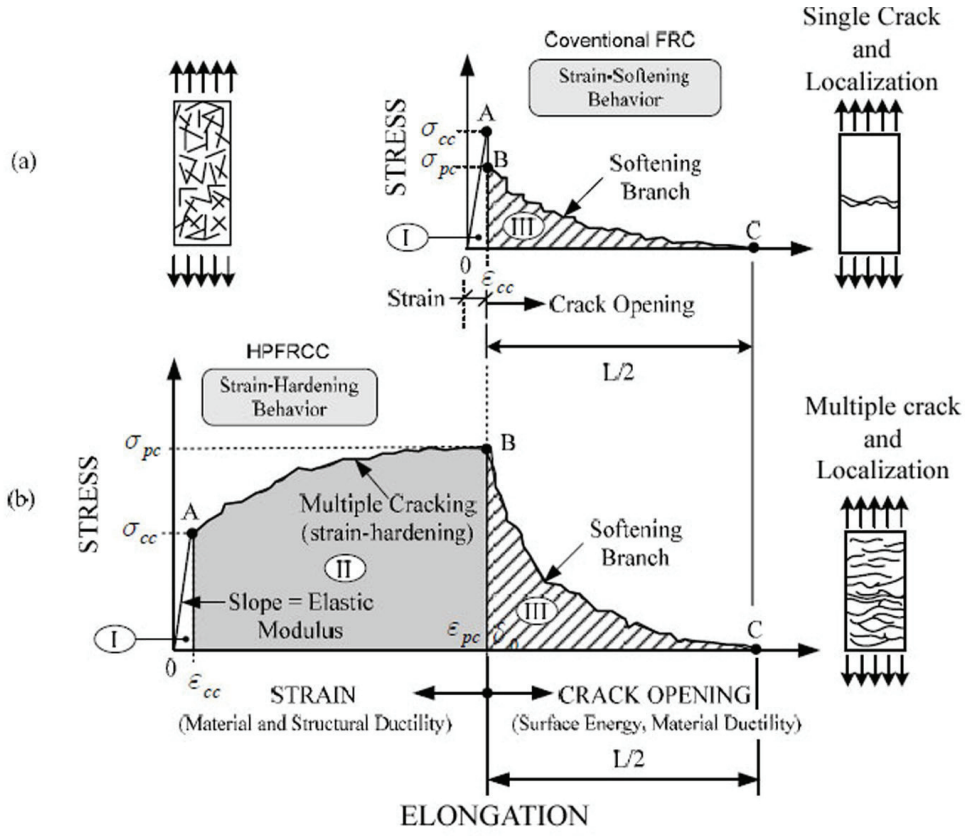

Figure 3.8: Stress strain diagram: (a) strain softening, (b) strain hardening

first linear and steep branch until the cracking resistance (Fig. 3.8b partI), after that a strain hardening behavior with multiple cracking occurred (partII). The coordinate in the point where the matrix reached the cracking resistance is defined by (σ_{cc} , ϵ_{cc}) and the peak point the the end of the strain-hardening behavior leads to a value defined by post-cracking stress strain (σ_{pc}, ϵ_{pc}). At the peak level, one crack localizes and a descending branch, which corresponds mainly to the opening of the critical crack, takes place (part III). Within this branch, fibers can pull out or fail and no more cracks develop. Naaman proposed to adopt the name "High Performance Fiber Reinforced Cement Composite" (HPFRCC) to describe the combination of high strength and toughness ductility (defined also as "'Strain Hardening behavior"') and the denomination "Strain Softening" to define classical Fiber Reinforced Concrete (FRC).

3.3.2 Properties of concrete

High Performance Concrete exceeds the properties of traditional concrete and special components are used to achieve the performance requirements. The main properties are developed for particular applications and environments. They can be summarized as follow:

- high strength;
- high early strength;
- high modulus of elasticity;
- high durability;
- low permeability;
- resistance to chemical attack;
- compaction without segregation.

The list of elements used during the design of mixture are reported in table 3.1 with their primary contributions, [22]. Not all properties can be obtained at the same time.

Materials	Primary contribution/ Desired property
Portland cement	Cementing material/ durability
Blended cement	Cementing material/ durability/high strength
Fly ash	Cementing material/ durability/high strength
Slag	Cementing material/ durability/high strength
Silica fume	Cementing material/ durability/high strength
Calcined clay	Cementing material/ durability/high strength
Metakaolin	Cementing material/ durability/high strength
Calcined shale	Cementing material/ durability/high strength
Superplasticizers	Flowability
High-range water reducers	Reduce water to cement ratio
Hydration Control admixtures	control setting
Retarders	Control setting
Accelerators	Accelerate setting
Corrosion inhibitors	Control steel corrosion
Water reducers	reduce cement and water content
Shrinkage reducers	Reduce shrinkage
Polymer/latex modifiers	Durability
Optimally graded aggregate	Improve workability and reduce paste demand

Table 3.1: Materials used in HPC, [22]

The factors affecting compressive strength and knowing how to modify those factors for the best solutions, are topics of great interest to manufacturers. Each variable should be studied separately during the mix design and the optimum value should be established. The cement contents vary from 400 to 600 kg/m^3. Fly ash, silica fume or slag are usually added a dosage rate of 5% to 20% by the mass of cementing material. The water-cement ratio should be adjusted according to the workability of the matrix. In high performance matrix the aggregate size, shape, surface, mineralogy and cleanness are very important. The aggregate diameter can be in a range from 20 to 2 mm. The strength and the bond or adhesion between the paste and the aggregates are important. Coarse washing of aggregates may require to remove detrimental coatings of dust and clay. The quantity of coarse aggregate should be the maximum consistent with the workability. It is also important the sequence in which solids and liquids are added in the mixer and the percentage of each material to avoid problems like balling cause by a dry uncompacted silica fume.

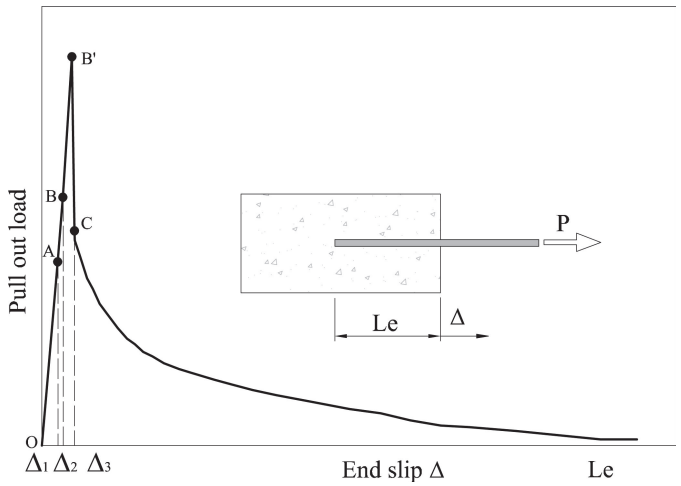

Figure 3.9: Smooth fiber: pull out load versus slip

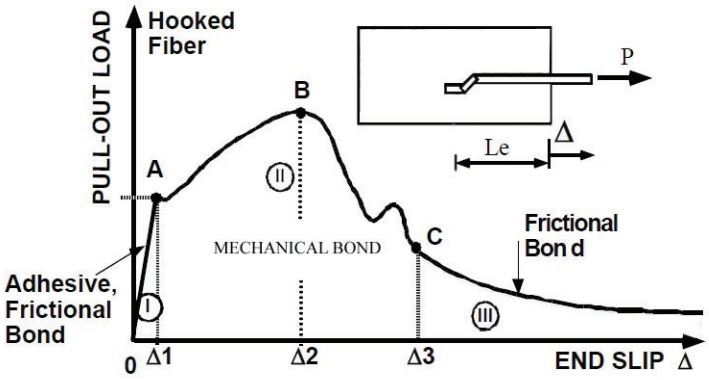

Figure 3.10: Hooked steel fiber: pull out versus slip [1]

3.3.3 Interface fiber and matrix

Experimental pull out test is essential to characterize fiber reinforced concrete behavior. This test is performed through the pull out of the single fiber or for small groups from the concrete matrix. Once established the fiber material an infinite combination of geometric properties can be chosen such as cross sectional shape, length, diameter and surface deformation. For steel, the cross section can be circular, rectangular, diamond, flat. To improve mechanical bond fiber surface can be made rough by inducing mechanical deformation. Authors such as Naaman analyzed the pull out phenomena for different surface roughness (smooth, hooked, twisted), [1]. The pull-out behavior of smooth fiber is shown in Fig. 3.9. The initial ascending branch (OA OAB OABB' according to the adhesion) occurred up to the peak load; after that, the load drops to level C and then it decreases slowly. The static friction and adhesion dominate the ascending branch, and after the dynamic friction occurs. The area under each branch correspond to the dissipated energy.

For hooked fiber Fig.3.10, the behavior for the first branch (OA) is the same of the smooth

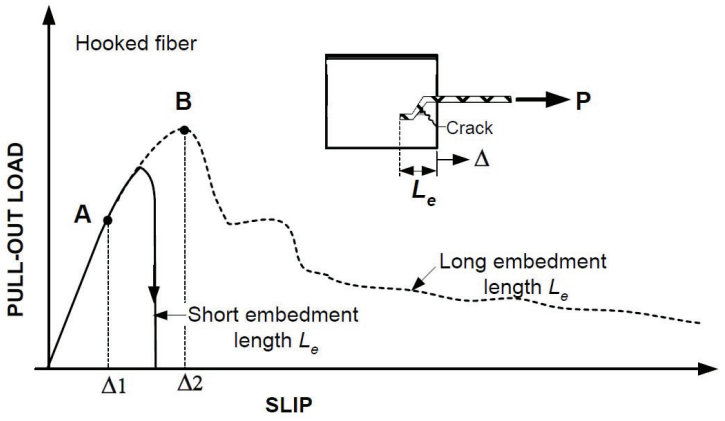

Figure 3.11: Effect of embedded length on the pull out phenomena [1]

fiber but the contribution for the second part (ABC) is clearly marked. Indeed two hinges for each corner of the hooked fiber are created while fiber slips into the matrix; after that, fiber is stretched and becomes straight and it can slide without any constraint. The comparison between the straight and hooked fiber, Figs 3.9 and 3.10, shows that the part (OA) is the same until Δ_1 where the large contribution (ABC) distinguishes the mechanical bond typical of hooked fiber. The displacement Δ_2 corresponds to the formation of the plastic hinges and in the point C the fiber is completely straight and free to slide. The area (II) indicates the energy released during the work of pull out phenomena that is much greater than the previous area (I). The hook has to be far away from the boundaries of the crack surfaces otherwise the branch (ABC) cannot develop. If the hook is to close to the edge, a crack occurs in the matrix up to reach fiber leading to a sudden drop in strength (Fig. 3.11). The embedded length of a hook is around 3 mm. Naaman [46] studied also the twisted typology fiber and the improvement behavior due to the

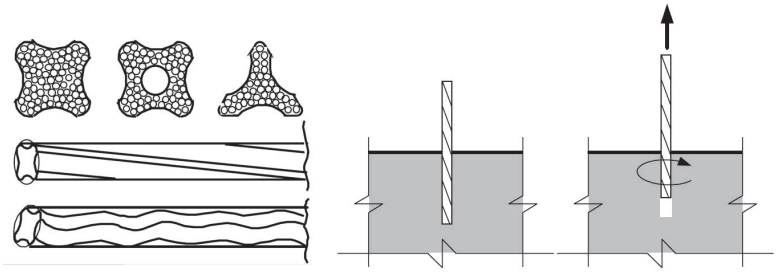

Figure 3.12: Geometry of twisted fiber and pull out mechanism

best anchoring effect, Fig. 3.12. The bond strength of smooth steel fiber is generally of frictional nature. Most fiber are mechanically deformed to improve their bond. Mechanical deformations correspond to hooked-end, buttoned end, indenting the surface and crimped, Fig.3.14. The fiber can also be twisted for improving the mechanical bond significantly. The pull-out mechanism is significantly different, Fig.3.13. Starting from the point (A) frictional and mechanical bond are activated simultaneously all the time up to complete pull-out. While sliding within the matrix fiber tried to un-twist and a torsional moment resistant occurred. The comparison in terms of pull out load and displacement for different geometry of fibers is summarized in Fig.3.13. Fiber

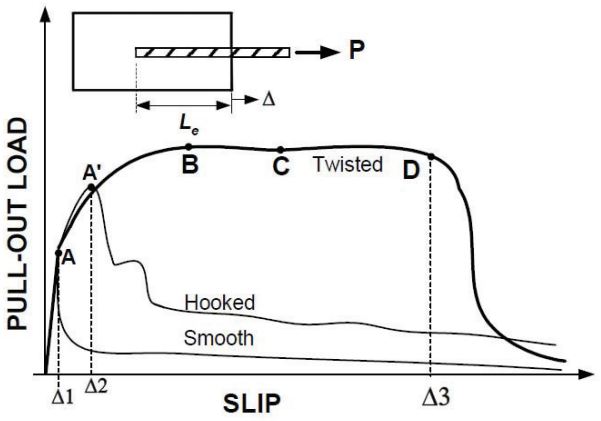

Figure 3.13: Influence of different fiber in the pull out mechanism

can be classified according to their characteristics as
the material:

- natural organic (cellulose, jute, bamboo)
- natural mineral (rock-wool)
- artificial (steel, titanium, glass, carbon, polymers, synthetic...)

the physical and chemical properties:

- density
- roughness
- chemical stability
- fire resistance

the mechanical properties:

- tensile strength
- elastic modulus
- stiffness
- ductility
- elongation to failure

geometry:

- cross section shape (circular, triangular, polygonal)
- length
- diameter or equivalent diameter in the general cross section

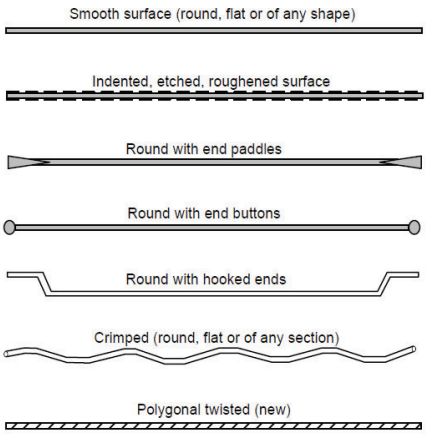

Figure 3.14: Typical geometry of steel fibers

- surface deformation (smooth, indented, crimped, twisted, with end hooks or other anchorage).

The volume fraction of the total composite depends on the applications as indicated in table 3.2, [46].

Material	**Range of V_f**	**Remark**
FRC Fiber Reinforced Concrete	$V_f \leq 2\%$	Fibers are premixed with the concrete matrix. Finer aggregates may be needed.
HPFRCC High Performance Fiber Reinforced Cement Composites	$V_f \geq V_{f-critical}$ $V_f \geq 1\%$	Strain hardening and multiple cracking characteristics in tension. With proper design, critical V_f can be less than 2%.
Shotcrete	$V_f \leq 3\%$	Applications in tunnel lining and repair
Spray Techniques (glass fibers)	$4\% \leq V_f \leq 7\%$	Applications in cladding and panels.

Table 3.2: Range of volume fraction

The presence of fiber leads to decrease workability of the matrix; also for this reason it is necessary to use superplasticizer. Furthermore, it is important the way that fiber are mixed to create a good dispersion and to avoid the group of coarse aggregates. In order to make effective the reinforcement, fibers must have the following properties, compared to the matrix as shown in the Fig. 3.15. The Young modulus varies from 200 GPa for fiber with a high and low percentage of carbon and 170 GPa for stainless steel fiber. The tensile strength has to be higher than the crack resistance of the matrix; the Young Modulus of fiber should be 3 times more than of the matrix; the bond strength has to be the same magnitude order of the tensile strength of the concrete. Generally, steel fibers are most commonly used for structural purpose and they have a length l_f between 6 mm and 70 mm and an equivalent diameter, d_f, between 0.15 mm and 1.20 mm. According to the CNR DT 204 [47] they can be classified according to their production process, the shape and the content of carbon, higher or lower to 0.20, or stainless steel.

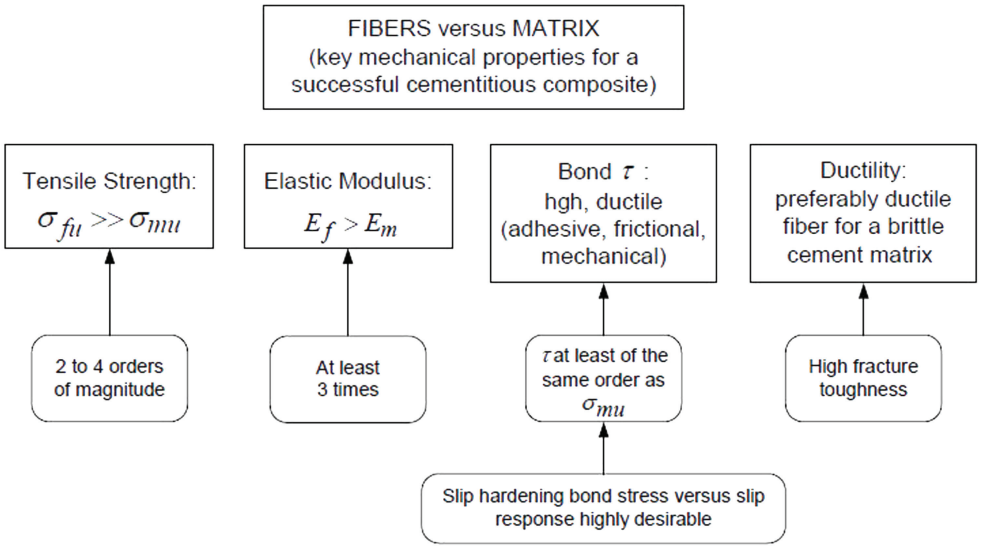

Figure 3.15: Fiber properties

3.3.4 Tensile behavior

The incorporation of steel fiber in the matrix exceeds the brittle behavior of plain UHPC under tensile stress. The UHPFRC can be classified according to the mechanical response in tension as "strain hardening" or "strain softening" according to the volume fraction of fiber, their bond and mechanical properties. According to CNR DT 204 the amount of fibers that determines the tensile hardening is about 2%, but acccording to Wille [2] is possible to decrease this value. He studied a matrix with compressive strength of 200 MPa and, in addition, different kind of steel fiber, smooth and high strength deformed. The research showed that a volume fiber of 1% is sufficient to obtain a strain hardening behavior with multiple cracking. The aims were to achieve a high tensile strength by improving the chemical and mechanical bond between fiber and concrete, to obtain a high ductility with an ultimate strain greater than 0.3% and to contain a relatively low amount of fibers less than 2.5%. The fibers analyzed were smooth and deformed. The last one can be distinguished in deformed at the end of the fiber and uniformly deformed such as twisted fibers. Different volume fractions were selected and the influence of the fiber shape was investigated through direct tensile tests. Figure 3.16 shows the tensile behavior with different amount of smooth fibers. An increase in volume fraction of reinforcement from 1.5 to 2.5% leads to an increase in tensile strength from 8 to 14 MPa and the strain from 0.17 to 0.24%. An increase from 1 to 2% of volume of hooked steel fiber, as shown in Fig. 3.17, involves an increment of tensile strength from 9 to 14 MPa, but the strain remains constant to 0.46%. Figure 3.18 shows the contribution of twisted fiber according to a volume fiber from 1 to 2% with increase in the tensile stress from 8 to 15 MPa. The post cracking branch increases from strain equal to 0.33 up to 0.61%. Even with low percentages of fibers and optimizing the geometry of the fiber, it is possible to reach a satisfactory values in terms of tensile strength and ductility.

For evaluating the tensile strength of HPFRC structural elements, the methods are explained in Standard rules (CNR DT 204/2006 and Model Code) and are here summarized.

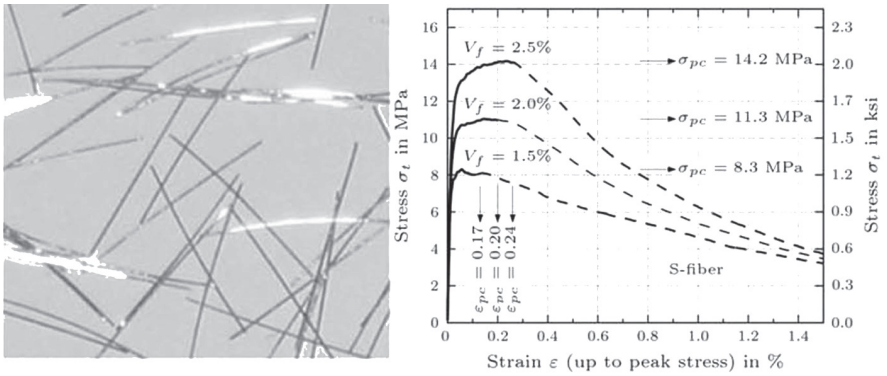

Figure 3.16: Stress versus strain for smooth fiber for different volume fraction [2]

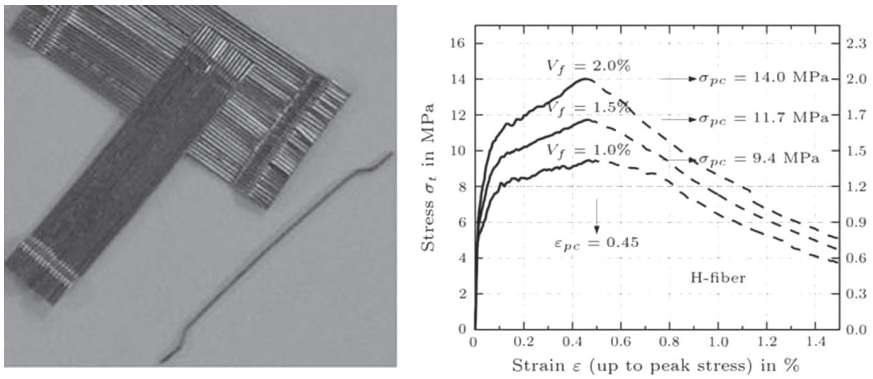

Figure 3.17: Stress versus strain for hooked fiber for different volume fraction [2]

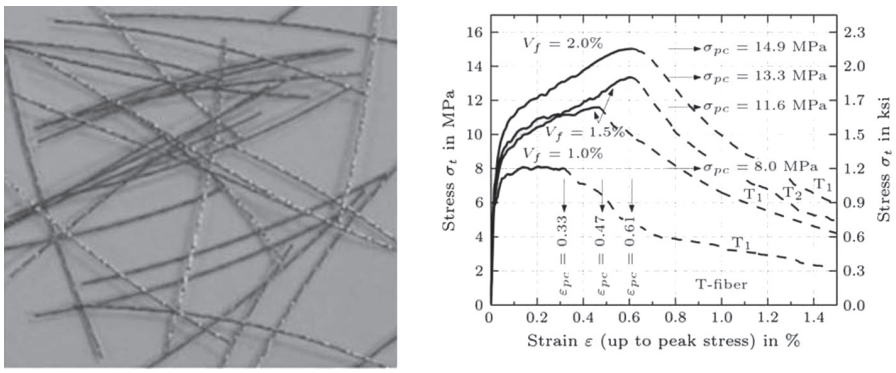

Figure 3.18: Stress versus strain for twisted fiber for different volume fraction [2]

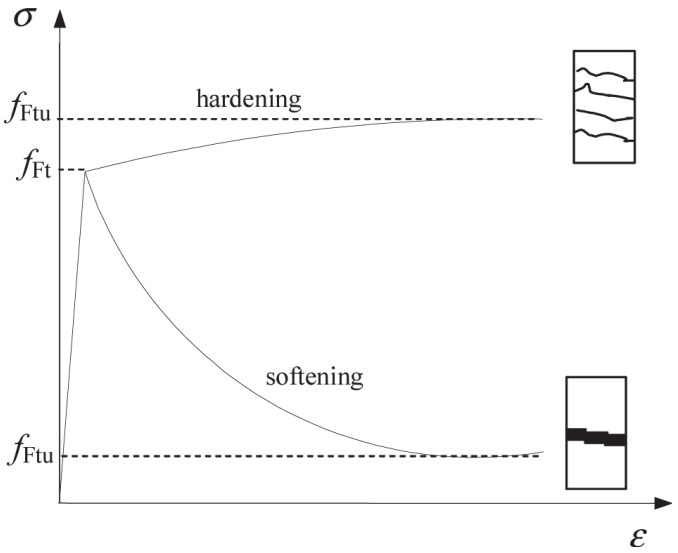

Figure 3.19: Tensile behavior from CNR DT 204

Italian National Guidelines CNR DT 204/2006

To identify the tensile behavior of UHPFRC, the Italian National Guidelines CNR DT 204/2006 proposes two models, softening for low amount of fiber and hardening behavior when multicracking phenomena take place (Fig. 3.19). The first cracking uniaxial tensile strength, f_{Ft}, can be assumed equal to the tensile strength of the matrix, f_{ct}, and for the softening material coincide with peak value. In both cases the pull out force can be computed from the equilibrium in the normal direction of fracture surface.

$$Q = \alpha \cdot V_f \cdot \frac{l_f}{d_f} \cdot \tau_m \tag{3.1}$$

where:

- V_f is the fraction volume of fiber;
- $\frac{l_f}{d_f}$ is the aspect ratio;
- α is a coefficient that considers the orientation of fiber;
- τ_m average tangential stress.

Equation 3.1 considers contributions such as the volume fraction, the aspect ratio but it does not take into account different aspects such as the shape of fiber and the casting flow. The post-cracking capacity can be defined through 4 point bending tests considering the values f_i which correspond to the assigned nominal values of crack opening or average value, f_{eqi}, in a range value of crack opening (Fig. 3.20). In case of notched beams the crack opening is referred to the CTOD. From bending test, it is possible to define two simplified laws stress versus crack opening: linear behavior (softening or hardening) and rigid plastic, Fig. 3.21. The value f_{Fts} represents the serviceability residual strength, defined as the post-cracking strength for serviceability crack openings and f_{Ftu} represents the ultimate residual strength. The crack opening, w_u, cannot exceed the value of 3 mm for bending elements and 1.5 mm for tensile elements in the case of

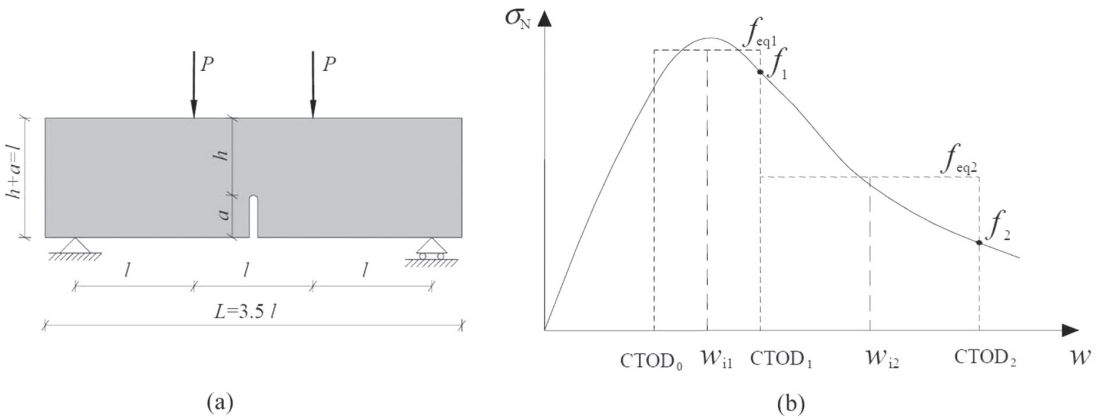

Figure 3.20: (a) Four point bending test and (b) values of tensile strength determined through bending test

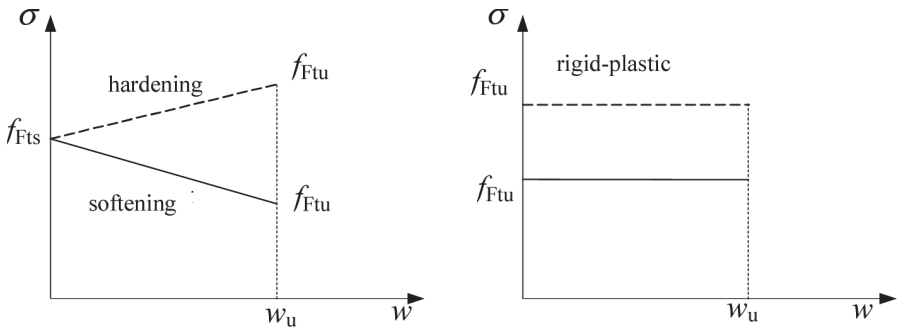

Figure 3.21: Simplified constitutive law, stress vs. crack opening

softening behavior. To get the definition of the constitutive laws in terms of stress-strain, the characteristic length has to be evaluated:

$$\epsilon = w/l_{cs}$$

In presence of traditional reinforcement the characteristic structural length, l_{cs}, can be estimated through Eqs. 3.2, 3.3.

$$l_{cs} = min\,(s_{rm}, y) \tag{3.2}$$

$$s_{rm} = \xi \cdot \left(50 + 0.25 \cdot k_1 \cdot k_2 \cdot \frac{\phi}{\rho}\right) \tag{3.3}$$

Where:

- s_{rm} is the average distance between crack expressed in mm;
- y is the distance of the neutral axis from the extreme tensile side;
- ξ is an adimensional parameter and it's depend on the aspect ratio ($\frac{l_f}{d_f} < 50$ $\xi = 1$; $50 \leq \frac{l_f}{d_f} \leq 100$ $\xi = 50$; $\frac{l_f}{d_f} > 100$ $\xi = 0.5$)
- d_f is the fiber diameter;
- l_f is the fiber length;
- ϕ is the bar diameter;
- k_1 is equal to 0.8 for high bond and 1.6 in the case of smooth bar;
- k_2 is 0.5 in the case of composite or pure bending when $y \leq h$ and 1 for the tension when $y > h$;
- h is the height of the section;
- ρ is the geometric reinforcement ratio.

In the case of section without traditional steel reinforcement and subjected to bending, bending and compression or tension, the quantity s_{rm} is equal to the depth of the specimen. This is valid for model of beam with plane section. For kinematic approaches as finite element, the structural characteristic length has to be changed. For hardening behavior the cracking occurs in a widespread way so a mean strain can be adopted and the ultimate strain is assumed equal to 1%. The stress vs. strain curve is shown in Fig. 3.22a and the simplified models are reported in Fig. 3.22b. To compute the value of f_{Fts} and f_{Ftu} that defined the constitutive strength parameter, two models are proposed by the Standard (Linear elastic model and rigid plastic model) and here reported.

Linear elastic model

The linear elastic model identifies two values, f_{Fts} and f_{Ftu}, based on the equivalent bending resistance through the following Eqs. 3.4 and 3.5.

$$f_{Fts} = 0.45 \cdot f_{eq1} \tag{3.4}$$

$$f_{Ftu} = k \cdot \left[f_{Fts} - \frac{w_u}{w_{i2}} \cdot (f_{Fts} - 0.5 \cdot f_{eq2} + 0.2 \cdot f_{eq1})\right] \geq 0 \tag{3.5}$$

where:

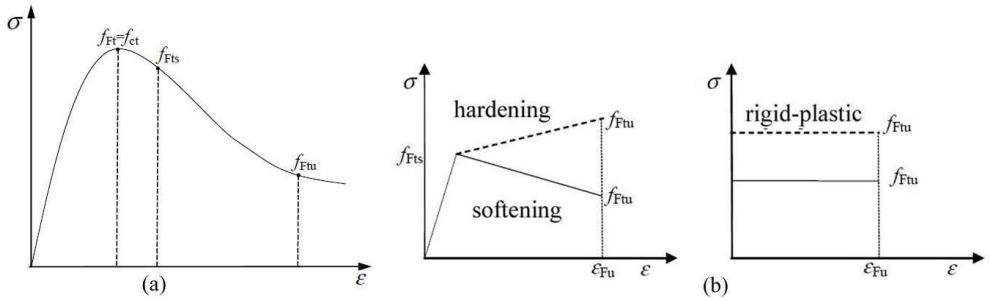

Figure 3.22: (a) Stress vs. strain, (b) simplified constitutive law

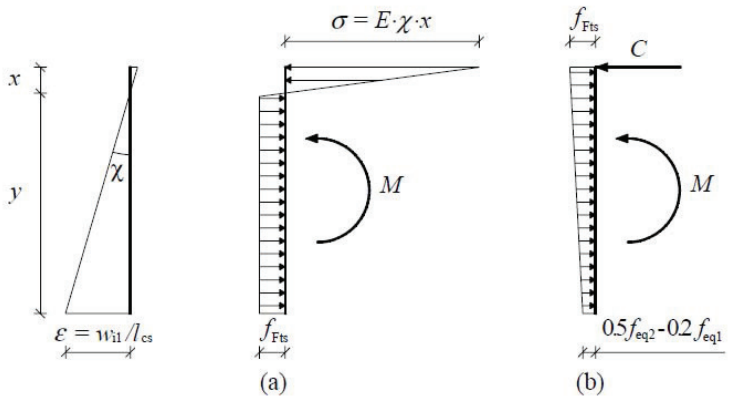

Figure 3.23: The tensional diagrams for the evaluation of tensile resistance

- f_{eq1} and f_{eq2} are the equivalent post-cracking resistance for the SLS and ULS respectively. In a notch beam the f_{eq1} is evaluated in the range of Crack Tip Opening Displacement 0≤w≤0.6 mm and the second one varies from 0.6≤w≤3 mm. For unnotched beam the post cracking strength f_{eq1} and f_{eq2} are estimated respectively in the COD range ($3w_I$ - $5w_I$), where w_I means the opening displacement at the maximum load evaluated in 0≤w≤0.1, and f_{eq2} is evaluated in the range ($0.8w_u$ - $1.2w_u$ mm) where $w_u = min(0.02 \cdot l_{cs}, 3mm)$.
- the coefficient k is equal to 0.7 for uncracked sections under tension and equal to 1 for the other situation;
- w_{i2} is the mean value of crack opening;
- w_u is the ultimate value of the crack opening.

The relationships, 3.4 and 3.5, can be computed by equilibrium equations on the rectangular cross section under bending load. In particular the Eq. 3.4 is referred to crack opening less than 0.6 mm and the following hypothesis are valid:

- plane section;
- the elasto-plastic behavior for tension where the maximum value is f_{Fts}, Fig. 3.23a;
- elasto-linear behavior in compression, Fig. 3.23b;

The unknown parameters are f_{Fts} and the curvature χ, the strain at the tensile side is:

$$\epsilon_{F1} = \frac{w_{i1}}{l_{cs}} \tag{3.6}$$

where

- w_{i1} is the average value of crack opening ($CTOD_0$ and $CTOD_1$);
- l_{cs} is the critical depth of the specimen section or the ligament depth;

so the equations system can be solved:

$$N = 0 \tag{3.7}$$

$$M(\epsilon_{F1}) = \frac{f_{eq1} \cdot b \cdot h^2}{6} \tag{3.8}$$

For critical section in a range from 40 mm to 150 mm, the value that correlates f_{Fts} to f_{eq1} is close to 0.45. Eq. 3.5 is obtained considering a linear relationship between w_{i1} and w_{i2} as shown in Fig. 3.24b. The stress corresponding to w_{i2} is computed by rotational equilibrium

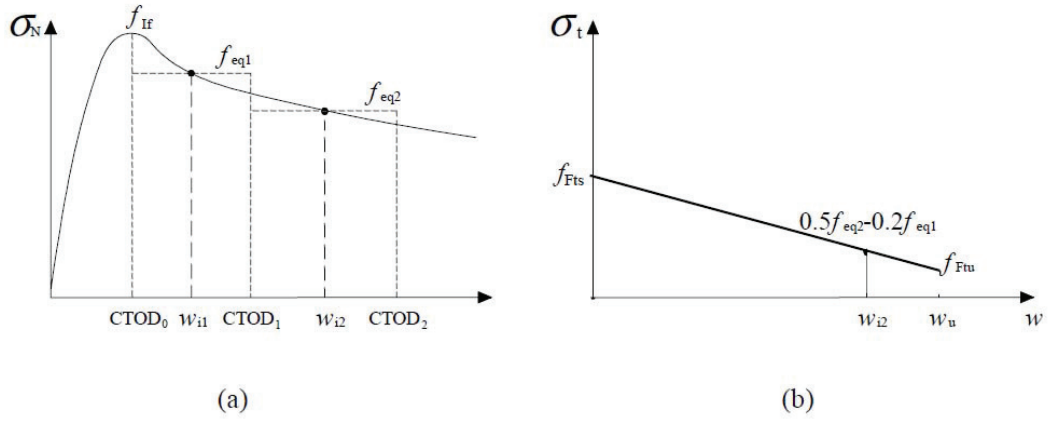

Figure 3.24: Linear softening model

(Eq.3.9), with the assumption that the resultant of compression is concentrated to the extrados, (Fig.3.23b) and that rigid linear softening determines the tensile behavior:

$$M(\epsilon_{F2}) = \frac{f_{eq2} \cdot b \cdot h^2}{6} \tag{3.9}$$

The strain value, ϵ_{F2} is referred to w_{i2}. The value σ_{Ft2} indicates the tensile strength at the bottom side.

$$M(\epsilon_{F2}) = M_{ULS} \tag{3.10}$$

$$\frac{1}{6} \cdot f_{eq2} \cdot b \cdot h^2 = \frac{1}{2} \cdot \sigma_{Ft2} \cdot b \cdot h^2 + \frac{1}{6} \cdot (f_{Fts} - \sigma_{Ft2} \cdot b \cdot h^2) \tag{3.11}$$

$$f_{eq2} = 2 \cdot \sigma_{Ft2} + 0.45 \cdot f_{eq1} \tag{3.12}$$

$$\sigma_{Ft2} \approx 0.5 \cdot f_{eq2} - 0.2 \cdot f_{eq1} \tag{3.13}$$

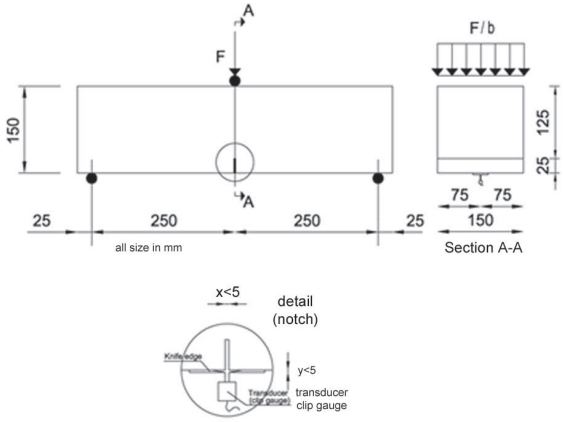

Figure 3.25: Set up for bending test EN 14651

By assuming $M(\epsilon_{F2})$ equal to the bending moment (Fig. 3.23), it is possible to identify σ_{Ft2} at the bottom chord (Eq. 3.13).

Rigid plastic model

The rigid plastic model proposes an unique setpoint, f_{Ftu}, on the basis of ultimate behavior.

$$f_{Ftu} = \frac{f_{eq2}}{3} \tag{3.14}$$

The Eq. 3.14 is obtained by imposing the equilibrium equation considering a linear diagram of tensile stresses, Eq. 3.15.

$$M_u = \frac{f_{eq2} \cdot b \cdot h^2}{6} = \frac{f_{Ftu} \cdot b \cdot h^2}{2} \tag{3.15}$$

Model Code 2010

The Model Code introduces the classification of fiber-reinforced composites and aims to become the reference text for definition of European Standards on concrete. The classification is based on the determination of several residual strength values obtained from the experimental curves Load-crack opening. In this case, the reference test is a three point bending test and strength values are measured at specific values of crack opening and not on the average equivalent values evaluated in an interval, Fig. 3.25. The Standard reference for the execution of the test is EN 14651 which requires the evaluation of four different strength values measured in correspondence of CMOD equal to 0.5, 1.5, 2.5, 3.5 mm, Fig. 3.26. In the Model Code only two characteristic flexural residual strength values,that are significant for serviceability f_{R1k} and and ultimate condition f_{R3k}, corresponding to CMOD equal to 0.5 and 2.5 mm, are taken into account.

$$f_{R,j} = \frac{3 \cdot F_j \cdot L}{2 \cdot b \cdot h_{sp}^2} \tag{3.16}$$

where:

- F_j is the is the load corresponding to $CMOD_j$;
- L is the span length;

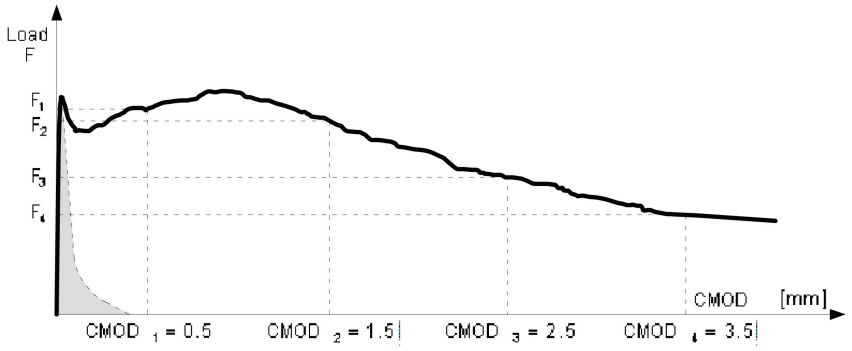

Figure 3.26: Load versus crack opening EN 14651 and comparison with plain concrete

- is the specimen width;
- h_{sp} is the distance between the notch tip and the top of the specimen (125 mm).

From the bending test results, two simplified approaches (stress-crack opening) may be inferred: a plastic rigid behavior, or a linear post-cracking behavior (hardening or softening) as it has already been indicated in CNR DT 204. The rigid-plastic model considers the static equivalence

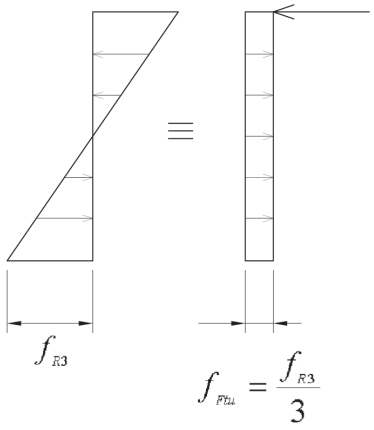

Figure 3.27: Simplified model adopted to compute the ultimate residual tensile strength

(Fig. 3.27) and the whole compressive force is concentrated in the top fiber of the section.

$$M_u = \frac{f_{R3} \cdot b \cdot h_{sp}^2}{6} = \frac{f_{Ftu} \cdot b \cdot h_{sp}^2}{2} \tag{3.17}$$

$$f_{Ftu} = \frac{f_{R3}}{3} \tag{3.18}$$

The linear model identifies two reference values, f_{Fts} and f_{Ftu}.

$$f_{Fts} = 0.45 \cdot f_{R1} \tag{3.19}$$

$$f_{Ftu} = f_{Fts} - \frac{w_u}{CMOD_3} \cdot (f_{FTS} - 0.5 \cdot f_{R3} + 0.2 \cdot f_{R1}) \geq 0 \tag{3.20}$$

The equation for f_{Ftu} and $w_u \neq CMOD_3$ is obtained by considering a linear constitutive law

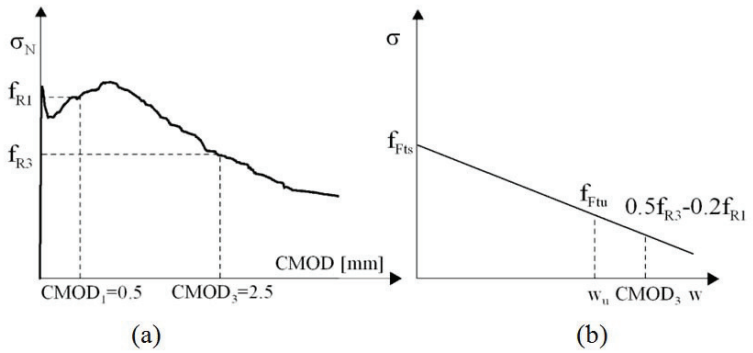

Figure 3.28: Typical results from a bending test on a softening material (a); linear post cracking constitutive law (b).

between points $CMOD_1$ and $CMOD_3$, up to the abscissa w_u (Fig. 3.28b). The stress value

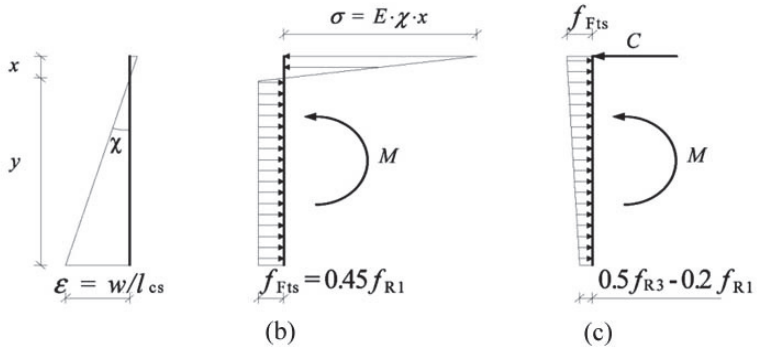

Figure 3.29: Stress diagrams for the determination of the residual tensile strength

corresponding to the crack opening $CMOD_1$ and $CMOD_3$ are determined from equilibrium, Eqs. 3.21 and 3.22, with the assumption that the compressive stress distribution is linear, Fig. 3.29b and that the tensile behavior is elasto-plastic until a crack opening displacement, Fig. 3.29c.

$$M(CMOD_1) = \frac{f_{R1} \cdot b \cdot h_{sp}^2}{6} \tag{3.21}$$

$$M(CMOD_3) = \frac{f_{R3} \cdot b \cdot h_{sp}^2}{6} \tag{3.22}$$

The Model Code proposes also constitutive laws more sophisticated which consider the uncracked behavior of the matrix before the peak load. A bi-linear stress-crack opening law is considered

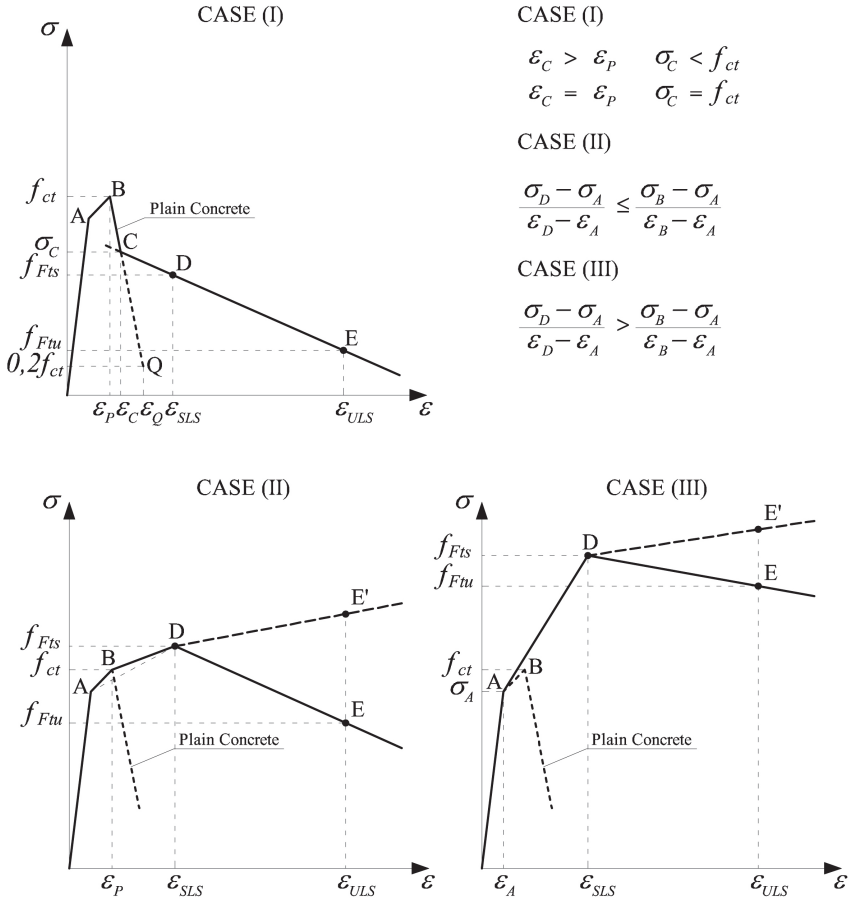

Figure 3.30: Bi-linear model: stress-strain relations

where the first branch is referred to cracking matrix and it is the same of plain concrete. The second branch is the contribution of fiber pull out. The post-peak crack propagation branch corresponds to the behavior of plain concrete until the intersection with the residual post-cracking behavior (Fig. 3.30). The point B is defined according to strength class as: for strength higher than 50 MPa the relationship is:

$$f_{ct} = 2.12 \cdot ln(1 + 0.1 \cdot (f_{ck} + 8)) \tag{3.23}$$

and the strain is equal to $1.5 \cdot 10^{-4}$. The point A is defined as $0.9 \cdot f_{ct}$. For softening material (CASE I) the post-peak propagation ($\overline{BC}$) is defined as:

$$\frac{\sigma - f_{ct}}{0.2 \cdot f_{ct} - f_{ct}} = \frac{\epsilon - \epsilon_P}{\epsilon_Q - \epsilon_P} \tag{3.24}$$

for $\epsilon_P \leq \epsilon \leq \epsilon_C$ with

$$\epsilon_Q = \frac{G_f}{f_{ct} \cdot l_{cs}} + \left(\epsilon_P - \frac{0.8 f_{ct}}{E_c}\right) \tag{3.25}$$

where G_f indicates the fracture energy of plain concrete. For softening behavior the residual strength (fourth branch) is defined by two points (ϵ_{SLS}, f_{Fts}) and (ϵ_{ULS}, f_{Ftu}) where the serviceability strain is equal to:

$$\epsilon_{SLS} = CMOD_1 / l_{cs} \tag{3.26}$$

and the ultimate strain

$$\epsilon_{ULS} = w_u / l_{cs} = min(\epsilon_{Fu}, 2.5 l_{cs}) \tag{3.27}$$

with $\epsilon_{Fu} = 1 - 2\%$. For hardening materials where f_{Fts} is greater than f_{ct} two possible cases are defined.
CASE II: the cracking propagation became stable until ϵ_{SLS} and the branch ($\overline{BD}$) is described as:

$$\frac{\sigma - f_{ct}}{f_{Fts} - f_{ct}} = \frac{\epsilon - \epsilon_P}{\epsilon_{SLS} - \epsilon_P} \tag{3.28}$$

for $\epsilon_P \leq \epsilon \leq \epsilon_{SLS}$.
CASE III: the cracking is stable until the ϵ_{SLS} and the branch ($\overline{A'D}$) is described as:

$$\frac{\sigma - \sigma_{A'}}{f_{Fts} - \sigma_{A'}} = \frac{\epsilon - \epsilon_{A'}}{\epsilon_{SLS} - \epsilon_{A'}} \tag{3.29}$$

where $\sigma_{A'} = 0.9 \cdot f_{Fts}$. For both cases the branch ($\overline{DE}$) or ($\overline{DE'}$) can be softening or hardening. In general, fiber distribution is assumed homogeneous and the orientation factor, K, is equal to 1. For unfavorable effects the orientation factor $K > 1.0$ otherwise for favorable effects is minor than 1. The serviceability and ultimate residual strengths are corrected by dividing for the orientation factor ki determined through experimental tests. The fibers orientation significantly determines the mechanical properties of the composites. Governing the orientation and dispersion of fibers could optimize the mechanical performances. Ferrara et al. [18] studied fresh state properties in order to obtain a self compacting matrix avoiding the vibration procedure. The mixture has to be an adequate viscosity to orient the fiber along the direction of the casting flow and to avoid segregation. To improve the mechanical performances the fiber have to be aligned in the direction of the principal stresses, that is possible by designing carefully the casting process.

3.3.5 Compressive behavior

During the uniaxial compression test, three are several mechanisms involved [48]. The first is the randomly generation of microcracks in parallel direction to the loading. The randomness of the cracking is due to the presence of weak point determined by the heterogeneity of the material. When the material is subjected to longitudinal compression, a tensile stress occurs orthogonally to compressive stresses. In the second phase, microcracks combine to create macrocracks always parallel to the compression. The macrocracks subdivide the concrete specimen in columns of varying shape and size. The diagonal cracks, that are formed in the last stage, joint together and create a sliding surface. In the curves load versus vertical displacement, the first two stages characterize the increase of load. After the appearance of diagonal cracks the load decrease with a softening branch governed by the propagation of the oblique cracks. The fiber could delay the formation of vertical microcracks and so delay the appearance of diagonal cracks improving the compressive resistance. However the fiber would have activated at microscale (at scale of cement paste), too small in comparison with the aggregate size. Moreover the presence of fibers can create an additional heterogeneity presence that can favor the appearance of vertical microcraks and also fibers are unable to oppose at the opening of diagonal cracks. A high amount of short fiber contrasts in part the diagonal microcraks and a lower content of long fibers play a role for diagonal and vertical macrocracks. Therefore the contribution of steel fiber in compression is concerned with an increase in ductility behavior at the structure level. To increase the compressive strength is necessary to optimize the mix design by using a low water cement ratio and a high percentage of silica fume. Figure 3.31 shows the behavior in uniaxial compression of plain concrete and

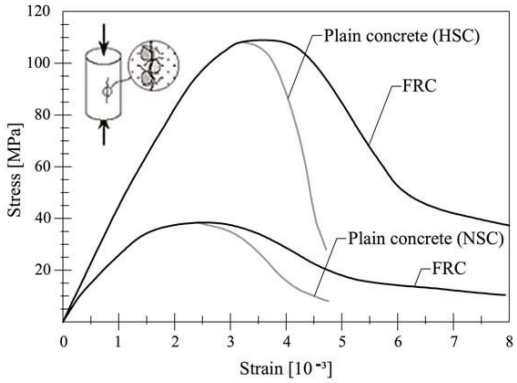

Figure 3.31: Main differences between plain and fiber reinforced concrete with normal and high strength

fiber reinforced concrete varying for the compressive class resistance. The fiber presence is quite irrelevant for the strength, but it can play a role for the ductility response.

3.4 Textile Reinforced Mortar

A quite new development of advanced cementitious materials is Textile Reinforced Concrete (TRC) where the combination of fine grained concrete and multiaxial fabric are employed [49]. The matrices used have to meet specific performances in terms of mechanical properties and workability, so in most cases the small maximum aggregate size is less than 2 mm. For this reason the matrix can be considered as mortar (Textile Reinforced Mortar, TRM). The use of textiles,

made by alkali resistant (AR) glass, carbon, Kevlar or aramid leads to a high effectiveness, because they are placed in the main stress direction unlike the randomly distributed short fiber such as glass fiber reinforced concrete (GRC). There are various collaborative research centers (Aachen University, Technische University in Dresden, Ben Gurion University at Israel and Ira A. Fulton University in Arizona) that investigate such as the basic mechanism regarding the load carrying capacity, the durability aspects, bonding characteristics and they suggest the guidelines for the dimensioning of thin TRC elements. TRC structural members are used under various environmental and loading conditions such as facades, tanks, containments, strengthening of existing structures, structural building elements and as integrated formworks.

3.4.1 Textile reinforcements

The arrangement, the volume fraction, the properties and the nature of the fiber materials have a great influences to the performances of the composite materials. Thus the nature and the layout of the textile have to meet various requirements. The characteristics of the reinforcement are high toughness and breaking elongation and equivalent Young modulus higher than that of the matrix. The equivalent modulus of textile is different from the elastic modulus of the fibers which depends on the production process of the textile. For example, a textile with leno weave has in the leno direction a smaller equivalent elastic modulus due to the fact that rovings are twisted. Two rules have to be considered to design cement composites with enhanced performances. It is necessary to increase both the ratios of tensile strength of fabric to the compressive strength of mortar and the ratio of the elastic modulus textile respect to the matrix. The rules take into account that in a cracked zone under tension the reinforcement contributes both in stiffness and in strength. The behavior of the cracked matrix is negligible.
Fiber can be distinguished in Low-End and High-End. The difference consists in the value of elastic modulus compared to the Young modulus of the concrete (low and high). Fiber with low elastic modulus are polypropylene, nylon and polyester. High performance fibers (glass or carbon) were available as early as 1960' in the aerospace industry and they became suitable for the concrete starting from the late 1980; in particular alkali resistant glass fiber were developed to minimize alkali reactions in the matrix. The requirements referred to the ratio of the elastic modulus can justify the not widely used in cementitious composites of Low-End fiber although their tensile strength was comparable with the steel-wire meshes. A comparison between mechanical properties of fibers used in thin cementitious composites and steel wires is reported in Tab. 3.3. Further characteristics of fibers are a good adhesion between the fabric and matrix,

Fiber Material	Density g/cm^3	Tensile strength MPa	Elastic Modulus GPa	Ultimate elongation %
AR Glass	2.8	1400	70-80	2
Glass E	2.5	2000-3500	70-80	3.5-4.5
Carbon, high modulus	1.85-1.9	2400-3400	390-760	0.5-0.8
Carbon, high strength	1.75	4100-5100	240-280	1.6-1.73
Aramid	1.44-1.47	3600-3800	62-180	1.9-5.5
Polymeric	1.1-1.25	40-82	2.6-3.6	1.4-5.2
Steel	7.8	up to 600	206	20-30

Table 3.3: Mechanical properties of fiber

low cost and small relaxation under permanent load.

Yarns are bundle filaments and the fineness is expressed in tex (g/km) depending on the number of filaments, the average diameter and the fiber density. The property of filaments depends on the applied size that is an organic compounds to bond the fiber together and stiffen them. Yarn can be made with a continuous strand of filaments (twisted or not) in a form suitable to be knitted or other working production process and they are stored in bobbins. Instead the denomination roving indicates an intermediate state between sliver and yarn. The fibers are composed of continuous filaments very thin and therefore difficult to manipulate individually. For this reason they are commercially available in various forms and the rule CNR DT 200/2004 [50] describes various forms in which fiber can be found on the market, Fig. 3.32. The tow is the product of the spinning machine and is constituted by a large number of filaments untwisted.

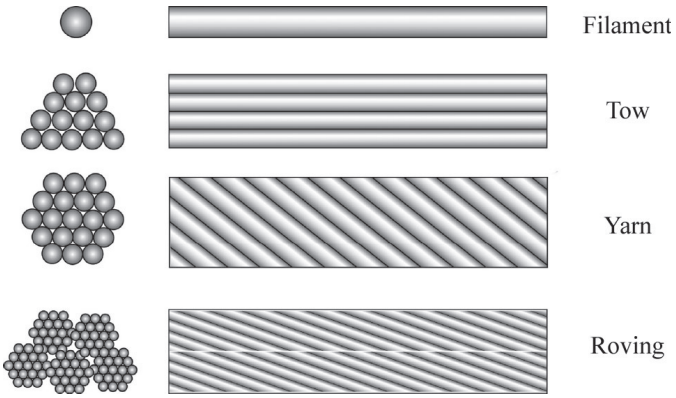

Figure 3.32: Types of fibers used in commerce

AR glass fiber

Alkali-resistant glass was developed in the 1970s and it based on silica-soda calcia with the addition of 16% of zircon. At temperatures up to 1350°C the silica sand, clay and limestone are melted in special furnaces and pulled off in hole with diameter from 9 to 27 μm with a certain speed. The melted glass falled in the holes creating a predefined number of thin filaments which are collected and directed to a spindle rotating at very high speed. The spindle pulls the fiber glass hence creating filament with diameter of a few microns. Yarn is obtained by the combination of a lot of filaments. After that a size made by organic polymers is applied on the filaments to favor the adhesion and the stress transfer between filament and the matrix. Table 3.4 shows different fibers commercially available.

Saint-Gobain vetrotex	Tex	Diameter [μm]	Number of filament
1	320	14	800
2	640	14	1600
3	1200	19	1600
4	2400	27	1600

Table 3.4: Alkali resistant glass fiber

Carbon fiber

Fibers are distinguished by their high modulus of elasticity and for their high strength. The modern technology of production of carbon fibers is based on the pyrolysis, that is, the thermal decomposition in the absence of oxygen of organic substances (called precursors) and the most used are the fibers of polyacrylonitrile (PAN) and rayon. PAN fibers are subjected to a thermal treatment at 200-240° C for 24 h in air, so that their molecular structure undergoes preferential orientation in the direction of the applied load. After that fiber with high tenacity are created with a carbonization at 1500° C in an inert atmosphere and fiber of high modulus of elasticity are performed through graphitisation incandescence process at 3000°C during which the crystalline structure of the fibers can develop similarly to a pure graphite.
Further characteristics are low density compared to AR glass fiber, good electric conductivity, high resistance to acid alkaline and organic solvents. They are used commonly in duroplastic and thermoplastic materials and only in some case in concrete. The disadvantages are the high cost and the difficult process avoiding deterioration of other fiber materials. When filaments break they become electrically conductive and hence all device and machine have to be shielded. Some commercially available carbon fiber are reported in Tab. 3.5.

Product type (Tenax fiber GmbH)	Tex	Diameter [μm]	Number of filaments
1	400	7	6000
2	800	7	12000
3	1600	7	24000

Table 3.5: Commercially available Carbon fiber

Aramid fiber

The nature of aramid fibers are organic and consisting of aromatic polyamides in the form highly oriented. The elastic modulus and tensile strength are intermediate between glass and carbon fibers. Aramid fibers have a lower density and brittleness compared to glass and carbon fiber. The disadvantages are low resistance in alkaline solutions and the negative heat expansion. Inside concrete material stresses can develop in adhesion area between fiber and concrete. In Tab. 3.6 some kind of commercially fiber are presented.

teijin Twaron BV	Tex	Diameter μm	Number of filament
1	167	12	1000
2	322	12	2000

Table 3.6: Aramid fiber commercially available

Fabrication technique

A fabric can be identified by the following properties:

- width of mesh;
- the way warp threads are arranged;
- the crosswise of the weft in the mesh;

- the nature of fiber;
- the weaving pattern of warp and weft.

There are variety of textile fabrication process and the most important feature is creating an open structure suitable for the full penetration of the matrix. To guarantee a good handling the threads must be interlacing and different manufacturing methods are available. The most

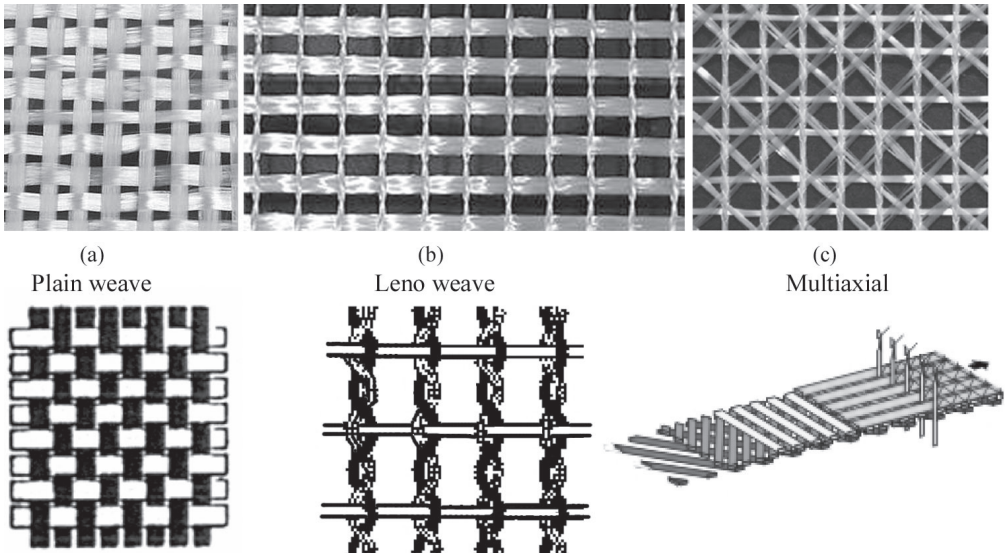

Figure 3.33: Different textiles pattern

widely used is woven fabric. It is characterized by two yarn sets as warp(0°) and filling(90°) and interlaced to each other to form the surface. It can be plane, twill and satin weaves. Figure 3.33 shows the most common example of textile fabrics: plane weave, leno weave and multiaxial. The kind and crossing weft and warp is called weaven and it influences the fabric properties. The plane (Fig. 3.33a) wave has a very high displacement stability, because every warp yarn twists in turn above and under a weft yarn. Nevertheless, the concrete has to penetrate inside the mesh so an open structure is necessary. Through impregnation with a plastic matrix, the fabric is so stabilised. Leno Weave (Fig. 3.33b), is the typical example used to weave meshes where warp and weft threads are twisted and joined by an additional binding thread. In recent years, several weaving machine manufacturers have developed increasing the efficiency of the productivity. Two needle reeds shift at the same time. One moves in the vertical direction and the other in the horizontal for the interlace. So different fabrics as well as crimps can be made increasing the variation possibilities. The best example of freedom in the mesh geometry is the multiaxial fabric that leads to a variety of interlacing indeed threads can be combined according to any angle, design of layer and weight for unit area, Fig. 3.33c. The variety of fabrication process allows to design tridimensional fabrics such as circular scrims with tubular shape, Fig. 3.34a and three-dimensional spacer warp knit, Fig. 3.34b. Circular scrims are adopted for reinforcing tubes and cable pits. The spacer fabrics can be realized with two fabrics with different mesh pattern and after linked to each other. For ensuring good handling and employing the whole potential in the material composites the fabric have to be fixed by impregnating with a coating. Besides ensuring cohesion and dimensional stability to the fabric, the coating has also the important function to guarantee for glass fabric the resistance against alcali. It is well known that glass does not rust,

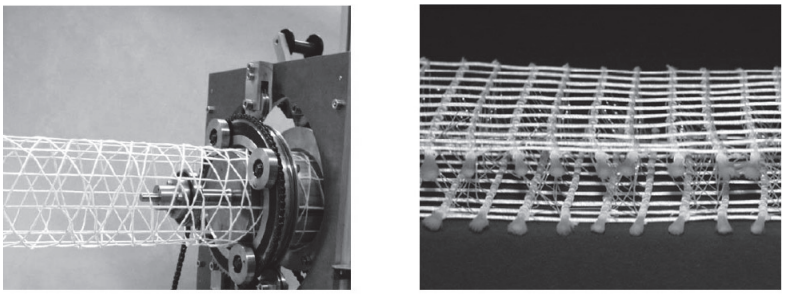

(a) (b)

Figure 3.34: Circular scrims fabric and biaxial fabric

not affected by biological agents, but it can be damaged if it is exposed to alcali solutions. The coating, made by water based polymer dispersion, is applied by a coater roll while a second one ensures the contact of the textile to the previous roll, Fig. 3.35. To obtain a uniform coating of fabric, it is important that the roll gives more coating material than the fabric can be absorb.

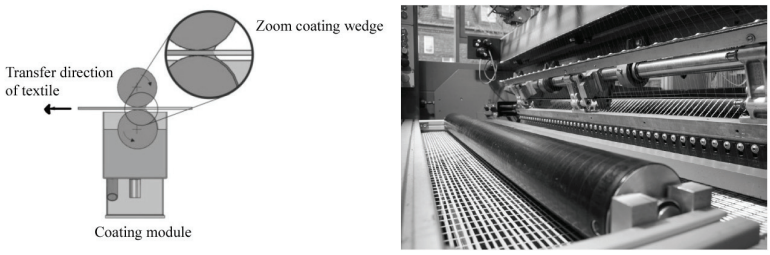

Figure 3.35: Coating procedure, [3]

Tensile strength

The properties of fabric are influenced by the sizing used and by the characteristics of filaments. The diameter of single filaments, the yarn fineness and material density have to be measured according to DIN EN ISO 2060-5079. The stress strain behavior of yarns is determined by the International Standard ISO 3341. To define exactly free clamping length, two resin blocks were applied at the ends of the yarn, Fig. 3.36. The tensile properties of fabric is obtained by direct

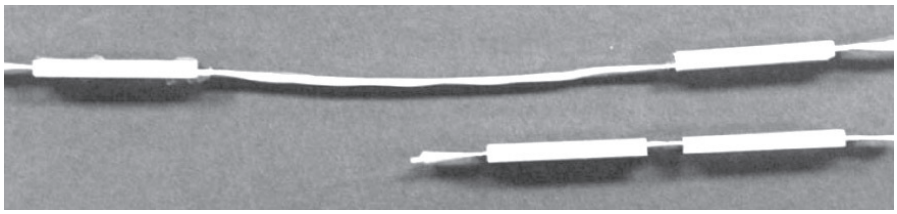

Figure 3.36: Epoxy resin in the end of the yarn

tensile test where in the clamp zone some layer of scotch are applied to avoid slipping (Fig. 3.38a). The difference tensile strength among filament, yarn and fabric is explained by considering unequal load acting in the filament of the yarn due to slipping phenomena but also the presence of

defects. This aspect was confirmed by the results obtained from tensile test on AR glass fila-

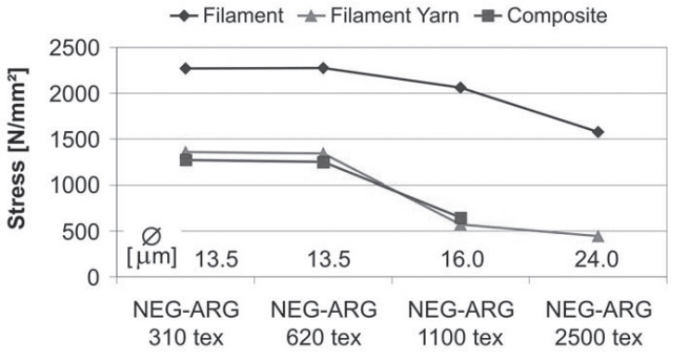

Figure 3.37: Dependence of tensile strength on the filament diameter or the yarn fineness in AR glass filament yarns [4]

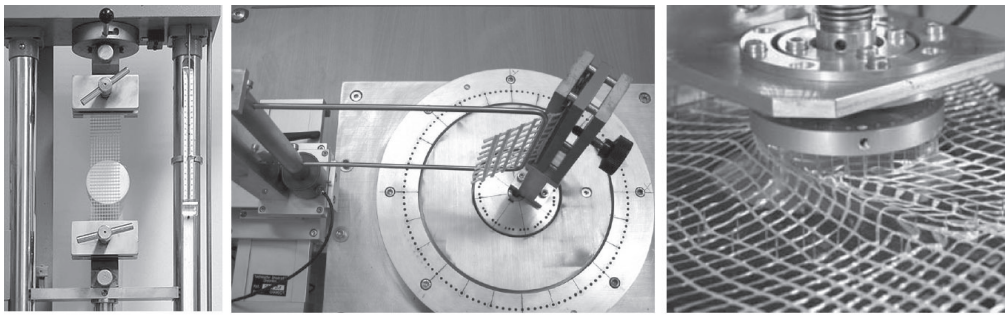

Figure 3.38: (a) Tensile, (b) Bending, (c) Stability Tests

ment and yarn [4] (fig. 3.37). To determine the structural stability of open structures, bending test with vertically specimen is performed, Fig. 3.38b. The specimen is fixed in perpendicular direction and it is is twirled around a bar. The turning moment is measured through the pressure load on the bar. For dimensional stability a special testing devices is developed by the Research Centre of Aachen to control the fabric properties, (Fig. 3.38c). A circular clamp is placed and rotated in the centre of the mesh. The strength is computed by the moment for a defined angle, [4].

Manufacturers can make available the characteristics of the yarn and the related certificates of conformity. To determine or verify the title of a thread can operate according to ISO 1889:1997.

$$T_x = \frac{P \cdot 1000}{L} \tag{3.30}$$

- where T_x is the the title of the thread expressed in Tex [g/km];
- P is the weight of sample in grams;
- L is the length of the sample expressed in meters.

The cross section of a wire (yarn, tow or roving), A, expressed in mm^2, is determinable starting from the title and the density of the yarn with the following relation:

$$A = \frac{T_x}{\rho \cdot 1000} \tag{3.31}$$

where ρ is the density expressed in g/cm^3. The data sheet of AR glass fabric has to contain the following properties, Tab. 3.7.

Properties	Direction	Units	Standard Rule
title	warp and weft	Tex	ISO 1889:1997(E)
density		g/cm^3	
number threads/cm	warp and weft	number/cm	ISO 4602:1997(E)
weight	total, warp, weft	g/m^2	ISO 3374:2000(E)
elastic modulus in tension	warp, weft	MPa	
tensile strength	warp	MPa	ISO 4606:1995(E)
tensile strength	weft	MPa	ISO 13934-1:1999
ultimate elongation	warp	%	ISO 4606:1995
ultimate elongation	weft	%	ISO 13934-1:1999

Table 3.7: Data sheet of fabric

3.4.2 Mix design

The design of the matrix is a complex assignment, because many requirements have to be fulfilled as well as mechanical parameters, production process, bonding behavior and durability. Usually the maximum aggregate size is less than 2 mm, so the matrix can be classified as mortar even if high performances, typically of fine grained concrete must be respected. The full penetration of the matrix inside the mesh is necessary to guarantee a good bond and loading behavior. Regarding durability problems, resistance to frost and impacts is required. Also mechanical properties are demanded and they will depend on the applications and on the overall composite materials. The matrix design has to be the best compromise considering all previous requirements and economic aspects for industrial production. A variety of mix compositions, developed in the collaborative research centre of Aachen University, are reported in Table 3.8. The cement type for all mix design is CEM 52.5. The high flowable consistency can be reached by using a small aggregate size around 0.6 mm, high binder amount and adding plasticizers. The strong decrease in alkalinity is due to the pozzolanic reaction of the silica fume with and the mass percentage is around of 25% compared to total binder content. Neverless it is hard to obtain a flowable consistency of the mixture with large quantities of silica fume so the maximum content of silica fume is restricted, lower than 10% by the mass of total binder content. Starting from the mixture PZ-0899-01, the second one FA-1200-01 differs for high content of fly ash to have a better durability. Fly ash and silica fume in matrix have beneficial effects because the pozzolanic reactions make the matrix dense, decrease the Calcium Hydroxide at the interface zone, and enhance the durability of composites. Moreover the fly ash can improve the viscosity properties of the matrix favoring the penetration of cement paste in the opening cross structure of fabric [51]. The third mixture has a high cement content and a low w/b so the structure is very dense and the strength is higher. This matrix was studied for mechanical reasons both in tension and compression [52]. Fresh and hardened properties were investigated [53], according to standard tests. Fresh concrete properties were determined through flow test, flow time and

Materials		Mineral based matrices		
		PZ-0899-01	FA-1200-01	RP-03-2E
Cement content	kg/m^3	490	210	980
Fly ash	kg/m^3	175	455	210
Silica fume	kg/m^3	35	35	210
Binder	kg/m^3	700	700	1400
Plasticiser	% by mass of binder	1.5	0.9	2.5
Siliceous fines (0-0.125mm)	kg/m^3	500	470	118
Siliceous sand(0.2-0.6)	kg/m^3	715	670	168
w/c		0.57	1.33	0.36
w/b		0.40	0.40	0.25

Table 3.8: Example of mix design

rheology measurements. The first test consisted in fulfilling of matrix the slump cone and measuring the flow on a horizontally plane, (Fig. 3.39a). A flow time test is the time in which the

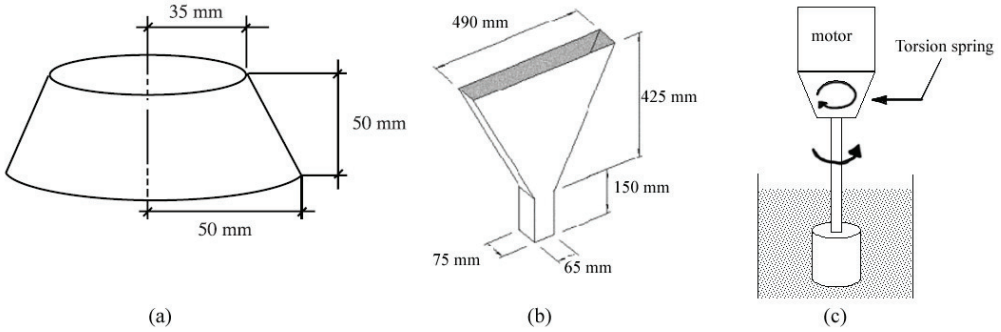

Figure 3.39: Slump test (a), flow time (b), rheology test (c)

concrete needs to flow through the V shaped funnel (Fig. 3.39b), after 10 and 30 minutes later the cast. Some results are reported in Table 3.9. Mechanical behavior can be influenced by the different rheology of the matrix modified by the presence of fly ash. Tests are carried out the mixes using a Brookefield Rheometer (Fig. 3.39c). The shear rate is varied during the tests from a higher rpm value at the start (20) to a lower value (10). The whole test finishes after 16 minutes. The rheological properties are computed starting from shear stress vs. strain diagram. Mobasher [51] studied the influence of fly ash on the mechanical and rheology properties. The results are represented in Fig. 3.40. The viscosity increase with the content of fly ash due to the ability of the fresh concrete to penetrate in the mesh. Contrariwise the yield strength decreases with increase a content of fly ash.

To characterize the hardened concrete properties, the traditional mechanical tests are performed (compressive, tensile strength, Young's modulus, shrinkage tests). Some results, obtained at Collaborative Research of Aachen (SFB 532) according to German Standard rules (DIN 18555-3 09.82, DIN 1048-5 06.91, DIN 52450 08.85), are reported in Table 3.10. All specimens are stored at 20°C. The compressive strength range from 32 to 98 MPa at 28 days and rather high shrinkage strains between 0.56 to 1.47 are observed. The right mixture should be chosen according to the planned applications.

Further experiments have been done to derive the constitutive laws in tension and in compres-

Fresh concrete properties		Matrices		
		PZ-0899-01	FA-1200-01	RP-03-2E
Air content	%	0.4	1.3	1.0
Density	kg/m^3	2239	2112	2140
Flow f_{10min}	mm	340	266	305
Flow f_{30min}	mm	340	263	320
Flow time f_{10min}	sec	6.5	4.4	7.0
Flow time f_{30min}	sec	7.2	4.8	9.0

Table 3.9: Example of fresh concrete properties, [23]

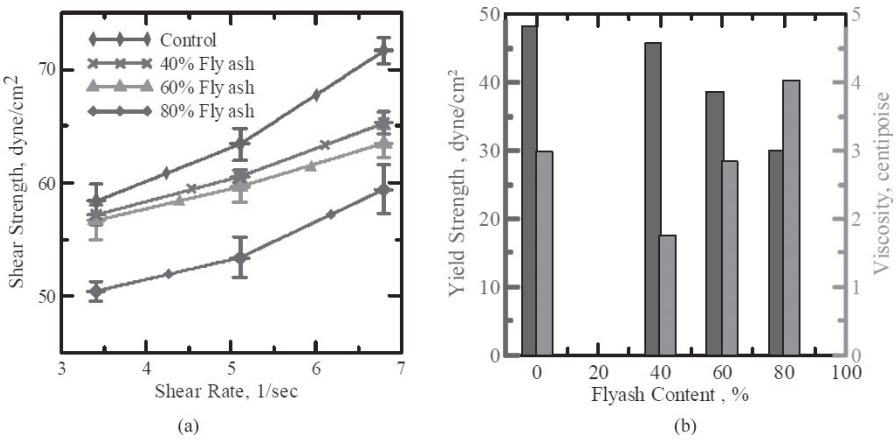

Figure 3.40: Shear Strength vs. shear rate and Shear Strength and Viscosity as a function of fly ash

Matrices	Compressive strength [MPa]		Flexural strength [MPa]		Young's modulus [MPa]	Shrinkage [mm/m]
	28 days	90 days	28 days	90 days	28 days	28 days
PZ-0899-01	74	89	7.6	8.1	33000	0.81
FA-1200-01	32	46	5.1	6.7	24800	0.56
RP-03-2E	98	108	8.1	9.4	26500	1.47

Table 3.10: Hardened properties, [23]

Specimen dimension	slenderness	PZ-0899-01	FA-1200-01	RP-03-2E
b x d x l	l/d	σ_c	σ_c	σ_c
mm^3	-	MPa	MPa	MPa
10 x 10 10	1	93.99	42.74	146.91
20 x 20 x 20	1	94.56	43.44	150.27
40 x 40 x 40	1	101.18	44.88	152.96
10 x 10 x 20	2	98.90	47.54	156.81
20 x 20 x 40	2	95.09	39.75	153.15
40 x 40 x 80	2	89.58	37.52	154.24
10 x 10 x 40	4	77.34	43.12	135.24
20 x 20 x 80	4	89.13	38.15	127.58
40 x 40 x 160	4	87.37	36.51	143.10

Table 3.11: Compressive strength results, [24] and [25]

sion.
In the approaches based on plasticity, the strength is independent from the dimension of the specimens, but experimental results show that quasi-brittle materials have a dependence of the nominal stress at ultimate load on the specimen size, this phenomena is known as size effect. Compression tests were performed by Brameshuber [25], to investigate size effects for varying specimen side length (d=10, 20, 40 mm) and different slenderness (λ=1, 2, 4). In particular, for the TRC applications it is important to investigate thinner structures (d$\approx$ 10 mm). Considering the results in Table 3.11, no significant size effect is observed. According to [24] and [25] no factors about scale effects are necessary.

3.4.3 Production process

The production processes are distinguished in manual production of small specimen or the mass series. The hand lay-up technique is the oldest and simplest method. A mould with different geometry is used: it can be as simple as a flat sheet or have curves and edges. The surface aspect is important because it determines the aspect of visible finished side of the specimen. The matrix is spread in the mould and a layer of textile is placed. It is also possible introducing fiber in the matrix. By using a roller, the air bubbles are worked out and an other matrix layer is cast. It is also possible matching in the matrix additives for coloring the concrete and putting widespread fiber to improve resistance, Fig. 3.41a. The advantages of this technique is the simple fabrication that allows to create different shapes with low capital investment. Even introducing the spray up variant that is faster, the lay up technique is suitable only for small series.
For large products the pultrusion technique is suitable (Fig. 3.41b). The fabrics are immersed in a slurry infiltration chamber and, after, it is pulled out in a set of roller where the matrix is compacted and the excessive paste is removed [54]. After making the specimen, pressure is applied on top of the composites to enhance bonding and penetration of the mortar inside the cross opening mesh. Usually the pressure is removed one hour after the casting procedure [51]. The pultrusion methods leads to create specimen with different widths, lengths and thickness.

3.4.4 Bond and Composite properties

The load bearing capacity of textile reinforced concrete is influenced by the material, amount and orientation of textile, the fine grained concrete and in particular by the bond behavior. The

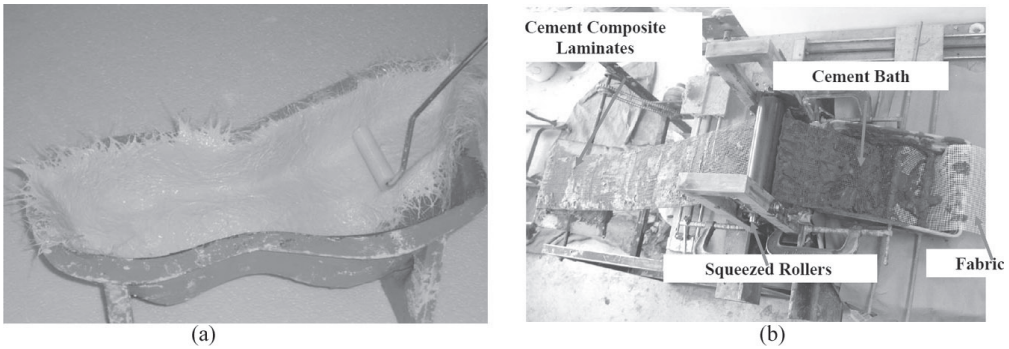

Figure 3.41: (a) Hand lay up and (b) pultrusion techniques

bonding behavior is completely different from steel bar because fabric has not homogeneous cross section. The rovings are made by filament that can be distinguished in two groups, outer and inner. The first are directly in contact with the matrix. Their contribution to bond performance is greater than inner (or sleeve) filaments, that are placed in the core of roving and they are stressed only indirectly. Experimental test and numerical models are developed to understand the bond characteristics of textile in a fine concrete. Actually the research is involved at three different levels (micro-meso-macroscale) and a systematic experimental research has done to obtain further information to optimize models for each level. Based on these models, design rules can be formulated in the future.

Bond mechanism

Bonding in the interface surfaces is very important because it determines the strength and ductility behavior of the material. If the bond is weak, the material shows a ductile behavior otherwise a brittle materials can be obtained. Textile reinforcements are composed of filaments. Only the outer one are embedded in cement paste and they have adhesion with surrounding concrete. The inner filaments can slip within the roving (Fig. 3.42a,b). The higher slippage leads to different stresses in the filaments and so the failure of filaments happens in different time, [55].
The use of epoxy resin can influence the internal bond because the inner filaments are not allowed to slip anymore. The anchorage contribution employs the whole filaments and they fail at the same time (Fig. 3.42c). Different approaches have been studied to idealize yarn-matrix system.

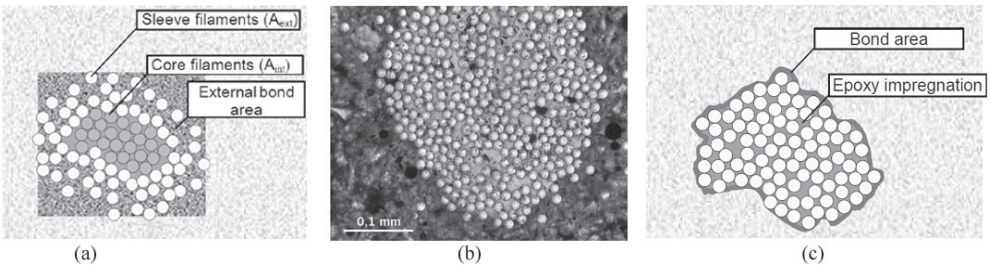

Figure 3.42: Detail of filaments in the roving : (a) (b) not fully infiltrated with cement, (c) epoxy impregnation

The telescopic and staggered failure are necessary to describe the roving behavior. In [5] the Yarn-Matrix-Bond (YMB) model, based on experimental tests, was presented (Fig. 3.43). The

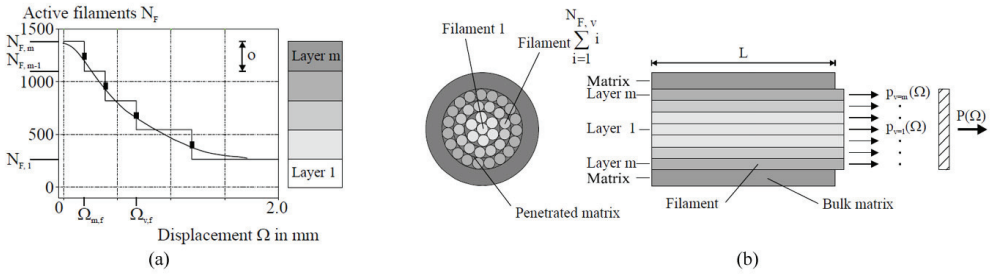

Figure 3.43: (a) Active filaments versus displacement, (b) idealisation yarn in concrete

idea was computing the pull out response of every filaments for every load step and the overall response of the yarn could be calculated by summation. The model adopted a layered system made of m layer for each of these the number of filaments is kept constant. With this model, the telescopic failure, that is noticed in the FILT (Failure Investigation using Light Trasmission properties) test, can be represented. The primary break down of the out filaments is followed by a failure of adjacent filaments until the core unit is pulled out. The active filaments versus displacement may be considered by a step function with a constant step (m the number of layer) (Fig. 3.43a). The YMB model considered as the main parameter, the decreasing interlayer contact area (embedded length L_v multiply for the contact perimeter $U_{c,v}$ for each layer). All embedded length of a layer L_{vi} can be considered as the summation of each contribution, L_v while ψ_v is the free length (Fig. 3.44). The load, transfered between filament and matrix in the not embedded length, was negligible. The pull out behavior is described as the contributions of two components: the slip of the filaments and the elongation resulting from the deformation of the free length. Banholzer [5] performed two kind of pull out tests in order to investigate the

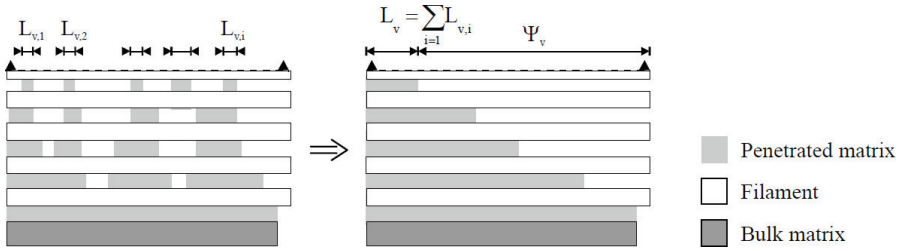

Figure 3.44: Micro structural idealization, [5]

bond slip behavior between a roving and the concrete matrix, one sided and two sided embedded tests. For the first typology a glass strand is placed in epoxy resin to prevent failure caused by clamping zone and for the other side is cast in a fine grain concrete matrix (50 x 50 x 30 mm^3 Fig. 3.45a). The pull out test is performed by using a testing machine with 0.1 mm/min until 1.7 mm. During the test, an artificial light is used to distinguish the strand that bright appearance (Fig. 3.45b). After a tensile failure the filament is unable to transfer the light and the bright appearance disappeared in the next image. This test is called FILT. The second kind of test was two sided embedment test that combined the advantages of the pull out with the possibility to measure the crack formation in the reinforced element. The specimen was a plate reinforced with fabric and it is cut from the edges so only one roving worked. The upper and bottom side is fixed to the tensile testing machine. By using a LVDT the crack opening of the specimen was

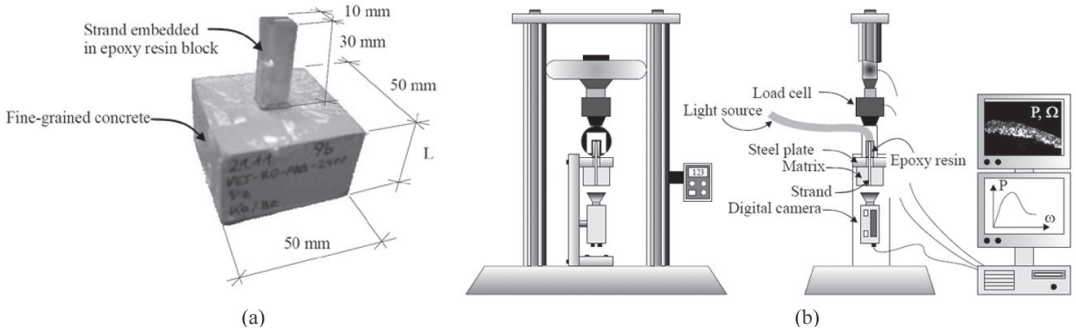

Figure 3.45: (a) Specimen for one sided test, (b) test set up

measured (Fig. 3.46).

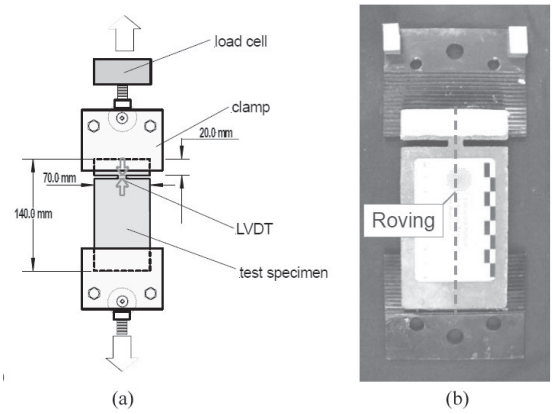

Figure 3.46: Two sided pull out test

Some results obtained by *Krüger*, [6], showed the difference bond slip behavior for different surfaces treatments of carbon and AR glass reinforcements (Fig. 3.47). The first part was linear elastic behavior until the peak load and after the load dropped to a low value and friction behavior dominated. When the peak was reached, a slip of the specimen occurred until the extraction of the roving from the concrete. The specimen impregnated with epoxy resin and sand coated showed the best bond resistance. In a lot of studies it was demonstrated that the geometry of fabric could have a significant influence on the bond behavior. To understand the influences of fabric geometry about bond performance, different contributions were analyzed by pullout tests, Fig. 3.48 ([56], [57], [58], [59], [60] and [61]). In particular pullout of a single yarn embedded in matrix, yarn from a fabric that was embedded in concrete matrix and pull out of a yarn from a free fabric without matrix, were considered. Furthermore different types of fabrics were examined, [62], woven and weft insertion knit fabric (Fig. 3.49) in order to understand the influences of yarn density, crimped structure and number of joints. The pull out test were performed by Instron machine with a cross rate of 15 mm/min and load versus slip curve were recorded. The effect of crimped geometry of the individual yarn in the woven fabric (Fig. 3.49a) was studied considering different crimp densities, amplitude wave and wave length (Fig. 3.50). Different trends were obtained comparing single yarn and yarn in fabric. In the first

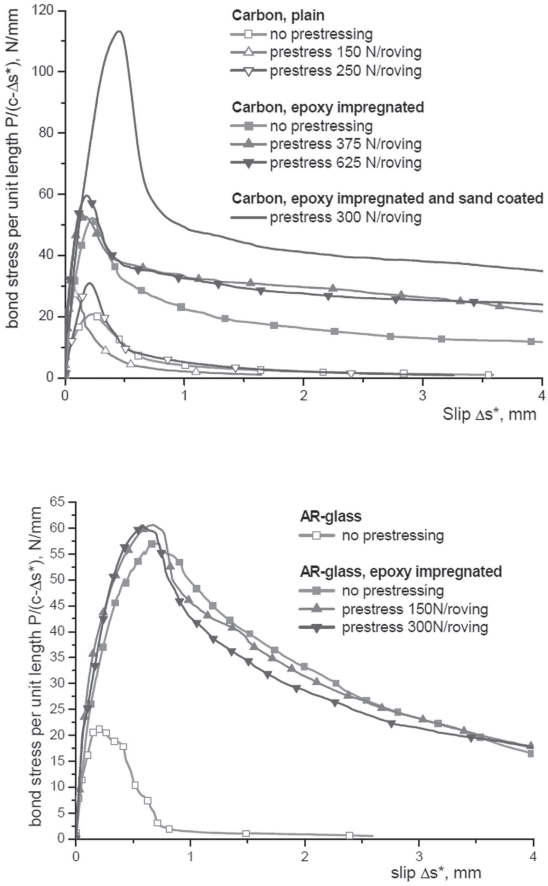

Figure 3.47: Bond slip behavior obtained by two sided pullout test, [6]

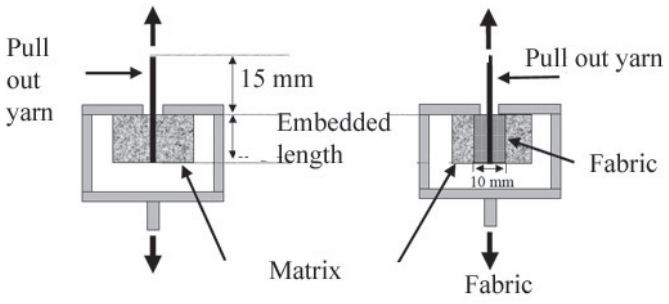

Figure 3.48: Pullout testing yarn

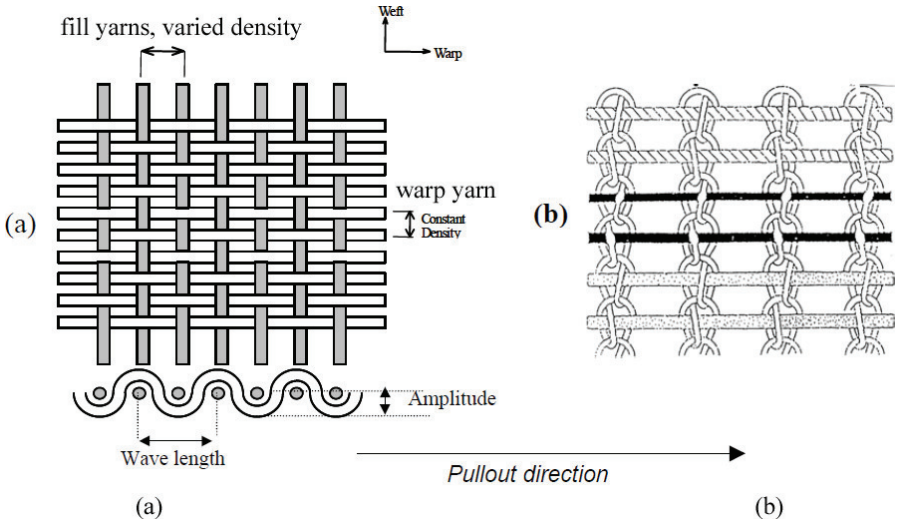

Figure 3.49: (a) Woven fabric, (b) weft insertion knit fabric

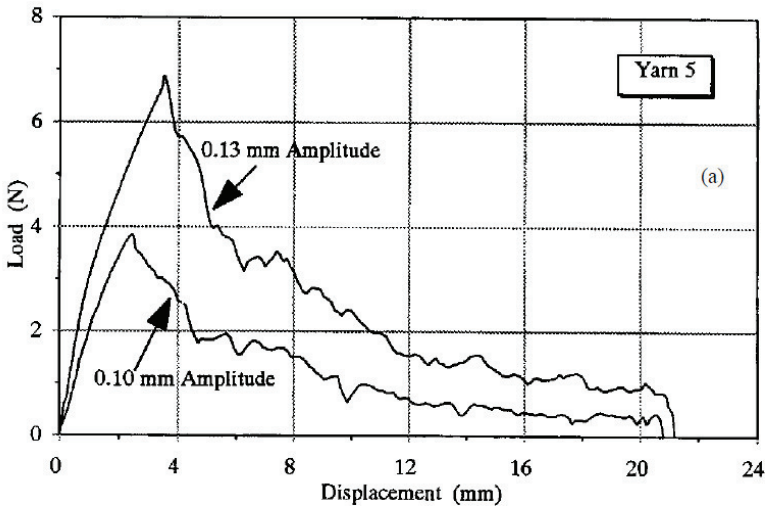

Figure 3.50: Effects of wave amplitude in the pull out resistance

case a linear correlation was found between bond stress and elastic modulus while in the second case others parameters should also be considered such as the geometry of the fabric because the woven geometry increased significantly the the bond in the cement matrix.

Mechanical properties of composites materials

The load bearing behavior is determined by bending or tension tests and the knowledge of cracking process is a crucial point. The direct tensile curve can be divided in three sections ([7] Fig. 3.51). At the beginning the linear elastic behavior depends on the stiffness of fine concrete (state I). After exceeding the concrete tensile strength, the whole stresses in the crack area is supported by the reinforcement. Increasing the strength additional cracks occur (state IIa). The crack pattern is influenced by the bond characteristics and tension failure of the matrix. In the stabilized phase (state IIb) no further cracks occur and the filaments are strained up. The stiffness should be equal to the Young Modulus of the reinforcement but usually it is 10 to 30 lower for the tension stiffening effect as well in steel reinforcement bar in concrete. In the state III there is no plastic branch, because the glass fiber has a brittle behavior. The failure mechanism of multifil-

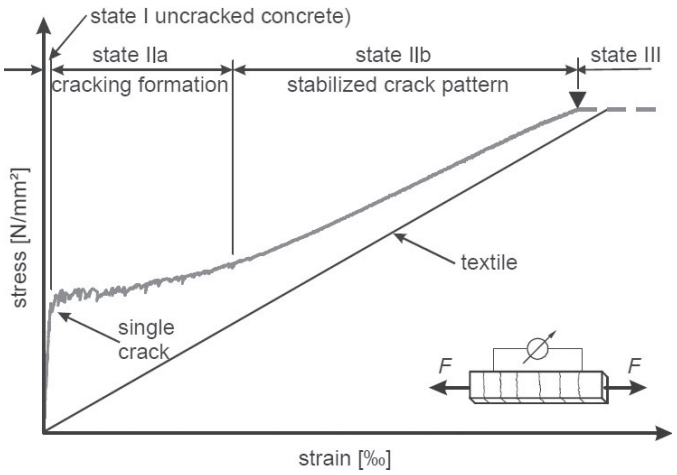

Figure 3.51: Direct tensile behavior, [7]

ament roving is very complex. Unlike the FRC that takes ductility from the pullout of the fiber from the matrix and the pullout load has to be lower than the fiber strength, the TRC failure mechanism is influenced by a lot of factors due to not homogeneous cross section. The external filaments (sleeve filaments) are in direct contact with the concrete and therefore are well bonded to the matrix, whereas the internal filaments (core filaments) are relatively free. This allows a telescopic failure, Fig. 3.52 [63], where the outer filaments are broken during loading where the inner filaments pulled out during loading. The sliding of the inner filaments leads high ductility to the material, mostly when brittle fibers are used.

The curve stress-strain is subjected to wide variations depending on a lot of factors such as the strength of fiber, adhesion fiber and matrix, impregnation of fiber, orientation of fiber, geometry of textile etc. As TRC is mostly used for tensile stress, two types of characterization test have commonly been used : direct tensile and bending tests. Different setup for direct tensile test are proposed by several researchers [8]. The dumbbell set up is used for specimen with increased section at the ends and a perforated plates was positioned in the mid-thickness to transfer the

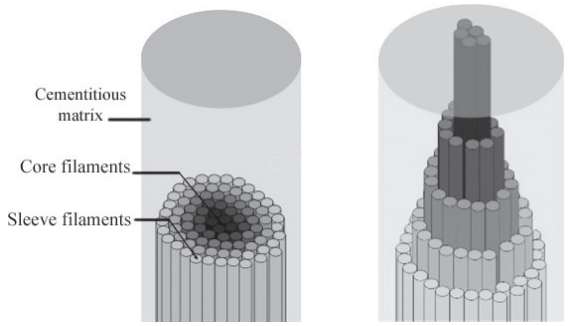

Figure 3.52: Core and sleeve filaments and telescopic failure

load (Fig. 3.53). The specimen is realized with vertical mold and shrinkage problem should be avoided. The problems are the difficulty to place the plates in the correct position and the unsuitability of thixotropic mortars. Another kind of specimen is the dog-bone (Fig. 3.54). The mould to realize the specimen is expensive. For transmitting the force to the specimen different methods are used standard clamps or steel cylinders passing through the specimen at the ends plate. The common problems of direct tensile tests are the non uniform stress distribution at the ends of the specimen and a possible parasitic bending moment due to the position of the clamping anchorages.

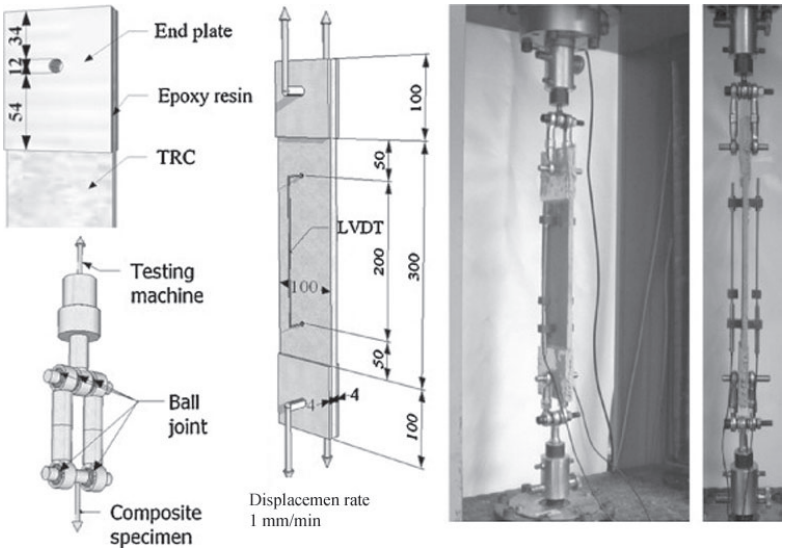

Figure 3.53: Set up for tensile test, [8]

The influence of different fiber material, AR glass and carbon, was investigated by Hegger ([64] Fig. 3.55). In the no cracked branch there was no influences by the highest stiffness of the carbon fiber. After that the carbon fiber had stiffness three time higher than AR glass due to the different Young modulus. The discrepancy between the ultimate resistance of roving taken from the fabric f_t and the strength in the composite material could be expressed by the following formula. The parameter k_1 was the effectiveness and for the AR glass was around 40% and for

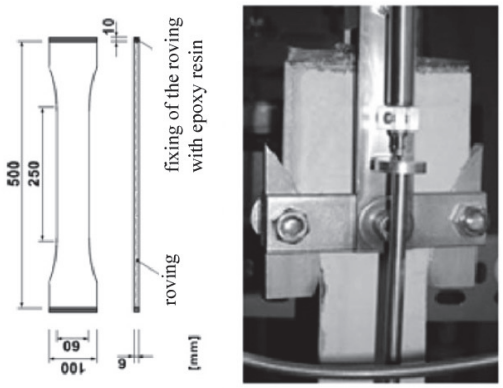

Figure 3.54: Dog-bone specimen

carbon 69%.

$$k_1 = \frac{\sigma_{max}}{f_t} \tag{3.32}$$

The influence of different roving has been studied by Molter[65] to understand the benefit

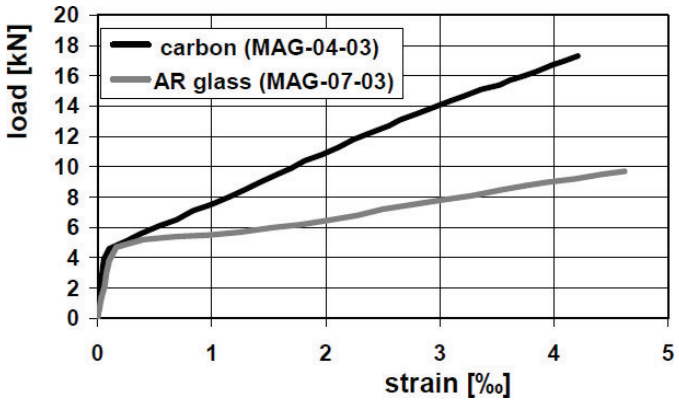

Figure 3.55: Load strain curves for AR glass and carbon fiber

due to the finest of roving in the bond behavior. The fabric used are reported in [66]. The textile MAG-01-03 had the finest roving and it showed the highest employment of fiber. The ultimate resistance diminished by enhancing roving thickness. This can be motivated by the theory deduced by [63] where the inner filaments had no direct contact with the matrix. So in the case of thick roving the inner filaments were greater. The effectiveness is influenced by the ratio between inner and outer filaments, Fig. 3.56.

The geometry of fabric can have a significant effect on composite properties, because it may increase bonding and give a hardening behavior. These influences are studied by four point bending test with a cross rate of 1.5 mm/minute with a span of 90 mm [9]. The specimens are made by lay up of 8 layer of fabric in cement mortar. Also specimens with straight yarn are considered to investigate the influence of crimp geometry. The fabric geometry are reported in

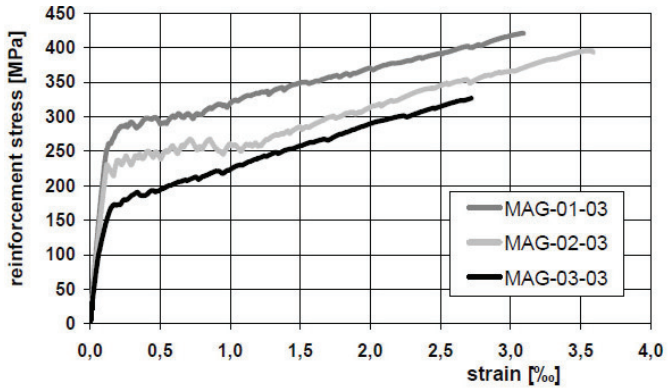

Figure 3.56: Stress strain curves for different titer rovings

Fig. 3.57. The results are showed in table 3.12 and Fig. 3.58 where the positive effect produced by the textile structure is evident compared to straight yarn. The special geometry may allow mechanical anchoring of the yarn in cement matrix due to the crimp geometry.

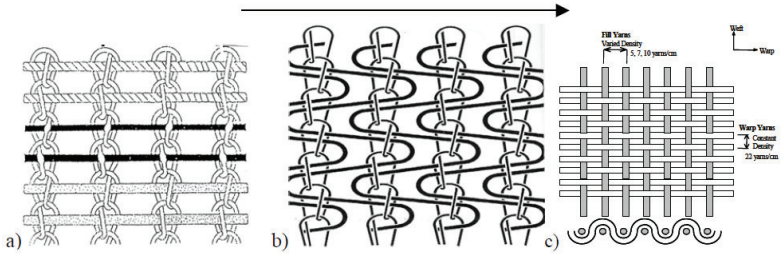

Figure 3.57: (a) weft insertion knit fabric, (b) short weft knit fabric, (c) woven fabric

The effect of fabric volume fraction was investigated by Singla [10] that used the same amount of reinforcement (two layers of AR Glass textile) embedded in specimens with different thickness. Increasing the reinforcement ratio, the ductility of the system improved due to the formation of distribute cracking (Fig. 3.59). Thinner specimen reached 6.7 MPa, whereas the other specimen 2.9 MPa. The reduction of thickness (around 33%) could allow an increase in strength of 56.7%.

Numerical Modelling

The TRM is characterized by a high degree of heterogeneity both for the reinforcement and for the matrix composition. Different kind of damage and failure are classified at collaborative research centers in Aachen and in Dresden. For simplicity the cement paste is regarded as homogeneous at all scale. Three levels are individuated (macro, meso and micro scale). At the macro-scale the textile is represented as a layer in an idealized cross section. In the meso-scale yarn are divided in two categories (core and sleeve filaments). The mechanisms involved are debonding yarn, crack development, crack bridges. In the micro-scale each filaments and their interactions are considered such as filament rupture, debonding filament.
The ACK (Aveston-Cooper-Kelly) model [67] described tensile behavior of TRM considering

Fabric type	Yarn type	Reinforcing yarn content in composite %Vol	Flexural strength [MPa]	Toughness N*mm	Flexural strength efficiency coefficient	Rel. factors of flexural strength efficiency coeff. fabric over straight yarn
7 yarn/cm woven	PE	5.7	18	4390	1.21	1.64
5 yarns/cm	Low mod.		15	4000	1.01	1.36
knitted short weft 3 yarns/cm	PE	2	16	4370	3.08	4.15
Knitted weft	PP Low Mod.	3.5	13	2990	0.74	0.70
Insertion 3 yarns/cm	HDPE High Mod.		19	4057	0.28	0.74

Table 3.12: Textile structure compared to straight yarn

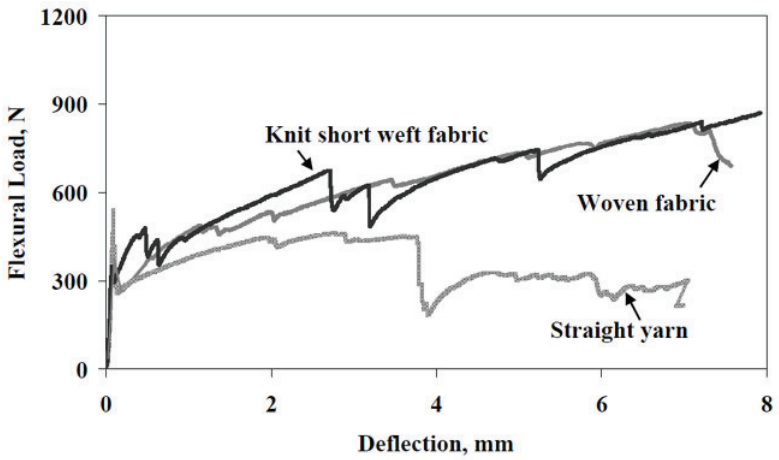

Figure 3.58: Flexural response results, [9]

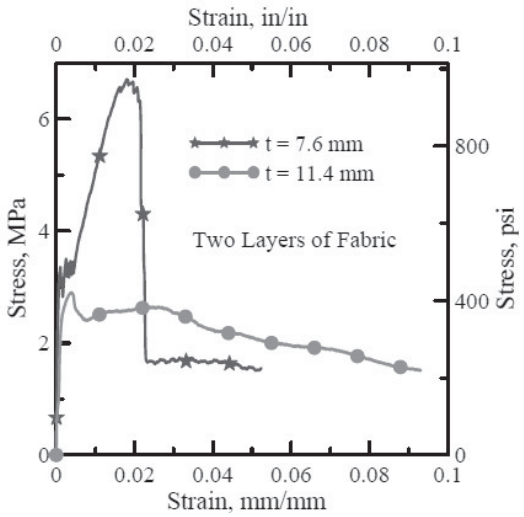

Figure 3.59: Influence of different thickness, [10]

the assumptions that when a crack occurred, debonding happened and the interaction between yarn and mortar became frictional with a constant value of shear stress. The behavior could be divided in three zones with different stiffness during the loading and unloading. The curve was determined by the pre-cracking branch (zone I), the multiple cracking (zone II) and the post-cracking branch (zone III).
Based on experimental tests the tensile [68] and bending capacity are studied. The tensile load bearing capacity is computed by eq. 3.33.

$$F_{ctu} = k_1 \cdot k_2 \cdot k_{0,\alpha} \cdot A_t \cdot \sigma_{max} \tag{3.33}$$

where

- F_{ctu} is the tensile load
- k_1 factor for the fiber effectiveness
- k_2 factor for biaxial loading
- $k_{0,\alpha}$ factor for the orientation of roving [69]
- A_t cross section of roving
- σ_{max} maximum tensile strength of the rovings

The bending capacity depended on the load bearing capacity in tensile state of the reinforcement and it could be computed in analogy with steel reinforcement concrete.

$$M_u = k_{fl,\rho} \cdot F_{ctu} \cdot z \tag{3.34}$$

- where $k_{fl,\rho}$ is a factor for bending load and is equal to 0.9 for AR Glass
- F_{ctu} is calculated according to eq. 3.33
- z moment arm

Durability problems

The durability aspect can be compared with FRC results present in the literature because on TRC there are still very few studies [70]. The interactions between fiber and matrix are time dependent over year. The loss strength during the time is different according to the fiber used (AR glass, polypropylene, carbon). The cause of the time dependent properties are of different types and the most common is fiber corrosion. The alkali are concentrated in the pore solution of the concrete and the pH can reach 13.7 deteriorating many fibers. Secondly, the continued hydration of the matrix that tends to densify the fiber-matrix interface increased hardness and the strength. So a crack will pass through the fiber and not around. Furthermore the bond between the outer filaments and matrix increases and the fiber failure dominates over the fiber pull out.
Two types of technique can be identified to simulate the behavior in time. The first is hot water ageing where sample are immersed in water at elevated temperature. The second is cyclic ageing to simulate cycles of temperature and moisture in alternative way. There are tests that involve fiber in accelerating ageing to evaluate their behavior in concrete. Fibers are immersed in alkaline solution and a reduction strength versus time is measured. Two are the approaches to improve durability by enhancing the strength of fiber versus chemical attack or by adopting modified cementitious matrices. Alkali Resistant glass fiber was developed in the 1970s and they are more durable but also subjected to degradation. By adding such coatings to AR glass fiber the hydration behavior is modified. These AR glass fiber are called of second generation. The second alternative is possible by reducing the precipitation hydration products or decreasing the pore solution alkalinity. It is possible modifying the cement matrix by adopting additives to Portland cement that reduce the pore solution alkalinity, [71].
The load bearing capacity of TRM is significantly improved by impregnating textile, [72]. Raupach studied the influence of a polymer impregnation on the durability of AR glass in alkaline environments. The degree of strength loss could be computed as:

$$\Delta f_{l,t} = 1 - \frac{f_t}{f_{t=0}} \tag{3.35}$$

where $\Delta\ f_{l,t}$ is the degree of strength loss at time t and f_t the tensile strength at time t.
The Fig. 3.60 indicates the degree of strength loss for filaments with epoxy resin and without before placed it in the alkaline solution at 50°. The pH value was 13.5 and the film thickness of epoxy layer was less than 1 μm. The tensile tests were performed at 7, 14 and 28 days of storage in alkaline solution. The degree of loss started from 40% until to 60%. It is necessary taking into account that the impregnation with epoxy resin was very low thickness around filaments instead of roving that had a much smaller attack area. The influence of attack area is shown in the Fig. 3.61 where dog bone, specimen stored in water, was tested. The impregnation textile showed a clearly lower degree of strength loss. This reduction could be due to the lower attack area of the alkaline solution and the enhanced thickness of epoxy resin around the roving compared to filaments.
A lot of models of durability were developed starting from empirical description up to analytical treatments based on micro-mechanical considerations. The models are based on the assumptions that damage is due to densification of the interface fiber and matrix and also for the fiber strength. The model of Katz and Bentur [73] was based on the physical densifying of the matrix. They considered the increased bond between fiber and matrix and the reduction of support length when fiber are inclined compared to applied force. The model considered also the non uniform fiber length due to breaking in the mixing phase.
Purnell model's [74] considered the strength loss in fiber caused by growth of surface flaws on fiber due to a stress corrosion process. In the model a relationship between the normalized stress

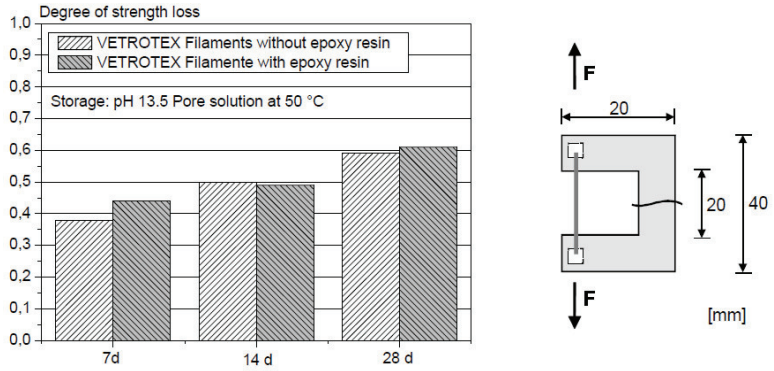

Figure 3.60: Influence of epoxy resin about degree of strength of filaments

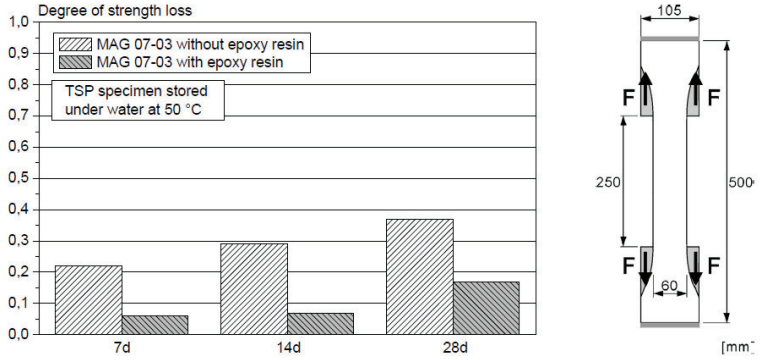

Figure 3.61: Degree of strength loss for specimen with and without epoxy resin

and time and parameter k, that was a function of temperature, was found.
Different models have been developed based on different approaches such as fiber corrosion models or matrix densification. There is not a correct model and the debate is still open. There are many aspects that have to be analyzed by the researchers.

Fire resistance

Textile elements are characterized by a thin structure compared to steel reinforcement concrete. Since the concrete cover is very small, textile has to stand very high temperatures. Therefore the fire resistance of TRM depends on the behavior of fabric at high temperature. Some tests showed the different loss in strength for different kind of fabrics. AR glass fiber showed a rapid decrease in tensile strength at temperature greater than 400°C, [4]. The best performance is reached by carbon fiber that showed a little decrease in tensile strength at temperatures of up 900°C. Another aspect of carbon fiber is the thermal expansion coefficient that is negative around $-0.4 \cdot 10^{-6} K^{-1}$. So the carbon fiber gets shorter at high temperature. The mechanical behavior of fine concrete is affected by the type of cement or binder. In particular different thermal expansion coefficient of cement and aggregate leads to a damage in the microstructure. However in fine concrete the pore volume is low so the micro-cracking is limited. Problem of spalling can be occurred when the water presents in the pore volume at 100°C can transform into vapor pressure and spalling the concrete after passing the tensile strength of the concrete.
The knowledge about textile reinforced concrete under high temperature is still quite limited because only a few tests were performed [75].

3.4.5 Existing and future applications

TRM is a composite material suitable for a wide structural and retrofitting applications. Characteristics of textile reinforcement are the possibility to be used in two dimensions and to adopt them self to complicated and curved geometry [76]. The use of fabric with high fluidity matrices leads to create elements with different shape. Furthermore TRM can be used in strengthening structural elements such as masonry or concrete wall, jacketing column and beam.

Retrofitting applications

Strengthen or upgrade existing buildings is a wide increase problematic. This necessity can be caused by different reasons such as damage by mechanical action, design requirements, change of structural system, construction mistakes or a deterioration due to the time. The increase of load carrying capacity can be reached by different methods. Near the classical methods as well shotcrete and FRP (Fiber Reinforced Polymers), the use of TRM is an extremely effective and promising technique. The main features of FRP are a high specific strength, corrosion resistance, easy and speed in the applications and minimum increase of the cross section. Despite these advantages the FRP has some drawbacks due to the organic resin adopted to bind the fiber. The high adherence of the resin leads to the development of high shear stresses in the interface area between concrete and retrofitting layer and so FRP may debond. The adherence between concrete and TRM is lower than the organic resin so the formation of crack and lower adherence are suitable for repairing old concrete. The main problems related to organic resin are the poor behavior a high temperature, high cost, lack of vapor permeability which may cause moisture accumulation in the interface. The substitution of organic binders with inorganic ones (cement matrix) seems to be very beneficial. The advantages of TRC is due to the combination of textile and concrete that leads to high tensile strength, low layer thickness, lower weight, high corrosion resistance. Different research projects in the retrofitting field has focused their attention on

TRM applied on masonry (Fig. 3.62) and concrete elements, because many are the advantages: fire protection, easiness to install, low cost matrix, compatibility with moist surfaces. Different studies have been conducted on system for rehabilitation masonry with textile reinforced concrete ([11], [26]). Structural tests demonstrated the ability of cement based material reinforced with textile to strengthen masonry wall and the best performance compared to FRP solution [77]. The TRC is suitable to strengthen for bending, shearing, torsion or axial force. It is also possible to repair complex and curved elements. In all cases it must be considered the load carrying capacity, the criterion of the minimum reinforcement and the necessity anchorage of textile layer. Recent studies explained the efficiency of TRM applied as confinement, shear and flexural strengthening [11], [78], [30], [60]. Before applying the strengthening layer, the old concrete element has to be treated with sandblast and the surface must be cleaned from any fine grains so the bond is improved. Then, an alternate layers of mortar and textile are applied to the old concrete surface.

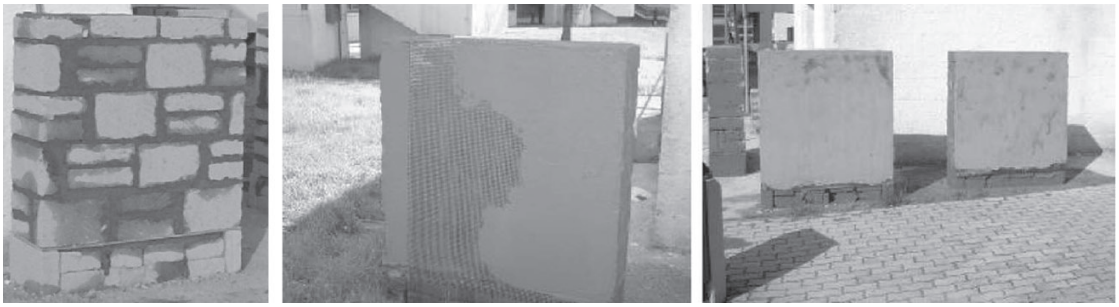

Figure 3.62: TRM applied on masonry wall, [11]

An experimental campaign was developed by Larringa [12] to investigate the effect of TRM in **flexural retrofitting** beams. Different kind of fabrics were used carbon, basalt and steel fibers with low and medium density. Rectangular beam (150 x 150 x 1500 mm) made by concrete with compressive strength of 17 MPa was chosen in order to simulate old concrete. Tensile surfaces of beam were made rough to enhance the bond with retrofitting layer that was applied by using a roller to compact the matrix. The specimens were tested by four point bending test with a displacement rate of 3 μm/s. Linear Variable Differential Transducers were applied to measure the displacement in the constant moment zone. The failure modes were different according to the fabric. For basalt and carbon fabric, the failure was due to the rupture of fiber when their maximum elongation was reached (Fig. 3.63a). For low density steel fabric, delamination in zone with maximum bending moment occurred (Fig. 3.63b) and for the medium density steel fabric a delamination happened at the end of the material composite (Fig. 3.63c). The use of TRM increased the maximum bending capacity by 40% for basalt, 48.5% for carbon and 94.5% to 148% for beam strenghened with steel fabric compared to control beam.

The flexural strengthening properties of textile reinforcement was also investigated by Weiland [13]. The slab specimen was 100 mm thick and has an effective span of 1.60 m (Fig. 3.64). The variables were the number of layers, the fiber nature (AR Glass and Carbon fiber) and three reinforcement ratio 0.2%, 0.34% and 0.5%. Before strengthening an artificial deterioration on specimen was applied. The slabs were tested in 4 point bending tests and the results were compared with a reference slab without strengthening layer. The load displacement curve of slab with TRC showed a higher first crack load compared to unstrengthened slab, because the moment of inertia was higher (Fig. 3.65). Due to retrofitting layer both load carrying capacity and also

Figure 3.63: Different failure modes [12]

Figure 3.64: Set up: four point bending test [13]

serviceability properties were improved. The displacement was limited. The crack pattern was visualized using water with ink on the surface of the slab and it was evident that besides the crack of predamage slab, new cracks occurred. The influence of different materials of fabric (AR Glass and Carbon fiber) was studied. The carbon fiber fabric was very competitive compared to AR glass fabric, because for the same bearing capacity, it was necessary 1/3 of AR glass area, Fig. 3.66.

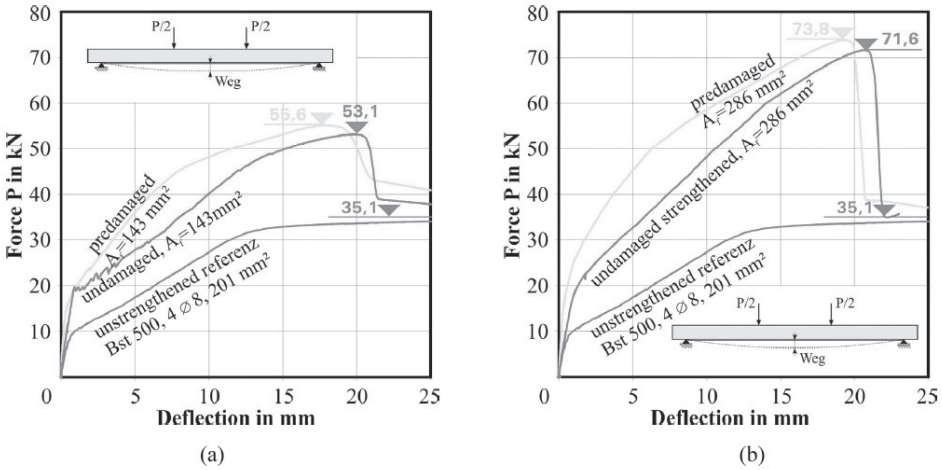

Figure 3.65: Results: (a) 3 layer of TRC, (b) 6 layer of TRC,[13]

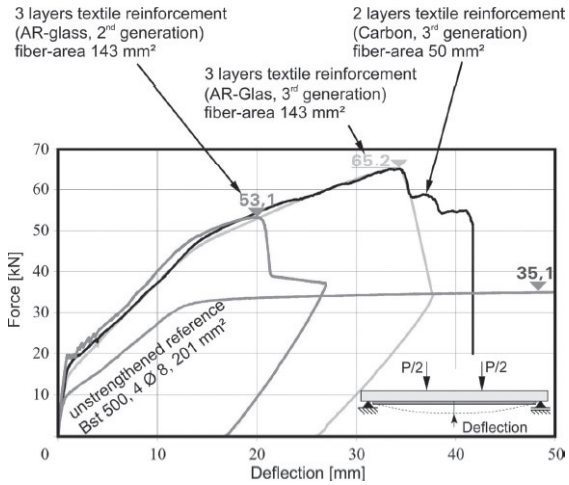

Figure 3.66: Compared different fabric, [13]

The design model used for steel reinforced concrete can be adopted also for the load carrying capacity of flexural strengthened beam and slab with an additional tension force due to the textile layer (Fig. 3.67 [14]). The hypothesis of Bernoulli, where the cross section remains straight during deformation, was still valid. The bond between old concrete and textile layer and fabric and mortar were considered to be rigid. The ultimate load was correlated to the

ultimate strain of retrofitting layer that derived from uniaxial tensile test even if there were some differences from the crack pattern obtained by a textile, while it worked as strengthened layer [14].

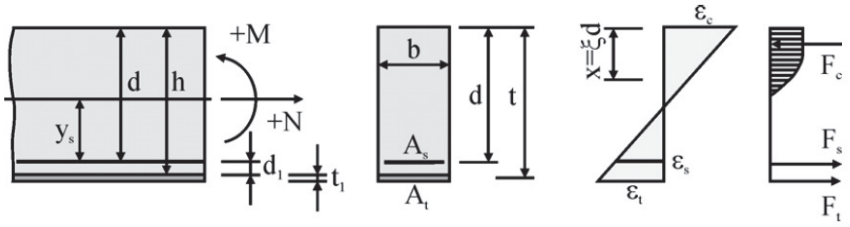

Figure 3.67: Bending model, [14]

Different failure modes could develop according to the kind of strengthening. It was important to know the weak points such as, for flexural strengthening layer of slab, the ends near the support (Fig.3.68). Where flexural strengthening is placed under slabs or beams, the repair layer itself must end before the support. So two were the main problems to compute the tension force transferred from the strengthening layer into the old concrete and to know anchoring length required [14].

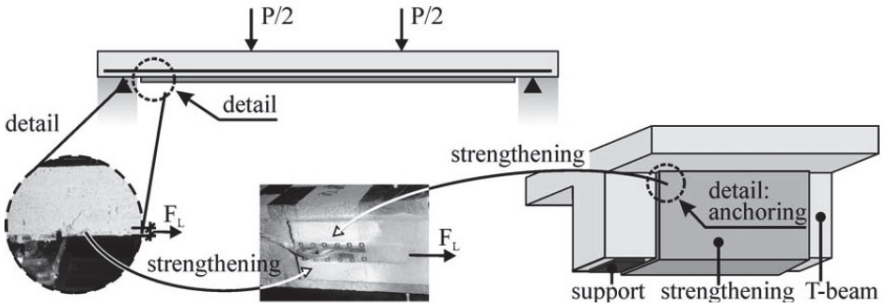

Figure 3.68: Weak points of anchoring [14]

The failure can start in different position and they were classified according to Ortlepp as in Fig. 3.69:

- failure mode 1 in the uncracked anchoring zone
- failure mode 2 for flexural cracks
- failure mode 3 for shear cracks
- failure mode 4 uneven concrete surface.

The collapse can happen at different layer: delamination of textile, failure of joint, and breaking of old concrete and pull out of fiber from the matrix layer (Fig. 3.70 [15]). The last one failure is not directly correlated to bond failure between old and repair layer. To avoid delamination in interface surface, the roughness of the old concrete element has been treated accurately. The best results were obtained by using high pressure water blasting followed by

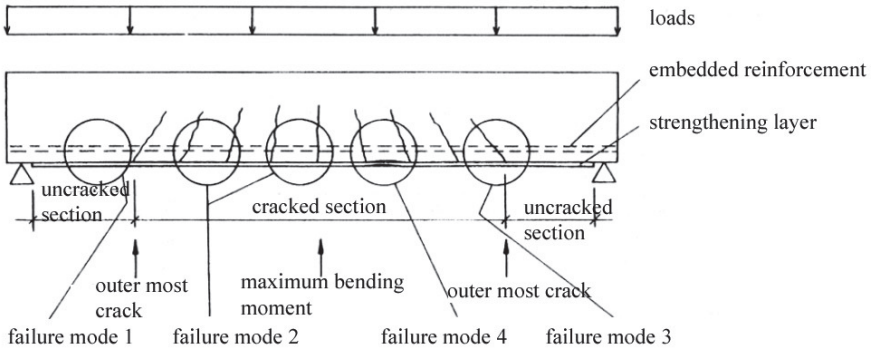

Figure 3.69: Bond failure modes of flexural strengthened concrete [4]

sandblasting.

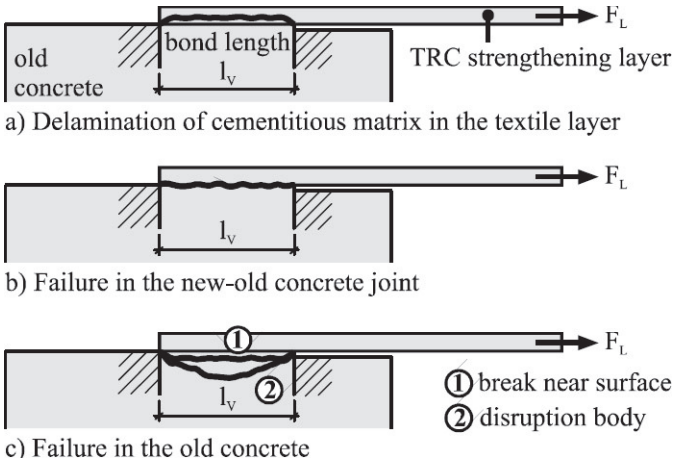

Figure 3.70: Failure modes, [15]

The main difference from the adhesive bonded plates (steel or FRP) was the absent of slip interface due to the presence of adhesive with a significantly lower Young modulus compared to strengthening layer. In TRC layer, crack region occurred with angle between 90° and 30° and they had a great influence on the deformation in the interface zone ([79] Fig. 3.71).

A bond simplified model was proposed by Ortlepp [15] based on strut and tie structure (Fig. 3.72). There was a correlation between the tension force in the retrofitting layer called F_L and the peel-off force T_i. The tension force T_i was perpendicular to F_L for the balance and it attempted to lift away from the old concrete. If the anchoring length l_V is too short, the perpendicular force lifted the strengthening layer and this failure was called peeling off. The failure layer was determined by the strength of several layer of the composite system.

Textile reinforced mortar can be used also as **jacketing material** to confine concrete. Usually the aim is to enhance the load carrying capacity of compression elements. Traditional confinement methods are steel jackets or FRP. Confinement increases strength and ductility concrete

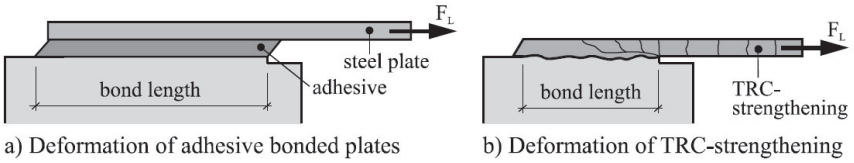

Figure 3.71: Adhesive bond compared to textile bond, [15]

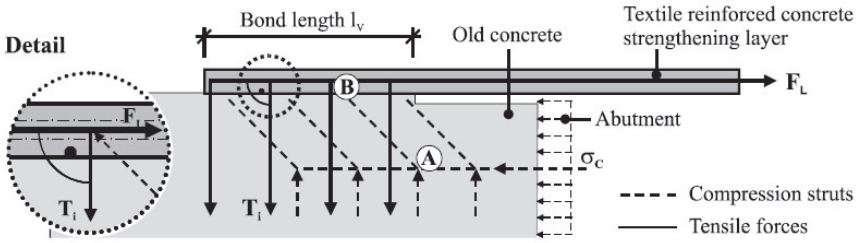

Figure 3.72: Strut and tie model, [15]

and it prevents buckling longitudinal reinforcement, while in seismic problems retrofitting techniques have the aim to increase the confinement pressure in the potential plastic hinge zone. An experimental investigations on concrete columns under compressive load reinforced by TRC was conducted by Jamous ([16] Fig. 3.73). The textile reinforcement improved working confinement and favored three axial state of stress. Circular short columns (diameter from 150 to 166 mm and 300 height) were used to avoid buckling phenomena. The traditional concrete was 35 MPa and two, four or six layer of glass textile were applied by wrapping the fabric reinforcement which was embedded for 8 mm in the matrix. Different anchoring length was considered varying from 90 to 200 mm. Vertical displacement on the top of the specimen was applied with a deformation rate of 2 kN/sec and the vertical displacement was monitored. The results are shown (Fig. 3.74) in terms of force versus strain where different measure of displacement were taken from the transducers. The test shows that according to the reinforcement ratio, there was an increase by up to 54% on the loading compared to the unstrengthened column. A simple model, to compute the

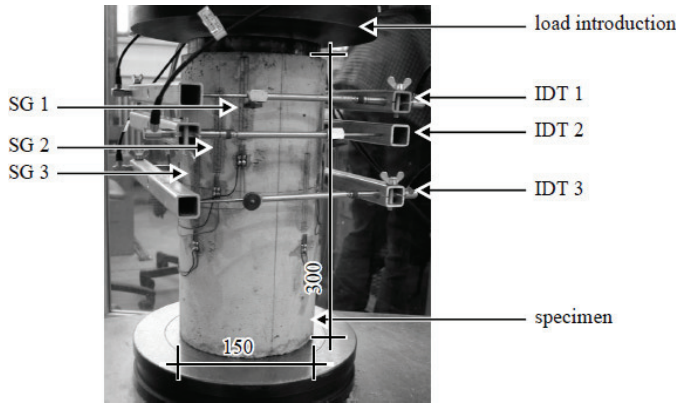

Figure 3.73: Test set up

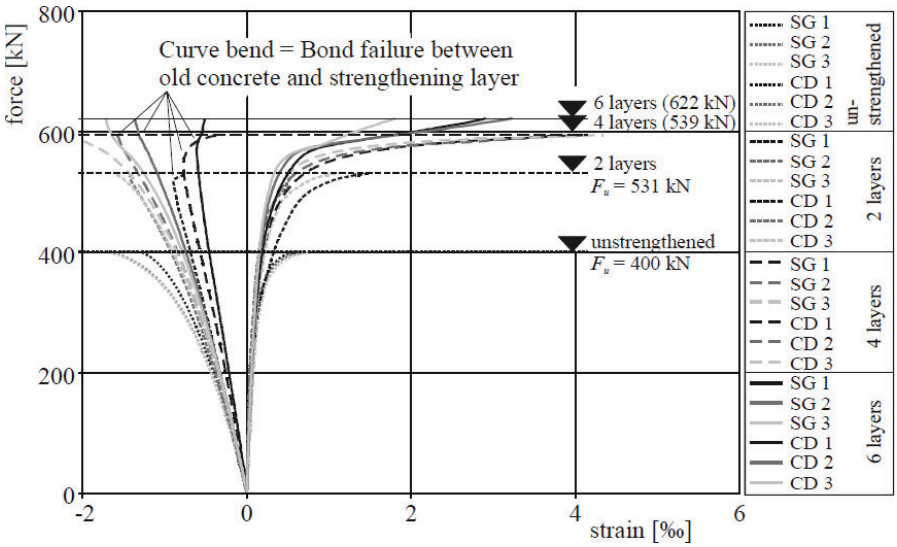

Figure 3.74: Results Force versus strain [16]

effect of strengthening layer in a confinement column, was proposed by [17]. If circular column was strengthened enough, transverse stretching was impossible and a triaxial state of stress was made. The circumferential stress can be computed according to eq. 3.36 [17].

$$\sigma_r = \mu \cdot \sigma_{c,l} = \mu \cdot E_c \cdot \Delta l / l \tag{3.36}$$

where σ_r is the peripherical stress
μ is Poisson ratio
$\sigma_{c,l}$ is the vertical stress in the old concrete with triaxial state of stress
E_c is the Young Modulus
Δl is the shortening of the support due to the normal load
l is the length of the column.
By the knowledge of the circumferential deformation, it was possible to compute the tangential tension in the retrofitting layer and accordingly the inner pressure in the old concrete (Fig. 3.75). The tangential tension force was computed by:

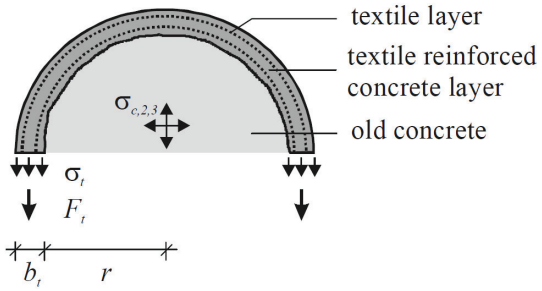

Figure 3.75: State of stress in the circle diameter, [17]

$$F_t = \sigma_t \cdot b_t \tag{3.37}$$

where σ_t is the normal tensile stress in the strengthening layer, b_t the thickness of TRC layer. The transverse stress in the old concrete with a radius, r, subjected to a triaxial state of stress was:

$$\sigma_{c,2,3} = b_t \cdot \sigma_t / r \tag{3.38}$$

By combining the contribution of the vertical stress $\sigma_{c,1}$ obtained from the load presented in the column and the transverse stress $\sigma_{c,2,3}$, the compressive resistance was enhanced due to the confinement effect. Hence the new load bearing capacity can be computed according to Eq. 3.39.

$$N_{c,3} = A_c \cdot \sigma_c \cdot \eta_c \tag{3.39}$$

where the A_c is the cross section of the old concrete, σ_c normal stress in the concrete, η_c the corrector factor for the multiaxial state of stress according to Dahl [17].
The complete interaction of both concrete layer can be considered according to Eq. 3.40 as shown in Fig. 3.76.

$$N = A_c \cdot \sigma_c \cdot \eta_c + A_t \cdot \sigma_t \tag{3.40}$$

where N is the vertical force of the column
σ_t normal stress in the TRC layer, A_t is the cross sectional area of strengthening layer.

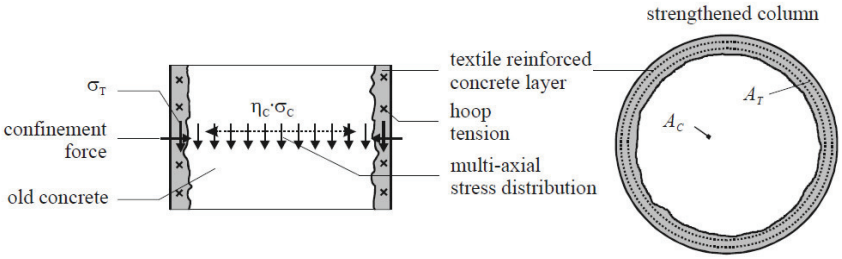

Figure 3.76: Stress distribution in the strengthening column [16]

One of the most common upgrading techniques involves the **jackets for shear resistance** in zone without suitable reinforcement. Experimental studies were conducted by Triantafilliou [30] to understand the effectiveness of shear reinforcement obtained by carbon textiles combined with cement based mortar and resin based matrix as just shown in chapter 02. The shear loading behavior of a textile strengthened element can be studied as strut and tie model both for steel reinforcement and textile. Different failure modes can occur in element with textile reinforcement subjected to shear:

- failure of steel stirrups
- failure of the strut
- failure of the strengthening layer
- peel off of the strengthening layer

The first and the second failure are typical of steel reinforced concrete. The contribution of TRC layer for shear strengthening has been computed by a model that considered the truss analogy.

Considering the angle β_i that fiber formed with the longitudinal axis of the element, the contribution V_t was established by Eq. 3.41 and Fig. 3.77 illustrated the geometry.

$$V_t = \sum_{i=1}^{2} \frac{A_{ti}}{s_i} \cdot (\epsilon_{te,i} \cdot E_{fib}) \cdot 0.9 \cdot d \cdot (cot\vartheta + cot\beta_i) \cdot sin\beta_i \tag{3.41}$$

where $\epsilon_{te,i}$ was the effective strain of TRC in direction i, E_{fib} was the elastic modulus of fiber, d was the effective depth of the cross section, A_{ti} was twice the cross section area of each roving in direction i, s_i was the spacing of roving in the longitudinal direction, ϑ was the angle between the shear crack and the element axis.

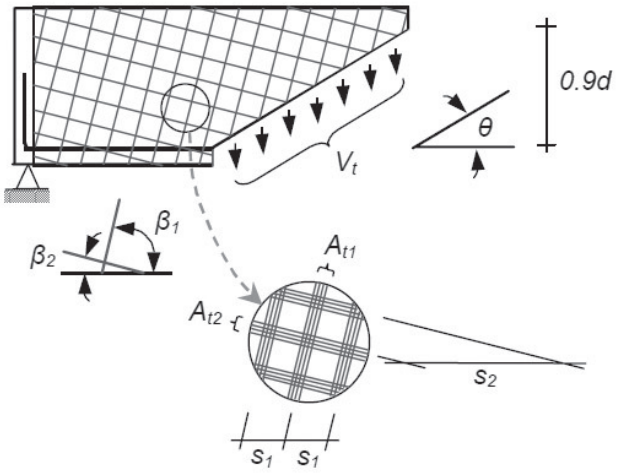

Figure 3.77: Contribution of reinforcement to shear resistance

Applications examples

The TRC material offers a wide spectrum of applications. The possibility to create thin concrete cover leads the construction of thin walled structural elements. Due to his high corrosion resistance, the concrete cover is minimized and slender structural elements can be design. Furthermore fine grain concrete matrix allows sharp-edged high quality aspect surfaces. These features lead to architects and engineers more freedom in the design. In the following some example are shown.

Grid shells offer load bearing capacity with a single or doubly curved surfaces. The curved surface can be divided into subareas with a polygon form. An example was diamond lattice grid [80] Fig. 3.78 where the whole structure was generated by the addition of the same rhombic element.

In order to study the capability of textile for shell structure application, the collaborative centre researchers at RWTH Aachen wants to create an experimental building where the roof is realized by doubly curved TRC shell Fig. 3.79 [80].

Figure 3.78: Diamond lattice grid

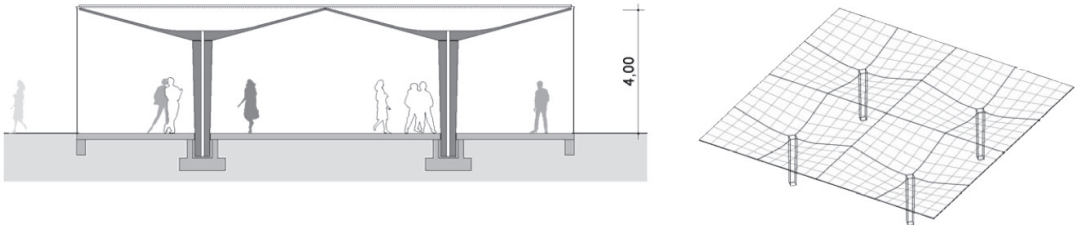

Figure 3.79: Experimental building

Sandwich panels made of TRC combined with insulation layers are an interesting choice for modern building and the RWTH collaborative research at Aachen studies the load bearing behavior of the composite element of TRC and foam core (Fig. 3.80). TRC panel has to satisfy a series of requirements such as low heat conductivity, noise protection and heat retention in concrete facings. First applications was conducted by Hegger [81] and further investigations on connecting devices, on the behavior of thin walled under temperature have to be done.

An extension building of Institute of Structural concrete RWTH Aachen University has been realized with cladding panels made of TRC. The existing building was extended for 5.4 m. The design of panel is shown in Fig. 3.81. This solution was less expensive than natural stone and a good cost efficient alternative for residential and commercial buildings. The TRC has been adopted for the facade of an office building "House Rheinlanddamm" in Germany. It had 6 stories and a height of about 21 m. According to the design, the building should get a rear-ventilated facade of large size. The panel had 25 mm thick and it was reinforced with AR glass fabric and additionally short fiber were used to enhance the crack prevention (fig. 3.82, [82]).
A small footbridge for pedestrians and cyclist has been held in Oschatz in 2006 and it has been designed by the Institute of Concrete Structures of Dresden University (Fig. 3.83). The total span width was 8.60 m and the width between the handrails 2.50 m. The bridge was made by TRM segment with a thickness of 30 mm and they were fixed together with un-bonded tendons. The transmission of shear within the joints was ensured by tendons.

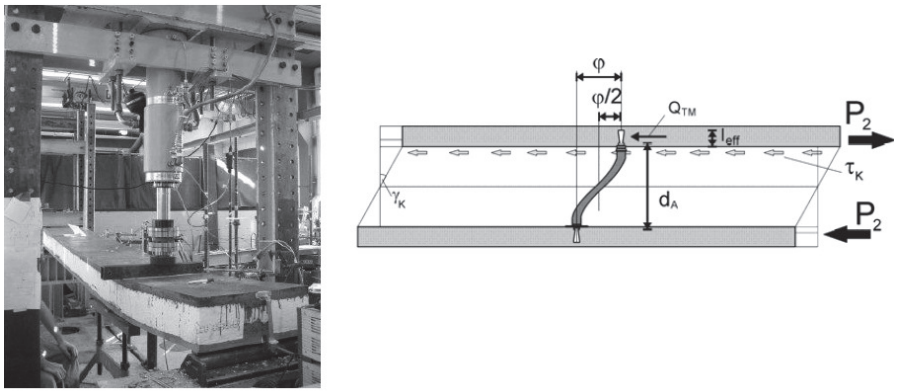

Figure 3.80: Sandwich panel

Figure 3.81: Sandwich panel used for curtain wall, Aachen University

Figure 3.82: House Rheinlanddamm

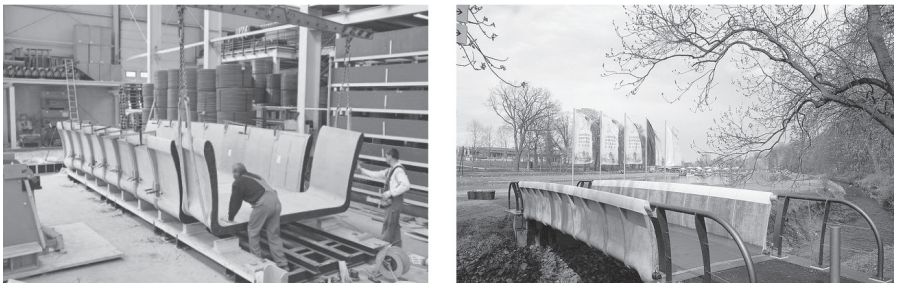

Figure 3.83: Pedestrian bridge in Oschatz 2006

Chapter 4

Mechanical characterization of retrofitting materials

The research project aims to investigate the effectiveness offered by innovative materials for retrofitting damaged concrete elements and to suggest the best solution comparing perfomance, costs and installation easiness. Thin layers can be used to strengthen traditional concrete: in particular 20 mm thick UHPFRC layers and 6 mm thick TRM layers are here proposed. The composite materials are considered by designers as a unique material whose mechanical features have to be indentified by proper tests nowadays under research investigations, such as notched and unnotched bending tests for fiber reinforced concrete and uniaxial tension unnotched tests for textiles. In this research activity the mechanical performance of UHPFRC has not been investigated and the research activity performed by Ferrara et al. [18], [83] has hence been taken as a reference; the whole mechanical characterization of TRM has instead been studied in this thesis [49].

4.1 UHPFRC

To optimize the peformance of UHPFRC is very important to control some parameters as the orientation, the dispersion of fibres in matrix through suitable fresh state properties and an accurate casting procedure. The fiber reinforced concrete used in all the experimental programme was made of short steel fibres (length 13 mm and diameter 0.16 mm) and characterized by a fiber volume fraction of 100 kg/m^3 that allowed a deflection hardening behaviour. The principal idea is that the matrix must be self compacting to avoid vibration because it may obstruct homogeneous fibre dispersion. The fresh state performance must have a suitable viscosity to orient fibres in casting flow direction and to avoid segregation due to higher specific gravity of fibre with respect to fluid mortar. The casting procedure must be realized to induce fibre aligning as close as possible with the direction of principal tensile stresses according to the use of structural element. In such way it is possible to achieve the efficient structural use of the composite, optimizing structure size, self weights, time and cost construction process. In order to follow these key ideas, fresh properties and the effect of fibre orientation on mechanical performance were assessed. The mix composition is shown in table 4.1 and it was already characterized by previous works [18], [83], [84]. All properties depend on the w/b ratio (0.18) and on the superplasticizer (SP) dosage and are linked to fresh state that was assessed through slump-flow, V-funnel, L-box, U-box and J-ring tests according to the standards [85], [86], [87], [88] as shown in fig. 4.1 and in table 4.2.

Content	Dosage (kg/m^3)
Cement type 52.5	600
Slag	500
Water	200
Superplasticizer	33 (l/m^3)
Sand 0-2 mm	983
Straight steel fibres (l_f=13 mm; d_f=0.16 mm)	100

Table 4.1: Mix design of fibre reinforced cementitious composite

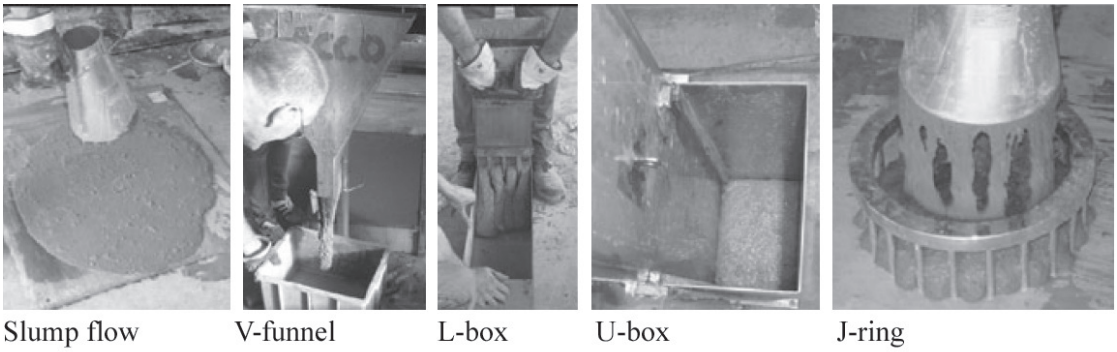

Figure 4.1: Fresh state tests

The results demonstrated the self leveling ability of the matrix.

Batch	Slum flow		V-funnel	L-box			U-box	J-ring
	Diameter (mm)	t_{50} (s)	Flow time t_v (s)	Height ratio	t_{200} (s)	t_{400} (s)	Height ratio	Diameter (mm)
1	770	7	23	-				735
2	730	7	-					-
3	775	4	20	1	2.5	4	0.98	755

Table 4.2: Results of fresh state characterization

Ferrara et al. [18] studied the influence of casting flow in fiber alignement. The beam specimens 150 mm wide and 500 mm long were cut from 30 mm thick slabs, as described by fig. 4.2. In the slab A the direction of casting flow was in some specimens parallel and other perpendicular to the beam axis. In the other case, B, the flow was radial. 4-Point bending tests were performed at a 5 μm/s rate, measuring the crack opening displacement COD over a gauge length of 200 mm.

Nominal stress versus COD curves (fig. 4.3) demonstrated the effectiveness to orient fibers in the direction of principal tensile stresses. To obtain the stress and strain values that define the constitutive law of the material according to the referred Guidelines [89], different length scales were involved. Concerning deflection hardening behavior, the pre-peak was determined by a multiple cracking regime in the central constant bending moment region, hence the length scale may be assumed equal to the COD gauge length (l=200 mm). After the multiple cracking

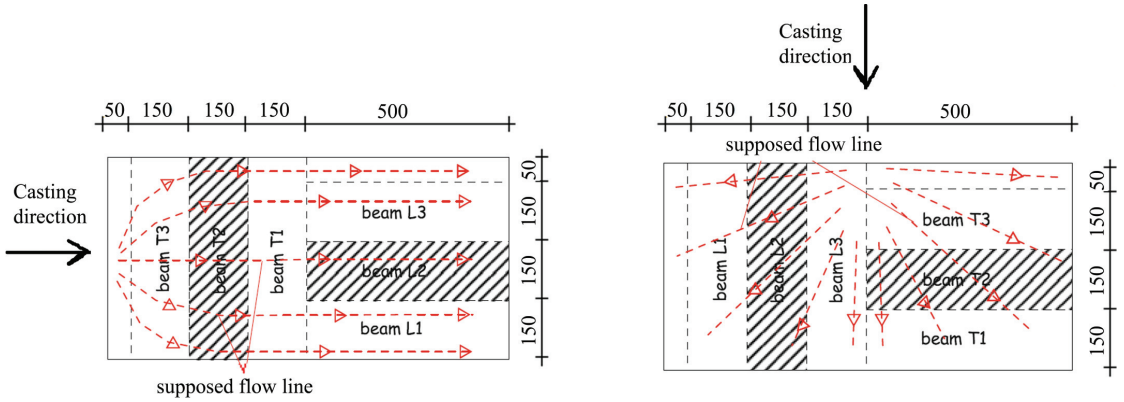

Figure 4.2: Scheme of casting procedure [18]

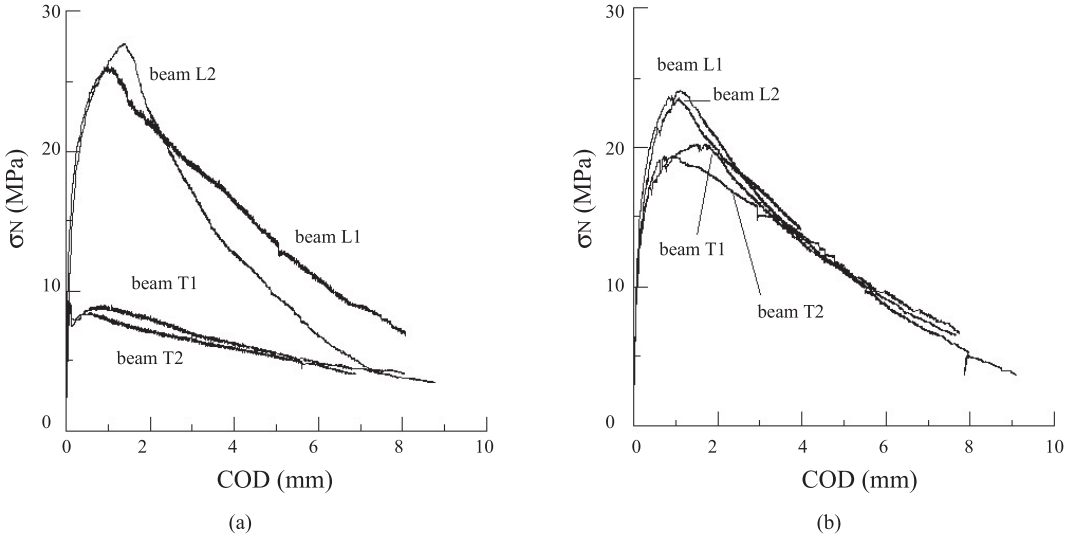

Figure 4.3: Results of 4 bending test (a) slab A (b) slab B [18]

stage, a single crack localized and the fracture governing length scale can be estimated equal to the thickness of the sample (h=30 mm). In the case where the behavior was deflection softening, as for beam with the axis orthogonal to the flow, the governing length scale was constant and equal to the thickness of the specimen. The equivalent post-cracking resistances were assessed with the following criteria:

- the first cracking strength, f_{If}, is defined as the maximum nominal resistance in the COD interval 0-0.1 mm and the corresponding crack opening is w_I (in this case w_I=0.1);
- the equivalent post-cracking strengths $f_{eq,1}$ and $f_{eq,2}$ are defined as the nominal stresses averaged in COD range 3-5 w_I and 0.02h ± 20% (0.48-0.72 mm). These values represent the serviceability and ultimate limit state. For very thin elements, the second COD may be not enough representative of the real ductility and deformation of the material. So higher COD ranges 0.04h ± 20% and 0.10h ± 20% are considered.

The crack opening ranges are redefined as follow:

- for $f_{eq,1}$: $(3 - 5 \cdot w_I - \epsilon_{peak} \cdot h) + \epsilon_{peak} \cdot l_{COD}$
- for $f_{eq,2}$: $(0.02h \pm 20\% - \epsilon_{peak} \cdot h) + \epsilon_{peak} \cdot l_{COD}$
- for further limits: $(0.04h \pm 20\% - \epsilon_{peak} \cdot h) + \epsilon_{peak} \cdot l_{COD}$
  $(0.10h \pm 20\% - \epsilon_{peak} \cdot h) + \epsilon_{peak} \cdot l_{COD}$.

The parameter of the constitutive law are identified through equilibrium of force and moment for the corresponding stress distribution fig. 3.23 and the constitutive law is reported in fig. 4.4. The value of β_1 was obtained by an inverse analysis to fit the experimental results. The tensile

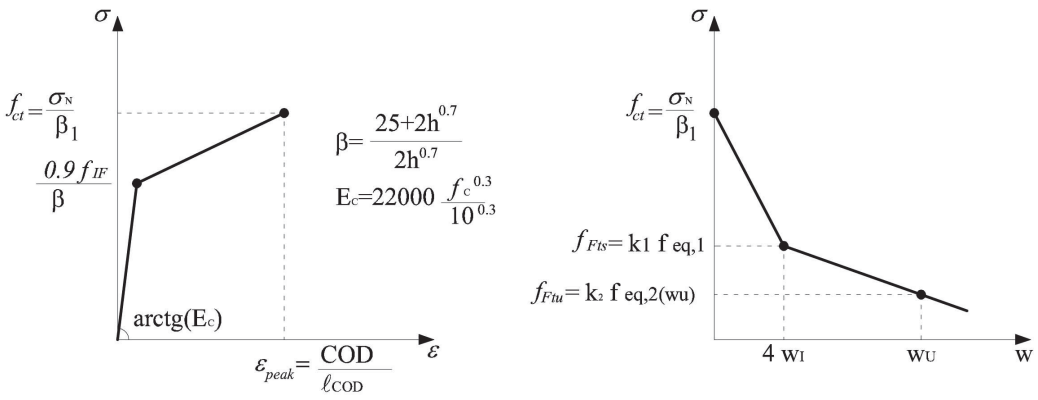

Figure 4.4: Pre-peak stress strain and post-peak stress crack

stress-strain and stress versus crack opening laws obtained by Ferrara et al. [18] are shown in fig. 4.5.

The bending response of thin UHPFRC structures was also studied by di Prisco [19], that identified constitutive relations starting from specimens (600 mm long, 150 mm wide and 23 mm average thick) prepared with the same mix design, as explained in the previous work [18], and tested by means of four point bending tests. The differences with the previous research are the thickness of about 23 mm but, in particular, the casting procedure. A slide of PVC 50 cm long and inclined at 60° was used to orient the fibers in the direction of principal tensile stresses (fig.

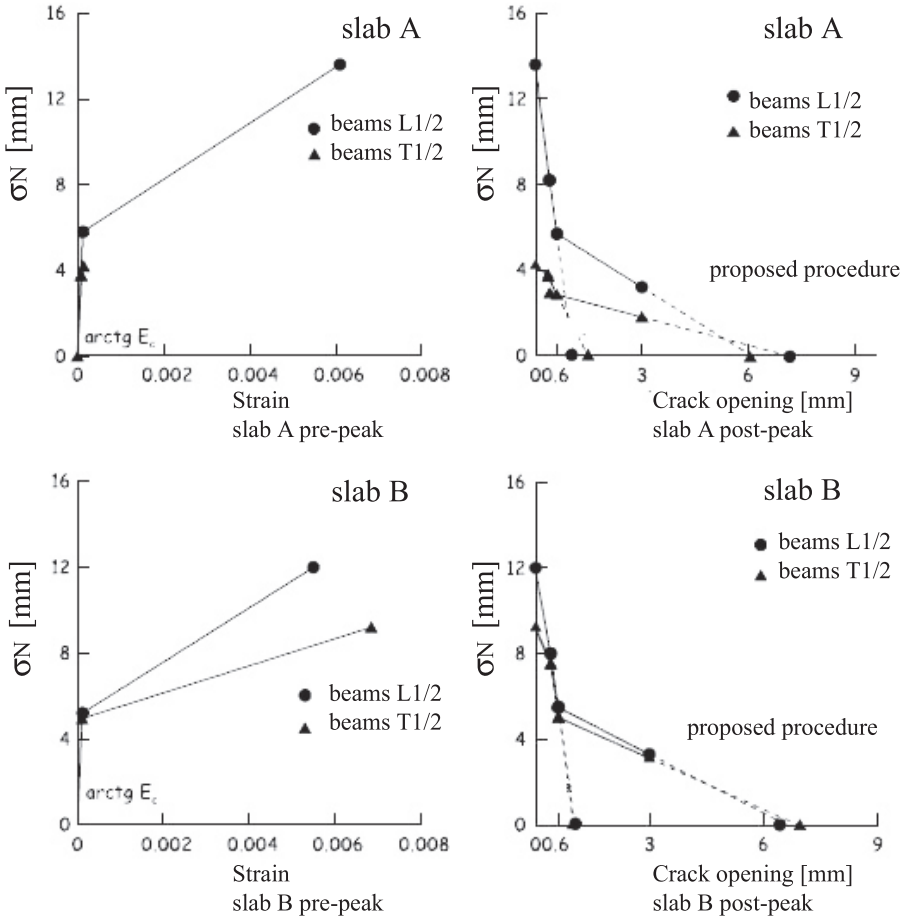

Figure 4.5: Tensile constitutive law, [18]

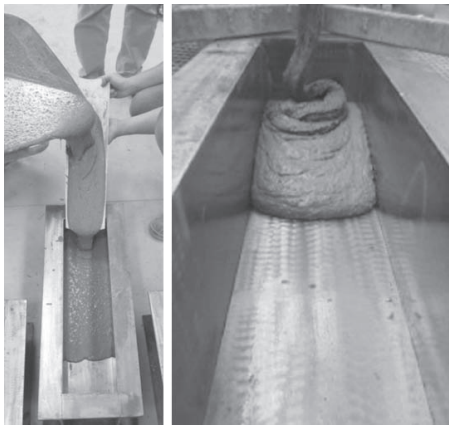

Figure 4.6: Casting procedure to orient fibres

4.6). Before performing bending test, the uniaxial compression strength of the UHPFRC matrix was determined by compressive tests on 150 mm size cubes after a curing of 28 days. The average cylindrical compressive strength f_c was equal to 104,6 MPa and corresponded to a C90 class with an elastic modulus E_c of 46 GPa. In the bending test the lower knives were placed at a distance of 450 mm, while the space between the upper ones was of 150 mm. An integral Crack Mouth Opening Displacement (CMOD) was measured by two displacement transducers (LVDT) on a gauge length of 200 mm. The vertical displacement was measured by four vertical displacement transducers, positioned near the loading knives. The tests were performed with a constant 1·10-4 mm/sec displacement rate until a stroke of 30 mm. Due to the high fibre orientation the composite material showed a stable behaviour up to a CMOD of 6 mm fig. 4.7b after that displacement, the LVDT was not able to record the softening phase as, instead reported in the load displacement curves fig. 4.7a. The constitutive law for UHPFRC was derived according to

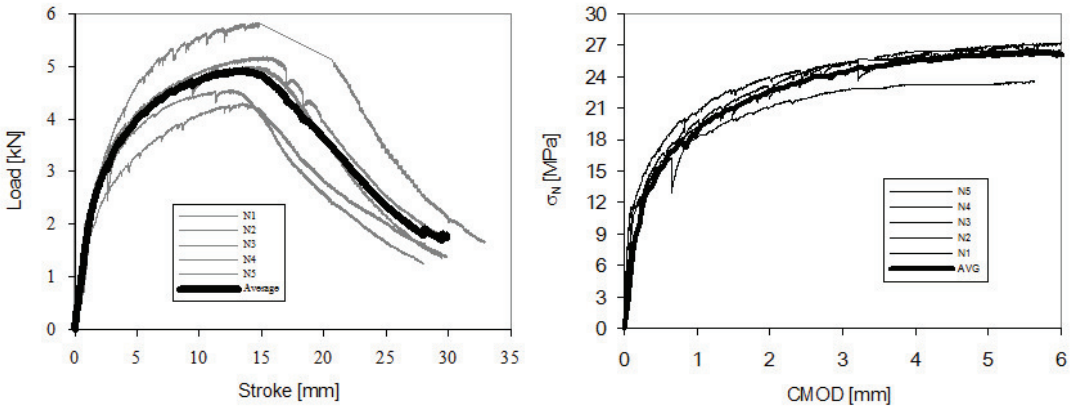

(a) (b)

Figure 4.7: Results curves (a) load stroke, (b) stress COD, [19]

the CNR-DT204 Guidelines [89] and Ferrara et al. [18]. Two characteristic lengths were taken into account: 200 mm pre-peak and the thickness of the specimen (23 mm) after the peak. The first cracking strength was computed as the average of the maximum nominal stresses values for a crack opening value w_I equal to 0,1 mm. On the contrary of [18], the composite material did not show a unique peak stress, so a conventional COD range $0 \div 0,7$ mm was considered (table 4.3).

COD_{peak}	0.7 mm
ϵ_{peak}	0.7 mm
l_{COD}	$3.5 \cdot 10^{-3}$
f_{If}	10.82 MPa
f_{peak}	17.94 MPa
β	2.36
$\sigma_{pre-peak}$	4.13 MPa
σ_{peak}	9.30 MPa

Table 4.3: Parameter of constitutive law

The value of σ_{peak} depends on β_1, value equal to 1.93 calibrated by inverse analysis to fit the

experimental results. The final results, obtained by averaging 5 tests, are summarized in table 4.4, 4.5, fig. 4.8 and more details are shown in [19].

$f_{eq,1}$ $[MPa]$ w=1-1.2 mm	$f_{eq,2}$ [MPa] w=2.6-3.5 mm	f_{Fts} [MPa]	**COD** f_{Fts} [mm]	f_{Ftu} [MPa]	**COD** f_{Ftu} [mm]
20.11	24.53	9.05	1.1	8.24	3.05

Table 4.4: Post peak parameters

Point	**Stress** [MPa]	**w**[mm]	**characteristic length** [mm]	**strain**[-]
A	4.13			$8.98 \cdot 10^{-5}$
B	9.30	0.7	200	$3.5 \cdot 10^{-3}$
C	9.05	1.1	23	$4.64 \cdot 10^{-2}$
D	8.24	3.05	23	0.13

Table 4.5: Stress strain value of tensile law of UHPFRC

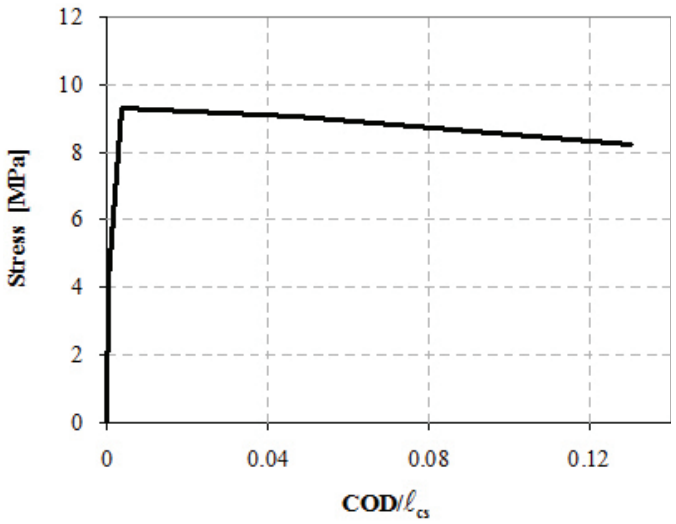

Figure 4.8: Tensile stress strain behaviour UHPFRC

4.2 TRM

Textile reinforced mortar exhibits a complex mechanical behaviour which derives from the heterogeneity matrix-reinforcement as well as from various bond mechanism between filament and adhesion at the fibre-cement interface. This contribution aims at analyzing the TRM behaviour highlighting the influence of several parameters considered as critical for the mechanical performances such as the nature of fibres, the reinforcement ratio, the geometry and interlacing of fabric, the impregnation of fibre, the curing procedure, the features of the matrix (bearing resistance, aggregate size, workability) etc. The mechanical characteristics of fabric and of composite material were determined through uniaxial tensile tests.

4.2.1 Concrete matrix

The specific properties of TRM require special rheological properties and a defined maximum grain size of the concrete to penetrate the mesh. Therefore, special concrete matrices adjusted to textile reinforced concrete were developed. Starting from the matrix used for HPFRCC, different matrix compositions were taken into account with different water-binder ratios and superplasticizer-cement ratios to enahance the workability. A small maximum grain size (<600 μm) was used and hence the matrix can be considered as mortar, but since it offered high performances it can be called fine grained concrete. One main aspect was to get full penetration inside the mesh, in order to guarantee efficient bond. So the consistency of concrete has to be adjusted according to the dimension of mesh pattern. In the case of hand lay up technique highly flowable consistencies are required, while for the lamination or pultrusion process plastic consistencies are necessary. Different mixture compositions were considered with superplasticizer-cement ratios of 7.3%, 8.3%, 9.3%, 10.3%. According to Standard Guidelines UNI EN 196-1[90], the bending resistance of mortar is defined by 3-point bending test on beam specimen (40 x 40 x 160 mm^3) with a load control of 50 N/s and the compressive tests are carried out on halves of the prism broken by bending tests. In order to estimate the mean axial tensile strength f_{ctm} from the mean flexural tensile strength $f_{ct,fl}$ the coefficient A_{fl} was used, according to the Model Code definition:

$$A_{fl} = \alpha_{fl} \cdot h_b^{0.7} / (1 + \alpha_{fl} \cdot h_b^{0.7})$$

where $\alpha_{fl} = 0.06$ h_b=is beam depth (40 mm) A_{fl}=2.26.
The results for different mix designs (M1, M2, M3, M4) are reported in the following tables from 4.6 to 4.9 for different superplasticizer-cement ratios. All the details concerning the matrix compositions are available also in appendix A.

Mix 1	
component	[kg/m^3]
Cem I 52.5	600
Sand 0-600 μm	957
water	209
Superplasticizer (Hp)	44
Slag	500

Table 4.6: Mix design M1 w/b=0.19 and Hp/c=7.3%

Mix 2	
component	[kg/m^3]
Cem I 52.5	600
Sand 0-600 μm	957
water	209
Superplasticizer (Hp)	49.8
Slag	500

Table 4.7: Mix design M2 w/b=0.19 and Hp/c=8.3%

The average values are reported in table 4.12 for the tensile and compressive strength; the fresh state properties of concrete were measured by means of slump test and flow time. In the first test the fresh concrete was poured in a slump cone and the flow was measured on a horizontally

Mix 3	
component	[kg/m^3]
Cem I 52.5	600
Sand 0-600 μm	957
water	209
Superplasticizer (Hp)	56
Slag	500

Table 4.8: Mix design w/b=0.19 and Hp/c=9.3%

Mix 4	
component	[kg/m^3]
Cem I 52.5	600
Sand 0-600 μm	957
water	209
Superplasticizer (Hp)	61.8
Slag	500

Table 4.9: Mix design M4 w/b=0.19 and Hp/c=10.3%

Mix 5	
component	[kg/m^3]
Cem I 52.5	600
Sand 0-600 μm	928
water	220
Superplasticizer (Hp)	44
Slag	500

Table 4.10: Mix design M5 w/b=0.20 and Hp/c=7.3%

Mix 6	
component	[kg/m^3]
Cem I 52.5	600
Sand 0-600 μm	855
water	248
Superplasticizer (Hp)	44
Slag	500

Table 4.11: Mix design M6 w/b=0.225 and Hp/c=7.3%

Hp/c [%]	f_{ct} [MPa]	f_c [MPa]	slump tets [mm]	flow time [sec]
7.3%	8.05	111.46		
8.3%	6.68	100.57	290	6.59
9.3%	6.02	100.61	300	4.4
10.3%	6.88	99.17	310	3.4

Table 4.12: Comparison for different quantity of superplasticizer

aligned glass plate; in the second test the flow was measured according to test methods for self compacting concrete. A V shaped funnel was filled with the fresh concrete and after that the bottom side was opened. The time that concrete needed to flow through the funnel was measured. The best performance in terms of resistance capacity was reached by the first mixture composition, but not for the workability properties.

Another considered parameter was the water-binder ratio and the following quantities 0.19, 0.20 and 0.225 were taken into account with a fixed value of superplasticizer (7.3%). The mix design and the strength parameters are reported in the following tables from 4.10 to 4.11.

The comparison in terms of tensile and compressive strength is shown in table 4.13. The compressive strength was reduced of about 30%. After these considerations the mix design used

w/b	Hp/c	f_{ct} [MPa]	f_c [MPa]
0.19	7.3%	8.02	112.47
0.20	7.3%	8.6	86.33
0.225	7.3%	6.56	76.91

Table 4.13: Comparison of resistance value for different water/binder ratios

for the TRM was the M1 and in some cases, where the workability was not good enough, the mix M3. After obtaining high compressive and tensile strength in all the investigated mix designs, the main problem remained the casting phase. As a matter of fact, if the mortar was not fluid enough, it was very difficult to spread it uniformly in order to obtain a 6 mm thick layer.

4.2.2 Fabric

The properties, the amount and the arrangement of the used fabric have a significant influence on the performances of the composite material. Therefore, the fiber and textile have to satisfy different demands. For an effective reinforcement the features are a Young modulus much higher than that of the matrix, high fiber toughness and breaking elongation. To define the great influences on the bearing behavior of the composite, many textile fabrics were considered and they were different in their basic properties. The mechanical characteristics of the textile reinforcement materials were determined by means of tensile tests in the warp direction with an electromechanical press INSTRON 5867 (maximum capacity 30 kN). For each type of fabric at least 3 samples of size 400 x 70 mm (size equal to that of the TRM specimen) were tested. In the 70 mm width a variable number of warp yarns were included depending on the mesh geometry. The fabrication technique was leno weave, where two warp wires are interlaced with the weft. On the same type of textile, the number of wires remained constant. The tests were performed with a displacement control equal to 1.67 mm/s and with a pressure, on the edge of the specimen, equal to 3.4 bar, fig. 4.9. At the sample ends, 4 layers of paper tape (5 cm high) were applied to allow a better adherence with the clamping device and to uniformly distribute the load. After several preliminary attempts, three different AR-glass fabrics (F1, F2 and F3) were adopted to

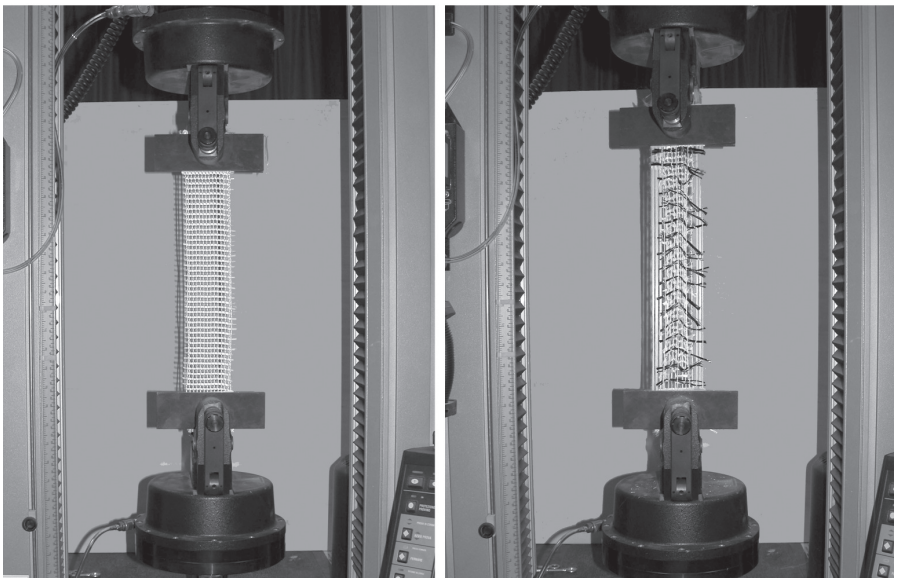

Figure 4.9: Set up of fabric tensile test

	F1	**F2**	**F3**
Material	AR-glass	AR-glass	AR-glass
Fabrication technique	Leno weave	Leno weave	Leno weave
warp wire spacing [mm]	4.4	4.9	4.9
weft wire spacing [mm]	5.0	7.1	10.1
warp [Tex]	2 x 320	2 x 640	2 x 1200
weft [Tex]	640	1200	1200
warp filament [μm]	14	14	19
weft filament[μm]	14	19	19
maximum tensile load [kN]	3.67	6.58	11.02

Table 4.14: Characteristics of fabric F1, F2, F3

reinforce the concrete matrix. The geometrical characteristics of each fabric are reported in table 4.14. The choice of these reinforcements has been done after several investigations, in order to optimize performances in terms of ductility and bearing capacity of the composite. The parameters involved in the previous studies, were the fabric geometry (dimension of the mesh), the roving size, the coating impregnation and also the fiber nature (Carbon and AR-glass). The experimental results in terms of load - stroke of the actuator are shown in fig. 4.10 and table 4.15, where in fig. 4.10d the average curves were compared. In the graphs, the thicker line indicates the average curve on 10 tests. The increment of the tensile load is proportional to warp cross section.

The nominal stress can be computed dividing the tensile load by the nominal area of the warp roving taking into account the number of roving for each fabric on 70 mm width (table 4.16). The area of one roving is computed dividing the Tex $[g/km]$ by the material density (for AR-glass is equal to 2500 kg/m^3). The tensile strength of the yarn was significantly lower than the total tensile strength of all filaments, because of the unequal loading of the filaments inside the yarn and also because of material defects. These reasons were supported by Curbach

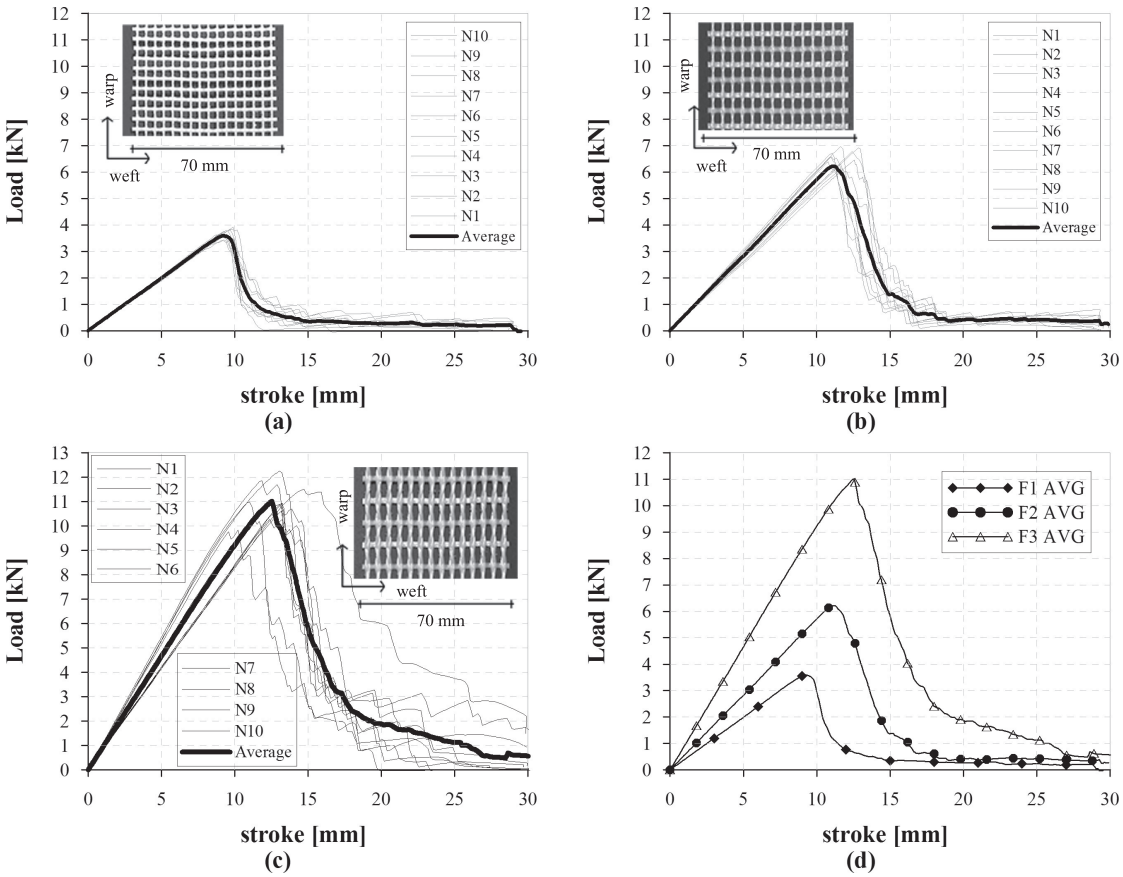

Figure 4.10: Load versus stroke curves for (a) F1, (b) F2 (c) F3 and (d) comparison F1, F2 ,F3

	F1 [kN]	F2 [kN]	F3 [kN]
N1	3.65	6.91	11.85
N2	3.44	6.45	10.97
N3	3.91	6.12	9.83
N4	3.78	6.77	11.04
N5	3.81	6.31	12.26
N6	3.68	6.58	10.27
N7	3.83	6.58	10.61
N8	3.58	6.71	10.92
N9	3.61	6.39	10.94
N10	3.47	6.97	11.50
Average	**3.67**	**6.58**	**11.02**
STD	0.16	0.27	0.72
STD %	4.25	4.09	6.52

Table 4.15: Fabric tensile load

theory ([4]) where the stress of filament (diameter 13 μm) was 2300 MPa and the corresponding resistance of yarn (310 tex) was about 1300 MPa.

	F1	F2	F3
warp roving on 70 mm	16	14	14
nominal area $[mm^2]$	4.096	7.168	13.440
nominal stress [MPa]	896	918	820

Table 4.16: Nominal stress value

For ensuring good handling, the fabric was fixed with coating in his ideal position. Coating is an adhesive applied with a solvent or a plastic melted to bond the fiber together to give a good physical stability. Different coatings (A, B, C, D), used on textile produced by Gavazzi industry, were considered to firstly evaluate the influence on tensile strength and after on the composite bearing capacity (fig. 4.11). The coatings are made of Styrene Butadiene and differ for the capacity to confer rigidity to the fabric. This property increases with the letter from A to D.

The fabric without coating (fig. 4.11a) showed the lowest tensile strength while the best performances were achieved by coating C and D, figs. 4.11d and 4.11e. The comparison of different fabrics is reported in fig. 4.11f. Also carbon fibre was taken into account. Fabrics, with the same geometry of F2 with the insertion of warp carbon rovings with no coating and coating C, were investigated fig. 4.12. The presence of coating gave stability to the fabric and all the filaments could be activated at the same time while in the fabric without coating single filaments were activated at different steps. For this reason the tensile resistance of fabric without coating was lower.

Other kinds of fabrics were considered (fig. 4.13) such as F4, with both warp and weft made of carbon fibers, F5 AR glass fabric where just the weft rovings were made of carbon and F6 where some warps and wefts were made by carbon, with and without coating. The geometric characteristics of fibers are shown in table 4.17 and the results are summarized in fig. 4.13. The best performance was obtained with fabric F6 (coating B) due to the dense mesh and due to the presence of impregnation that glued all filament to create a homogeneous cross section.

4.2.3 Production technology

The hand lay up technique is the simplest and most commonly used manufacturing method for fiber reinforced composite such as organic resin and glass fiber. This method has been adopted for TRM specimens due to the simple fabrication technology, low production costs and the possibility to produce complex shaped specimens. A suitable amount of matrix was spread over a formwork with a transparent bottom plate introduced to check the penetration of the matrix inside the mesh. Some overlapping steel rails were placed, in order to fix the fabric at different

	F4	F5	F6
Material	Carbon	AR-glass and weft carbon roving	AR-glass and carbon
Fabrication technique	Leno weave	Leno weave	Leno weave
warp [Tex]	400	640	640 AR glass and 400 C
weft [Tex]	400	1200 AR glass and 400 C	1200 AR glass and 400 C

Table 4.17: Geometric characteristics of fabric F4, F5, F6

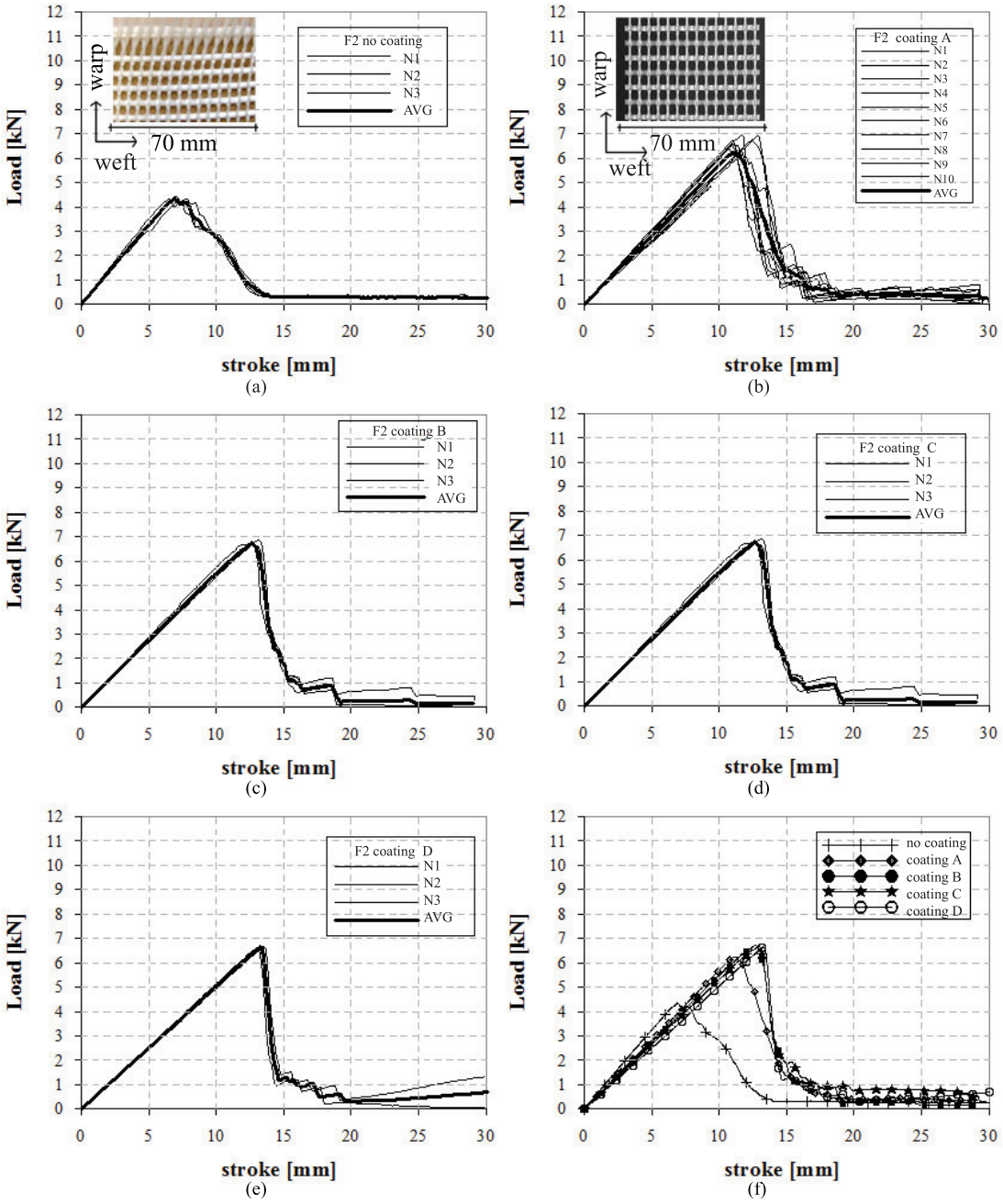

Figure 4.11: Different coating applied on F2 fabric, (a) no coating, (b) coating A, (c) coating B, (d) coating C, (e) coating D, (f) comparison

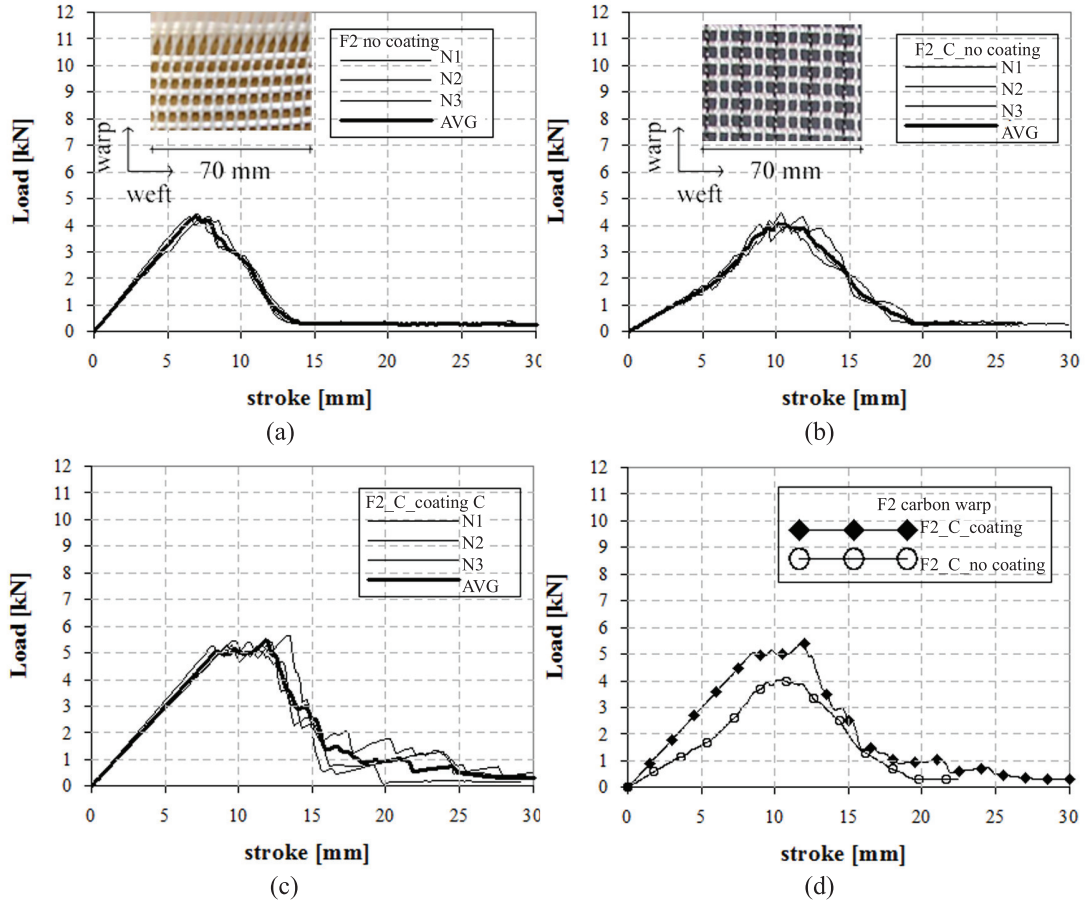

Figure 4.12: Influence of carbon roving in fabric F2 (a) F2 no coating, (b)F2-C no coating, (c) F2-C coating C, (d) comparison F2-C with and without coating

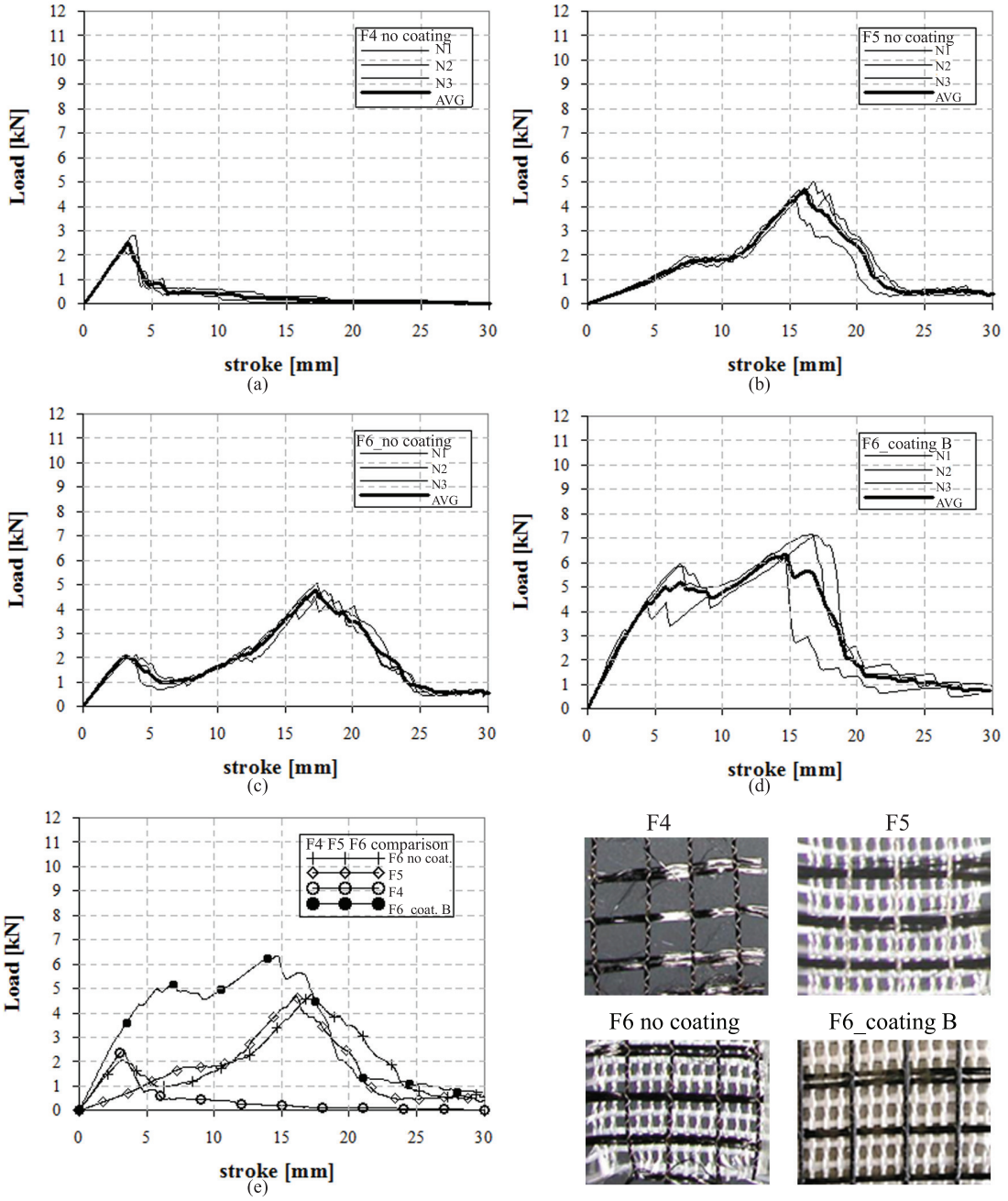

Figure 4.13: Different fabrics with carbon roving in warp and or weft direction, (a) F4 no coating, (b) F5 no coating, (c) F6 no coating, (d) F6 coating B, (e) comparison, (f) fabrics

levels. By using a roller, the air bubbles presented in the matrix could be significantly reduced. After that, the textile was tightened and fixed at the edge of the formwork and another layer of matrix was spread. A multilayer specimen can be reproduced by iterating this procedure. The hand laminating technique (fig. 4.14) is not belonging to the traditional concrete technology and a disadvantage were the rheology properties of fresh cement that must be able to penetrate the open texture of the reinforcement. The specimen were demoulded after one day and they were cured in a climatic chamber at 98% RH, placed in vertical position so that the shrinkage was the same on both sides, preventing planarity losses.

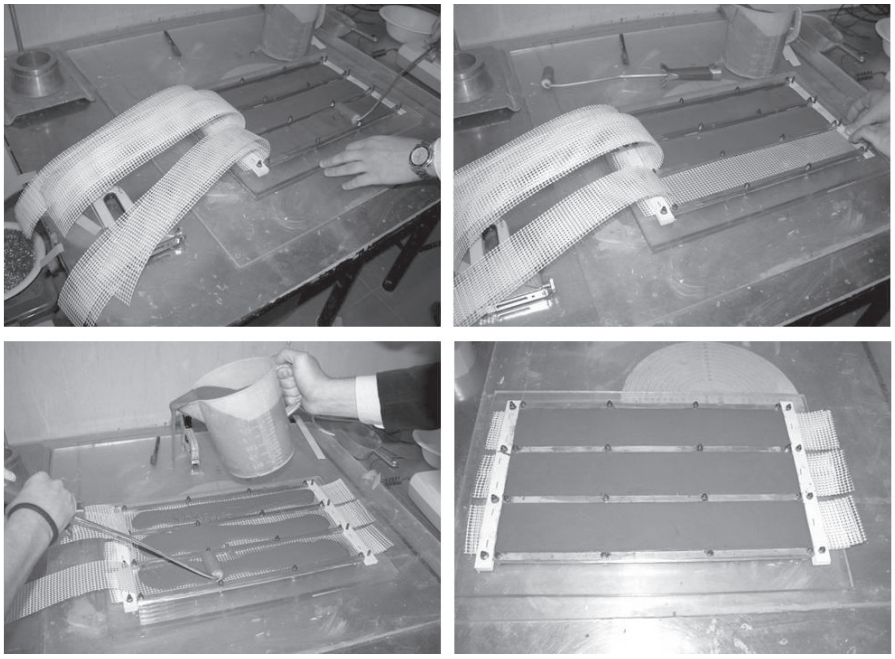

Figure 4.14: Production process of hand lay up technique

4.2.4 Composite material

In order to understand the role played by the number and the position of fabric layers, several TRM specimens, 400 mm long, 70 mm wide and 6 mm thick with different reinforcement ratios were considered:

- 1 single fabric in the middle
- 2 overlapped fabrics in the middle
- 2 layers divided by a thin layer of mortar
- 3 layers divided by a layer of mortar with a total thickness of 12 mm

The load bearing behavior was evaluated by means of direct tensile tests. At the edge zones perspex plates 75 x 70 mm or steel plates 55 x 70 mm were glued to homogeneously distribute the load, fig. 4.15. To prevent torsional and bending moment due to a misalignment of the

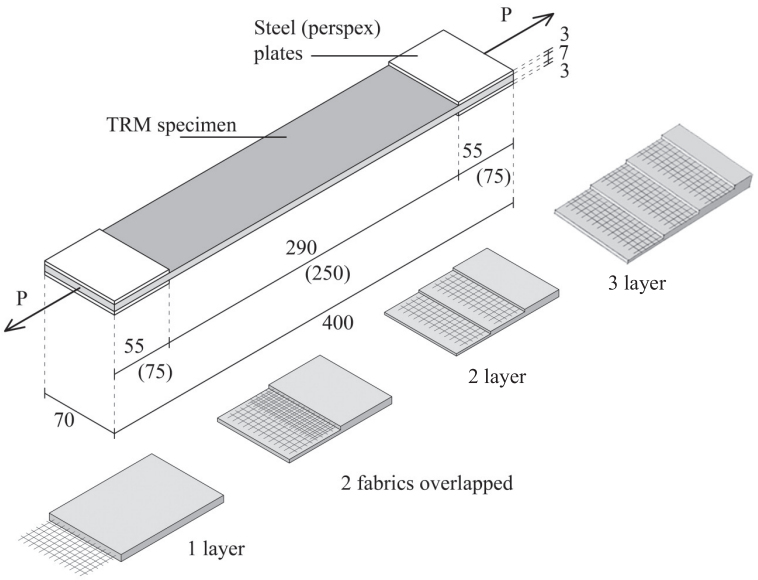

Figure 4.15: TRM specimen dimensions

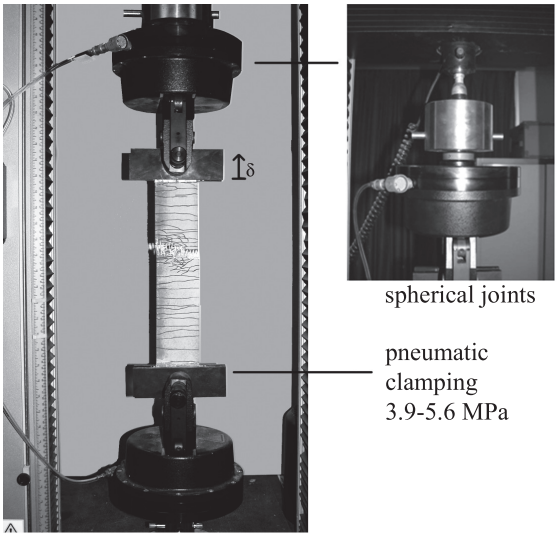

Figure 4.16: Set up tensile test

constraints, spherical joint were introduced. The tests were carried out at a constant displacement rate of 0.02 mm/sec, fig. 4.16.

The stress strain diagram of textile reinforced mortar under uniaxial loading was characterized by a non linear curve that can be divided in three sections, fig. 4.17. At the beginning the stiffness of the uncracked material (stage I) corresponded to the Young modulus of the matrix. Overcoming the tensile resistance, the first crack occurred and the load in the cracked area was transferred by the fabric. Enhancing the tensile load, a multicracking pattern was developed (state IIa). The cracking space and width depended on the property of the reinforcement (resistance capacity and bond behaviour). In the multicracking branch the load increased of very low amount. In state IIb no more cracks appeared and while the load increased, the filaments were strained up until reaching the ultimate tensile resistance of the reinforcement. The stiffness in state IIb should be equal to the Young modulus of the fabric but, as in steel reinforced concrete, tension stiffening effect occurred and the slope remained parallel to the stress strain curve of the pure fabric. The AR glass and Carbon fabric did not develop a ductile branch (state III) because they do not have plastic capacity; for this reason, the TRM failed when the ultimate strength of the fabric was reached.

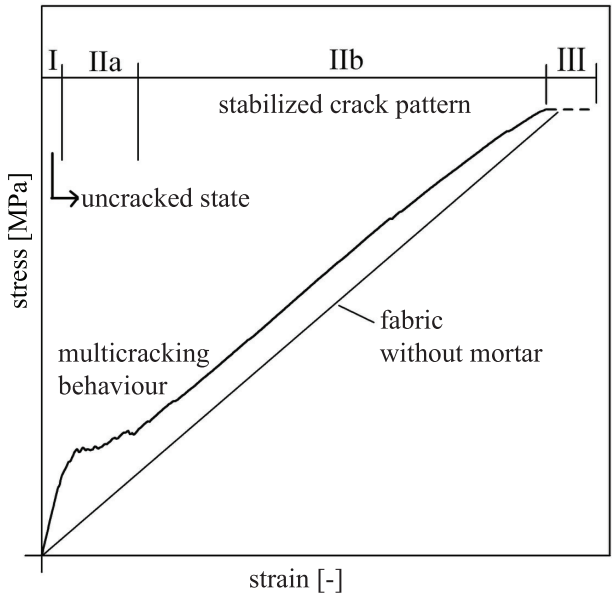

Figure 4.17: Stress strain diagram of TRM under uniaxial loading

Numerous tests were performed to understand the influence of many parameters on the different branches of tensile response. In particular, the following aspects are discussed in the thesis:

- geometric reinforcement ratio and position inside the specimen thickness
- fabric geometry
- different coating
- curing procedure (air, water, oven)

- strain rate
- size effect
- high temperature.

Geometric reinforcement ratio effects

The first variables considered were the quantity of fabric and the position in the thickness. Fabrics F1 and F2 with coating A were used to obtain different percentage of reinforcement by adopting more than one layer in the thickness. The reinforcement area (Af) has been computed by means of the Tex of each single roving, the number (n) of roving in the specimen width (16 for F1 and 14 for both F2 and F3) and the AR-glass density (ρ_d):

$$A_f = n \cdot Tex/\rho_d \tag{4.1}$$

In the case of fabric F1 and F2 different geometrical reinforcement ratios (Af/Ac where Af is the equivalent section area of AR-glass fabric and Ac is the cross section of the specimen) were achieved by using different fabric layers in the specimens thickness:

- 1 layer (ρ=0.97%, 6 mm thick)
- 3 layers (ρ=1.46%, 12 mm thick)
- 1 layer where 2 fabrics were overlapped called "2 fabrics" (ρ=1.94%, 6 mm thick)
- 2 layers with 2 detached fabrics called "2 layers" (ρ=1.94%, 6 mm thick).

The results are shown in terms of stress vs. strain fig. 4.18. Nominal stress is obtained by dividing the load by the specimen cross section, while normalized displacement is the applied stroke displacement (δ) divided by the initial distance between the clamping edges. It worth noting that, in all the graphs, each average curve is interrupted when the first of the three nominally identical specimens reaches the ultimate normalized displacement; thus the peak of the average curve is different from the average of peak values shown in table 4.18. For each reinforcement ratio 6 tests were performed. Typical crack patterns were pointed out for each specimen fig. 4.19.

specimen	thickness [mm]	maximum load[kN]	δ_u [mm]	σ_{max} [MPa]	ϵ_u [-]	$\sigma_{cracking}$ [MPa]	$\epsilon_{cracking}$ [-]	$\epsilon_u/\epsilon_{cracking}$ [-]
ρ=0.97%	6.8	3.81	1.98	8.02	0.0080	5.92	0.0022	3.96
ρ=1.46%	12	9.25	6.52	10.98	0.0219	2.73	0.0020	11.04
ρ=1.94%	7.1	6.72	5.19	13.52	0.0210	6.40	0.0026	8.40
ρ=1.94%	6.3	7.92	6.33	17.88	0.0219	4.57	0.0009	24.97

Table 4.18: Average on 6 values for each amount of reinforcement, Mix M1

Increasing the percentage of reinforcement, the peak load enhanced and crack pattern became very dense. Looking at the case F1 - 1 fabric (Figs. 4.18a, 4.19a,b), the second and the third branches typical of TRM multi-cracking behavior are absent. Looking at the crack pattern, just few cracks appear in the specimen; this should be explained by an energy release at the onset of crack that is too large to allow stress redistribution between mortar and reinforcement, thus causing the failure of the composite itself. This situation is similar to a RC section characterized

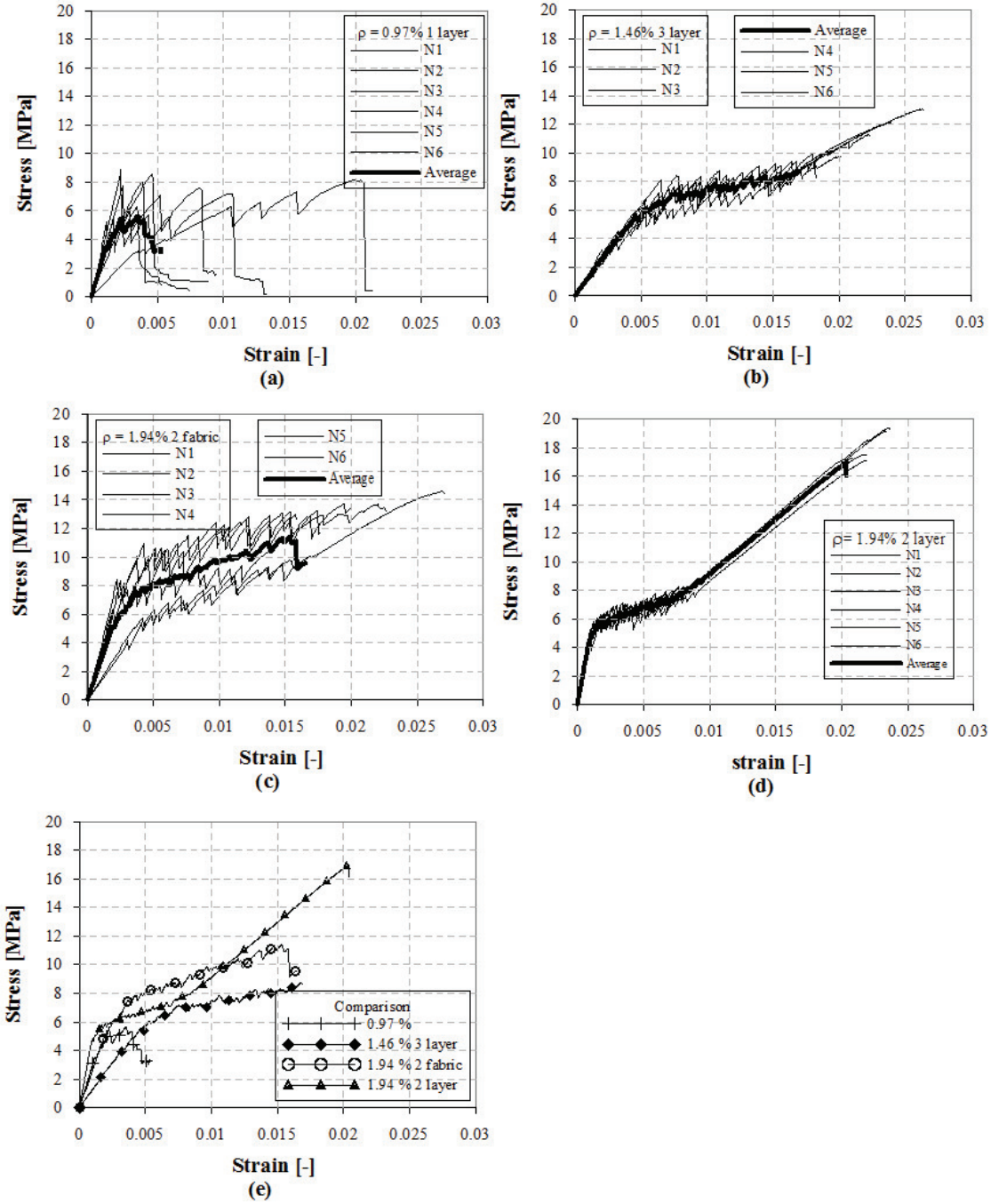

Figure 4.18: TRM (fabric F1) Stress-strain curves (a) ρ=0.97%, (b) ρ=1.46%, (c) ρ=1.94% 2 fabrics, (d) ρ= 1.94% 2 layer, (e) comparison

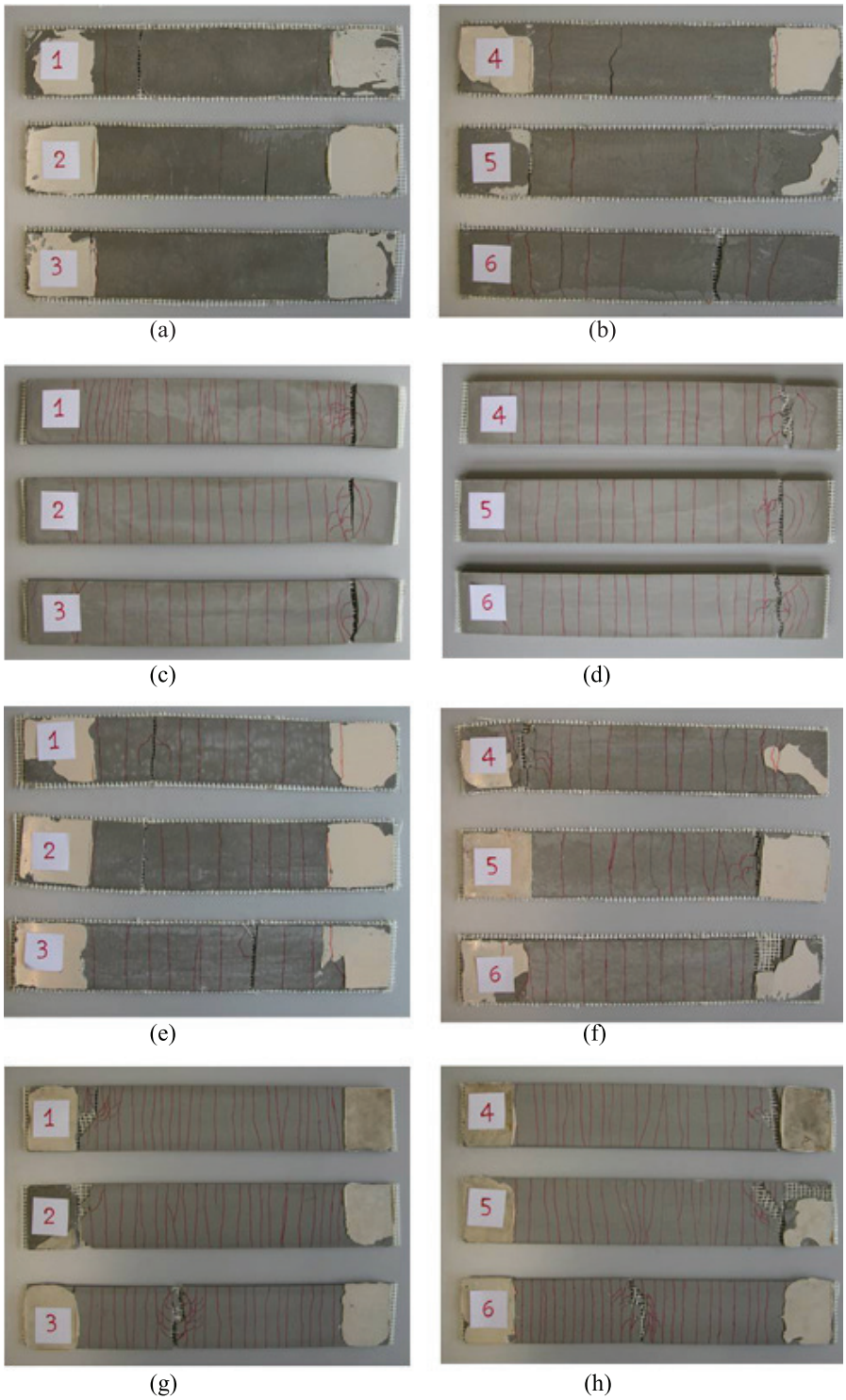

Figure 4.19: Crack pattern F1: (a) (b) 0.97%, (c) (d) 1.46%, (e) (f) 1.94 2 fabric%, (g) (h) 1.94 2 layer%

by a minimum reinforcement endowed by a negligible ductility. The case with three fabric layers corresponded to a low reinforcement ratio (1.46%, 12 mm) due to the difficulty to insert three textile layer in 6 mm with hand lay up technique. The specimen made by 3 layers was tested without the presence of steel plates due to the thickness of 12 mm. Hence, the first cracking strength was lower due to the lack of redistribution of load at the clamping areas figs. 4.18b and 4.19c,d. In the case F1 - 2 fabrics (Fig.4.18c) a bond failure prevents the onset of the branch IIb despite the increase of the total reinforcement, causing a progressive sliding of the fabric highlighted by a longer IIa branch. The best performance was reached by ρ=1.94% 2 layer, where bond between matrix and fabric was better, compared to two overlapped fabrics, because the area in contact with the cement paste was greater, fig. 4.18d. The maximum stress was 17.88 MPa (table 4.18) and cracks were very dense (one for each weft step), maximizing the mechanical performances, fig. 4.19g,h. When two fabrics were in contact, sliding phenomena between fabric wires and matrix occured. Bond is the fondamental parameter to determine the property of a composite material. The TRM behaviour is quite different if compared to steel reinforced concrete due to the inhomogeneity of the mesh cross section. Textile is composed by thousands of filaments where only the external ones are in contact with the matrix, while the inner filaments can slip inside the roving. In Banholzer theory [5] the roving pull out was schematized with a cylinder model made by concentric rings where each of them was composed by several filaments. The failure started from the outside filaments until reaching the inner filaments fig. 4.20. According to this model, the case where fabrics were detached by a thin layer

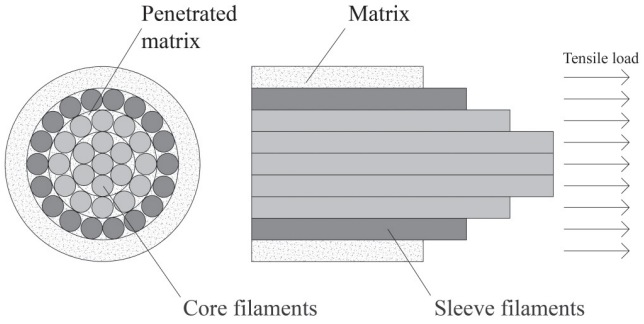

Figure 4.20: Roving pull out taken from Banholzer theory

of mortar, showed the best performance compared to 2 overlapped fabrics due to a greater area in direct contact with the matrix. The tensile strength varied from 8 to 17.88 MPa (table 4.18) and the ultimate strain was of about 2%. Good repeatability for all the tests was noticed with a scattering around 1%. The three layers showed a cracking resistance lower than the one of the sole matrix, due to the presence of defects in the specimen. The same procedure has been done for specimens made with mix design M3 and reinforced with fabric F2 coating A. Three tensile tests were performed for each nominal reinforcement ratio:

- 1 layer ($\rho = 1.71\%$)
- 3 layers ($\rho = 2.40\%$)
- 1 layer two overlapped fabrics (“2 fabrics” $\rho = 3.42\%$)
- 2 detached layers (“2 layers” $\rho = 3.42\%$)

The results in terms of stress vs. strain are presented in fig. 4.21. The crack pattern are shown in fig. 4.22 for different reinforcement quantities and the average values are presented in table 4.19.

specimen	thickness [mm]	max load[kN]	δ_u [mm]	σ_{max} [MPa]	ϵ_u [-]	σ_{cr} [MPa]	ϵ_{cr} [-]	ϵ_u/ϵ_{cr} [-]
ρ=1.71% 1layer	6.3	5.02	5.57	11.36	0.0193	3.47	0.0008	24.71
ρ=2.40% 3layers	12.1	12.58	6.46	14.82	0.0219	4.86	0.0018	13.43
ρ=3.42% 2 fabrics	7.0	10.95	7.08	22.37	0.0245	4.48	0.0010	25.73
ρ=3.42% 2 layers	6.2	10.65	6.45	24.42	0.0224	4.62	0.0009	24.68

Table 4.19: Average on 3 values for each amount of reinforcement F2 (a) 1.71% 1 layer, (b) 2.40% 3 layers, (c) 3.42% 2 fabrics, (d) 3.42% 2 layers, mix design M3

In all these cases the three branches typical of TRM tensile tests were clearly visible. The best performance in terms of stress was achieved by $\rho = 3.42\%$ 2 layers, fig. 4.21d and table 4.19 showed the comparison in terms of stress versus strain for all the reinforcement amount and the maximum tensile stress was equal to 24.42 MPa. The ultimate strain was comparable for the following percentages $\rho = 2.40 - 3.42\%$ and it was about 0.02. The cracking strength (table 4.19) was lower than the value f_{ct} equal to 6.02 MPa computed by means of bending tests (table A.4) but it was comparable to the tensile strength obtained, from direct tensile test on specimen without fabric, and was equal to 4.77 MPa. Dividing the peak load of TRM specimen by n_{fabric} times the peak load experimentally detected by stretching only the fabric (F1 or F2), an Effectiveness Factor EF can be evaluated. If EF is less than 1, a bond weakness is immediately highlighted. Sometimes EF can be larger than unity, thus experiencing a positive interaction with the matrix which exerts a tension stiffening effect. EF factors are computed and shown in appendix B (B.1, B.2, B.3, B.4). Looking at the results the 2 layers solution is generally characterized by a higher strength than 2 fabrics solution because, despite of the same reinforcement ratio, the 2 layers solution has a large contact surface between matrix and reinforcement. The TRM tensile strength grows from 13.52 MPa to 17.88 MPa for the fabric F1 and from 22.37 MPa to 24.42 MPa for fabric F2, despite a not negligible decrease of EF factor values. Crack distance decreases with increasing reinforcement ratio until a crack at each weft roving is obtained, maximizing the mechanical performances of the composite. The ultimate strains reached in the cases of 2 fabrics and 2 layers are comparable and greater than 2%. Good repeatability was achieved in all the tests with a scattering always smaller than 1%.

The best performance was achieved with the geometric reinforcement ratio equal to 3.42% obtained by 2 detached fabric layers. So this result was compared to the tensile behaviour of a specimen reinforced by 1 layer of fabric F3 coating D (tables 4.14 and 4.15) with $\rho = 3.20\%$ fig. 4.23, table 4.20 and the crack pattern fig. 4.24 was dense.

specimen	thickness [mm]	maximum load[kN]	δ_u [mm]	σ_{max} [MPa]	ϵ_u [-]	$\sigma_{cracking}$ [MPa]
ρ=3.20%	6.2	07.51	7.44	17.13	0.0257	4.03

Table 4.20: Average on 3 values for each amount of reinforcement F3

The optimum amount of reinforcement was obtained by using two detached layers F2 (ρ=3.40%) or a single layer F3 (ρ=3.20%). The comparison between these two solutions is shown fig. 4.23c-d. After the first linear branch, a multicracking phase occurred and the first cracking strength for fabric F2 is higher than for fabric F3 (appendix B fig. B.5 line 10 mm); this difference is

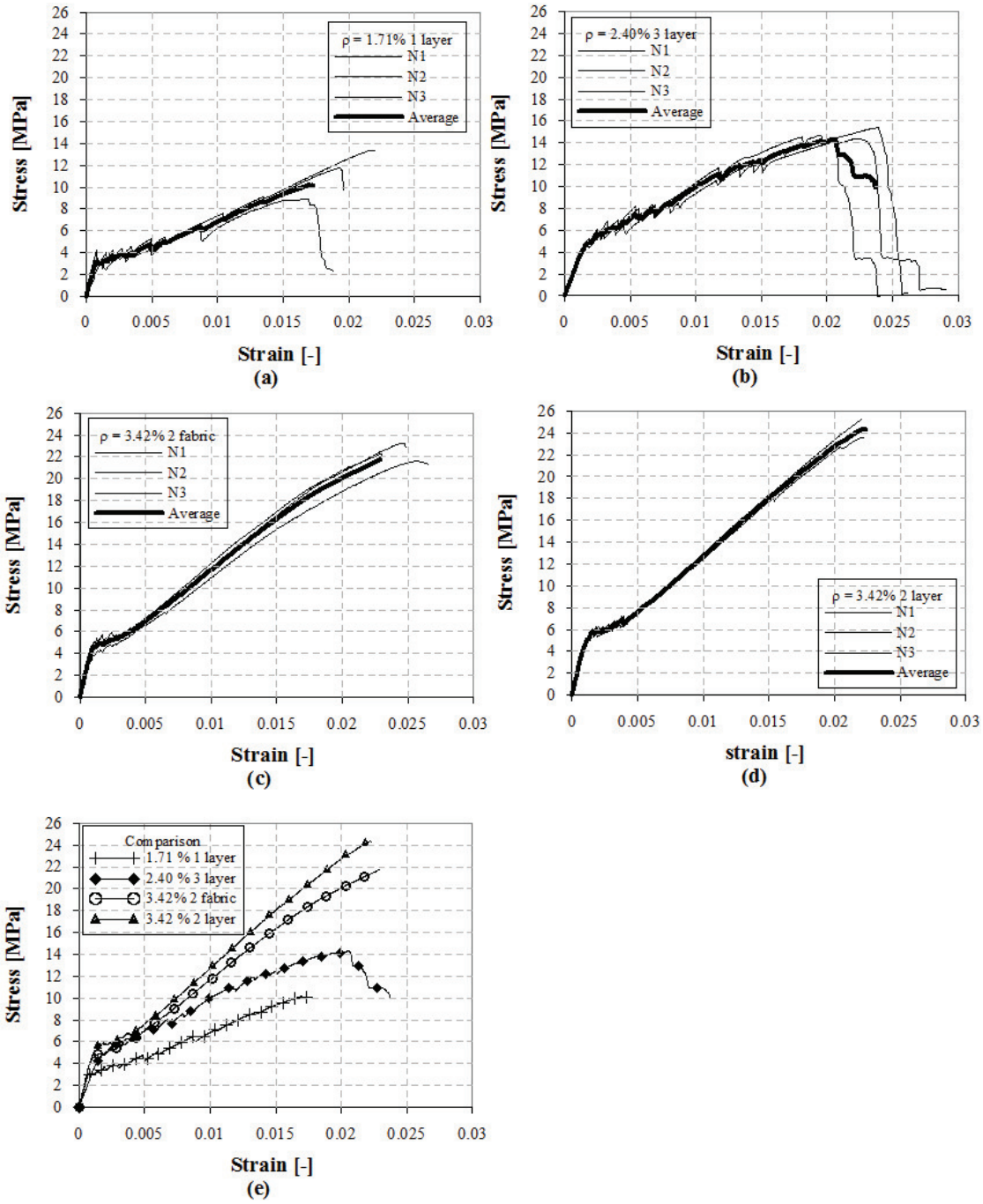

Figure 4.21: Stess-strain curves TRM (fabric F2 mix M3): (a)1.71%, (b) 2.40%, (c) 3.42% 2 fabric (d)3.42% 2 layer (e) comparison

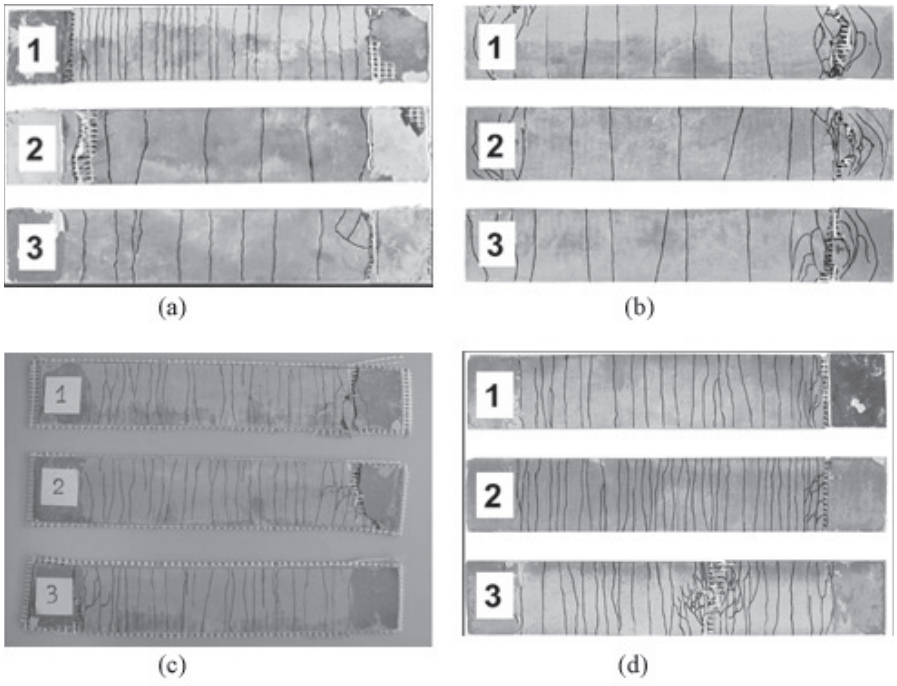

Figure 4.22: Crack pattern fabric F2 for different reinforcement ratio: (a)1.71%, (b) 2.40%, (c) 3.42% 2 fabric (d)3.42% 2 layer

comparable with the scattering of the tensile strength of mortar in different batches and is justified by a further decrease of EF, that reaches 0.68. The EF decrease also affects the stiffness of the last branch, where no further cracks occurred. The peak strength reached is equal to 25 MPa for F2 and to 15 MPa for F3. The ultimate strain is lower than 2% and the crack pattern for the samples with fabric F3 showed a larger distance between cracks (about every 30 mm fig. 4.24). As a matter of fact, the bond area in contact with the cementitious matrix is larger in the case of 2 layers so that the roving is better anchored to the matrix. According to Banholzer theory, in fabric F3 the number of inner filaments, that can slide between each other is higher, while with two layers more area is in contact with the matrix enhancing the bond mechanism. For this reason, the solution with two layers seems to be the best, even tough the solution with 1 layer can be easier in retrofitting applications.

Influence of coating

To understand the influence of coating in the tensile behaviour, these samples reinforced with 2 layers of fabric F2 were considered:

- 3 specimens made by 2 fabrics without and with coating A, mix design M1;
- 3 specimens made by 2 fabrics coating B and mix design M6;
- 3 specimens made by 2 fabrics coating C and mix design M6;
- 3 specimens made by 2 fabrics coating D and mix design M6.

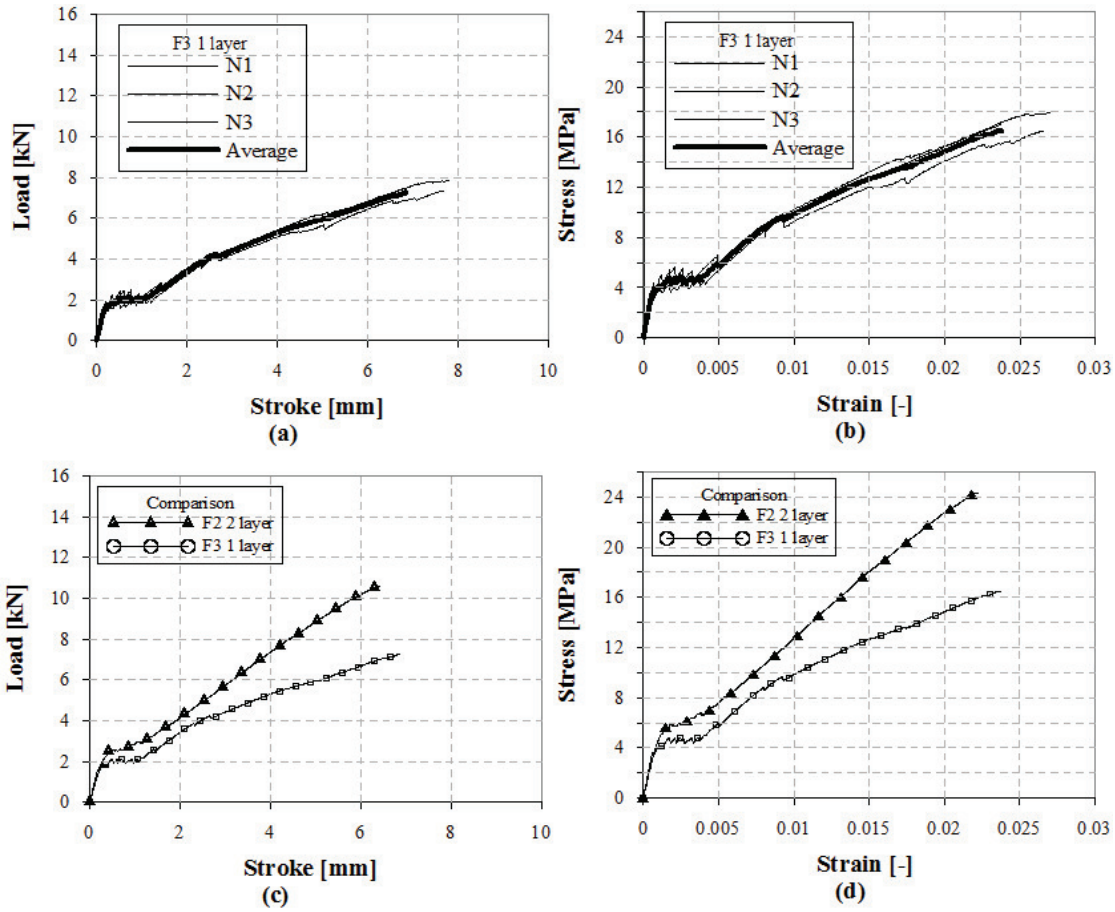

Figure 4.23: Tensile behaviour: (a) (b) TRM reinforced with F3 1 layer, (c) (d) comparison F3 1 layer and F2 2 layer

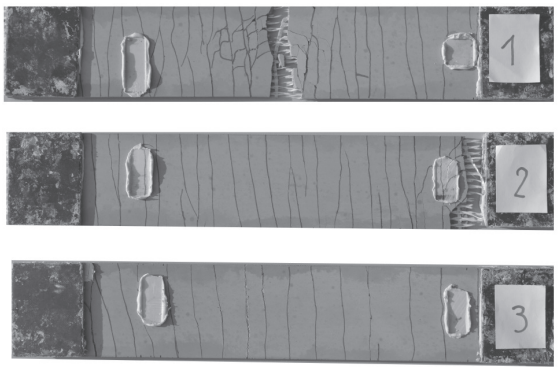

Figure 4.24: Crack pattern TRM reinforced with 1 layer F3

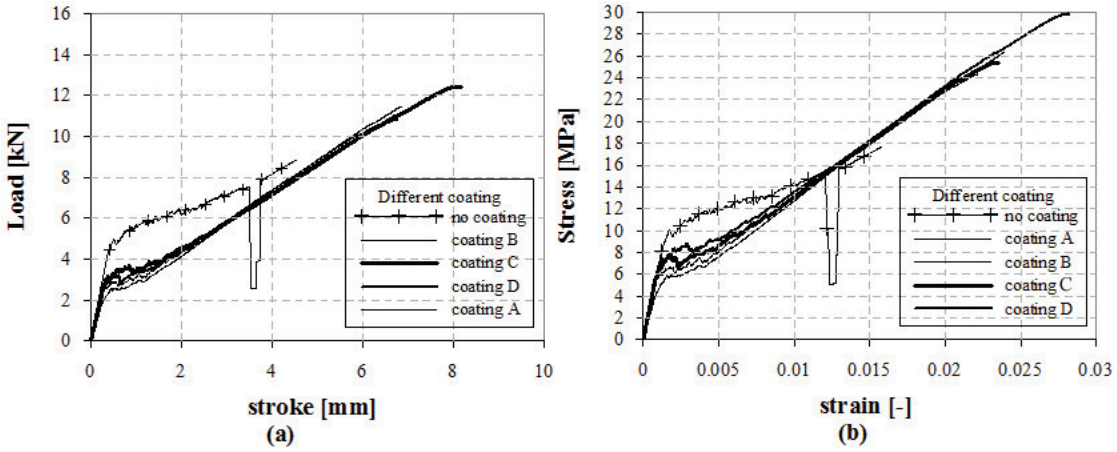

Figure 4.25: Influence of different coatings on TRM reinforced with 2 layers of F2

From the average results curves, it can be noted that maximum stress (29.9 MPa) was achieved by coating C, while in terms of ductility (ratio between ultimate strain and cracking strain) coating B showed the best performance (28.74) table 4.21. The fabric without coating presented the highest multicracking branch but no ductility phase. The fabric without coating was not taken into account as possible solution because no good handling can be guaranteed. The Effectiveness Factor confirmed that coating C is the best solution, table 4.22.

specimen	Mix design	thickness [mm]	max load[kN]	δ_u [mm]	σ_{max} [MPa]	ϵ_u [-]	σ_{cr} [MPa]	ϵ_{cr} [-]	ϵ_u/ϵ_{cr} [-]
no coating	M5	7.1	8.15	3.87	16.41	0.0135	9.29	0.0014	9.49
coating A	M1	6.2	10.65	6.45	24.42	0.0224	4.62	0.0009	24.68
coating B	M6	6.2	12.00	7.32	27.53	0.0255	5.61	0.0009	28.74
coating C	M6	6.0	12.48	8.15	29.93	0.0283	7.74	0.0012	23.77
coating D	M6	6.1	10.96	6.98	25.79	0.0241	6.45	0.00010	25.66

Table 4.21: Average values of tensile tests for different coatings

specimen	P_{TRM} [kN]	n	P [kN]	P_{fabric} [kN]	EF
no coating	8.15	2	4.08	4.34	0.94
coating A	10.65	2	5.33	6.5	0.81
coating B	12.00	2	6.00	6.8	0.88
coating C	12.48	2	6.24	6.71	0.93
coating D	10.96	2	5.48	6.68	0.82

Table 4.22: Effectiveness factor for different coatings

Influence of carbon roving in warp direction

Specimens reinforced by 2 layers of fabric F2-C were subjected to tensile load to evaluate the influence of carbon rovings in the tensile behavior, in comparison with the samples reinforced with 2 layers of F2. Two types of specimens were studied:

- specimens with 2 layers of F2-C no coating mix design M5
- specimens with 2 layers of F2-C coating C mix design M6.

The results showed that in the case of no coating, the specimens reinforced with a fabric with carbon roving reached a multicracking branch fig. 4.26a with higher stresses values than the ones related to F2 without coating fig. 4.26e. In the case of coating also the third branch occurred fig. 4.26c,d and the slope of the curve was stiffer fig. 4.26f due to different elastic modulus between carbon (210 GPa) and glass fiber (70 GPa). The main disadvantage of carbon instead of glass fiber is the cost.

Different weft roving step

Bond in a cementitious matrix is a quite complex issue and it is influenced by fabric geometry and by matrix itself. The textile fabric, as discussed before, has no homogeneous cross section and its bond behavior is governed by inner and outer filaments properties. The influence of weft as a direct anchor plays an important role in the global bond-slip behavior of the fabric. In order to analyze bond in a fabric, the contribution offered by the yarns perpendicular to the load direction and by the joint connection among roving have also to be considered. A schematic model proposed by Soranakom [91] provides sequential stages of debonding and failure of the joints. As the load increases, a series of debonding step is expected, starting from the longitudinal debonding along the roving parallel to the load direction till reaching the anchoring point, which consists in the node where warp and weft are connected. In this thesis, the geometrical anchorage mechanisms, offered by the transverse yarns, was studied by means of tensile tests on specimens with different weft spacing but with the same warp cross section. Starting from fabric F3-1 layer, three nominally identical tests have been performed for different spacing values (10, 20, 30 and 50 mm). The results in terms of nominal stress vs. normalized displacement are reported in Fig. 4.27 and summarized in Table 4.23. Further details can be found in appendix B (fig.B.5). The first cracking strength is in the case of the smallest weft spacing (about 4 MPa), because of the less effective tension stiffening induced along the warp. In bond effectiveness the weft could play a double role: on one hand it could act as a direct anchorage to the warp sliding; on the other hand it represents a defect in the matrix cross section that could favor both warp delamination and/or cracks propagation along weft direction. In the case of small weft spacing the weft defect action prevails on the contribution of the weft as direct anchor. When weft spacing is wider, the tension stiffening action prevails and the first cracking strength reaches values of about 7 MPa. In the case of 30 mm and 50 mm weft spacing, the stiffness of multicracking branch is higher because the process of longitudinal delamination is prevented by a longer bond length. In terms of ductility, the specimens with 10 mm weft spacing are characterized by a larger ultimate strain because the longitudinal crack propagation, caused by the dense presence of defects due to weft, allows the roving to stretch out. Fig. 4.27 shows the different crack patterns: it is possible to observe that, in the case of 30 mm weft spacing, cracks occur also between the weft rovings. It is worth noting that the peak load is roughly the same for all the weft spacing considered. Therefore weft spacing investigated affect only tension stiffening, but never Effectiveness Factor EF (appendix B fig.B.5).

Curing methods

Different shrinkage conditions could have some influence on bond properties. Hence, different curing methods such as air for 28 days, 60°C for 6 days and water for 28 days, were analyzed. Specimen made by mix M3 and reinforced with 1 layer of fabric F3 were cured under these

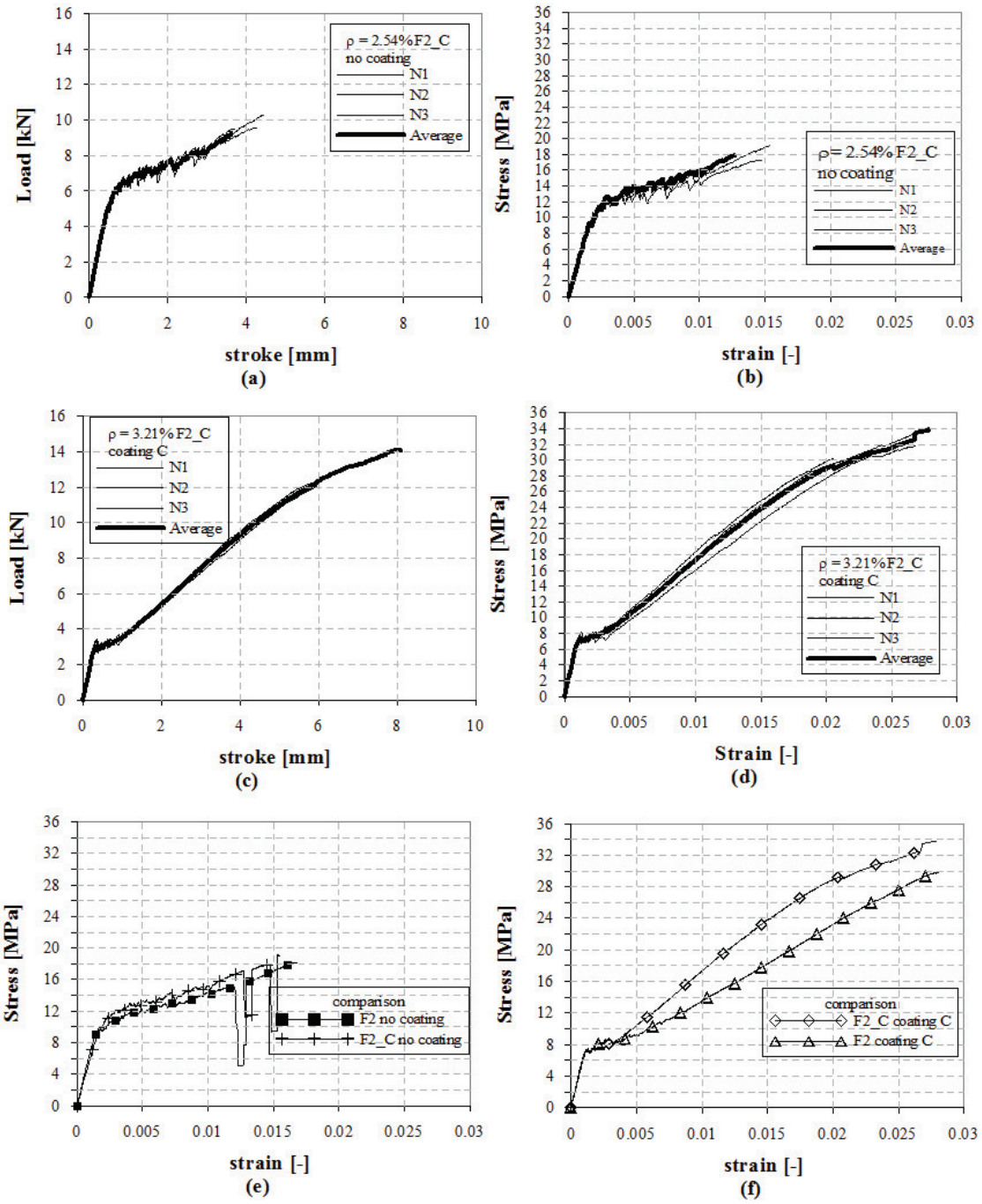

Figure 4.26: Load-stroke and stress-strain results on tensile test F2-C: (a) (b) no coating, (c) (d) coating C, (e) (f) comparison

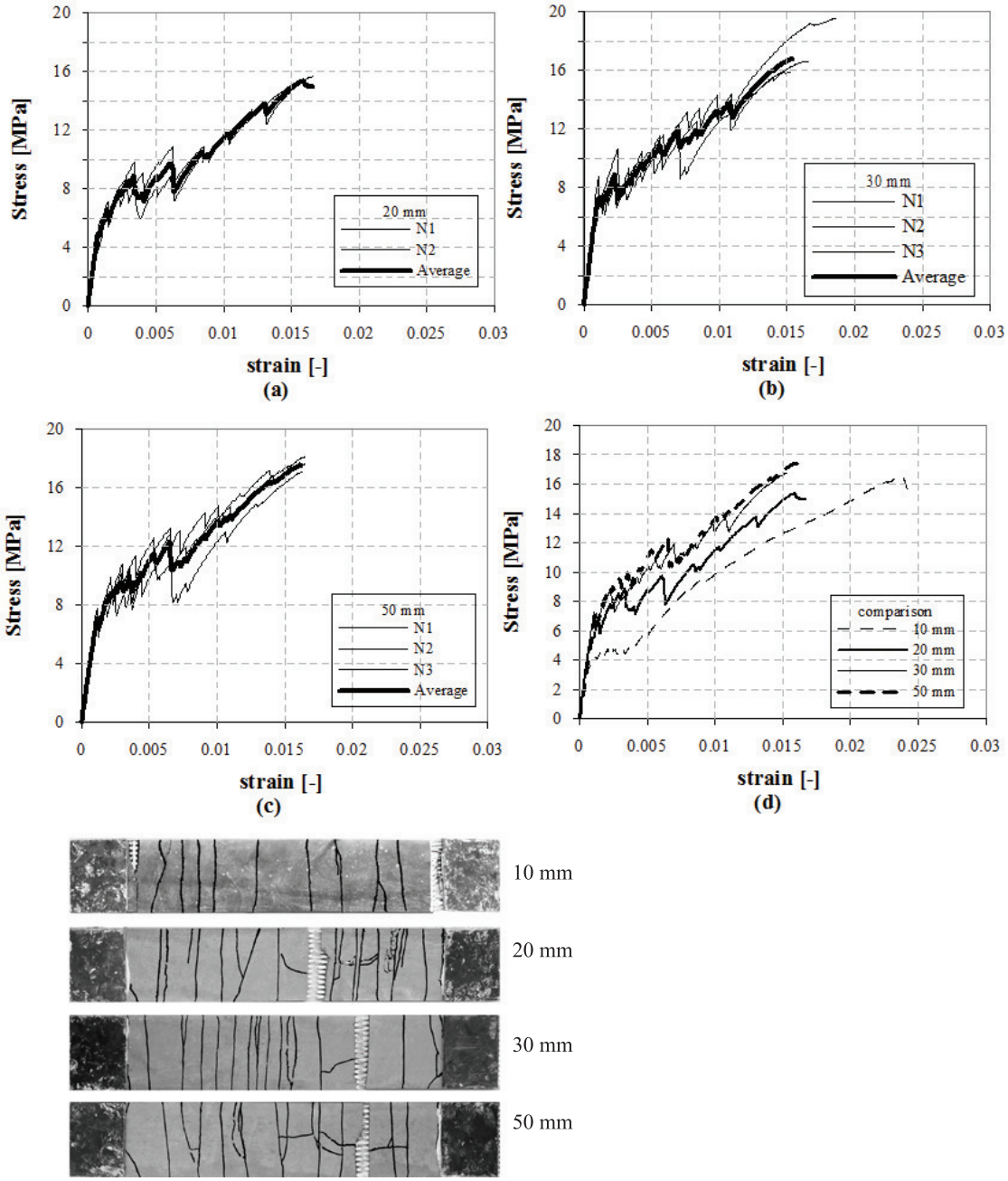

Figure 4.27: Contribution of weft spacing roving in the tensile behaviour: (a) 20 mm, (b) 30 mm, (c) 50 mm, (d) comparison

Weft spacing	thickness [mm]	P_{max} [kN]	δ_u [mm]	σ_{max} [MPa]	δ_u/ℓ	σ_I [MPa]
10 mm	6.2	7.51	7.44	17.13	0.0257	4.03
20 mm	6.8	7.36	4.64	15.51	0.0161	5.46
30 mm	6.3	7.60	4.86	17.35	0.0168	7.72
50 mm	6.2	7.63	4.74	17.58	0.0164	7.22

Table 4.23: average values for different weft spacing mix design M3

different situations before being tested. The results in terms of stress versus nominal displacement are shown in Fig. 4.28 and the values are summarized in Table 4.24 and further detail are shown in appendix B (fig. B.6). Specimens cured in water showed a first cracking strength lower than the other cases and a final branch with a lower stiffness. A possible cause is the water penetration between roving and matrix that make a telescopic failure easier, damage the fabric and reduce the bond. The best performance was achieved by air cured method, where the first cracking and ultimate strength were greater and the crack pattern was denser. This result can be due to the higher shrinkage phenomena that enhanced bond between matrix and reinforcement. The first cracking value of 6 MPa was comparable with the average tensile resistance f_{ctm} obtained by bending tests as indicated in tables A.4 and 4.24. The average curve of specimens cured at 60°C for 6 days is placed between the two other cases: this intermediate behavior is due to the shrinkage compensation obtained with oven curing and the slow initial hydratation of slag [92].

curing condition	thickness [mm]	P_{max} [kN]	δ_u [mm]	σ_{max} [MPa]	δ_u/ℓ	σ_I [MPa]
water	6.2	7.51	7.44	17.13	0.0257	4.03
60°C	6.5	10.25	7.25	22.40	0.0252	5.40
air	6.2	11.57	7.19	27.13	0.0250	6.10

Table 4.24: Different curing conditions: average value

Displacement rate

The influence of displacement rate on TRM mechanical behavior is a topic open to further investigations. Some studies were conducted in Silva [93] to investigate TRM subjected both to low and high-rate tensile loading ranging from 0.0001 to 50 s^{-1} and, in particular, the effect of the addition of short fibers on the static and dynamic response. The displacement rate generally used in the literature and in all the tests of this thesis was $2 \cdot 10^{-2} mm/s$, so the ranges of chosen displacement rates (corresponding at different strain rate) are the following (included in static and quasi-static regimes):

- 2 mm/s ($0.69 \cdot 10^{-2} s^{-1}$)
- 2 mm/s $\cdot 10^{-2}$ ($0.69 \cdot 10^{-4} s^{-1}$)
- 2 mm/s $\cdot 10^{-4}$ ($0.69 \cdot 10^{-6} s^{-1}$).

The strain rates were computed dividing the displacement rate by the gauge length of the specimens. Three tests were performed for each range on specimen reinforced with 1 layer of fabric

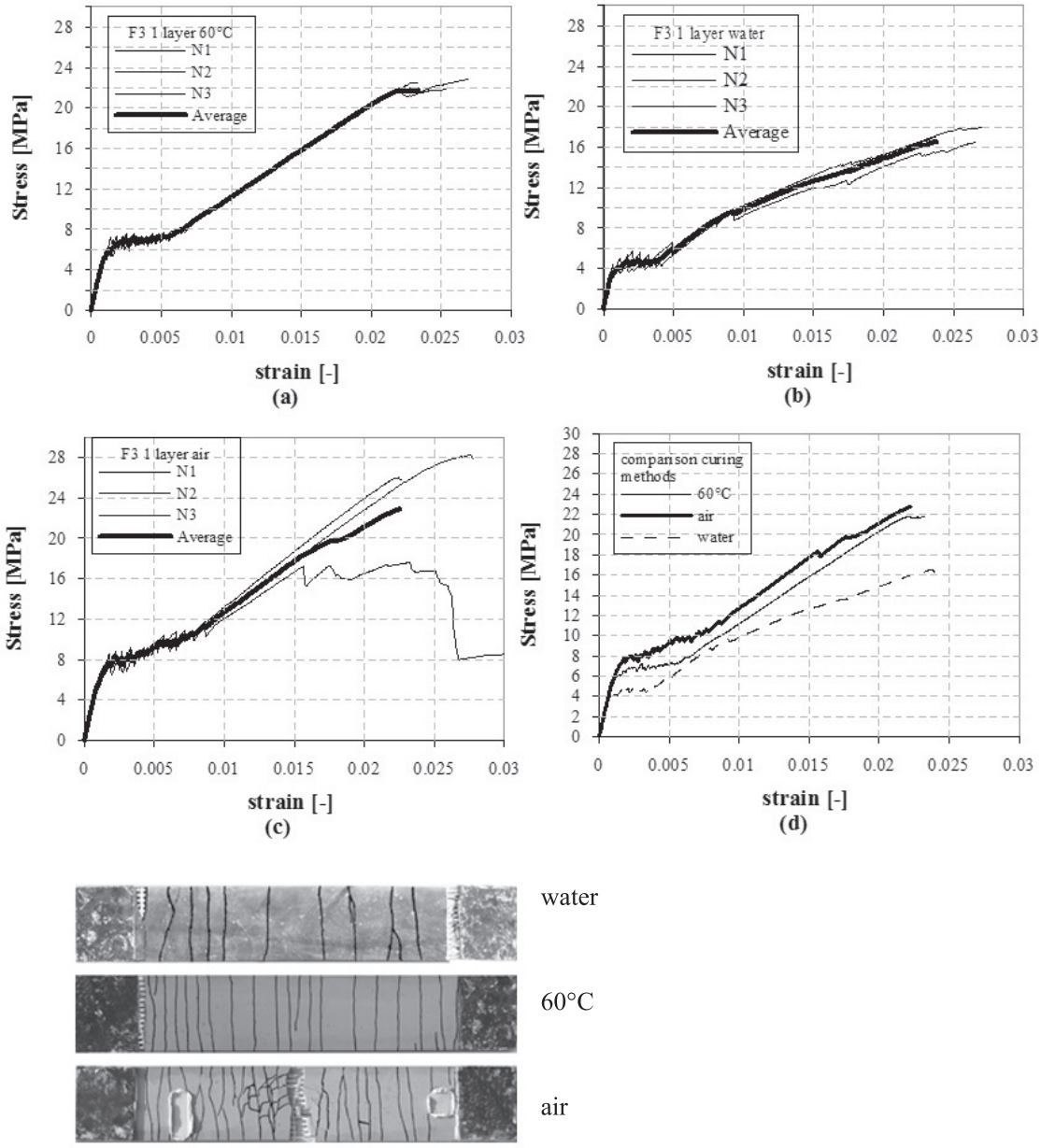

Figure 4.28: Curing methods

F3 and mix design M3. The results are shown in fig. 4.29, (table 4.25 and appendix B fig. B.7). For the higher displacement rate (2 mm/s) it is possible to observe the typical behavior of TRC characterized by 3 branches: the first one corresponds to the linear-elastic behavior, then, when the first crack occurs at about 6.3 MPa, a multiple crack formation can be observed; at the end, after a low stress increase, the cracks widen until failure. In all specimens and specially in number 2 and 3 a change of stiffness at about 16 MPa of nominal stress takes place. This discontinuity could be related to an apparent stiffness increase due to creep effect. It is worth noting that the final slope of all the strain rates investigated are almost the same. The typical behavior of TRM could also be observed for the intermediate displacement rate ($2 \cdot 10^{-2}$ mm/s), that is the common speed used for TRM tensile tests. The second phase starts at a lower stress value (about 4 MPa) and also the peak stress reached is lower in comparison with the higher displacement rate considered before (about 17 MPa instead of 22.4 MPa). For the lowest displacement rate considered ($2 \cdot 10^{-4} mm/s$) the 3 branches could not be clearly identified because, after a first linear-elastic phase, only a multicracking phase up to failure can be observed. At this displacement rate, when the first crack occurs (at stress ranging from 3.7 to 5.1 MPa), a reduction of bond strength between matrix and fabric is observed and sliding occurs. The strength reached in this last case is even close to 13 MPa. Looking the results, it is possible to notice a loss in strength and ductility with the decreasing of displacement rate. Besides, a coarser crack pattern is experienced passing from 10^{-2} to $10^{-6} s^{-1}$ (Fig. 4.29). A loss in strength of about 23.5% could be observed both passing from 10^{-2} to 10^{-4} s^{-1} and from 10^{-4} to 10^{-6} s^{-1}. The significant role played by strain rate here observed could be related to both glass material and interface bond strength. Further research is required to better understand the roles of each mechanism.

displacement rate	thickness [mm]	P_{max} [kN]	δ_u [mm]	σ_{max} [MPa]	δ_u/ℓ	σ_I [MPa]
2 mm/s	6.3	9.97	8.15	22.42	0.0283	6.39
$2 \cdot 10^{-2}$ mm/s	6.2	7.51	7.44	17.13	0.0257	4.03
$2 \cdot 10^{-4}$ mm/s	6.6	6.07	6.27	13.10	0.0217	4.53

Table 4.25: Different displacement rate: average results

Size effect

In order to appreciate the role of size effect in uniaxial tension hardening behavior due to multicracking phenomenon controlled by bond effectiveness, three different specimen lengths were investigated (290, 150 and 75 mm). For all the lengths experienced, specimens reinforced with F3 - 1 fabric (reinforcement ratio equal to 3.07%) were considered. Fig. 4.30 and Table 4.26 indicate the results related to TRC specimens. Fig. 4.30 shows that all the average curves obtained for the different lengths are overlapped for displacement values lower than 0.2 mm. This could be explained considering that the displacement measured by the mechanical press is given by the sum of two components: the specimen elongation and the specimen sliding in the clamps. As a matter of fact, in the first linear-elastic branch the sliding contribution is predominant, so the curves seem to be overlapped. On the contrary, looking at the stress vs. strain curves obtained by dividing the relative displacement by the free length, a different initial stiffness (Fig. 4.30) can be observed. Therefore the initial slope of nominal stress versus normalized displacement curves should represent the elastic modulus of the mortar, that is the same for all the specimens, but the results are altered because of the specimen sliding between the clamps as explained. With reference to post cracking behavior, the curves highlight a tension stiffening controlled by the specimen length: the longer the specimen, the smaller the ductility. The crack pattern (Fig.

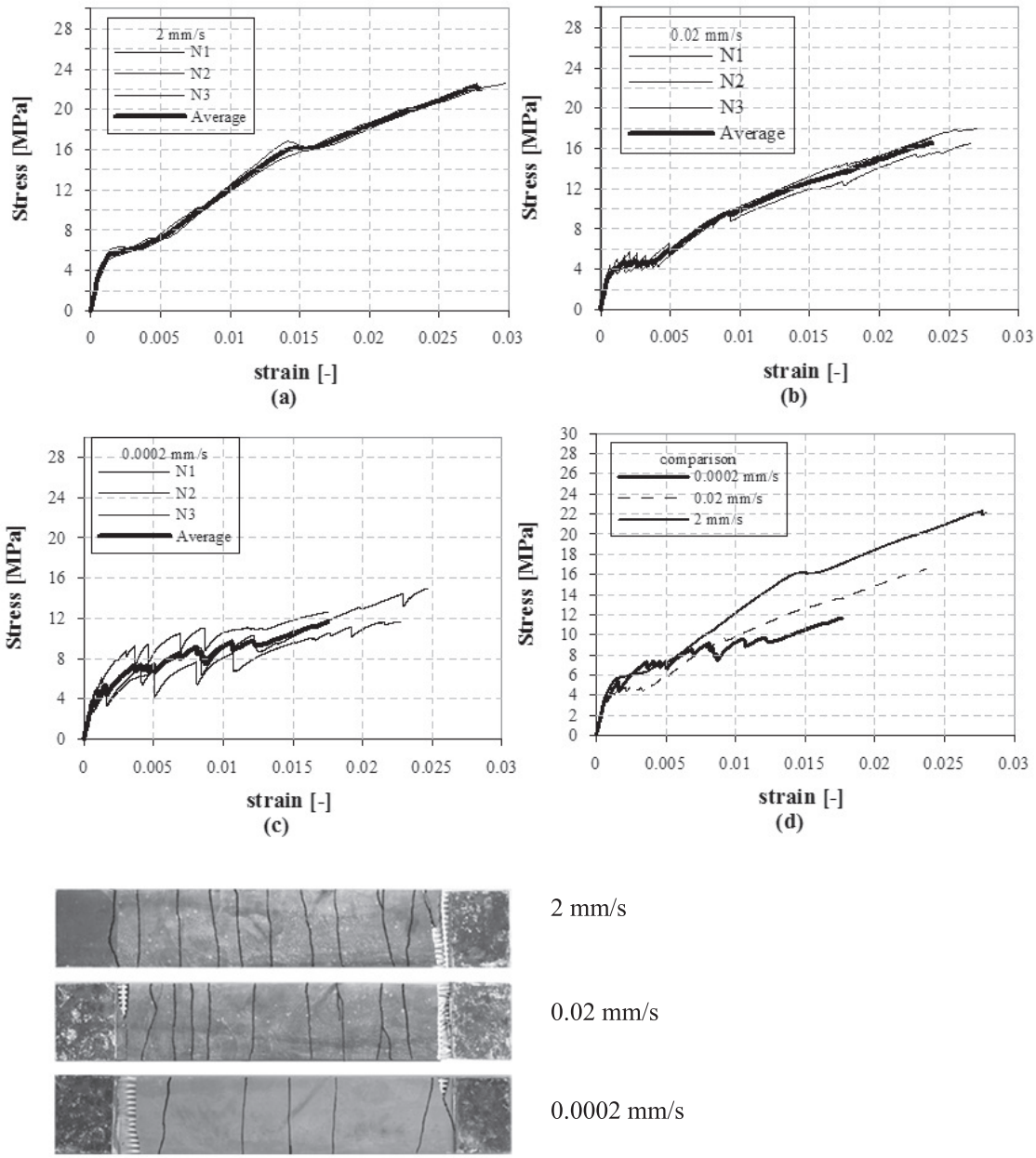

Figure 4.29: Displacement rate

4.30c) shows a finer cracking for shorter specimens and this justifies the previous results. Further details are available in appendix B (table. B.8).

specimen size	thickness [mm]	P_{max} [kN]	δ_u [mm]	σ_{max} [MPa]	δ_u/ℓ	σ_I [MPa]
290 mm	6.2	7.51	7.44	17.13	0.0257	4.03
150 mm	6.5	9.51	3.81	20.67	0.0261	5.72
75 mm	6.4	9.29	2.70	20.65	0.0366	5.19

Table 4.26: Different specimen size for TRM specimen

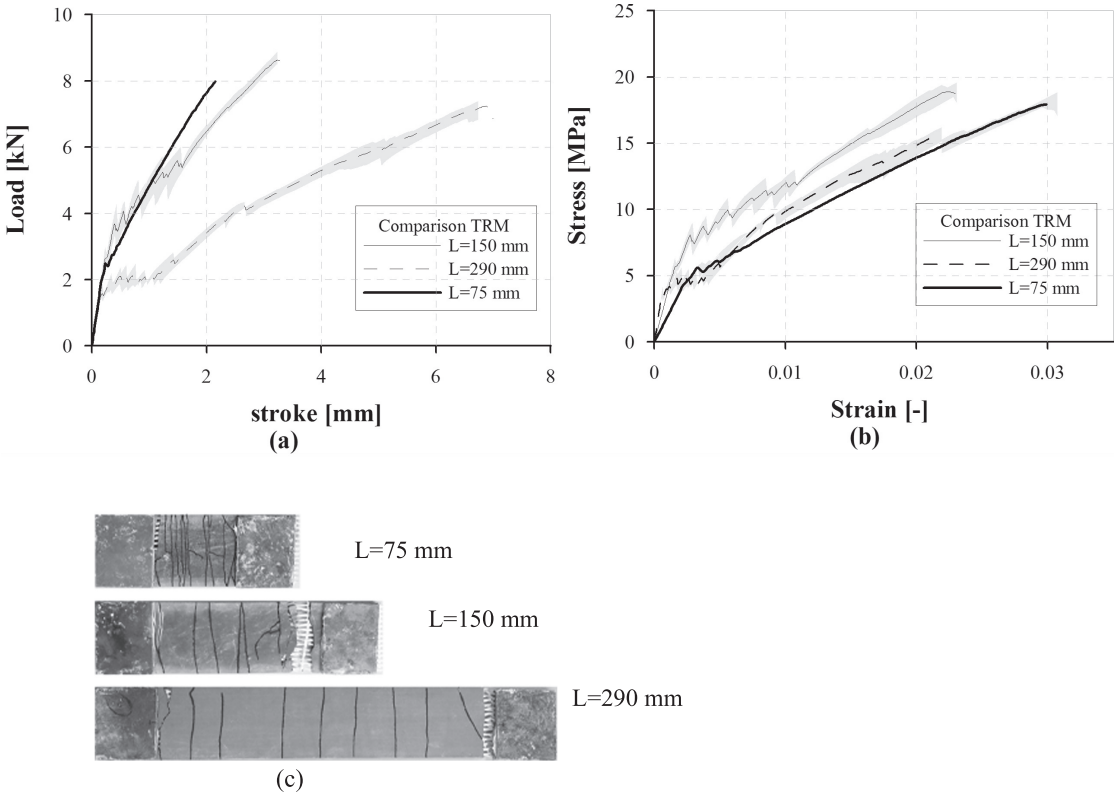

Figure 4.30: Size effect (a) (b) TRM specimen, (c) crack pattern

Effect of high temperature

The AR glass textile embedded in cement matrix is subjected to loss in strength during the time. Some researcher have studied durability models to calculate the quantity of the strength loss related to material, humidity and temperature [94], [95]. Few studies have been conducted on TRM exposed to high temperatures. In the experimental program, uniaxial tests were performed to investigate the residual mechanical properties of the material. Specimens made by mix design M5 and reinforced with 2 layers of fabric F2 were cured in a wet environment for 28 days and after that they were placed in a oven fig. 4.31 and exposed to thermal cycles up to three different maximum temperatures (200 - 400 - 600°C) fig. 4.32. The maximum temperature was reached

with an heating rate equal to 30°C/h and, after 2 hours of stabilization phase, a cooling branch of 15°C/h was performed. For each range, 3 nominally identical tests were performed and they were compared with three specimens not thermally damaged.

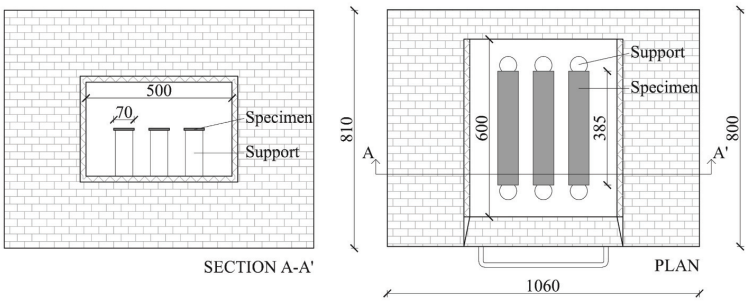

Figure 4.31: TRM specimens inside the oven

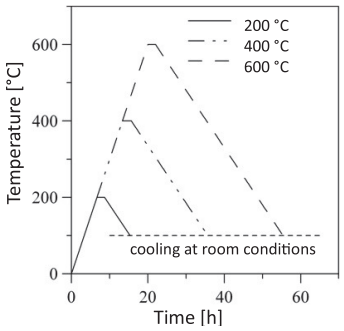

Figure 4.32: Heating rates

specimen	σ_{max} [MPa]	ϵ_{max} [-]	$\sigma_{cracking}$ [MPa]	$\epsilon_{cracking}$ [-]
20°C	19.76	0.0212	5.53	0.0010
200°C	20.64	0.0189	9.86	0.021
400°C	6.90	0.0113	3.95	0.0011
600°C	4.00	0.0010	4.00	0.0010

Table 4.27: Average results value of tensile tests after thermal cycles

A common behavior can be observed for the temperatures 20°C and 200°C where the three non linear stages occurred. On the contrary, the behavior of 400°C and 600°C specimens was respectively characterized by a multicracking branch and by a linear brittle phase. The comparison in terms of stress versus strain for all temperatures is shown in fig. 4.33 and an increment in the first cracking resistance was evident for 200°C, if compared to 20°C table 4.27. This improvement in the tensile strength was due to greater shrinkage at high temperature that enhanced the bond between matrix and reinforcement. Conversely, 400°C and 600°C degraded the coating, thus favoring sliding phenomena.

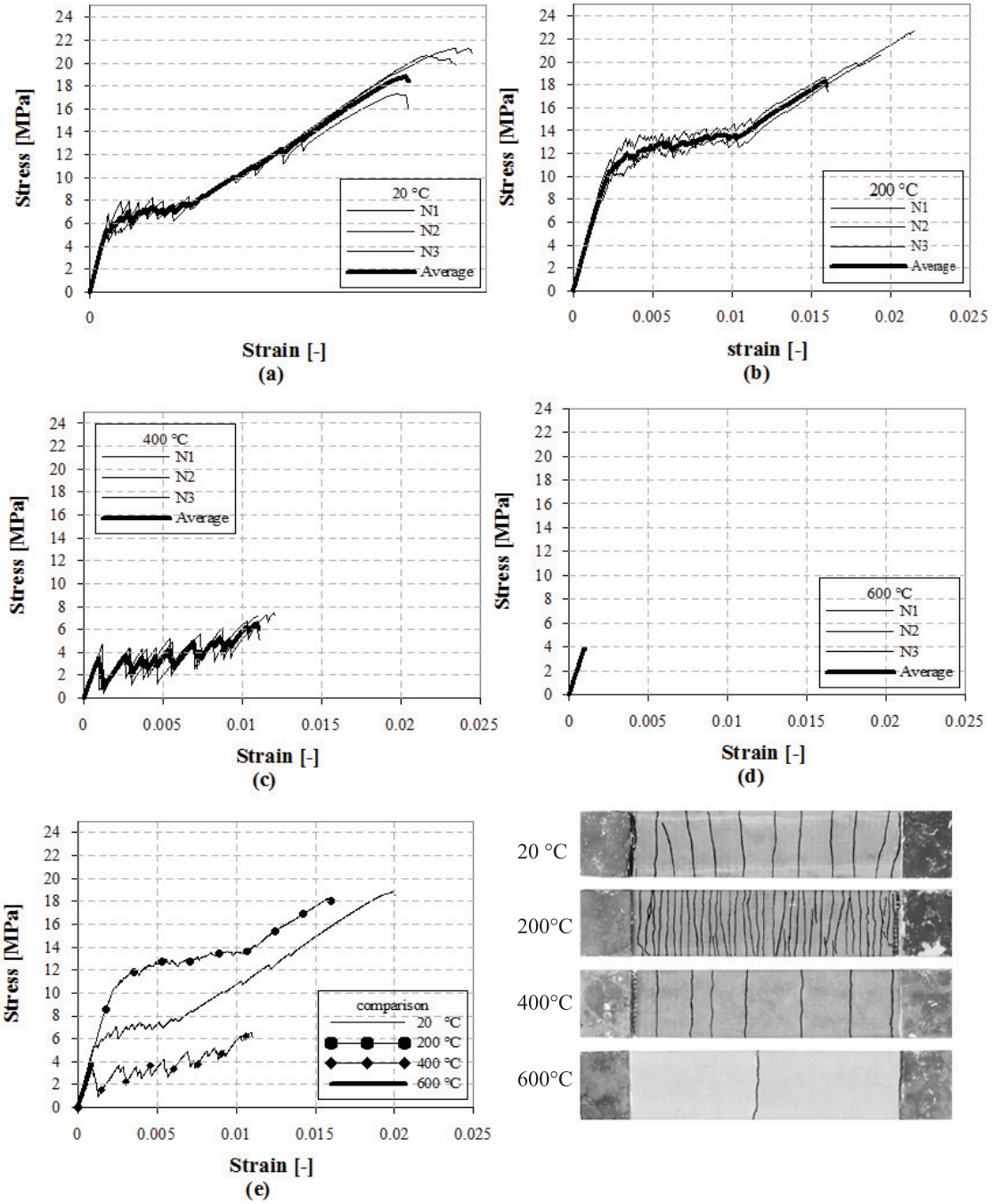

Figure 4.33: Results to thermal cycles for different rates temperature

Chapter 5

Retrofitting solutions: experimental programme

Nowadays, it is known that a lot of existing structures no longer meet today's safety standard. The solution should be found in repair and retrofitting technologies. The success often depends on the choice of materials. The purpose of this thesis is to illustrate the potential enhancement of structural safety limit state brought by the use of an advanced cementitious composites. From the comparison between TRM and UHPFRC, one material will be suggested for the best solution. It is generally recognized that the bond between the repair material and the substrate material is a key issue. Failure can start from an interfacial defect causing delamination in the case of a weak bond and spalling in the case of overlay strong bond and brittle repair material. For analyzing the contribution in the post-crack behavior due to the retrofitting material, a new technique, Double Edge Wedge Splitting (DEWS)was adopted to investigate tensile behavior. Furthermore compression tests were also performed. The effectiveness of the reinforcement were investigated referring both to uncracked and crack situation for the existing structure; in the case of cracked condition, SLS and ULS crack opening were considered. The retrofitting materials were applied over a substrate layer made of traditional concrete that represents the structural element to be retrofitted.

5.1 Substrate and specimen preparation

The specimen used as substrate layer was a R/C concrete plate with dimension of 30 x 30 x 10 cm and characterized by two notches in the upper and in bottom side, fig.5.1a. The concrete plate was reinforced with a steel welded mesh made by 6 mm diameter rebar, 150 mm spacing. The mesh was placed in the central section of the specimen, fig. 5.1b.

A set of 16 specimen were casted at each time by using a proper formwork which geometry is reported in fig. 5.2.

A series of wood elements divided the different samples and in the center of each portion the steel welded mesh was positioned. Along the longest side of each subdivision a steel parallelepiped with a triangular base, fig. 5.3 was fixed to create the V shaped notch.

Sixty plates and ten cubic specimen were casted (fig. 5.4) and cured at room conditions for one month. After that, the concrete plates were sawed to create the vertical notch of 30 mm long (fig. 5.5).

After the curing period, concrete plates were precracked at two different levels: w=0.3 mm

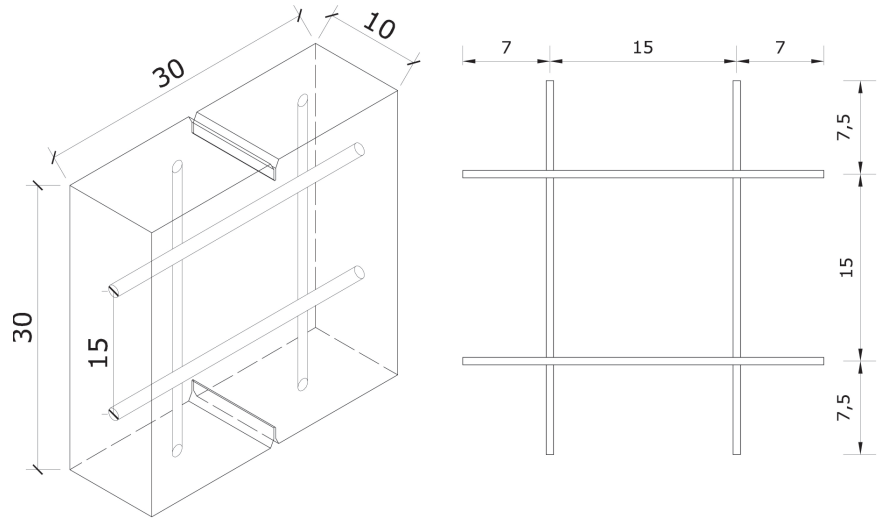

Figure 5.1: (a) Concrete specimen, (b) steel welded mesh

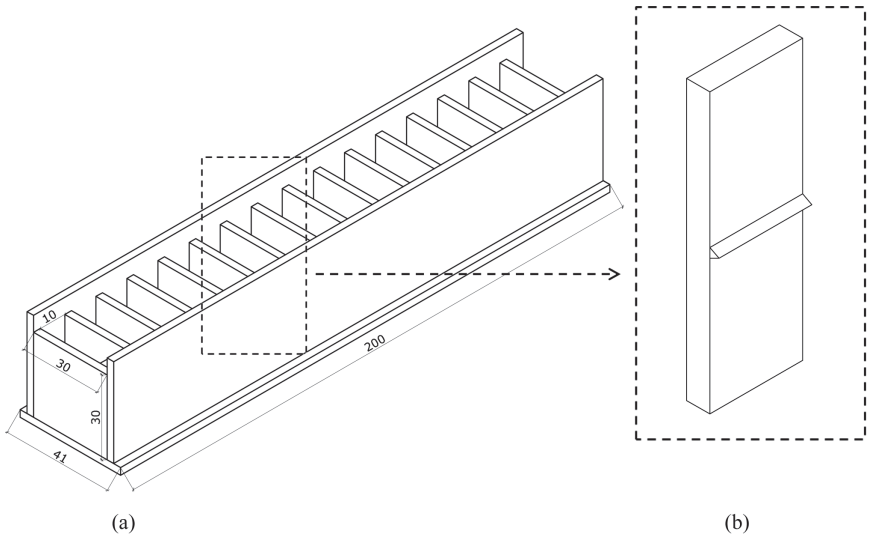

Figure 5.2: Formwork for concrete plates (a) scheme, (b) detail

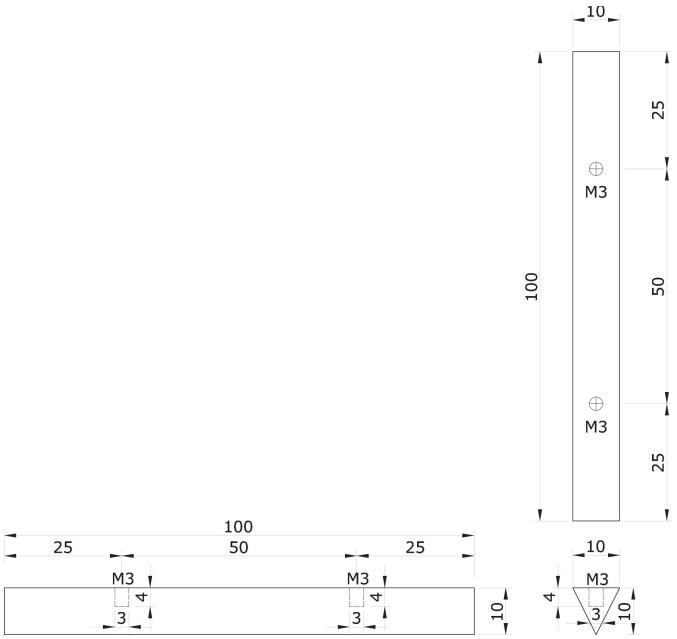

Figure 5.3: Detail of steel parallelepiped element

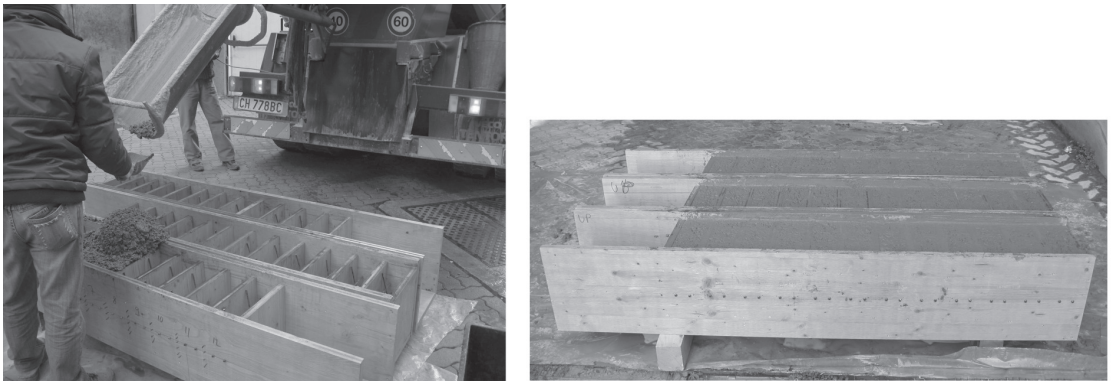

(a) (b)

Figure 5.4: Cast of concrete plates

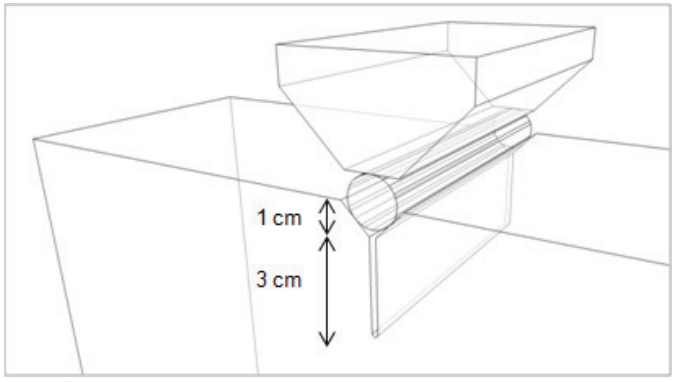

Figure 5.5: Detail of the V shaped notch

to simulate SLS condition and w=3 mm to represent ULS. DEWS test, that explained in the following chapter, was used to create such cracked conditions. The crack opening was measured in the central section on both sides of the specimen. Once reached the desired crack opening, the specimens were unloaded and prepared for the retrofitting layer application.

Before casting the retrofitting layer, to enhance the bond, the concrete surfaces were treated by a disk of a angle grinder to make the interface rough. The retrofitting materials were applied on both sides of the substrate. Two different casting methods were adopted according to the repairing technique. The TRM was cast in a horizontal plane and the notches were closed with hot glue to avoid that the matrix filled the notches fig.5.6a. A thin layer of mortar was spread on specimen and after placing the AR glass fabric, a roller was adopted to compact the mortar, fig. 5.6e. The matrix M5 already presented in Chapter 04 reinforced with fabric F3 was adopted.

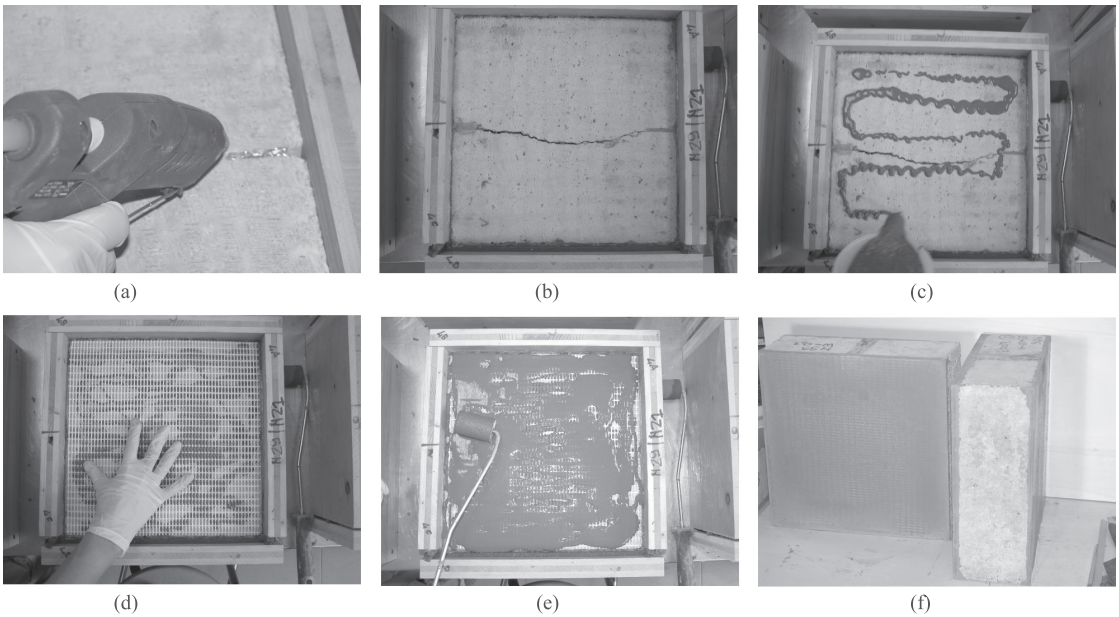

Figure 5.6: Casting procedure of TRM retrofitting layer

UHPFRC was cast in vertical direction from one side to improve fiber alignment to the tensile stress direction and also to lead air bubbles to go out (fig. 5.7). The formwork has been realized with two transparent sides to control casting flow direction.

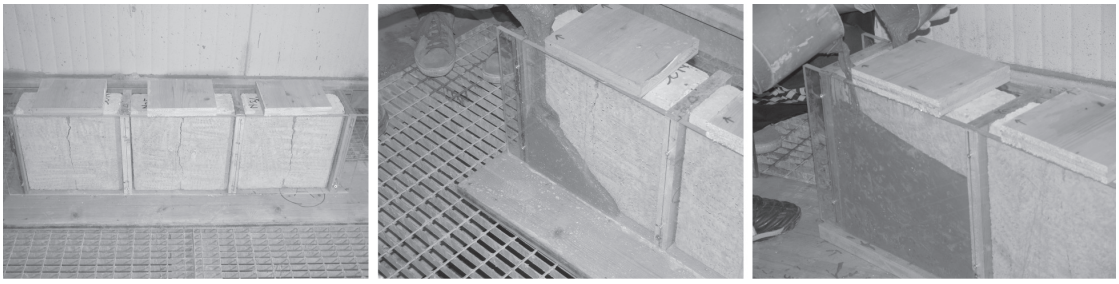

(a) (b) (c)

Figure 5.7: Casting procedure for UHPFRC retrofitting layer

Mix design and mechanical properties of the material have been already discussed in chapter 04. Once hardened the specimen were demoulded and cured in a climate chamber at 98% RH for 28 days. For each crack opening levels 6 plates reinforced with TRM and 6 with UHPFRC were prepared in order to use three samples for tensile and three for compression tests (table 5.1). Three concrete plates undamaged and 2 plates for each damage levels were used as reference samples for both tests.

Damage level	concrete plates no strengthening layer	n° plates with TRM	n° plates with UHPFRC	Tests
0 mm	3	3	3	DEWS
	2	3	3	compression
0.3 mm	-	3	3	DEWS
	2	3	3	compression
3 mm	-	3	3	DEWS
	2	3	3	compression

Table 5.1: Specimen quantity for DEWS and compression tests.

5.1.1 Substrate mechanical characterization

Concrete and steel were characterized by standard tests, compression and tensile tests respectively.

Concrete

The concrete was characterized by a maximum aggregate size of 14 mm and the mix design is reported in table 5.2.

Standard compressive tests on cubic specimen (15 cm side) were carried out to characterize the mechanical property of the material. The results of 10 tests are shown in table 5.3.

Component	Content [kg]
Cement 42.5	340
Water	170
Dracril 1100	3.4
Sand	1490
Sand sieved	379
Density [kg/m^3]	2382

Table 5.2: Mix design of concrete

Specimen 150x150x150 mm^3	R_c [MPa]
1	37.51
2	33.06
3	32.76
4	31.14
5	32.98
6	32.57
7	32.53
8	33.06
9	35.09
10	37.78
R_{cm}	34
ST.D	2.21 %
R_{ck}	30.40 MPa

Table 5.3: Cubic compressive resistance of traditional concrete

Steel

The tensile behavior of steel bar (6 mm of diameter) was defined by direct tensile tests. A mechanical press with maximum load capacity of 100 kN with a constant stroke rate of 0.05 mm/sec was adopted. The strain was computed by dividing the vertical displacement measured with a transducer over a gauge length of 50 mm. The behavior was defined by the following states: a first elastic branch until the yield stress, a hardening phase, and finally a necking phase until the failure of the bar. Fig. 5.8 (a) shows the stress vs. vertical displacement curve and (b) shows the stress vs. strain curve before the necking.

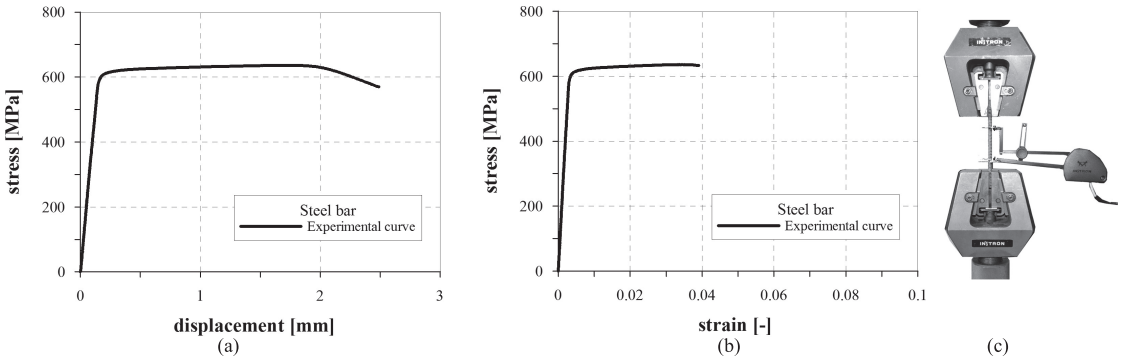

Figure 5.8: Tensile behavior of steel bar : (a) constitutive law stress vs displacement, (b) stress vs strain curve, (c) set up

5.2 DEWS technique

Double Edge Wedge Splitting test (DEWS) (fig.5.9) [96] is an indirect tensile test that can be considered as an extension of Wedge Splitting (WS) [97]. The most important aim was to reproduce the stress distribution on the sections of a notched specimen loaded in pure tension, without any crosswise compressive stresses.

In Bending (fig. 5.10) and Brazilian test compressive and tensile stresses act on the bending and splitting plane respectively. The elastic tensile stress along the ligament are shown in fig. 5.11.

Contrarily to WS, in DEWS technique two opposite wedge-shaped cuts are introduced and steel plates are placed on the notch lips to guarantee low sliding friction with steel cylinders used to apply the load. This set-up reproduces also a sort of Double Punch test proposed by Chen and Yuan ([98], fig. 5.12). In this test the specimen is a concrete cylinder placed vertically in a uniaxial compression. The load is applied by two steel circular punches centered at top and bottom side. A typical failure mechanism presents three radial fracture planes but from some experimental results the number of fracture planes ranges from two to four (fig.5.13 [20]).

An advantage of the DEWS as in traditional splitting tests, is the possibility of carrying out tensile test by applying compressive loads so avoiding the problem typical of the direct applications of tensile load. Indeed no steel plates glued at the extremities of the specimen or other load-transferring device are needed. Moreover, as clear from the comparison between the elastic tensile stress distribution of the 2 test (Brazilian and DEWS fig. 5.11), the absence of highly localized compression stresses is an advantage in the case of ductile material where significant plastic deformation can occur. The set-up used to apply the compressive load is made

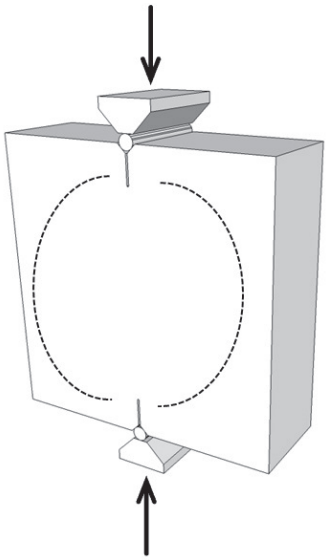

Figure 5.9: Dews technique

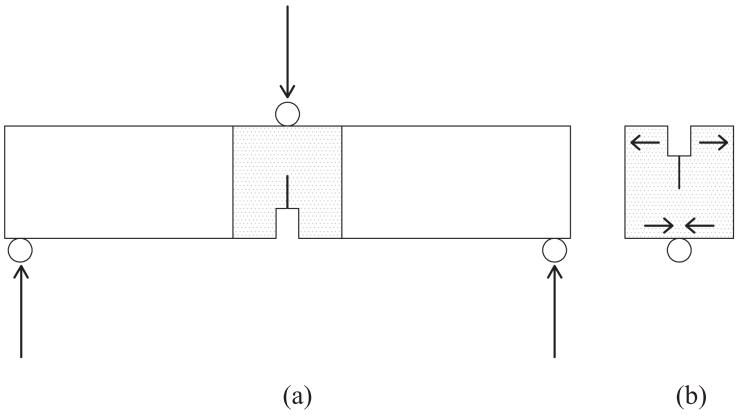

Figure 5.10: Analogies between (a) bending and (b) wedge splitting tests

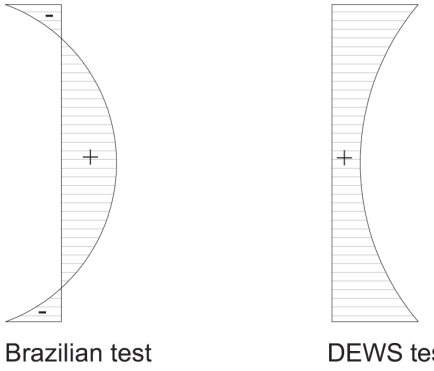

Figure 5.11: Distribution of stresses for Brazilian and DEWS test

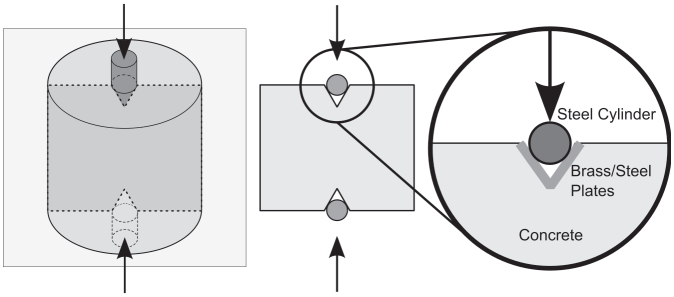

Figure 5.12: Analogies between Punch test and DEWS as section of Punch test

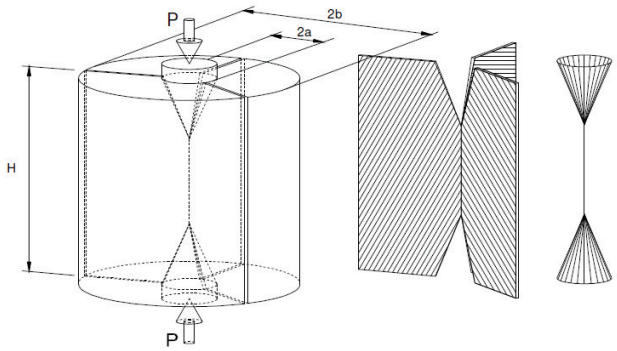

Figure 5.13: Double punch test arrangement, mechanism of failure, [20]

by two steel cylinders acting on 45° shaped notches in which steel plates are placed. Thanks to the particular arrangement two compressive stress arches are defined between the loading points. The compressive arch is clearly visible in fig. 5.14 where the vectors representing the smallest principal stress are shown. In the same figure can be observed that such principal stresses, in the central region of the specimen, are parallel to the ligament direction; this means that the mid span section is subjected to uniaxial tensile stresses and the strength should be very close the tensile strength measured in uniaxial tensile test.

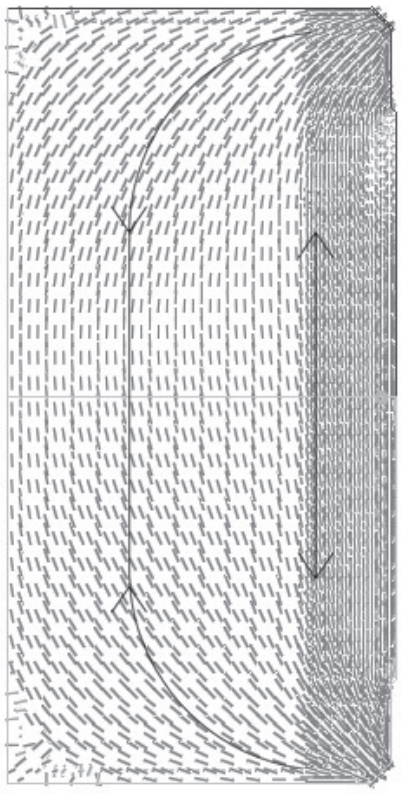

Figure 5.14: Direction of compression vectors in the plate

The tests were performed by means of an electromechanical DMG machine with the maximum capacity of 100 kN and a precision class of 0.5. A detail of the loading device is given in fig. 5.15 and the technical specification of the cylinder used as load knife (fig.5.16) according DIN 6325 are reported in table 5.4.

Material	100Cr6
hardness	Hrc 60 ± 2
Length	100 mm
diameter	10 mm

Table 5.4: Dowel pins specifications

A couple of 100x10x1 mm steel plates were fixed to the specimen in the internal surface of the V-shaped notched in order to uniformly distribute the load applied by means of the cylinder.

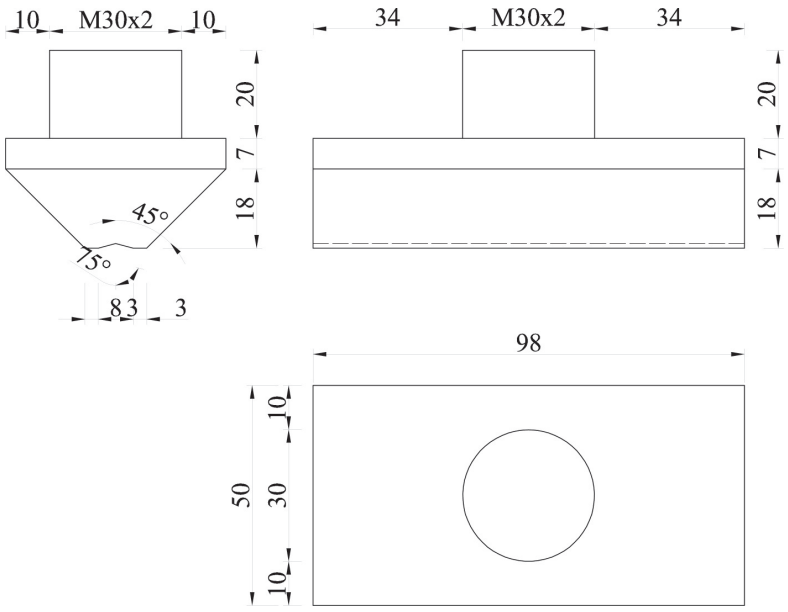

Figure 5.15: Device of DEWS set up

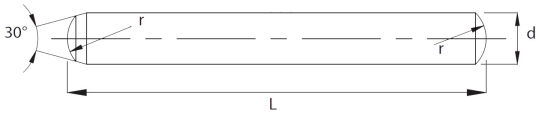

Figure 5.16: Dowel pins DIN6325

The friction between the cylinder and the steel plates decreased the load applied on the specimen and introduced a tangential component on the sliding surfaces. The coefficient was taken from experimental results obtained from tests conducted by di Prisco [96]. Different metal coupling and lubrificants were confronted to estimate the friction reduction between the cylinders and the metal sliding area. Three solutions were considered: brass and steel directly in contact, PTFE layer insertion and use graphite as lubrificant. A particular test device for simulating the behavior of sample subjected to vertical load by measuring the tensile force transmitted to the fracture area was made. The best solution was obtained by using steel plates and graphite as lubrificant (named Molykote U-n) and the friction coefficient was equal to 89%. The splitting force was computed referring to the situation of fig.5.17 with ϑ=45° and using the following formula, eq. 5.1:

$$F_{sp} = \mu \cdot P/2 \tag{5.1}$$

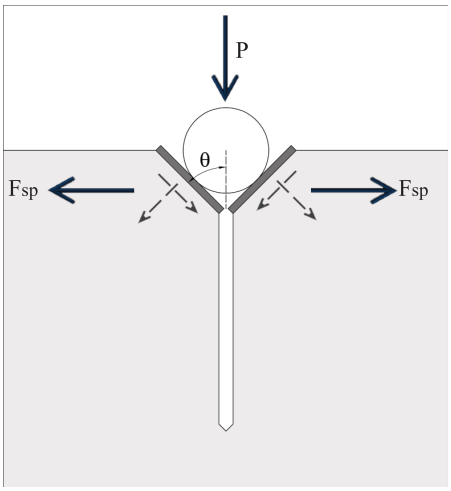

Figure 5.17: Relation between compressive and splitting force

In order to measure the crack opening on the specimen, 3 LVDT transducers were applied on each side of the specimen: one at the tip of both the notches and one in the middle of the ligament. In order to monitor any detachment between the different material layers, one LVDT was applied perpendicular to the specimen plane close to the central point of the specimen on both sides. A detailed scheme of the specimen instrumentation is given in figure 5.18.

The LVDTs used are full bridge HBMWA10 fig. 5.19a which characteristic are summarized in table 5.5.

	unit	WA10
Bridge type		full bridge
Nominal displacement	mm	10
Nominal sensitivity	mV/V	80
Characteristic tolerance	%	±0.2
Linearity deviation	%	±0.2

Table 5.5: Transducer specifications

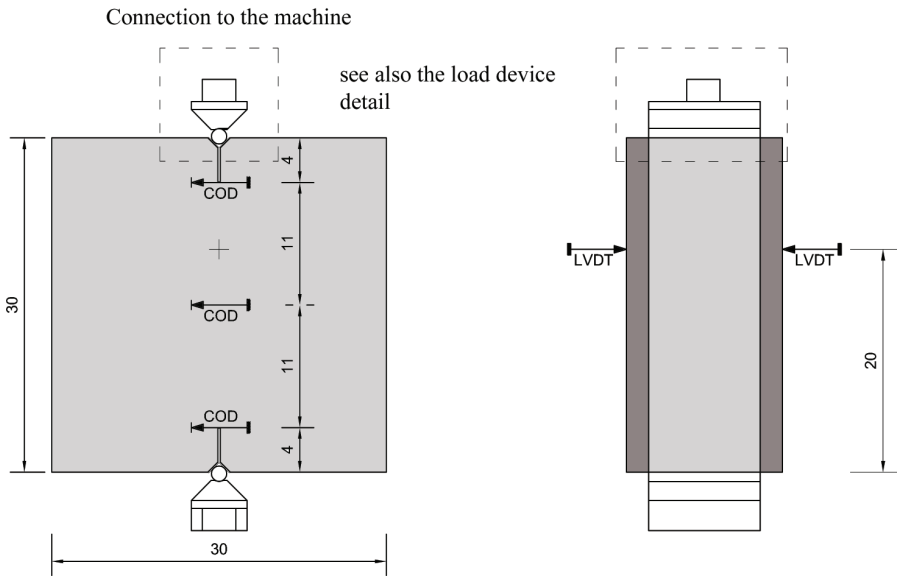

Figure 5.18: Scheme of DEWS setup

(a) (b)

Figure 5.19: LVDT and SPIDER8

Data acquisition in the whole tests was performed by using the electronic measurement system SPIDER8 by HBM fig. 5.19b and the characteristics are described in table 5.6.

	unit	value
Accuracy class		0.1
Digital resolution	digit	±25000
Measured value buffer	Meas.	< 20000
Sampling rate per channel	1/s	19600
Transducer eccitation voltage	V_{rms}	2.5
Carrier frequency	Hz	4800

Table 5.6: Electronic measurement system SPIDER8 specifications

5.3 Set up compression tests

The compression tests was performed rotating specimens of 90 degrees with respect to dews tests in this way, when cracked situation is considered, the crack was perpendicular to the compressive load direction. The loaded surfaces were those not characterized by the notch and before the test were coated with a layer of mortar to make the surfaces smooth and plane thus avoiding possible localized failure where defects appear, fig. 5.20.

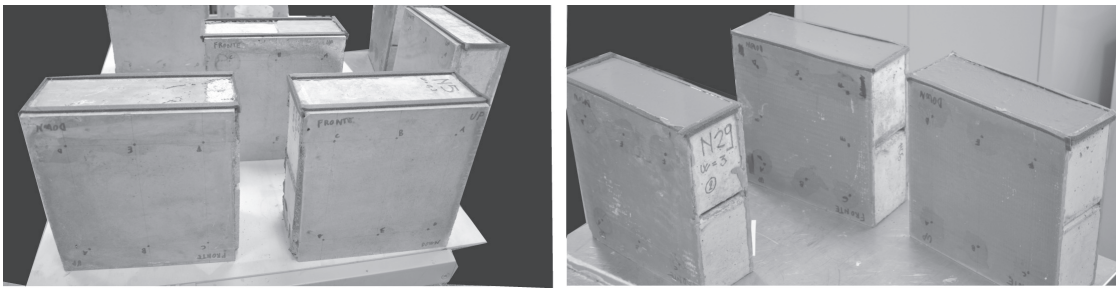

Figure 5.20: Concrete covering to make the surface smooth

The load was uniformly distribute by steel plates (10 mm thick) placed in the upper and bottom side (fig. 5.21) just on the surface of concrete substrate. The load transfer in the retrofitting layer was guaranteed by bond on the interface surface.

On both sides three displacement transducers were placed perpendicular the specimen plane in order to measure detachment of the strengthening layer. Furthermore two LVDTs were placed measure the stroke vertical displacement, fig. 5.22. The compressive tests were performed by a hydraulic press Controls Advantest with maximum load of 3000 kN by imposing constant stroke rate 0.05 mm/sec on specimen with and without strengthening layer for all the damage levels. The LVDTs and data acquisition system were the same used for DEWS tests.

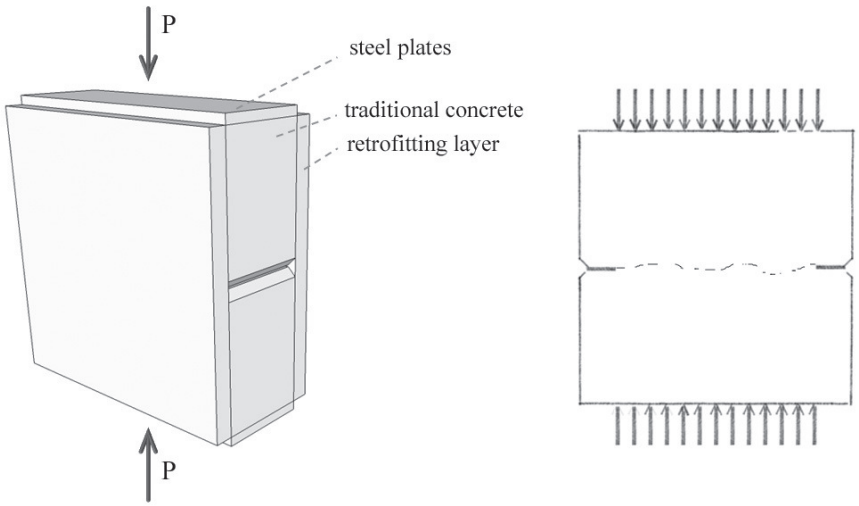

Figure 5.21: Scheme of compression tests

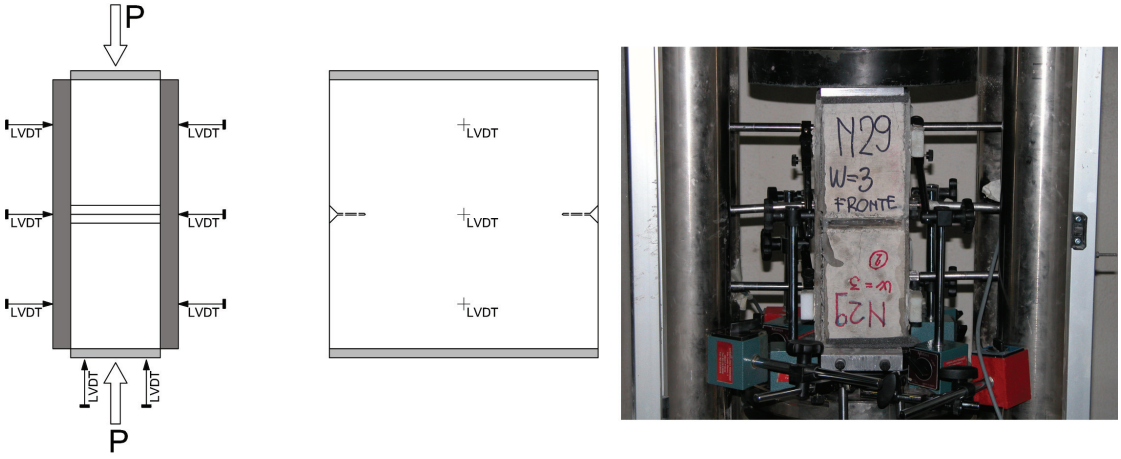

(a) (b) (c)

Figure 5.22: Set up compressive tests

Chapter 6

Retrofitting solution: experimental results

The aim of this chapter is to describe the results obtained by performing the experimental programme described before. This section will be divided in the Double Edge Wedge Splitting tests (DEWS) and compression tests on strengthened plates. The experimental results are described referring to the average behavior for each crack opening considered and for both retrofitting materials taken into account, UHPFRC and TRM.

6.1 DEWS tests results

First of all, DEWS tests were performed on the concrete plates without strengthening layers to be used as reference. The results are shown in terms of load vs. vertical displacement and by splitting force vs. the crack opening displacement measured by the transducer placed in the middle of the section, (fig. 6.1a,b). The thick solid line represents the average curve that was stopped at the end of the first of the three curves. The first branch is linear until reaching the cracking strength of the concrete (splitting cracking force equal to 30 kN). After that, the contribution of the steel bars was activated until the bar yielding and failure (fig. 6.2). Fig. 6.3 shows the crack opening displacement vs. vertical displacement referred to specimen number one. The crack opening is not symmetric: in most of the cases it started from the bottom side may be favored by the movement of the press machine from that side. Fig. 6.4 shows the development of the rotation on both specimen sides, rear and front, calculated as in eq. 6.1 where ℓ is the ligament equal to 220 mm:

$$rotation = (COD_{up} - COD_{down})/\ell \tag{6.1}$$

The rotation (fig. 6.4) was increasing at a stroke value of 2.3 mm and immediately after it decreased in range between 2.4 and 3.4 mm. The decrease of rotation, fig. 6.5, is justified by the fact that the crack opens in asymmetric way and then the crack propagation along the ligament tends to make uniform the crack opening value. At a stroke value of 3.4 mm the crack is uniformly open at both edges, so the rotation starts again to increase because of a not perfectly symmetrical behavior of the bars may be caused by random defects both in steel and bond surface.

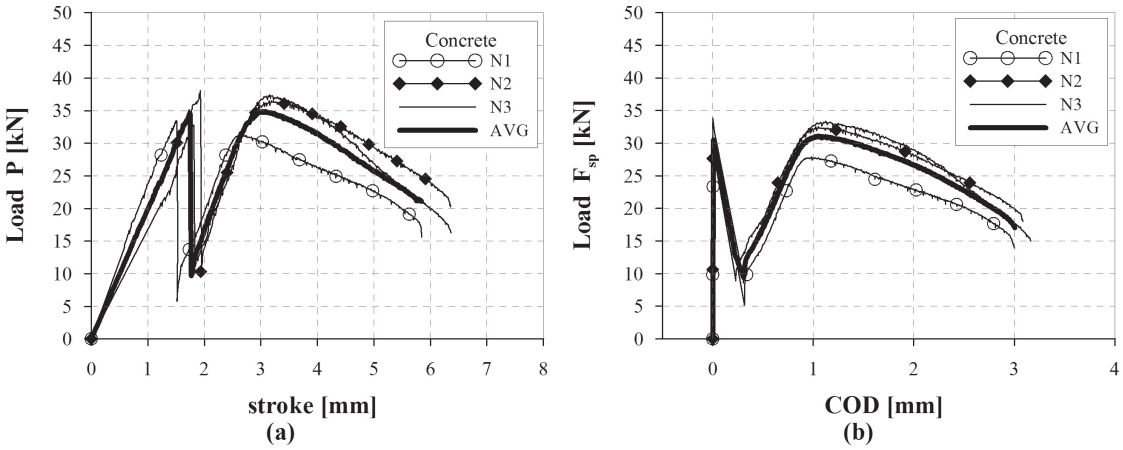

Figure 6.1: Concrete plates: (a) Vertical Load vs. vertical displacement, (b) Splitting force vs COD average

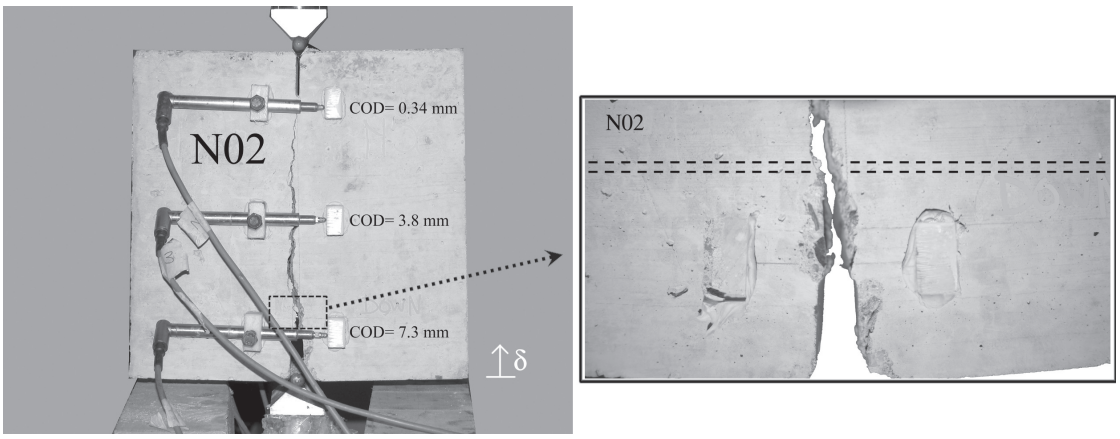

Figure 6.2: (a) Concrete plates N02, (b) breaking of the steel bar

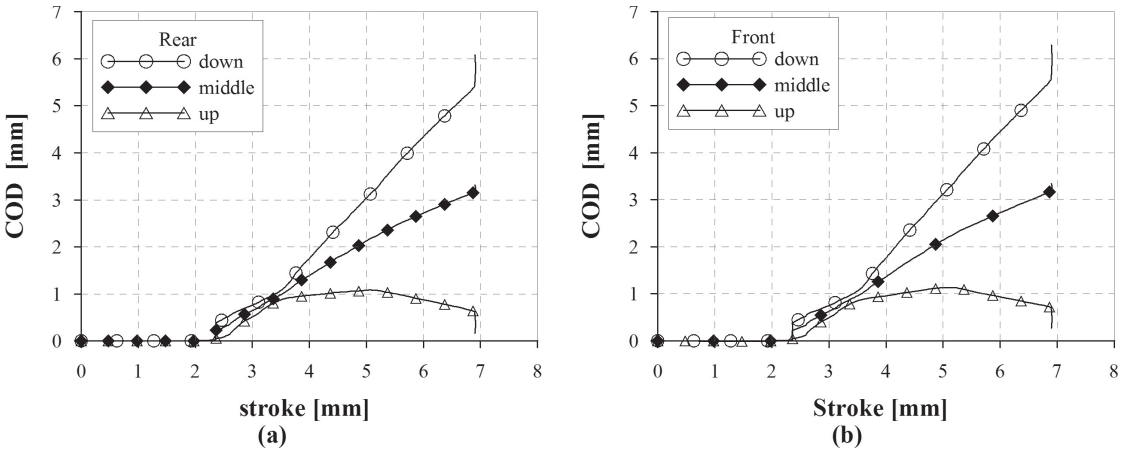

Figure 6.3: COD vs. vertical displacement (a) rear side, (b) front side

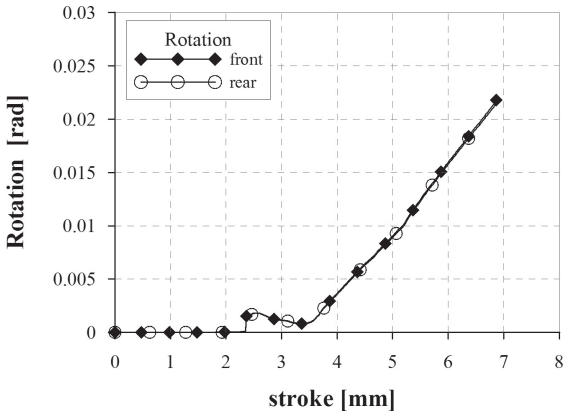

Figure 6.4: Rotation vs. vertical displacement, front and rear side

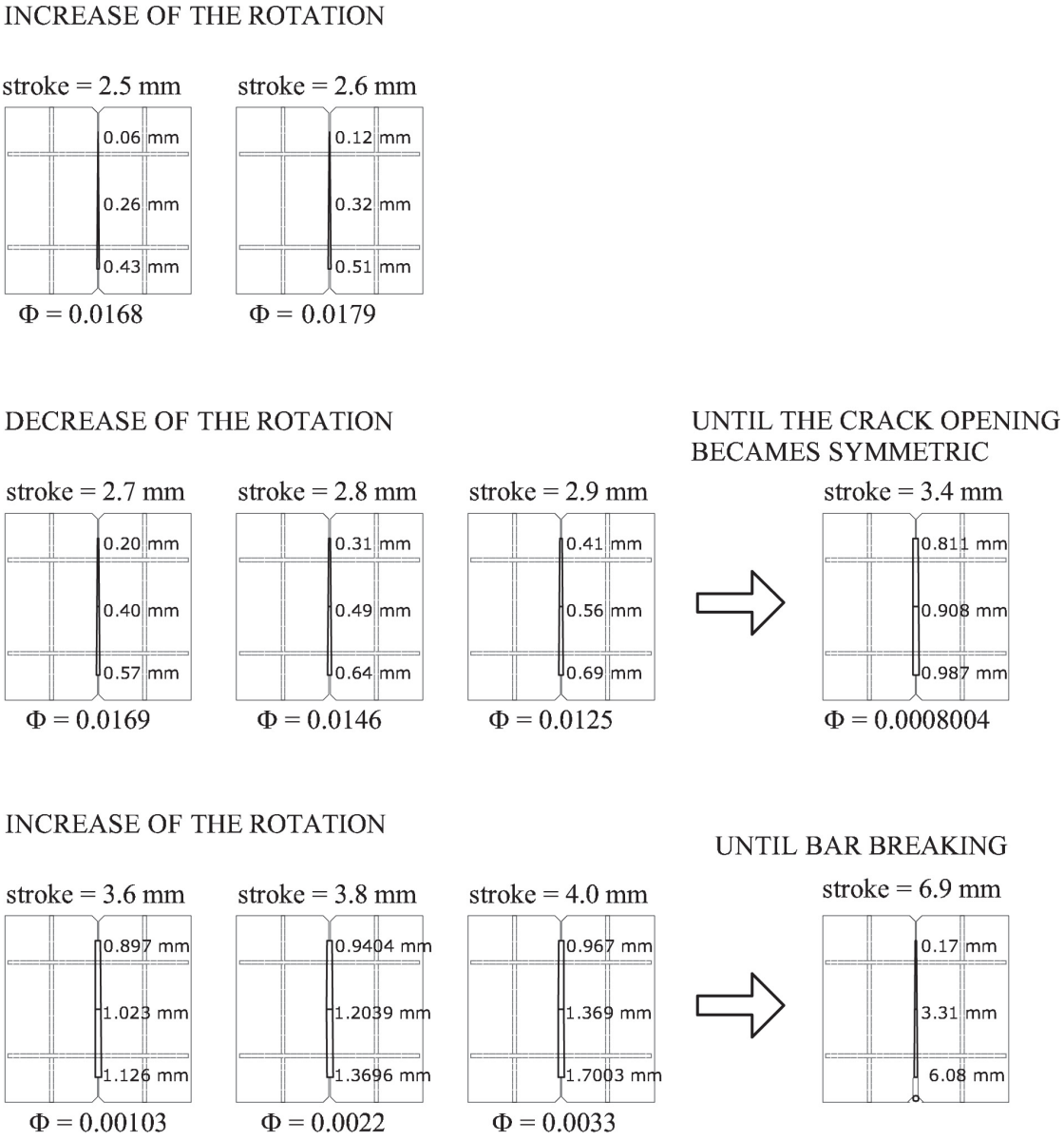

Figure 6.5: Cracks evolution compared to the rotation

6.1.1 TRM solution

The typical failure mechanism for TRM strengthening layer was associated to the multicracking phenomena guaranteed by the AR glass fabric. In the central section TRM experienced a delamination for a length of about 50-70 mm and consequently multicracking occurred. In some regions the TRM matrix was detached from the original support maybe because of local crushing due to the eccentricity between the interface plane on which the tangential stresses acted and the middle plane of TRM where tensile forces are transferred (fig. 6.6). It is worth noting that the load was applied only on the existing substrate concrete and it was transferred to the retrofitting layer by bond at the interface surfaces. For this reason a tension and a bending state of stress was generated and thus the local crushing due to eccentric load originated takes place at the external surface (fig. 6.7).

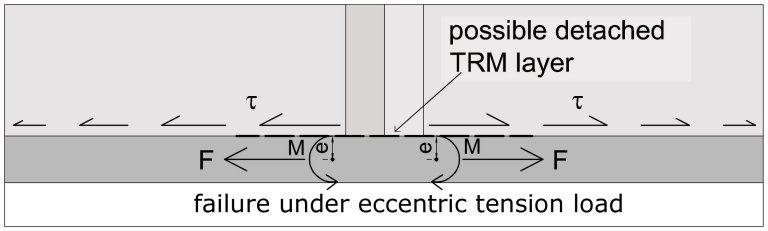

Figure 6.6: Detail of the detached of the TRM matrix

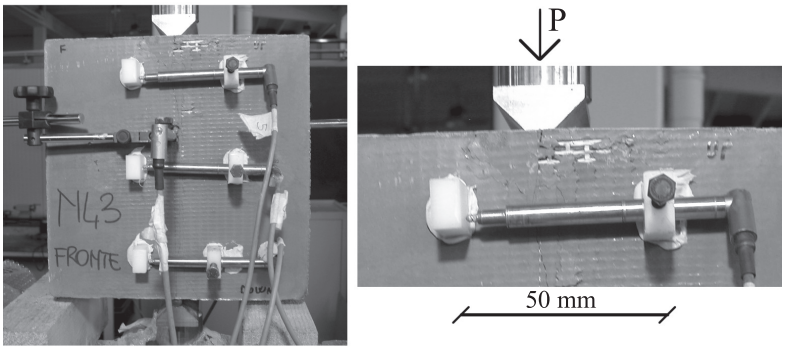

(a) (b)

Figure 6.7: DEWS test on TRM w=0 mm (a) multicracking zone, (b) detail

The results of concrete undamaged plates (w=0 mm) reinforced with two layers of TRM are shown in fig. 6.8a in terms of vertical load vs. vertical displacement. The first branch was linear until the crack strength of the matrix was reached (P = 65 kN, stroke displacement=2.9 mm). TRM layer started to multicrack in the central section over a length of 50 mm. In fig. 6.8b the splitting force vs. the crack opening are shown where the COD indicates the average between the front and rear COD measures taken in the central position. The Crack Opening Displacement are measured on both sides at three levels: up, middle and down (see figs. 6.8c,d referred to sample number one). COD values increase after a stroke value equal to 2.9 mm. For sample number 2 the test was stopped at stroke value 5.8 mm because the maximum capacity (100 kN)

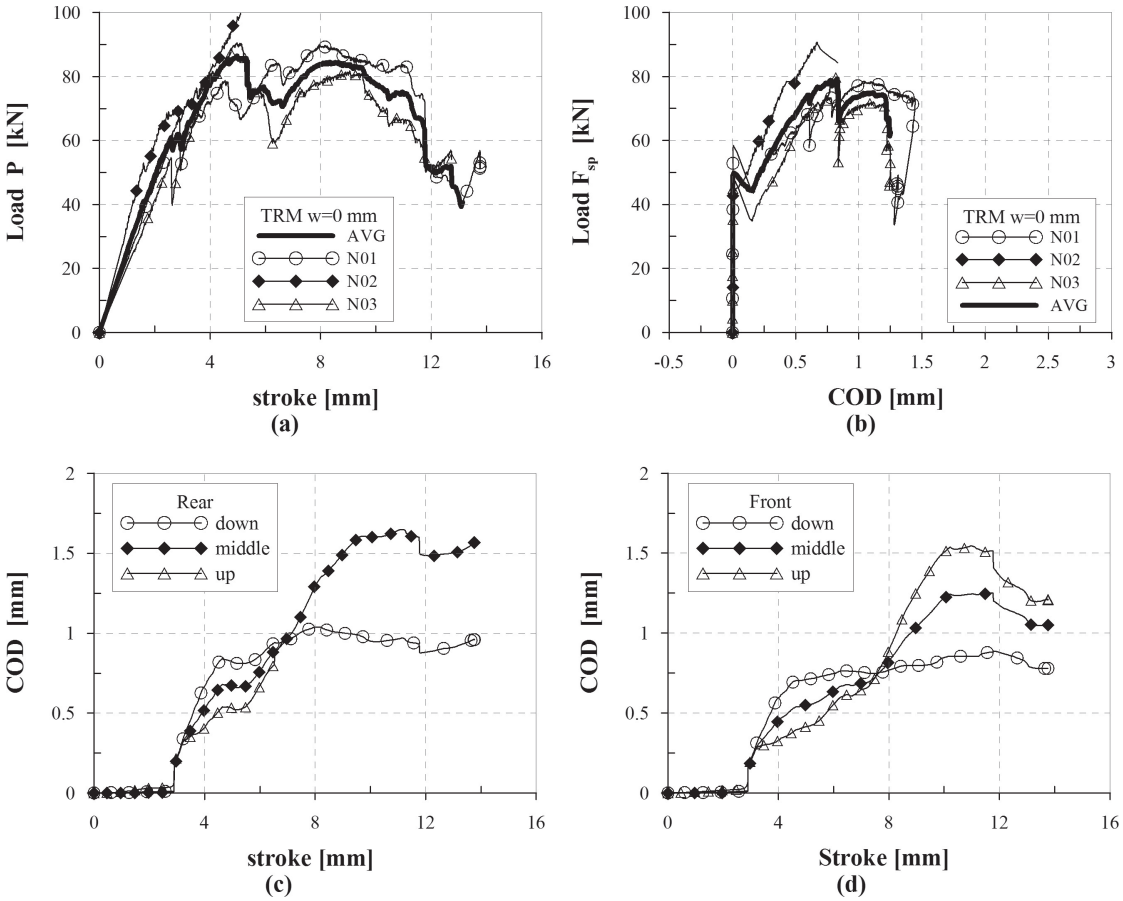

Figure 6.8: TRM w=0 mm (a) Load vs. stroke, (b) Splitting force vs. COD, (c) e (d) rear and front COD vs. stroke specimen N01

of the machine was reached. All the COD measures were stopped before the end of the test due to the TRM matrix detachment, where the instruments were glued. The whole set of test was stopped when the loading knife was completely penetrated inside the notch.

Fig. 6.9a,b showed the behavior referred to samples precracked at 0.3 mm and 3 mm while fig. 6.9c reported the comparison for the whole set of crack opening levels. The first two cases (uncracked and 0.3 mm) reached the same peak load for both the solutions: about 90 kN. In the case w=3 mm the TRM retrofitting was able to restore and to increase the initial strength of the reference condition, reaching a maximum load of 40 kN. Further detail about DEWS tests (TRM and UHPFRC) are shown in appendix C.

6.1.2 UHPFRC solution

The DEWS tests were performed for specimen strengthened with UHPFRC for the same three crack opening displacement previously discussed. The results in terms of vertical load vs. vertical displacement are reported in the following fig. 6.10. Two failure mechanisms were observed: the cracking in the ligament section and delamination of strengthening layer. The observed mechanism for this solution involved both delamination of one or both repairing layers and

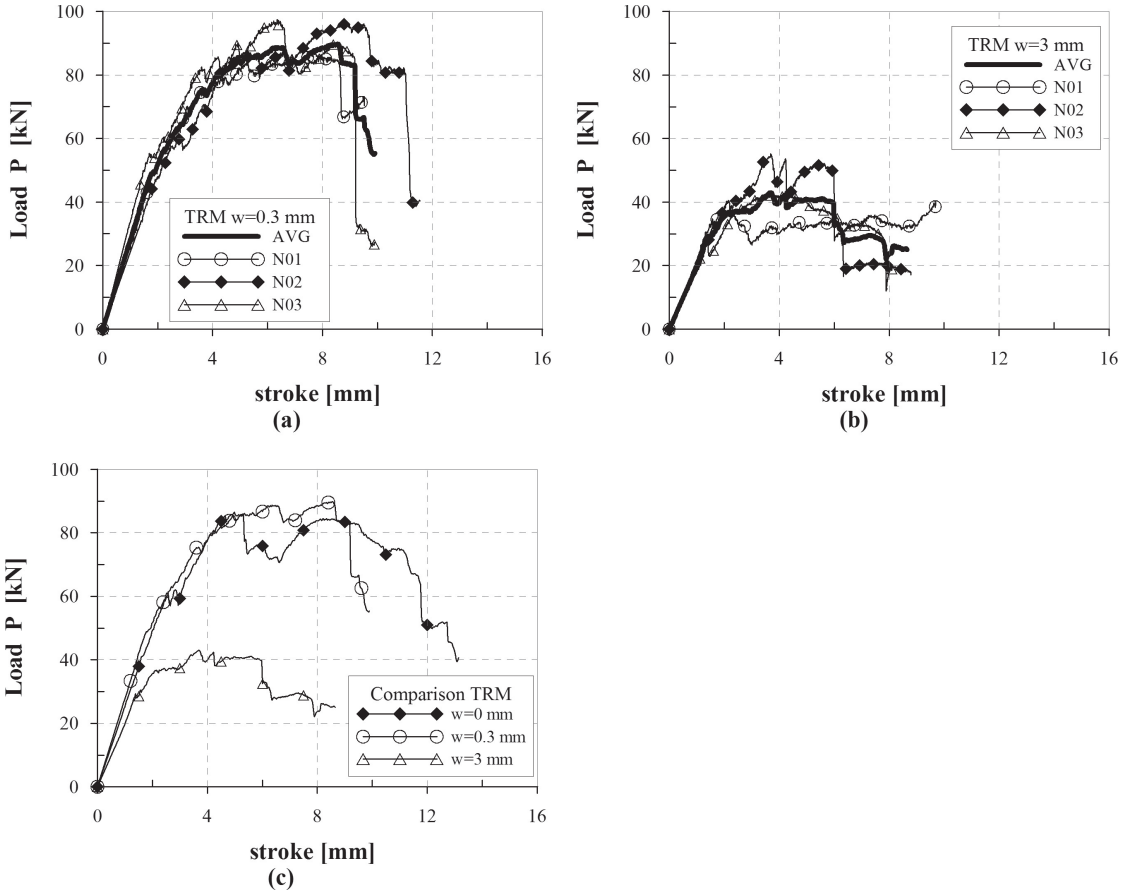

Figure 6.9: Load vs vertical displacement: (a) precracked 0.3 mm, (b) precracked 3 mm, (c) comparison for precrack levels

uniaxial tensile crack propagation along the critical plane. In the case of w=0 mm, two specimens (N01, N02 fig. 6.10a) activated the delamination failure mechanism on both sides together with the crack propagation along the ligament region of the subgrade concrete. The third specimen (N03 fig.6.10a) showed delamination on only one side and a consequent eccentric tension on the remaining portion of the specimen. In the case w=0.3 mm (fig. 6.10b) no delamination occurred in the three nominally identical specimens tested and on both sides only one crack localized and was observable at a visual inspection. The results of the specimen N01 are reported in fig. 6.11 where the graph (b) and (c) shows the evolution of the crack opening displacement for both side at three levels (up, middle and down). In the last case w=3 mm two specimens (N01, N02 fig. 6.10c) showed delamination on both sides without any visible crack on the retrofitting layers and in the last specimen (N03 fig. 6.10c) only one side experienced delamination while the remaining portion was subjected to a central traction with a visible crack localization of the active retrofitting layer. The results of the whole tests are collected in the appendix B.

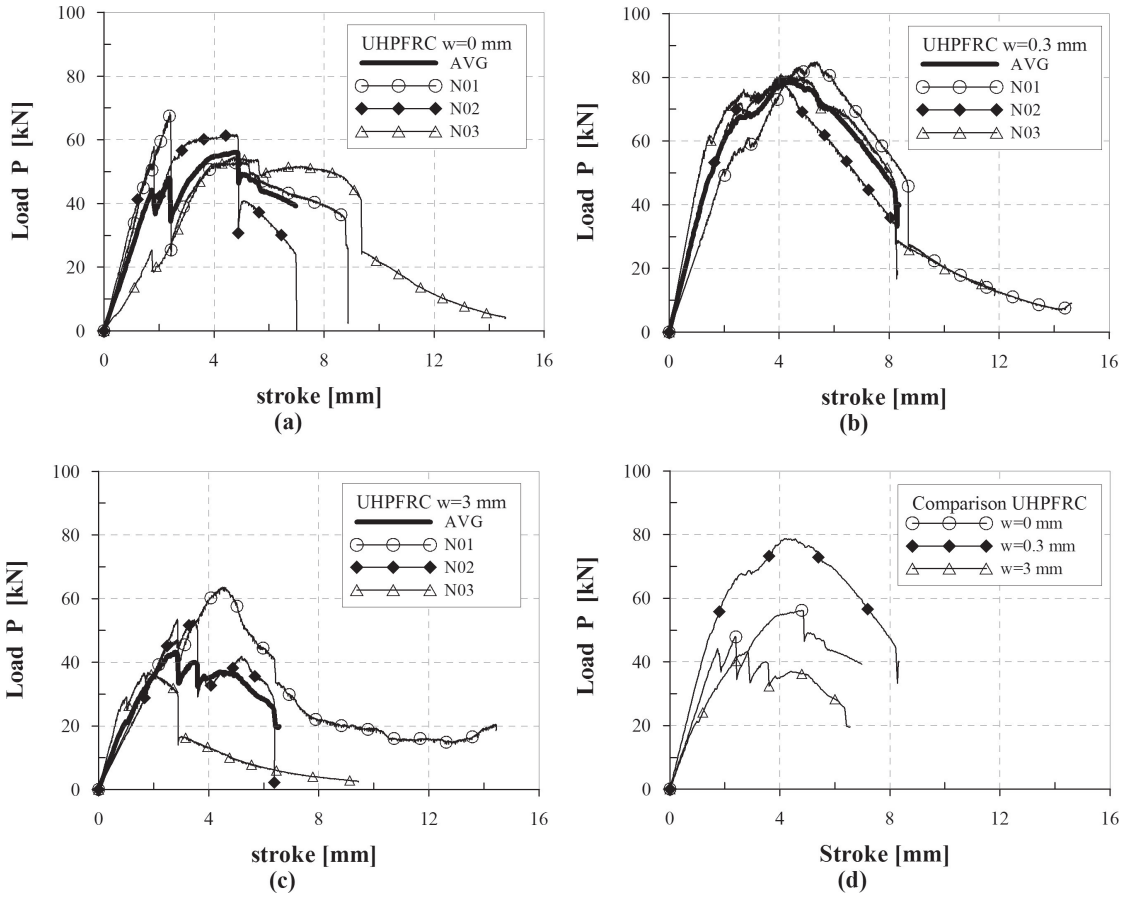

Figure 6.10: Specimen reinforced with UHPFRC: Load vs vertical displacement (a) w=0 mm, (b) w=0.3 mm, (c) w=3 mm

The main cause of the failure mechanism involved in the UHPFRC solution was the strain shrinkage which for this matrix is close to $\epsilon_{sh} = 10^{-3}$. The presence of the substrate restrained the shrinkage thus avoiding any curvature. For this reason, self-stresses caused delamination starting from the ends of the specimen up to the central section. The main difference with the

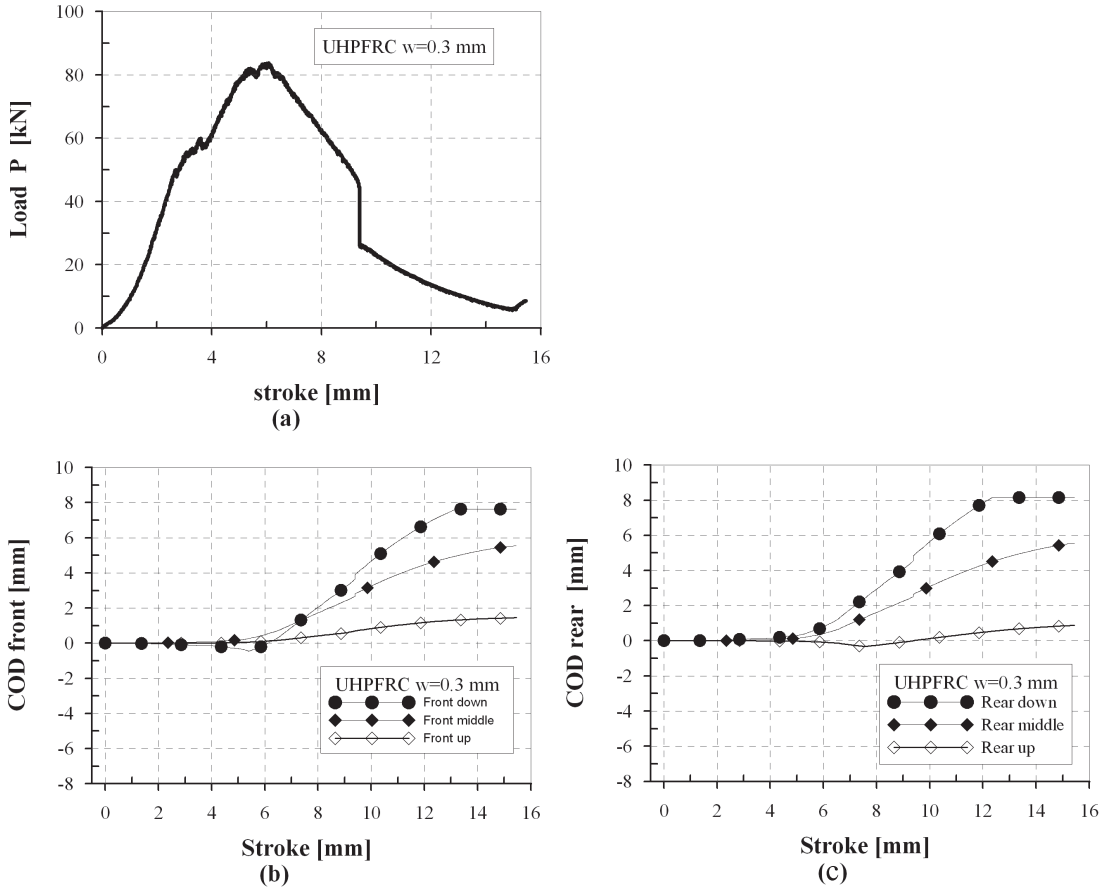

Figure 6.11: (a) Load vs. vertical displacement, (b) rear side COD vs. vertical displacement, (c) front side COD vs. vertical displacement

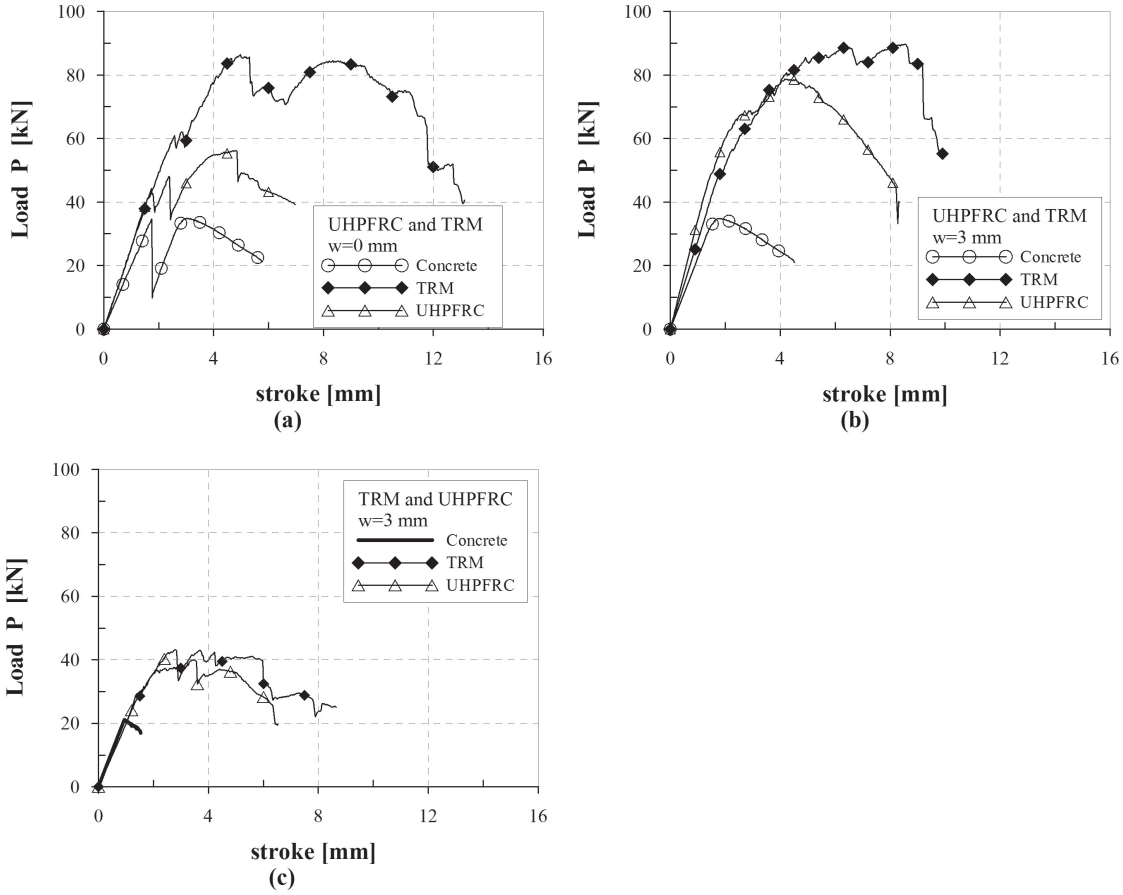

Figure 6.12: Comparison TRM and UHPFRC average curves: (a) w=0 mm, (b) w=0.3 mm, (c) w=3 mm

TRM solution was the thickness layer. Indeed the moment associated to the shrinkage curvature increased with thickness and is given by eq. 6.2 (fig. 6.13).

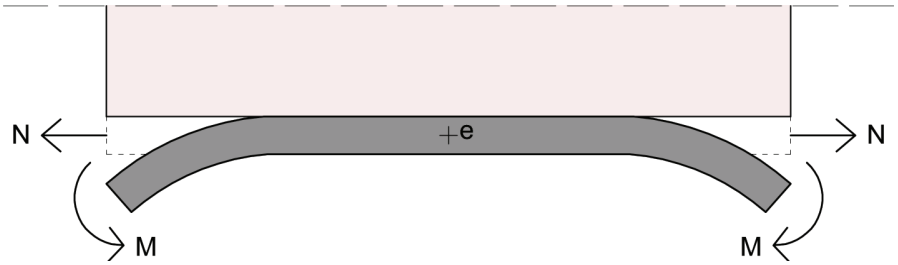

Figure 6.13: Scheme of shrinkage effects

$$M = E \cdot I \cdot \vartheta = E \cdot t^3/12 \cdot \epsilon_{sh}/\left(t/2\right) \tag{6.2}$$

where t is the retrofitting layer thickness, E the retrofitting material elastic modulus and ϵ_{sh} the shrinkage strain. The influence of shrinkage on the axial force (fig. 6.13) can also be computed considering the system concrete and retrofitting layer as two springs working in parallel. By means of the force method, the force X in fig. 6.14, representing the force generated on the subgrade by the shrinkage of the retrofitting layer, can be computed by eqs. 6.3, 6.4 and 6.5:

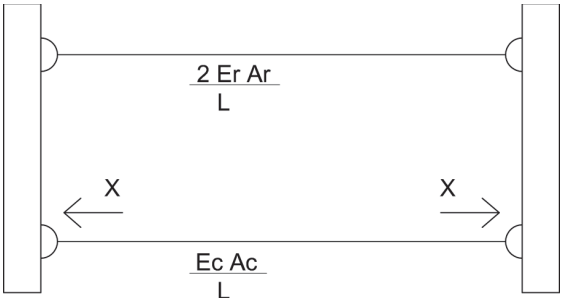

Figure 6.14: Scheme of force method

$$X \cdot \delta_{11} + \delta_{10} = 0 \tag{6.3}$$

$$\left(1/\left(2 \cdot E_R \cdot A_R/L\right) + 1/\left(E_c \cdot A_c/L\right)\right) \cdot X + \epsilon_{sh} \cdot L = 0 \tag{6.4}$$

$$X = \epsilon_{sh} \cdot 2 \cdot A_c \cdot E_c/\left(E_c \cdot A_c/\left(E_R \cdot A_r\right) + 2\right) \tag{6.5}$$

Increasing the stiffness $(E \cdot A)$ of the reinforcement layer, the axial force increases. Both actions (axial force and moment) influence the failure delamination mechanism dominating on the UHPFRC solution.

Shrinkage contribution seems to be relevant both in the case of uncracked solution and of w=3 mm, while in the first case the stiffness of the uncracked subgrade worked as a significant constraint for the retrofitting material shrinkage; in the last case the reinforcement bars were already yielded before retrofitting applications and therefore their irreversible plastic strains may

play a key role in enhancing once again constrain to the retrofitting material shrinkage. In the case of w=0.3 mm, no significant effect of shrinkage strain was observed, maybe because of the subgrade governed by the cracked elastic behavior of the subgrade cross section.

The stress transfer by means of bond occurred and the UHPFRC layer could be activated creating a crack in the center section. In this way it was possible to achieve higher peak load (80 kN) and displacement (8 mm), if compared to the other two cases. The ductility was guaranteed by the controlled growing of the crack in the retrofitting layer due to the presence of steel fiber, while in the two previous cases the ductility was apparent because it was due to delamination of the material but without any visible cracks.

The comparisons of the two solutions in terms of load vs. vertical displacement curves are presented in fig. 6.12 for the three damage levels. For the first two cases, TRM showed the best performances while for the last situation both retrofitting materials are equivalent in terms of maximum load and displacement. Table 6.1 summarizes the maximum load for all the conditions and the ratio between the maximum load of strengthened plates and concrete specimens.

Precrack	Concrete [kN]	TRM [kN]	UHPFRC [kN]	ratio TRM	ratio UHPFRC
w=0 mm	35	86.5	56.12	2.46	1.60
w=0.3 mm	34.8	89.7	78.7	2.62	2.29
w=3 mm	21.09	43	43	2.05	2.05

Table 6.1: Maximum load value

TRM and UHPFRC retrofitting solutions showed a strength more than twice the one of the reference situation. The only exception was the case of UHPFRC for uncracked situation, where the increment was equal to 1.6. Both materials seem to be suitable as retrofitting layer. TRM seems to be the most effective choice from the experimental results and in addition other advantages of TRM are:

- easiness in casting procedure because no formworks are needed;
- no fiber segregation, a typical problem of UHPFRC casting in vertical direction;
- thickness reduced to 6 mm instead of 20 mm with the consequent decrease of the dead load.

Also comparing the cost, TRM is the most convenient choice; considering AR glass fabric (3 Euro/m^2), mortar (140 Euro/m^3)and matrix with steel fibers (440 Euro/m^3), the prices for the two materials according to the considered thicknesses are:
TRM

$$3.3 + 140 \cdot 0.006 = 3.84 Euro/m^2 \tag{6.6}$$

UHPFRC

$$440 \cdot 0.02 = 8.8 Euro/m^2. \tag{6.7}$$

6.2 Compression tests

Before performing the compression tests explained in the previous chapter, the compressive strength of plain concrete was evaluated by compressive tests on cubic specimens (150 X 150 X

Precrack level [mm]	Concrete [kN]	TRM [kN]	ratio TRM [%]	UHPFRC [kN]	ratio UHPFRC [%]
w=0	901.6	752.7	-16.5	779.6	-13.5
w=0.3	718.3	827.0	15.1	780.7	8.7
w=3	724.2	486.7	-32.8	606.3	-16.3

Table 6.2: Maximum compressive loads value

150 mm^3). The cubic value, averaged on 10 tests, was 34 MPa and, considering the area between the notch, the maximum compressive load was computed as follows:

$$A_{net} = 220 \cdot 100 = 22000mm^2 \tag{6.8}$$

$$P_{max}^{exp} = 34 \cdot 22000 = 748kN \tag{6.9}$$

6.2.1 w=0 mm

The failure of concrete substrate (fig.6.15a) presented an elastic behavior until peak load, obtained as average of the peak load of 2 tests, equal to 901 kN and after a brittle collapse. The maximum compressive value was higher to the theoretical strength obtained from the compressive tests on cubic specimen (748 kN). The reason could be due to confinement effect favored by the friction on the longest bases. This was due to the absence of stearic acid between steel plates and specimen during the tests. The friction offered a confinement effect that increased the load of about 17% (eq. 6.10).

$$(901 - 748)/901 = 17\% \tag{6.10}$$

When retrofitting layers were introduced, the reached peak loads were lower than the reference concrete plates ones, as shown in table 6.2. The compressive strength of the only retrofitting layer could be evaluated as:

$$F_{TRM} = f_c \cdot Area = 100MPa \cdot 12mm \cdot 300mm = 360kN \tag{6.11}$$

$$F_{UHPFRC} = 126MPa \cdot 40mm \cdot 300mm = 1512kN \tag{6.12}$$

These contributions of the strengthening materials were not activated because a delamination due to shrinkage occurred during the tests. Even before the tests, the specimens showed partial delamination favored by the larger ageing in relation to the DEWS tests. From studies performed by BASF company, the shrinkage strain at 60 days was around 0.001050. Furthermore, in the strengthened plates, the stresses transfer were quite complex due to the geometry of the specimen and the equilibrium mechanism was explained in Fig. 6.17. The precrack in the ligament section was absent so the applied load was equilibrated both by retrofitting layer and concrete. The eccentricity of the vertical loads respect to strengthening layers favored a detachment of the layer on the upper side and a crack propagation on the central section of concrete. Fig. 6.16 shows the collapse for concrete and UHPFRC strengthened plate. The reason for which the peak load obtained from the experimental results in the strengthened plate was lower than the load of reference concrete plates, has to be found in the complex stress transfer that is different for the two section planes as indicated in fig. 6.18.

In the XY plane the stress are confined in the section ligament and they are transferred to the strengthening layers in the section where the notch of the concrete plate was absent. In the

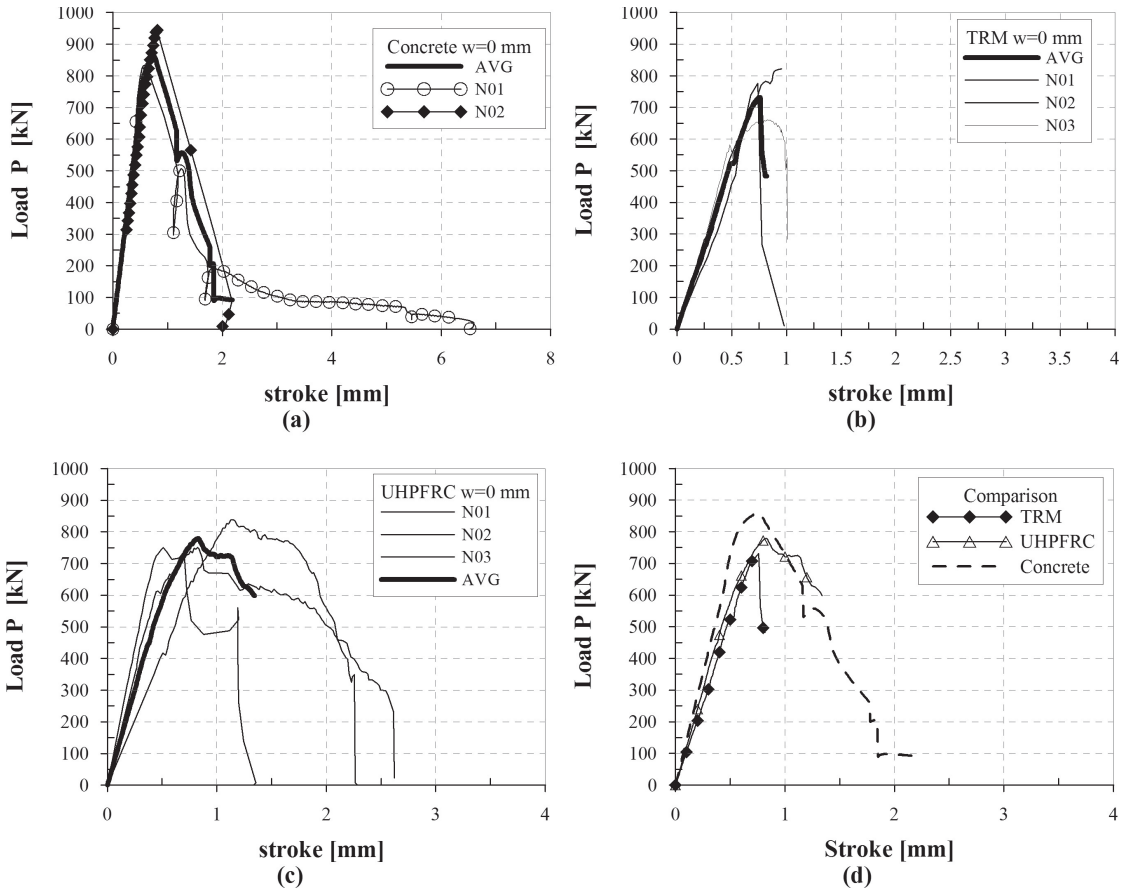

Figure 6.15: Compression tests on sample with w=0 mm, (a) concrete, (b) TRM, (c) UHPFRC layer, (d) comparison

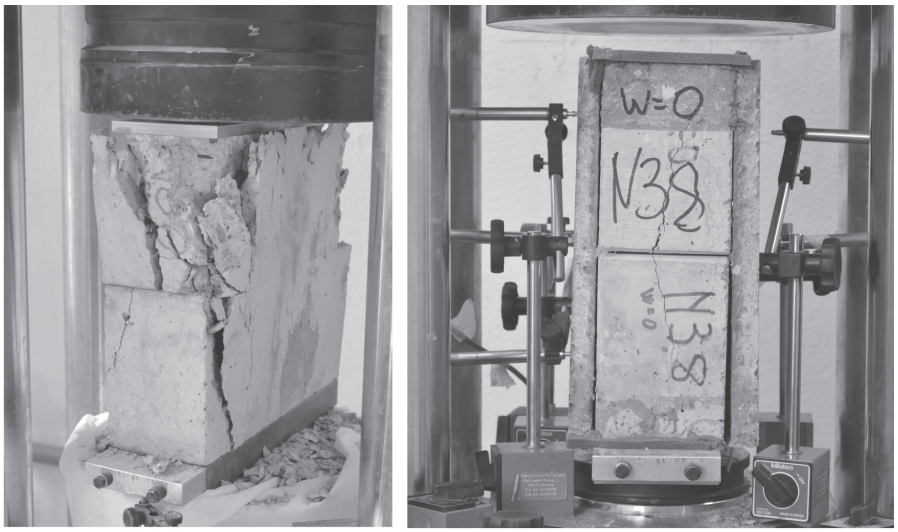

(a) (b)

Figure 6.16: (a) Failure of concrete sample, (b) failure of sample reinforced with UHPFRC for w=0 mm precrack level

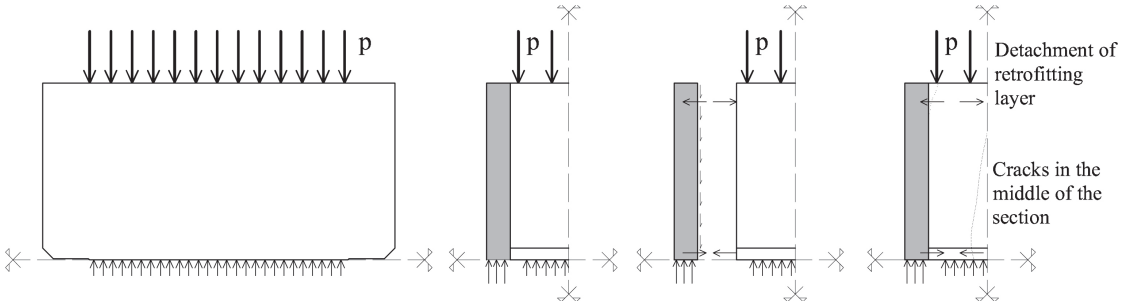

Figure 6.17: Equilibrium for strengthened plates in the case of w=0 mm

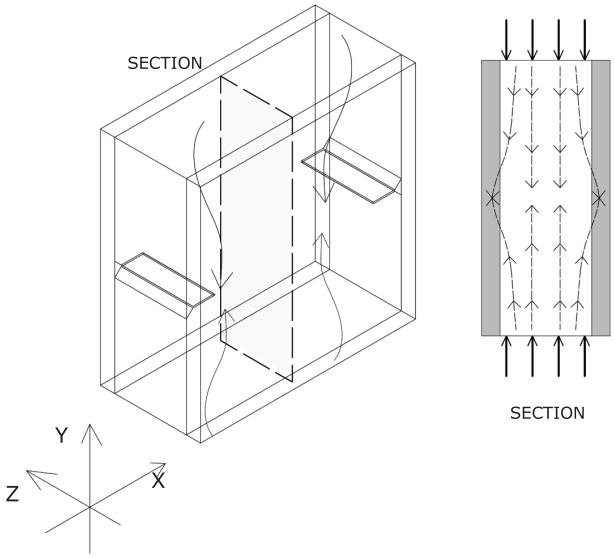

Figure 6.18: The stress transfer in strengthened plates

transverse plane two sections have to be considered: one at the notch level and the second in the central section of the specimen where the notch was absent. In the first case the transmission of stress from the concrete plates to strengthening layers was negligible while in the second section the stresses are transmitted partly to the reinforcement and partly to the concrete plates in the upper side.

6.2.2 w=0.3 mm

In the case of w=0.3 mm the failure of concrete plates were characterized by two behaviors: one was elastic until a peak load around 844 kN and a brittle branch occurred (N02 fig.6.19); the second after reaching a peak load lower than 592 kN, a softening branch took place (N01 fig.6.19). These different collapse mechanisms were influenced by the precrack initial phase, because in the case of specimen N01 the precrack opening was symmetric for the both sides while for specimen N02 the crack width as indicated in table 6.3 were quite different. In the

specimen	rear side [mm]	front side [mm]
N01	0.29	0.21
N02	0.4	0.031

Table 6.3: Precrack values

initial branch of the curves, the slope was lower because there was the reclosure of the precrack. For specimen N02 this phase was not symmetric and a compressive-bending state of stress took place. The different collapse mechanisms of concrete plates, were absent in strengthened plates because the retrofitting layers make stable the crack propagation. The strengthened plates (fig. 6.19b,c) reached maximum peak load higher than concrete plates (table 6.2) with increments respectively 15.1% for TRM and 8.7% for UHPFRC. The greater increment offered by TRM

layer can be due to penetration of the matrix inside the crack, because the aggregate size was 0.6 mm instead of 2 mm. In this crack level the shrinkage strain was less restrained, as already explained for DEWS test, so the delamination should be delayed.

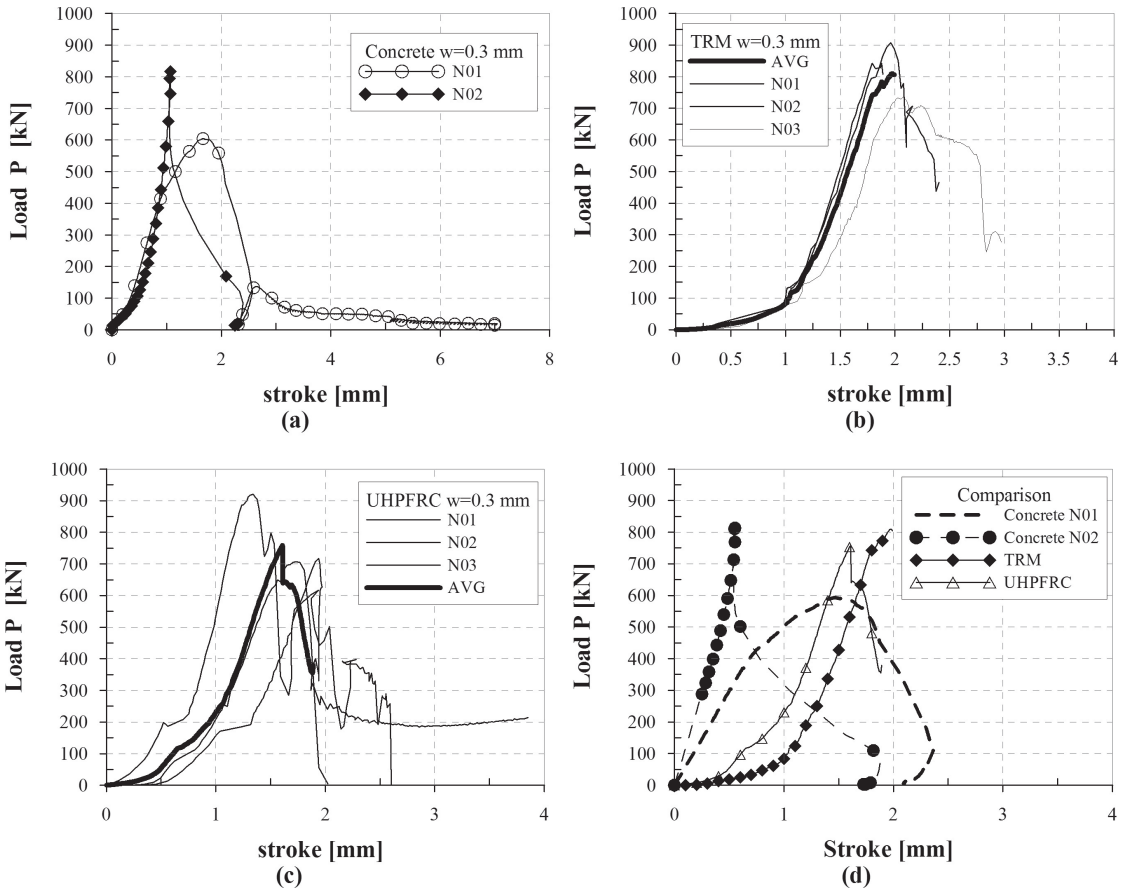

Figure 6.19: Compression tests on sample with w=0.3 mm

6.2.3 w=3 mm

Fig. 6.20 shows the results obtained for plates precracked at 3 mm. For concrete plates two behaviors were highlighted as in the previous crack level case. The different precrack values of both sides are indicated in table 6.4.

specimen	rear side [mm]	front side [mm]
N01	3.01	2.8
N02	3.01	1.57

Table 6.4: Precrack values for 3 mm of damage

Comparing the results with the retrofitting specimens, a decrease of 16.3% for UHPFRC and 32.8% TRM can be observed. In this case the precrack was so high that the complete reclosure of

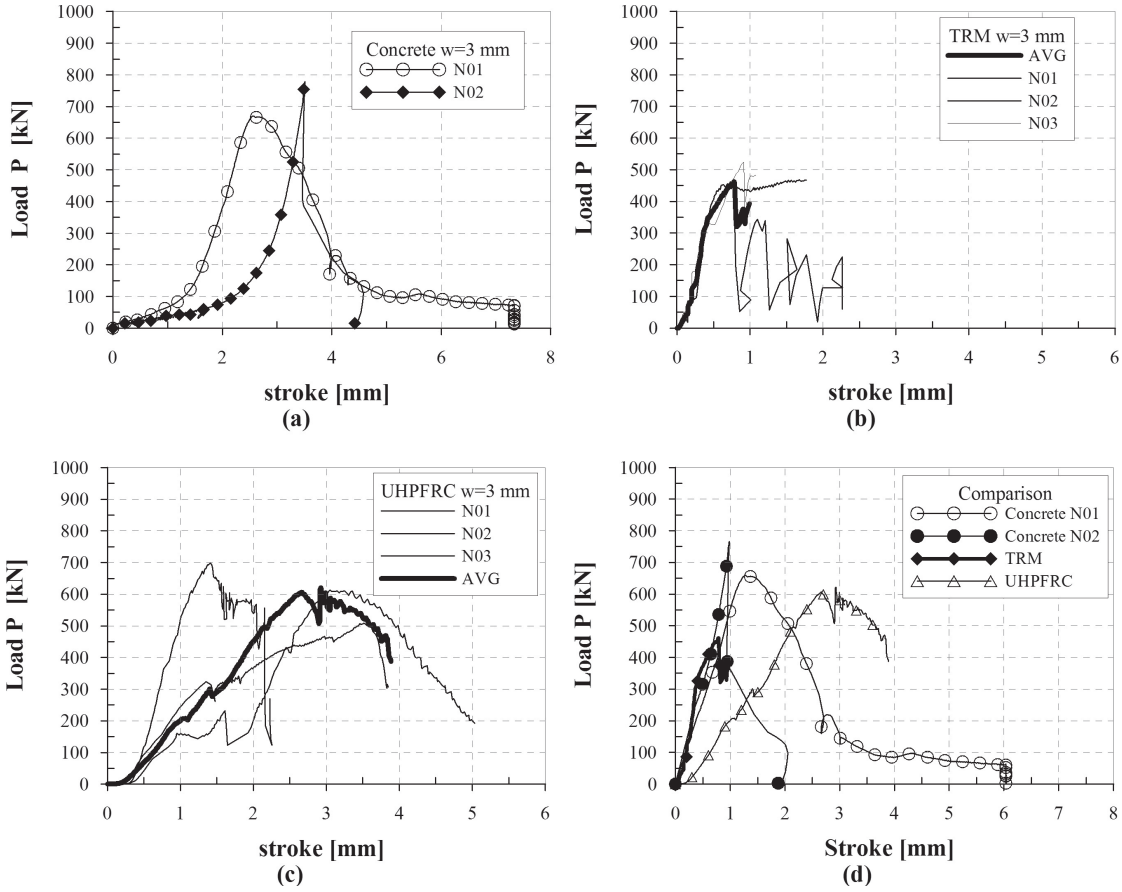

Figure 6.20: Compression tests on sample with w=3 mm

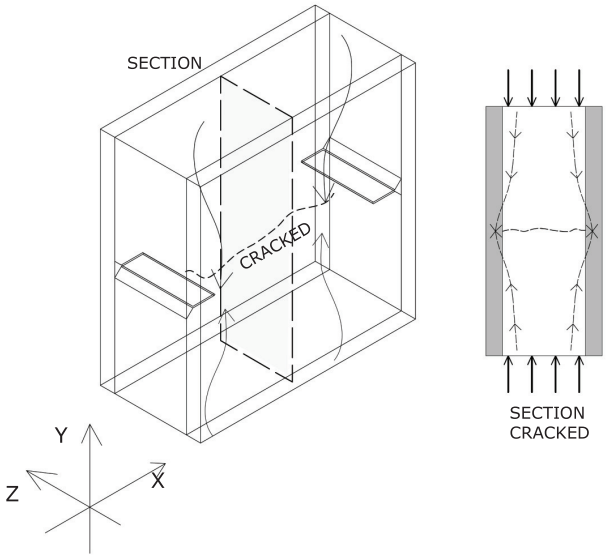

Figure 6.21: Stress transfer mechanism

the cracks was impossible considering the interlocked effect that can be occurred. Furtermore the compressive stress could be transmitted only in the retrofitting layer as shown in fig. 6.21. This mechanisms could influence the peak load value. The details of all tests are shown in appendix D.

Chapter 7

Test results discussion and design prediction

A simplified model was studied to understand mechanisms involved in tensile experiments. The tensile tests performed in the experimental programme presented two aspects very important to be take into account: the geometry and the presence of different materials with which the specimen was made of.

Upper and bottom notches significantly influenced the tensile stress distribution . It is widely known that if a discontinuity is considered, a stress intensity factor has to be considered. The stress distribution differs from the unnotched specimen under tensile load, because tensile stresses are not uniformly distributed along the section present this intensification of the stress value near the notch tips that decreases moving away from the notch.

According to the specimen geometry adopted, when the retrofitting layer experienced to shrinkage phenomenon the related strains are restrained by the inner substrate concrete layer. This means that before starting the tests, the concrete plates had a sort of confinement state of stress and that in the strengthening layer a curvature arises since the not symmetrical shrinkage conditions inside the layer itself. A series of mechanisms were involved during tensile tests. After reaching the tensile strength in the concrete subgrade, crack in the centre of the specimen occurred starting from the tip. Once this crack propagated, also some sliding of the reinforcement bars can occur. This delamination of the steel reinforcement could propagate up to the welded joint with the transverse steel bar providing a direct anchoring. The anchoring capacity of the welded bar depends on bearing load of the weld between the bars. This direct anchor plays a key role in the global stiffness of the sliding mechanism, as a matter of fact just the 10% of stiffness is guaranteed by the indirect anchor provided by the steel bar surface. At the same time the stresses were transferred to the retrofitting material by bond at the interface surfaces. The treatment of the concrete surface is a key issue to improve the bond between the layers. This is the main problem common to all retrofitting applications. The cracks could propagate along the interface between the two layers causing a delamination that when controlled can help to improve the global ductility (as in TRM), but when it involved the whole interface region can even prevent the activation of the retrofitting layer.

7.1 Notch effect

The defects in materials are often considered as the main causes of brittle failure. The effects of stress concentration near the irregularities have long been investigated. If we consider a notch, the stress tends to infinity near the crack tip, fig.7.1. The stress limit is given by the strength of the material.

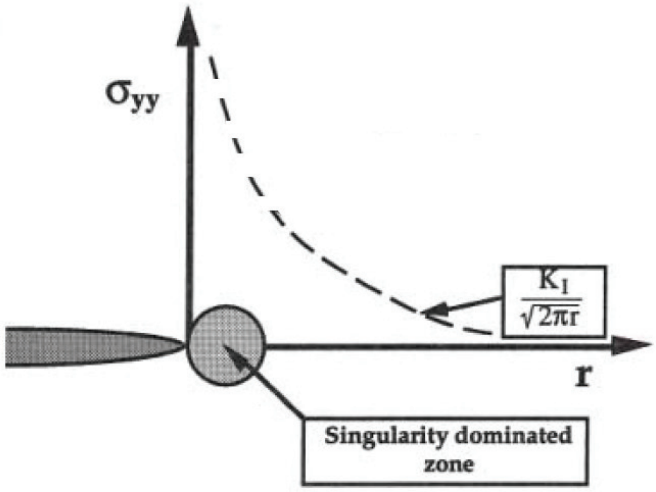

Figure 7.1: Stress distribution near a crack

It is well known from the literature that for defining the state of stress near the crack tip the stress intensity factor (K_I) has to be computed.

$$\sigma = K_I/\sqrt{2 \cdot \pi \cdot a} \tag{7.1}$$

where the parameter a is the crack length and the maximum stress reached corresponds to the tensile strength of the material. The stress intensity factor is tabulated for common tests specimens (Single Edge Notched Tension, Single Edge Notched Bend, Centre Cracked Tension, Double Edge Notched Tension, Compact Specimen) and it depends on the size of the notch (a) and the height of the specimen (W) by function f(a/W).

$$K_I = P/\left(B \cdot \sqrt{W}\right) \cdot f\,(a/W) \tag{7.2}$$

In the model, the presence of the two textile layers can reduce the notch effect because the strengthened material can make stable the crack propagation phase. For this reason it was not taken into account the coefficient proposed by the literature but a coefficient was calibrated by comparing the peak load of the experimental results to the theoretical ones. This parameter was computed equal to 0.55.

7.2 Simplified model

The simplified model considered the DEWS test on undamaged concrete plates reinforced with TRM layers. The TRM layer was chosen as strengthening material because, considering the experimental results, it gave the best performance in terms of maximum load and ductility.

Furthermore, TRM material, unlike the UHPFRC, has not yet standard rule. So this model aims to give some indications, limitations for the designer. In particular, the model takes into account the delamination problem that involves both the steel bar and the retrofitting layers. The effect of the direct anchoring guaranteed by the transversal bar of the mesh was also considered. The idea is to give range values in which the delamination length occurred for the different materials used for retrofitting to understand the portion in which the reinforcement and steel bars were activate.

7.2.1 Reference experimental results

As shown in the previous chapter, the specimen behavior (precracked level equal to w=0 mm) reinforced with two layers of TRC subjected to DEWS tests was shown in fig. 7.2. The model was calibrated considering the splitting force vs. the crack opening displacement as the average of rear and front sides (fig. 7.2b). One of the three tests was stopped because the limit of the machine was reached (100 kN). From the displacement values measured by LVDT at upper, middle and lower levels of the plate and for rear and front side, it is possible to notice that the behavior is quite symmetric in the plane of the specimen. Referring to test N01, the displacement values and rotation vs. the crack opening measured in the middle of the section (average of two values rear and front) are reported as example, fig. 7.3. The maximum crack opening displacement reached was in a range between 1 mm and 1.5 mm for both sides. Considering fig. 7.3a the experimental results are quite near to an ideal line at 45°, that should represent a symmetrical behavior. The rotation was measured dividing the difference between upper and lower crack opening displacement by the height of the ligament (220 mm) fig. 7.3b.

7.2.2 Model description

Starting from the experimental results some assumptions were made. The rotation was equal to zero, so the crack opening was constant along the ligament section and out of plane rotation were equal to zero, so the behavior can be considered in the plane of the specimen and symmetric. The model scheme is represented in fig. 7.4. The contribution for the equilibrium were offered by the concrete plate, the steel bars and TRM layers.

Because of the horizontal equilibrium the sum of each contribution is equal to the splitting force (F_{sp}). The equilibrium equation is expressed in eq.7.3:

$$F_{sp} = F_{concrete} + F_{Steel} + F_{TRM} \tag{7.3}$$

The three forces acted as three spring that worked in parallel where the total displacement was the same for each springs while the total force was the sum of each element, fig.7.5. The splitting force is a function that depends on the crack opening displacement:

$$F_{sp} = F(w) \tag{7.4}$$

The parameters involved are the characteristic lengths (TRM and steel bars) and the positive increment of the crack lengths ΔL_{cs}:

$$L_{cs,TRM} < \bar{L1} \tag{7.5}$$

$$L_{cs,steel} < \bar{L2} \tag{7.6}$$

$$\Delta L_{cs,TRM} > 0 \tag{7.7}$$

$$\Delta L_{cs,steel} > 0 \tag{7.8}$$

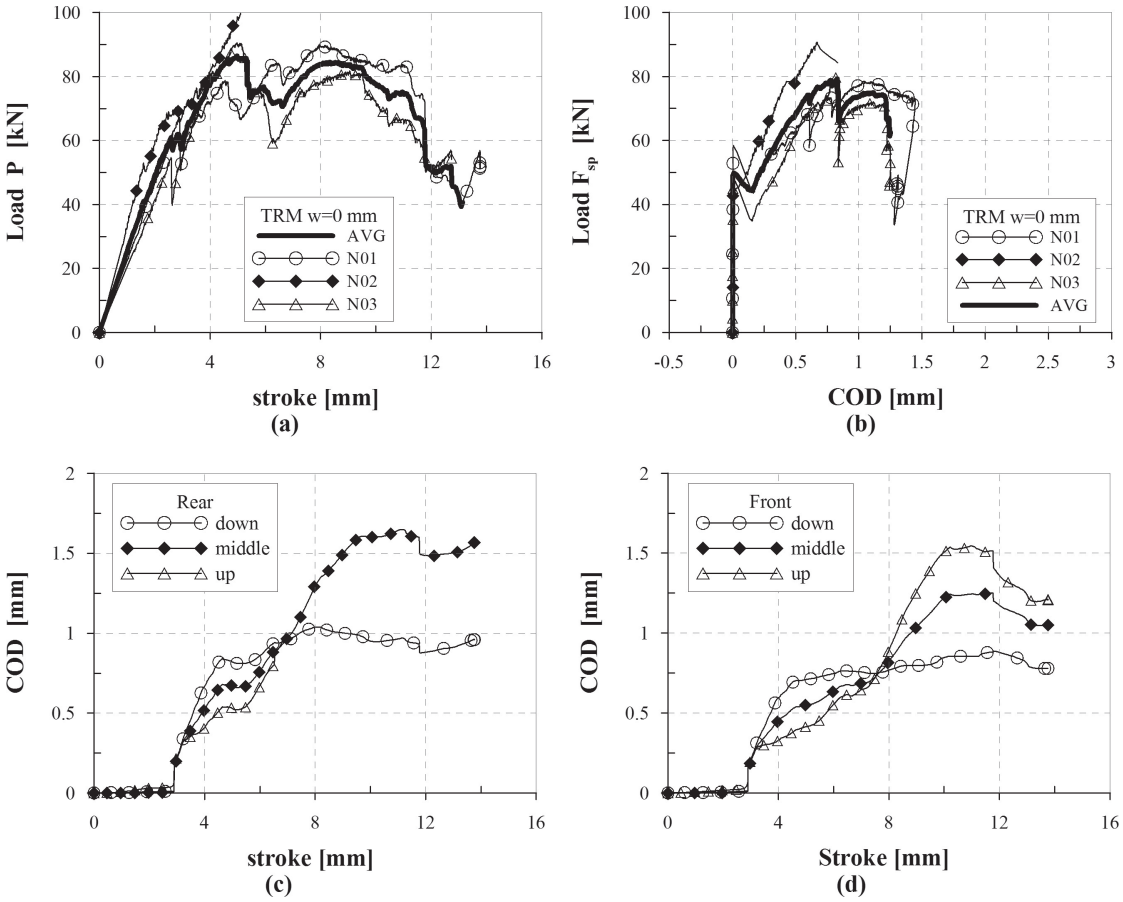

Figure 7.2: Specimen retrofitting with TRM under DEWS test (a) Vertical load vs. displacement, (b) splitting force vs. COD (c), (d) rear and front displacement vs. stroke, see also fig. 6.8

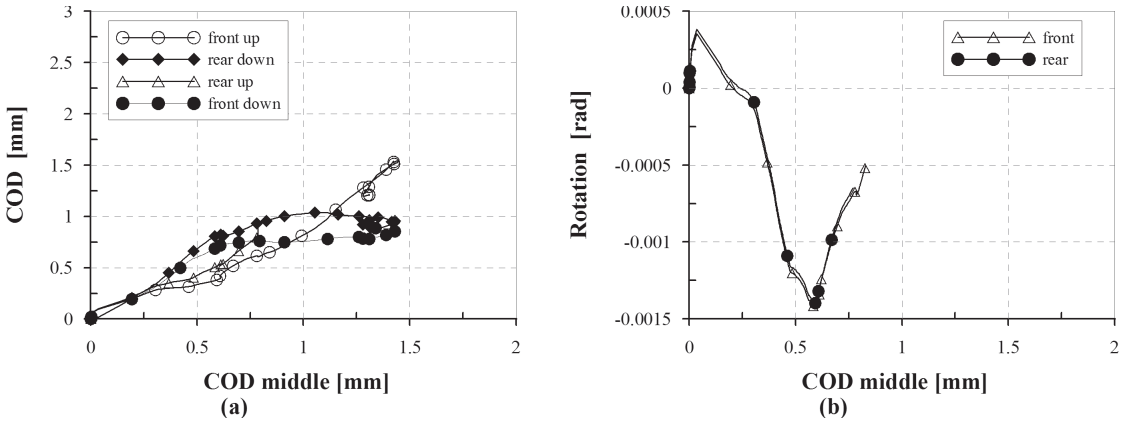

Figure 7.3: (a) COD front and rear for up and down level, (b) curvature rear and front vs. COD measured in the middle of the section

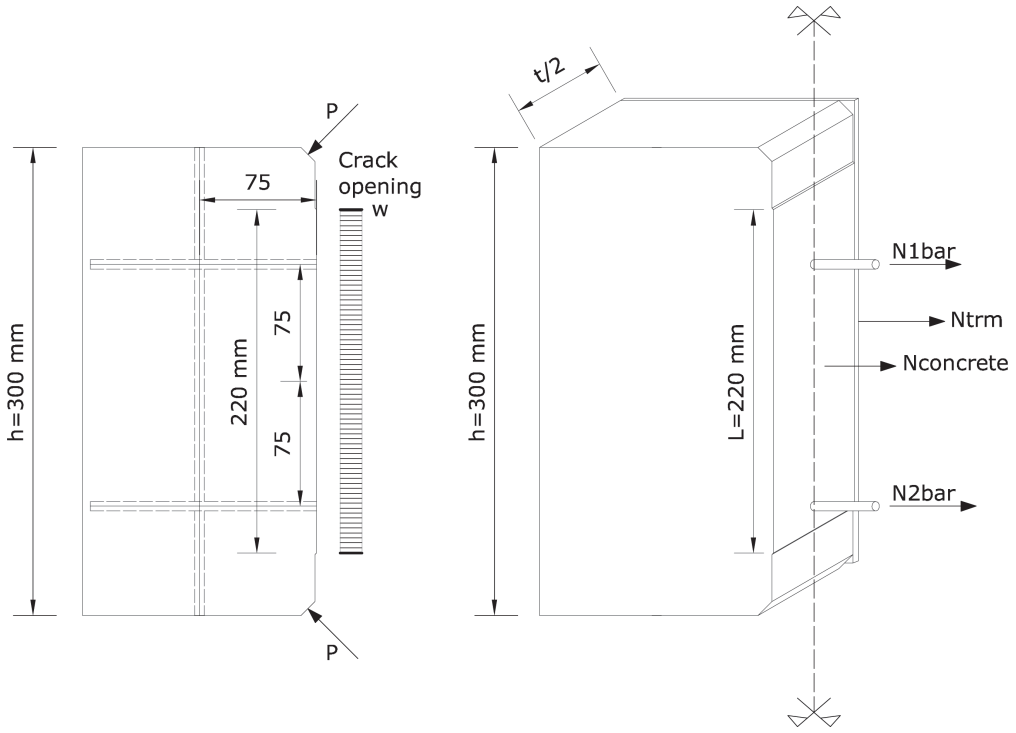

Figure 7.4: Model scheme 2D and 3D sections

Both the values of L_{cs} (TRM and steel) had a geometric limits ($\bar{L}1$=300 mm, size plate and $\bar{L}2$=150 mm, distance of the two vertical bars). The constitutive laws of steel and TRM are defined in terms of stress vs. strain and are discussed in the following paragraph. For this reason and since the kinematic description is given by a uniform crack opening distribution, a structural characteristic length has to be defined for all the materials the strain and stress values. Because of delamination, the length over which anchoring is missing define this characteristic length for TRM and reinforcement bars. Other contributions like the direct anchoring have to be taken into account and they will explained in the next paragraph.

7.2.3 Constitutive laws

The constitutive law of subgrade concrete was expressed in the pre-peak phase by a bilinear according to the MC2010 [99], while the post peak was defined by a Hordijk curve. From an elastic analysis it was estimated the length over the tensile stresses dominated that was the distance where two compressive arches occurred. So a distance of 150 mm was considered to compute the crack opening starting from the strain values. The relationship was shown in fig. 7.6 where the stress values in points A and B are the following eqs. 7.9, 7.10 and collected in table 7.1:

$$\sigma_B = f_{ctm} = 0.3 \cdot (f_{ck})^{(2/3)} = 0.3 \cdot 20.22^{(2/3)} = 2.23MPa \tag{7.9}$$

$$\sigma_A = 0.9 \cdot f_{ctm} = 2.007MPa \tag{7.10}$$

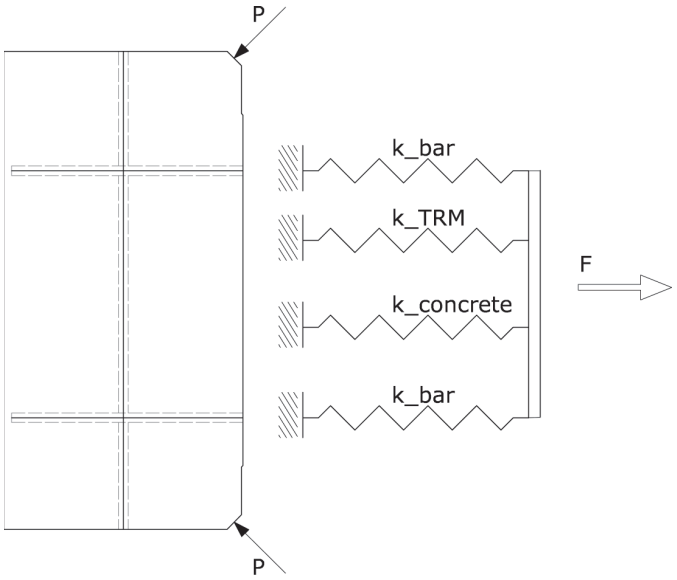

Figure 7.5: Scheme of the forces

point	stress [MPa]	strain [-]
A	2.007	0.0000943
B	2.23	0.00015

Table 7.1: Stress and strain values

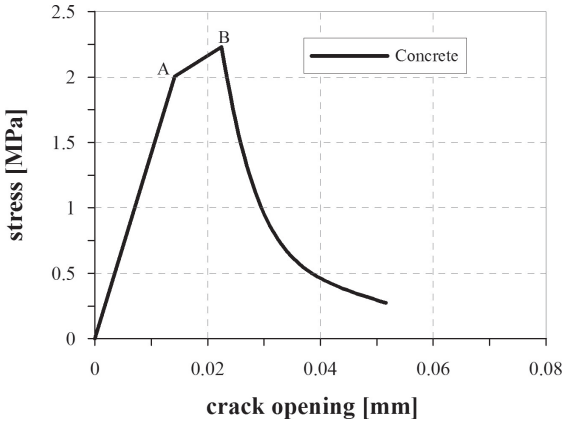

Figure 7.6: Constitutive law of concrete stress vs. crack opening

Along the section the stresses of the concrete were variable according to the constitutive law so the area between the notches was discretized in several steps. The concrete force was obtained by the sum of the forces for every step.

Starting from the experimental characterization, the constitutive laws of TRM and steel were extrapolated (fig. 7.7) in terms of stress vs. strain (table 7.2). The dashed line in fig. 7.7(b) indicates necking in the bar and the strain was computed dividing the vertical displacement of the machine by the diameter of the bar. By imposing the crack opening suitable characteristic lengths were calibrated based on experimental results.

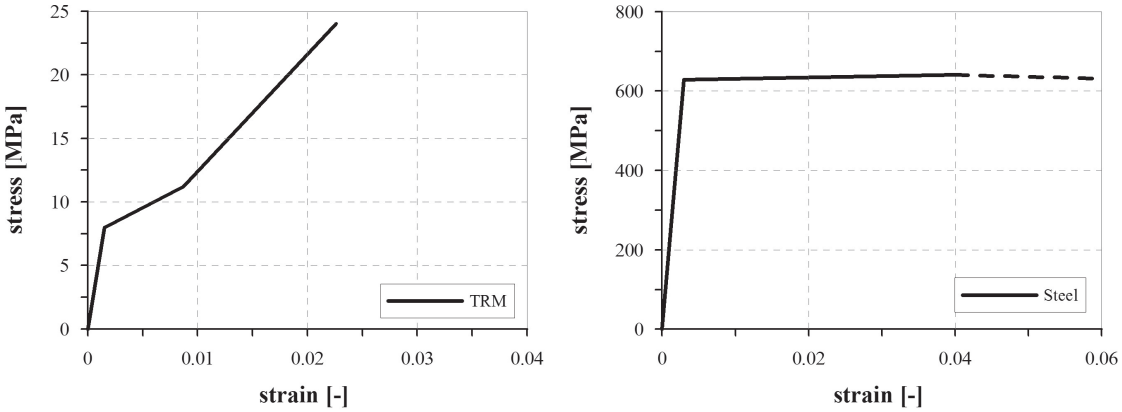

Figure 7.7: Constitutive laws of (a) TRM and (b) steel

TRM		STEEL	
stress [MPa]	strain [-]	stress [MPa]	strain [-]
0	0	0	0
8	0.0015	628	0.003
11.2	0.0087	641	0.04
24	0.02258	478.83	0.4

Table 7.2: Constitutive parameter for TRM and steel

7.2.4 Contribution of steel welded mesh

The stress transfer from steel bar to concrete occurred by bond. After reaching the maximum tangential strength, delamination started and propagated along the bar. The maximum delamination length was 150 mm that is the distance between the two transverse bars of the mesh. After that, the direct anchoring, guaranteed by the presence of the welded in the intersection of the two steel bars, start to be active. This can be schematized as a spring (K_{II}) that works in series with the stiffness (K_I) associated to the elongation of the bar, fig.7.8. Two points have to be considered in the node: the weld and the flexibility of the vertical bar. Considering the second one as the weakest mechanism, the transverse bar could be subjected to bending for a displacement δ.

The contribution provided by transverse bar has just been estimated by di Prisco [100]. The experimental campaign was conducted for a research project financed by Pigazzi Reti Cortenova.

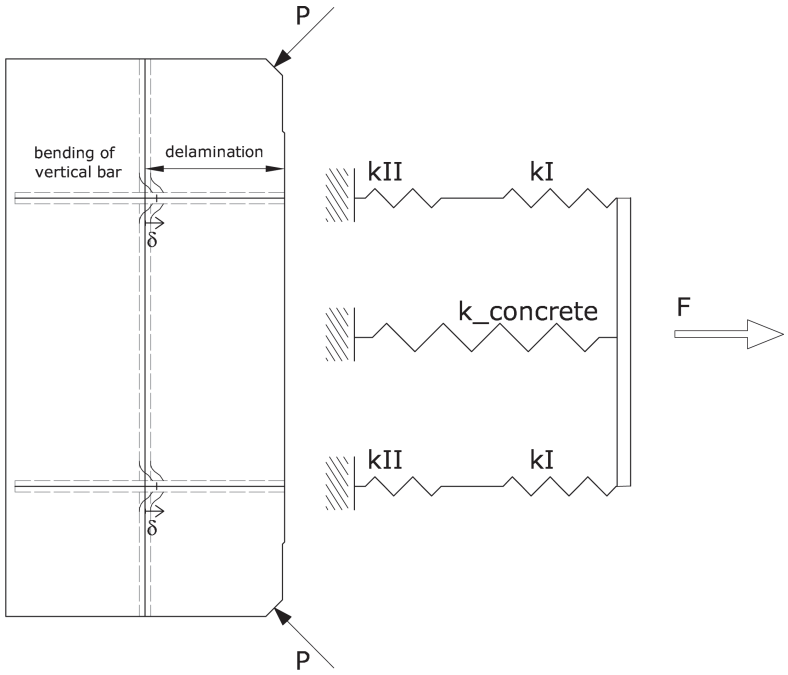

Figure 7.8: Direct anchoring and bending of the vertical bar

The welded mesh had diameter of 8 mm embedded in concrete C20/25 for a total length of 200 mm and with a transverse welded bar of 8 mm diameter. The tests were divided in three groups according to the percentage of longitudinal bar in contact with the concrete (0, 50, 100%) of the embedded length. The contribution provided by the trasverse bar was studied by decoupling the longitudinal bars from the concrete by means of a plastic pipe. The stiffness of the spring that represented the contribution of the trasverse bar was computed around 40 kN/mm that represents the 91% of the global stiffness of the whole anchoring mechanism so, just the 9% was related to indirect anchor, after pull-out.

7.2.5 Experimental and prediction comparison

The design model was calibrated according to the experimental results in order to investigate the stiffness offered by direct and indirect anchoring and the contribution of TRM. The model was calibrated on the experimental curve, obtained as the average of three experimental test, that was divided in different branch as shown in fig. 7.9. In particular the aim of the model is to define the bond length of TRM and reinforcing bars that guaranteed the equilibrium with the experimental splitting force for a given crack opening value. For each branch considered a proper bond length evolution law was assumed to best fit the experimental results. For all branches investigated the delamination length and the distribution of stresses assumed are reported.

Branch OA - AB

The first branch (OA) (fig.7.9) was linear until when the tensile strength of the subgrade concrete was reached. The peak load was computed considering the contribution of the concrete and TRM, and a coefficient due to the notch effect experimentally calibrated and acting in the range P-P'

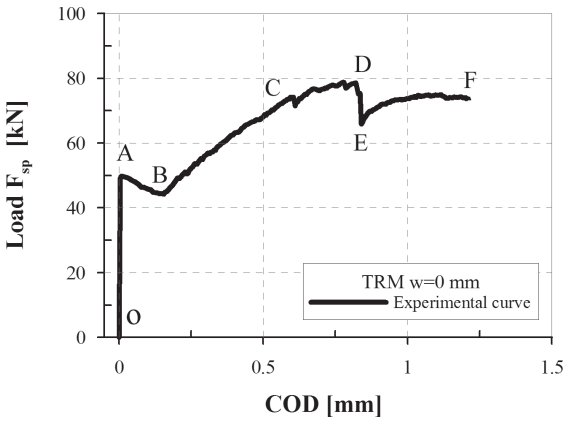

Figure 7.9: Experimental curve

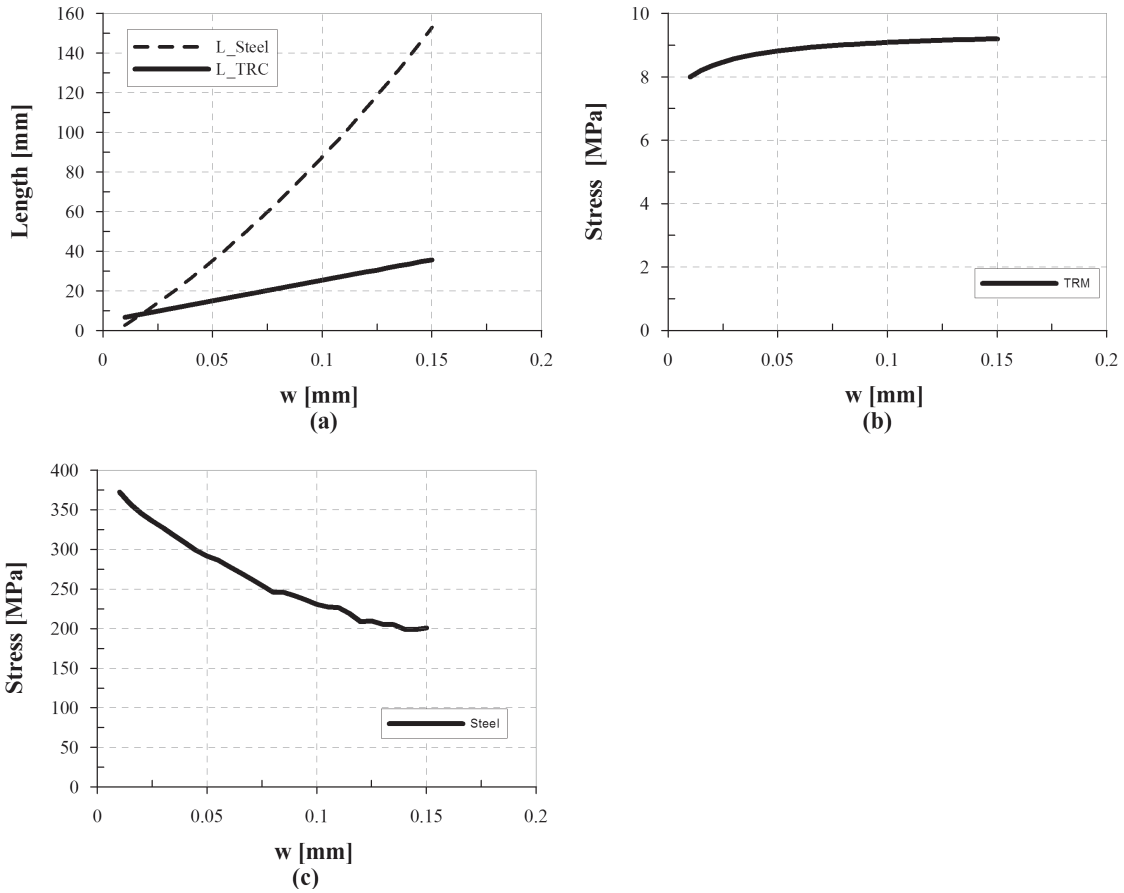

Figure 7.10: Branch AB (a) Delamination length TRC and steel vs. w (crack opening) , (b) Stress TRM vs. w, (c) Stress steel vs. w

(fig. 7.14b), until a crack opening of 0.04 mm. After reaching the tensile strength (branch AB w=0.01-0.15 mm), the TRM layer and the steel bar were activated. The load decreased because delamination phenomena occurred. In this phase the steel bars delaminate up to a distance of 150 mm, fig.7.10a. This measure corresponded to the distance between the two vertical bars of the mesh that offered a direct anchoring. The TRC layer in this branch presented microcracks along distance of 6-35 mm. These values were measured by means of a visible inspection carried out through a micrometer. The stress distribution of TRM layer and steel bars are shown in fig. 7.10b, c. In the point A the TRM layer has a stress equal to 8 MPa corresponding to the onset of multicracking in agreement with the TRM constitutive law.

7.2.6 Branch BC

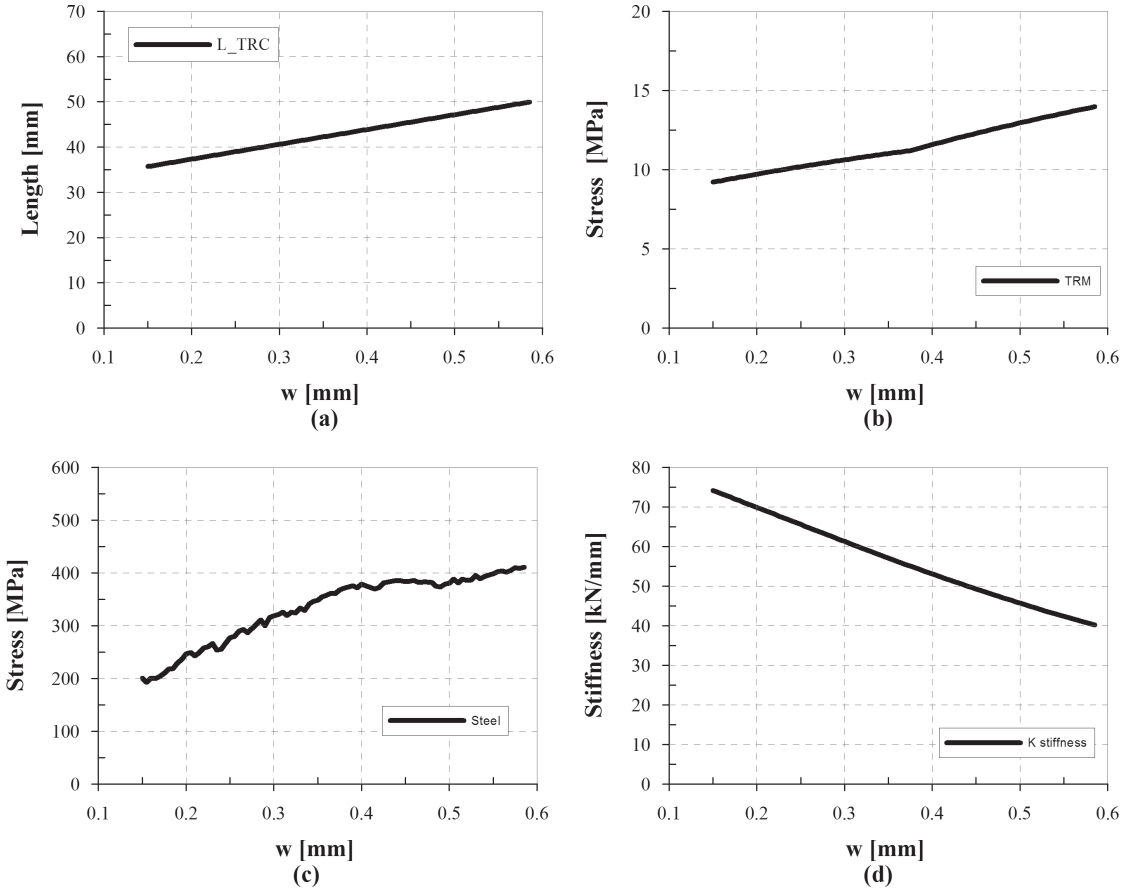

Figure 7.11: Branch BC (a) Delamination length TRC vs. w, (b) Stress TRM vs. w, (c) Stress steel vs. w, (d) Stiffness vs. w

In the branch BC (w=0.15-0.6 mm) the load increased until a value equal to 74 kN. The delamination of TRM grew up to a value of 50 mm always measured by means of a visible inspection, while in the steel bar no further delamination occurred and the welded mesh direct anchoring was activated (fig.7.11) by assuming to neglect tension stiffening out this stage. The stiffness (KII) of the spring due to the intersection node with the transverse bar was found and

decreased from 70 to 40 kN/mm. Considering the delamination length of the bar limited to 150 mm, the remaining contribution due to the KII spring was computed. As said before, the two springs worked in series, so the total displacement was given by the sum of the two elements. The tensile stress in the TRM layer reached the value of 14 MPa, while in steel bar was equal to 415 MPa still corresponding to the elastic branch of the constitutive law.

7.2.7 Branch CD

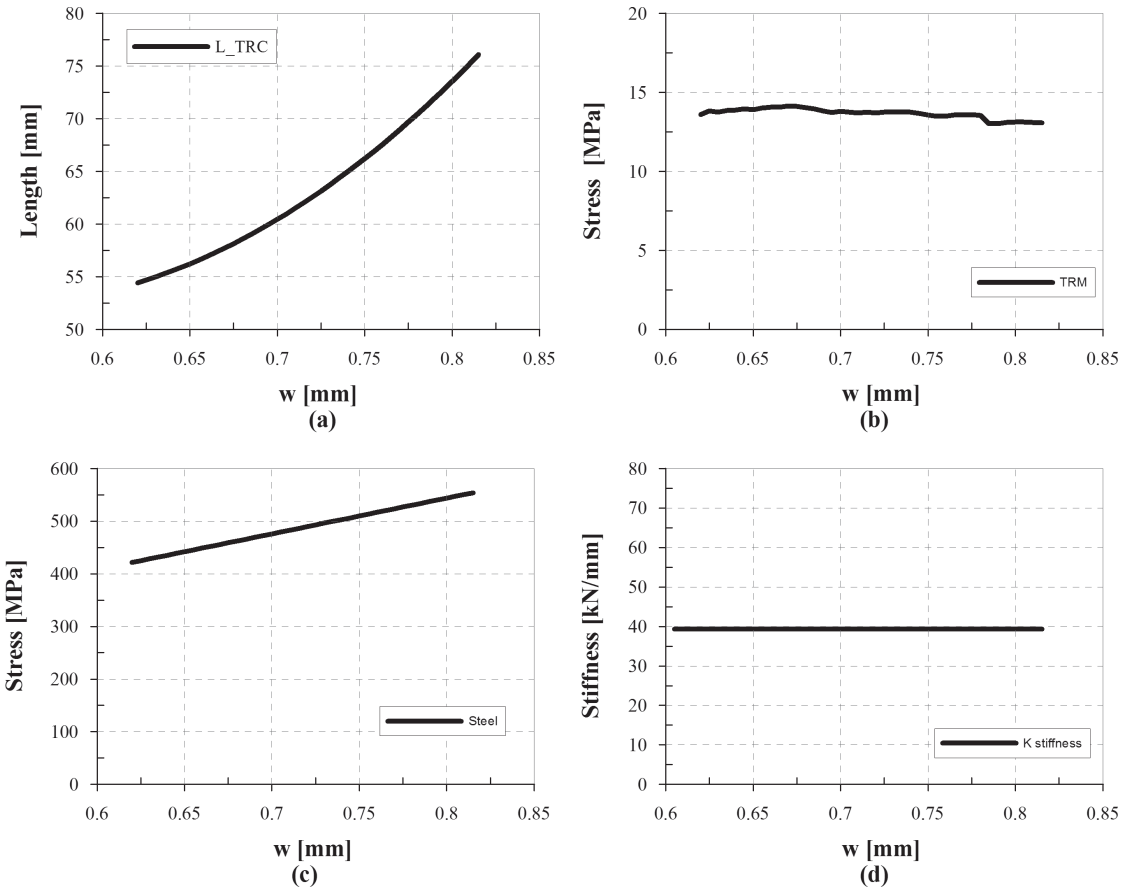

Figure 7.12: Branch CD (a) Delamination length TRC vs. w, (b) Stress TRM vs. w, (c) Stress steel vs. w, (d) Stiffness vs. w

In the point C the load vs. crack opening displacement curve showed a discontinuity where the load decreased from 74 to 71 kN. This decrease may be due to further detachment of the TRM layer at w=0.61 mm resulting from 50 mm to 55 mm. After that, the delamination portion increased until 78 mm and the tensile stress distribution remained around the value of 13 MPa for all branch. The results are presented in fig. 7.12. The stiffness of the direct anchoring of the mesh remained constant and bar stress was so known and from equilibrium the TRM stresses were computed (fig.7.12d). This last information allows to identify the TRM delamination crack evolution. The stresses of the bars grew until value of 554 MPa.

7.2.8 Branch EF

The final branch was characterized by a clear decrease of the load in the point E from 78 to 68 kN because a further detachment of the TRM layer occurred. In particular delamination happened for a length of 162 mm (fig. 7.13)a. The tensile stress decreased from 12 to 9 MPa in the range 0.82 to 0.84 mm (fig. 7.13)b while in the bar the tensile strength was quite constant at 627 MPa (fig. 7.13)c. The experimental tests were stopped when the load knife was completely inside in the V shaped notch not reaching the steel bars failure. Also in this simplified interpretation the stress of the steel was lower than the yield value.

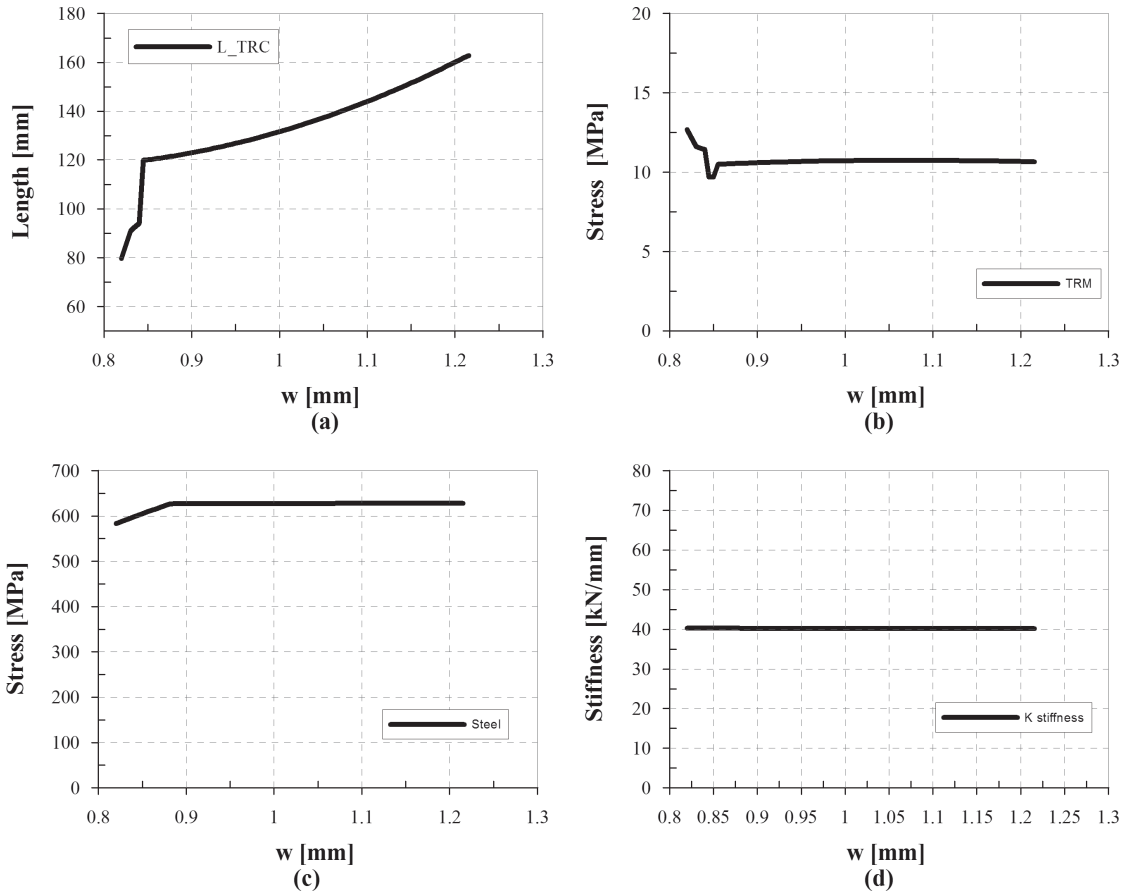

Figure 7.13: Branch EF (a) Delamination length TRC vs. w, (b) Stress TRM vs. w, (c) Stress steel vs. w, (d) Stiffness vs. w

The comparison between the experimental curve and the simplified model and the evolution of delamination length of the TRM are reported in fig. 7.14.

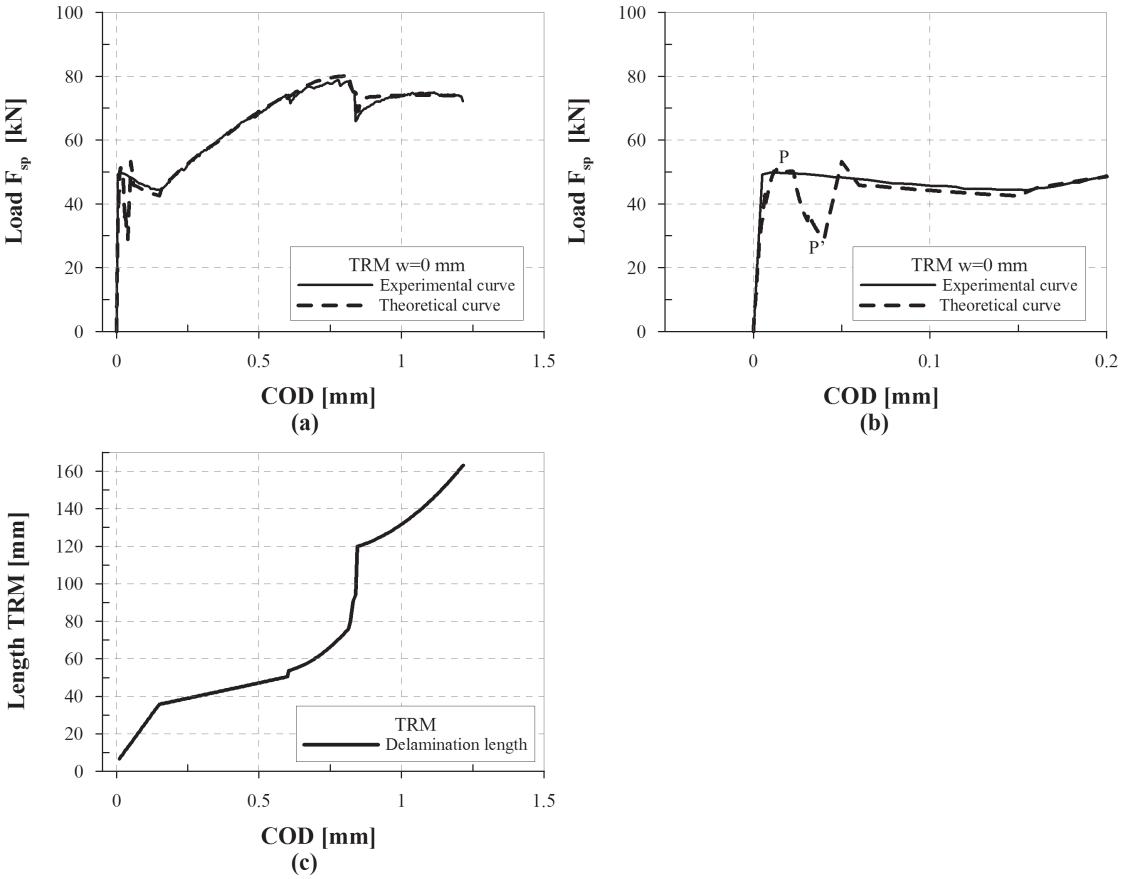

Figure 7.14: (a) Comparison with experimental curve, (b) detail of the peak, (c) evolution of delamination length of TRM

Chapter 8

Concluding remarks and further developments

8.1 Conclusion

This thesis investigates the use of two materials Textile Reinforced Mortar (TRM) and Ultra High Performance Fiber Reinforced Concrete (UHPFRC) for strengthening and seismic retrofitting of concrete structures. The research aims to study the mechanical characterization of the materials and their coupling with traditional reinforced concrete. The retrofitting of building damaged by earthquake is a very important issue. As a matter of fact is quite important to look for a retrofitting technique that can ensure the global structural safety of the building, the speed of the placing operations and the durability of the solution. All these aspects are crucial in order to restore the full functionality and safety of the damaged buildings. The reduction of the time for the retrofitting operations is very important to reduce all the costs related to provisional housing and to the inactivity of the business activities. In this sense the use of TRM and UHPFRC can be a good way to achieve a strong and fast retrofitting solution.

A real innovation was the technique adopted to investigate the effectiveness of the reinforcement layer. Up to now DEWS test has been used to identify the residual strength in the post-cracking regime of Fiber Reinforced Concrete. Using this technique it was possible to combine several advantages. In principal the possibility of carrying out tensile tests by applying compressive loads, thus avoiding the typical problem of the direct tensile test on the specimen such as glued plates on the edges of the specimen to distribute the load. This aspect is common with other indirect tensile test such as bending and Brazilian test, but with this technique, it is possible to minimize the structural effects. In particular the new test produces the stress distribution on the ligament of a notched specimen loaded in pure tension, without any crosswise compressive stresses. Furthermore DEWS test allows to compare the retrofitting specimen with the unstrengthened ones in terms of load capacity but above all in terms of ductility. The ductility is driven by the deformation of the strengthening material and by the delamination between retrofitting and subgrade. So when the stresses are transmitted from the support to retrofitting layer, the last one could deform over a length in which the material is detached from the substrate.

A comprehensive experimental program was carried out in order to provide a better understanding on the effectiveness of TRM and UHPFRC as retrofitting layer as a means of increasing the bearing and deformation capacity of Reinforced Concrete (RC) structures and some impor-

tant conclusions can be highlighted. By comparing the maximum load reached by using TRM and UHPFRC layer in the three damage levels, TRM showed the best performances. Indeed the ratio between maximum load of the retrofitting solution and of the reference specimen is here reported (table 8.1) as just shown in chapter 06.

Precrack	Concrete [kN]	TRM [kN]	UHPFRC [kN]	ratio TRM	ratio UHPFRC
w=0 mm	35	86.5	56.12	2.46	1.60
w=0.3 mm	34.8	89.7	78.7	2.62	2.29
w=3 mm	21.09	43	43	2.05	2.05

Table 8.1: Maximum load values

In terms of ductility it is not possible to compare the crack opening displacement of the concrete specimen with the strengthened ones, because for the last one the tests were stopped before the failure of the steel bars or the retrofitting layer. Nevertheless the major ductility was reached in the TRM solution because the good bond at the interface surface allows to transfer the tensile stresses from the support to the strengthening layer. TRM multicracks in the central region where a portion of the layer is detached from the concrete plate. On the contrary UHPFRC solution presented a delamination over all the interface before developing his tensile strength and no cracks were observed on the surface. The whole detachment occurred as a rigid body motion. Enhancement in bond interface has to be investigated to employ the tensile properties of the material.

The ductility of TRM is guaranteed by the delamination range and in the design model it is possible to evaluate a quite gradual variation of the bond length. The aim of the model is to estimate for each crack opening displacement, the detachment of TRM layer and consequently the stress strain distribution. The maximum detachment evaluated by the model is equal to 160 mm, that is half of the specimen size, and the maximum stress reached in the TRM layer is equal to 14 MPa that is less than the maximum tensile strength of the material.

By comparing the two TRM and UHPFRC solutions, it is concluded that TRM layer is an extremely effective and promising strengthening technique for reinforced concrete. Other advantages are the reduced thickness (6 mm instead of 20 mm), the cost (3.84 $Euro/m^2$ instead of 8.8 $Euro/m^2$), the easy application since no formwork are needed.

8.2 Future prospectives

In the experimental investigation performed during this work different bond surface geometries were not take into account. Usually in the real application a sandblasting treatment is used to make the surface rough: in this case different pressure and size sand can be adopted. The treatment of the interface is the first aspect to be considered for ensuring the stress transfer. Furthermore also the use of direct anchoring will be investigated in the future.

An other aspect, that may be investigated, is larger crack opening displacement in order to reach the failure of the specimen. In this case other possible failure mechanisms can be evident such as the failure of retrofitting layer or steel bar. The aim is to define the ductility offered by the strengthening layer when the material has reached his maximum tensile strength.

For better understanding the behavior under compressive load, the effect of the notch on the stress distribution should be investigated. In particular the geometry of specimen may be modified removing the notch that causes a possible deviation of the compressive stress distribution.

Appendix A

Mix design

specimen	batch	f_{ctf}[MPa]	f_{ctm} [MPa]	f_c [MPa]	
N1	1	14.98	6.63	114.81	103.60
N2	1	16.97	7.51	106.38	126.68
N3	1	17.86	7.90	107.30	107.63
N4	2	19.51	8.63	99.74	108.53
N5	2	19.15	8.47	114.33	113.05
N6	2	20.72	9.17	114.71	121.11
Average		18.20	8.05	111.46	
STD		2.05	0.91	7.54	
STD%		11.26	11.3	6.76	

Table A.1: Bending and compressive strength M1 (0.19 w/b, 7.3% Hp/c)

specimen	Pmax [N]	b [mm]	h [mm]	f_{ctf} [MPa]	f_{ct} [MPa]
N1	6125.8	40.1	39.8	14.4	6.30
N2	6886.9	39.46	39.7	16.5	7.30
N3	5980.4	39.3	39.8	14.3	6.30

Table A.2: Bending strength M2 (0.19 w/b, 8.3% Hp/c)

Specimen	Fc [kN]	A [mm^2]	f_c [MPa]
N1	143.6	1600	89.7
N2	164.2	1600	102.6
N3	175.6	1600	109.7
N4	160.3	1600	100.1
N5	121.3	1600	75.8
N6	140.7	1600	87.9

Table A.3: Compressive strength M2 (0.19 w/b, 8.3% Hp/c)

specimen	batch	f_{ctf}[MPa]	f_{ctm} [MPa]	f_c [MPa]	
N1	4	13.82	6.11	98.69	114.29
N2	4	17.45	7.72	103.23	107.47
N3	5	11.76	5.20	94.90	92.38
N4	5	12.32	5.45	97.92	80.34
N5	5	13.58	6.01	94.22	94.86
N6	6	13.65	6.04	103.26	95.79
N7	6	12.72	5.63	92.39	93.01
N8	6	13.62	6.03	97.43	100.55
Average		14.25	6.02	100.61	
STD		1.83	0.76	6.75	
STD%		12.906	12.6	6.71	

Table A.4: Bending and compressive strength M3 (0.19 w/b, 9.3% Hp/c)

specimen	Pmax [N]	b [mm]	h [mm]	f_{ctf} [MPa]	f_{ct} [MPa]
N1	6644.3	39.31	39.78	16.0	7.0
N2	5270.8	39.22	39.81	12.7	5.6
N3	7534.5	39.41	39.94	17.9	7.9

Table A.5: Bending strength M4 (0.19 w/b, 10.3% Hp/c)

Specimen	Fc [kN]	A [mm^2]	f_c [MPa]
N1	161.74	1600	101.0
N2	145.56	1600	90.9
N3	187.13	1600	116.9
N4	153.72	1600	96.0
N5	162.5	1600	101.5
N6	141.42	1600	88.3

Table A.6: Compressive strength M4 (0.19 w/b, 10.3% Hp/c)

specimen	Pmax [N]	b [mm]	h [mm]	f_{ctf} [MPa]	f_{ct} [MPa]
N1	7802	40.33	39.98	18.1	8
N2	7697	39.72	39.86	18.2	8
N3	8629	39.89	39.98	20.3	8.9
N4	7657.51	39.87	39.39	18.5	8.1
N5	8822.52	39.95	39.75	20.9	9.2
N6	8547.58	40	40.1	19.9	8.8

Table A.7: Bending strength M5 (0.20 w/b, 7.3% Hp/c)

Specimen	Fc [kN]	A [mm^2]	f_c [MPa]
N1	138.33	1600	86.4
N2	127.46	1600	79.6
N3	144.56	1600	90.3
N4	135.62	1600	84.7
N5	142.3	1600	88.9
N6	140.82	1600	88
N7	124.99	1600	78.1
N8	139.19	1600	86.9
N9	136.4	1600	85.2
N10	158.38	1600	98.9
N11	142.55	1600	89
N12	128.12	1600	80

Table A.8: Compressive strength M5 (0.20 w/b, 7.3% Hp/c)

specimen	Pmax [N]	b [mm]	h [mm]	f_{ctf} [MPa]	f_{ct} [MPa]
N1	6558	40	39.2	16	7
N2	6646	40.1	39.55	15.8	7
N3	6103	40.2	38.5	15.1	6.69
N4	6004	39.9	39.02	15.1	6.6
N5	6584	39.9	39.7	15.6	6.9
N6	5637	39.9	39.55	13.5	5.9
N7	5916	39.9	39.8	14	6.1
N8	5916	39.9	39.8	14	6.1

Table A.9: Bending strength M6 (0.225 w/b, 7.3% Hp/c)

Specimen	Fc [kN]	A [mm^2]	f_c [MPa]
N1	117.25	1600	73.2
N2	122.31	1600	76.4
N4	124.73	1600	77.9
N5	119.19	1600	74.4
N6	121.87	1600	76.1
N7	116.11	1600	72.5
N8	132.47	1600	82.7
N9	136.85	1600	85.5
N10	118.27	1600	73.9

Table A.10: Compressive strength M6 (0.225 w/b, 7.3% Hp/c)

Appendix B

TRM mechanical characterization

	Specimen	t [mm]	P_{max} [kN]	δ_u [mm]	σ_{max} [MPa]	δ_u/l [-]	σ_I [MPa]	EF [-]
F1 – 1 fabric	N1	6.9	3.75	0.59	7.76	0.0024	7.76	1.02
	N2	6.7	4.17	0.56	8.90	0.0022	8.90	1.14
	N3	6.9	4.13	1.12	8.55	0.0046	5.55	1.12
	N4	6.7	3.55	2.02	7.56	0.0081	5.13	0.97
	N5	6.7	3.37	2.65	7.19	0.0107	5.18	0.92
	N6	6.8	3.87	4.92	8.14	0.0199	3.00	0.84
	Average	6.8	3.81	1.98	8.02	0.0080	5.92	1.00
	s.d.	0.10	0.32	1.66	0.64	0.0067	2.10	0.12
F1 – 2 fabrics	N1	7.1	6.56	4.35	13.19	0.0174	8.30	0.89
	N2	7.1	6.50	3.73	13.07	0.0148	8.40	0.89
	N3	7.2	6.91	4.77	13.71	0.0195	6.03	0.94
	N4	7.2	7.35	6.65	14.58	0.0268	5.06	1.00
	N5	7.3	6.56	6.22	12.84	0.0253	4.17	0.89
	N6	6.7	6.42	5.41	13.69	0.0220	6.41	0.87
	Average	7.1	6.72	5.19	13.52	0.0210	6.40	0.91
	s.d.	0.21	0.35	1.12	0.63	0.0046	1.70	0.05
F1 – 2 layers	N1	6.3	8.44	6.73	19.14	0.0234	4.23	1.15
	N2	6.2	8.39	6.77	19.33	0.0235	2.93	1.14
	N3	6.3	7.49	5.89	16.99	0.0204	4.42	1.02
	N4	6.5	7.67	6.30	17.52	0.0218	5.25	1.04
	N5	6.2	7.48	6.00	17.24	0.0208	5.80	1.02
	N6	6.5	7.78	6.27	17.08	0.0218	4.79	1.06
	Average	6.3	7.92	6.33	17.88	0.0219	4.57	1.07
	s.d.	0.14	0.43	0.36	1.06	0.0013	0.99	0.06

Figure B.1: Test results for specimen reinforced with fabric F1

	Specimen	t [mm]	P_{max} [kN]	δ_u [mm]	σ_{max} [MPa]	δ_u/l [-]	σ_I [MPa]	EF [-]
F1 – 3 layers	N1	12.1	7.89	5.37	9.32	0.0181	2.41	0.72
	N2	12.2	8.33	5.94	9.75	0.0201	2.96	0.76
	N3	12.0	10.16	7.10	12.10	0.0237	2.39	0.92
	N4	12.1	11.05	7.796	13.04	0.0262	2.14	1.00
	N5	12.0	8.74	6.07	10.41	0.0204	3.28	0.79
	N6	11.8	9.32	6.61	11.28	0.0222	3.23	0.85
	Average	12.0	9.25	6.52	10.98	0.0219	2.73	0.84

Figure B.2: Test results for specimen reinforced with fabric F1-3 layers

	Specimen	t [mm]	P_{max} [kN]	δ_u [mm]	σ_{max} [MPa]	δ_u/l [-]	σ_l [MPa]	EF [-]
F2 – 1 fabric	N1	6.0	5.63	6.28	13.39	0.0219	4.20	0.86
	N2	6.5	4.07	4.85	8.94	0.0168	3.19	0.62
	N3	6.5	5.35	5.60	11.76	0.0193	3.01	0.81
	Average	6.3	5.02	5.57	11.36	0.0193	3.47	0.76
F2 – 2 fabrics	N1	7.3	11.05	7.43	21.62	0.0257	3.81	0.84
	N2	6.8	11.07	7.15	23.26	000247	4.63	0.84
	N3	6.9	10.74	6.66	22.25	0.0230	4.99	0.82
	Average	7.0	10.95	7.08	22.37	0.0245	4.48	0.83
F2 – 2 layers	N1	6.5	10.72	6.39	23.57	0.0222	4.69	0.81
	N2	6.1	10.86	6.49	25.42	0.0225	3.91	0.83
	N3	6.1	10.37	6.47	24.28	0.0224	5.27	0.79
	Average	6.2	10.65	6.45	24.42	0.0224	4.62	0.81

Figure B.3: Test results for specimen reinforced with fabric F2

	Specimen	t [mm]	P_{max} [kN]	δ_u [mm]	σ_{max} [MPa]	δ_u/l [-]	σ_l [MPa]	EF [-]
F2 – 3 layers	N1	12	12.08	6.63	14.38	0.0223	4.89	0.6
	N2	12.3	13.24	7.04	15.38	0.0239	4.43	0.62
	N3	12	12.35	5.72	14.71	0.0194	5.24	0.6
	Average	12.1	12.58	6.46	14.82	0.0219	4.86	0.606

Figure B.4: Test results for specimen reinforced with fabric F2-3 layers

	Specimen	t [mm]	P_{max} [kN]	δ_u [mm]	σ_{max} [MPa]	δ_u/l [-]	σ_I [MPa]	EF [-]
10 mm	N1	6.2	7.86	7.80	17.97	0.0270	3.48	0.71
	N2	6.3	7.32	7.66	16.45	0.0265	4.36	0.66
	N3	6.1	7.35	6.85	16.97	0.0237	4.26	0.67
	Average	6.2	7.51	7.44	17.13	0.0257	4.03	0.68
20 mm	N1	6.8	7.31	4.50	15.34	0.0156	5.82	0.66
	N2	6.7	7.40	4.78	15.67	0.0166	5.09	0.67
	Average	6.8	7.36	4.64	15.51	0.0161	5.46	0.67
30 mm	N1	6.0	8.19	5.36	19.55	0.0186	7.43	0.74
	N2	6.3	7.43	4.78	16.62	0.0165	6.99	0.67
	N3	6.5	7.18	4.43	15.87	0.0153	8.74	0.65
	Average	6.3	7.60	4.86	17.35	0.0168	7.72	0.69
50 mm	N1	6.0	7.34	4.75	17.59	0.0165	6.94	0.67
	N2	6.4	7.84	4.69	17.06	0.0162	7.76	0.71
	N3	6.1	7.72	4.76	18.08	0.0165	7.00	0.70
	Average	6.2	7.63	4.74	17.58	0.0164	7.22	0.69

Figure B.5: Test results for specimen reinforced with fabric F3 considering also different weft spacing

	Specimen	Batch	t [mm]	P_{max} [kN]	δ_u [mm]	σ_{max} [MPa]	δ_u/l [-]	σ_I [MPa]	EF [-]
water	N1	10	6.2	7.86	7.80	17.97	0.0270	3.48	0.71
	N2	10	6.3	7.32	7.66	16.45	0.0265	4.36	0.66
	N3	10	6.1	7.35	6.85	16.97	0.0237	4.26	0.67
	Average		6.2	7.51	7.44	17.13	0.0257	4.03	0.68
60 °C	N1	12	6.5	10.43	7.75	22.86	0.0269	5.14	0.95
	N2	12	6.5	10.30	6.70	22.50	0.0233	5.54	0.93
	N3	12	6.5	10.01	7.29	21.84	0.0253	5.53	0.91
	Average		6.5	10.25	7.25	22.40	0.0252	5.40	0.93
air	N1	13	6.0	11.01	6.47	26.04	0.0225	7.31	1.00
	N2	13	6.1	12.13	7.91	28.21	0.0275	5.85	1.10
	N3	13	6.4	7.81[d]	4.48[d]	17.25[d]	0.0157[d]	5.14	0.71[d]
	Average		6.2	11.57	7.19	27.13	0.0250	6.10	1.05

[d] problem occurred during the test (crack formation in the clamping area) – values not considered in the average

Figure B.6: Test results for specimens reinforced with F3 at different curing conditions

	Specimen	Batch	t [mm]	P_{max} [kN]	δ_u [mm]	σ_{max} [MPa]	δ_u/l [-]	σ_I [MPa]	EF [-]
2 mm/s	N1	10	6.4	10.20	8.61	22.62	0.0298	5.06	0.93
	N2	10	6.2	9.62	7.84	22.05	0.0273	6.07	0.87
	N3	10	6.4	10.10	8.02	22.57	0.0277	5.59	0.92
	Average		6.3	9.97	8.15	22.42	0.0283	5.57	0.91
2×10^{-2} mm/s	N1	10	6.2	7.86	7.80	17.97	0.0270	3.48	0.71
	N2	10	6.3	7.32	7.66	16.45	0.0265	4.36	0.66
	N3	10	6.1	7.35	6.85	16.97	0.0237	4.26	0.67
	Average		6.2	7.51	7.44	17.13	0.0257	4.03	0.68
2×10^{-4} mm/s	N1	10	6.4	5.24	6.58	11.66	0.0227	3.73	0.48
	N2	10	6.5	6.85	7.15	14.98	0.0247	4.74	0.62
	N3	10	6.9	6.12	5.08	12.64	0.0175	5.12	0.56
	Average		6.6	6.07	6.27	13.10	0.0217	4.53	0.55

Figure B.7: Test results for specimens reinforced with F3 at different displacement rate

	Specimen	Batch	t [mm]	P_{max} [kN]	δ_u [mm]	σ_{max} [MPa]	δ_u/l [-]	σ_I [MPa]	EF [-]
290 mm	N1	10	6.2	7.86	7.80	17.97	0.0270	3.48	0.71
	N2	10	6.3	7.32	7.66	16.45	0.0265	4.36	0.66
	N3	10	6.1	7.35	6.85	16.97	0.0237	4.26	0.67
	Average		6.2	7.51	7.44	17.13	0.0257	4.03	0.68
150 mm	N1	14	6.8	10.41	4.49	21.92	0.0304	6.41	0.94[e]
	N2	14	6.5	9.56	3.75	20.65	0.0259	6.24	0.87[e]
	N3	14	6.3	8.56	3.18	19.43	0.0219	4.50	0.78[e]
	Average		6.5	9.51	3.81	20.67	0.0261	5.72	0.86
75 mm	N1	14	6.5	10.63	3.26	23.38	0.0450	5.70	0.96[e]
	N2	14	6.2	7.93	2.17	17.75	0.0294	5.09	0.72[e]
	N3	14	6.4	9.32	2.68	20.82	0.0355	4.79	0.85[e]
	Average		6.4	9.29	2.70	20.65	0.0366	5.19	0.84

[e] The strength of the 400 x 70 mm fabric was considered

Figure B.8: Test results for specimens reinforced with F3 for different specimen size

Appendix C

DEWS test

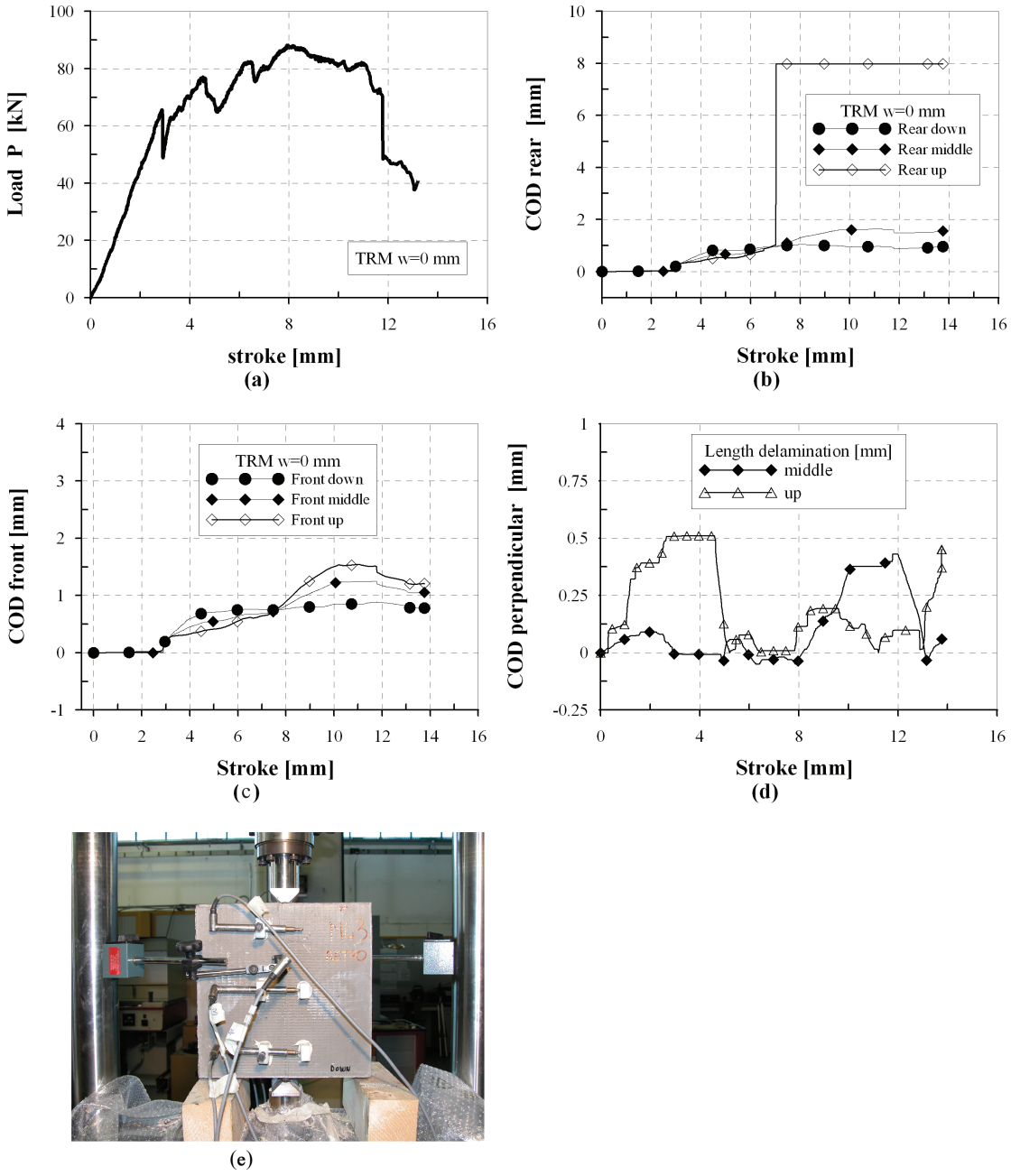

Figure C.1: TRM w=0 mm N01

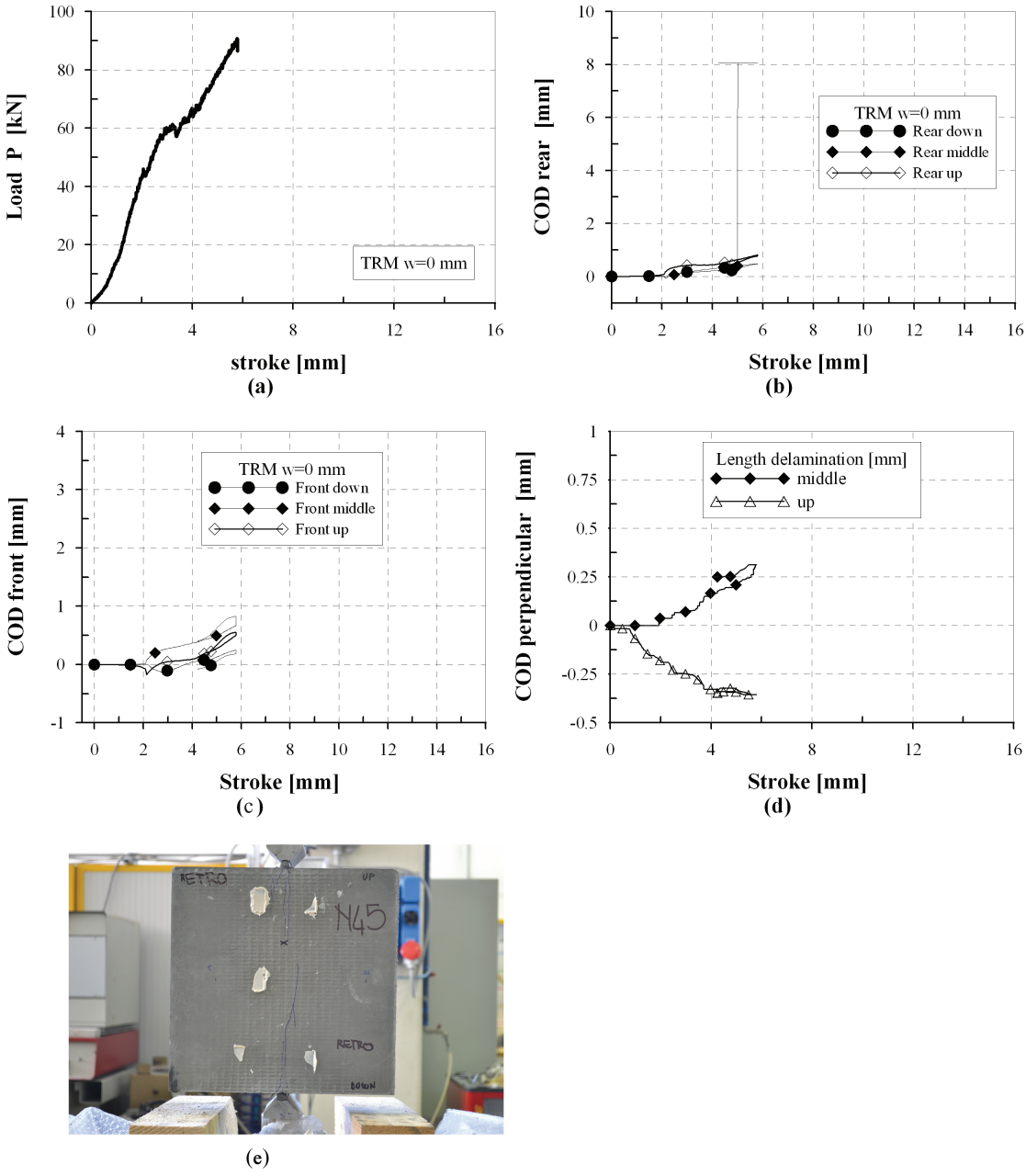

Figure C.2: TRM w=0 mm N02

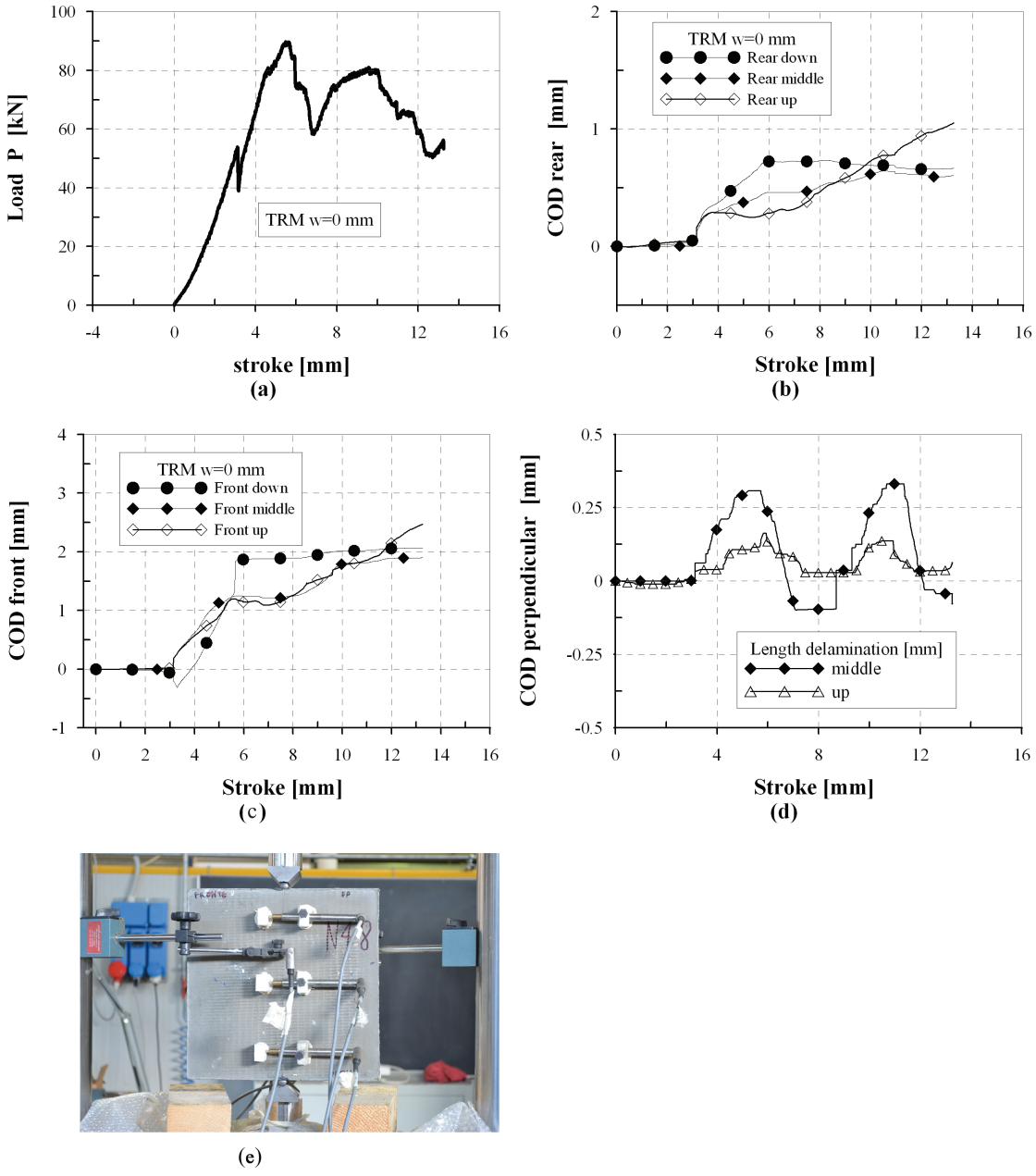

Figure C.3: TRM w=0 mm N03

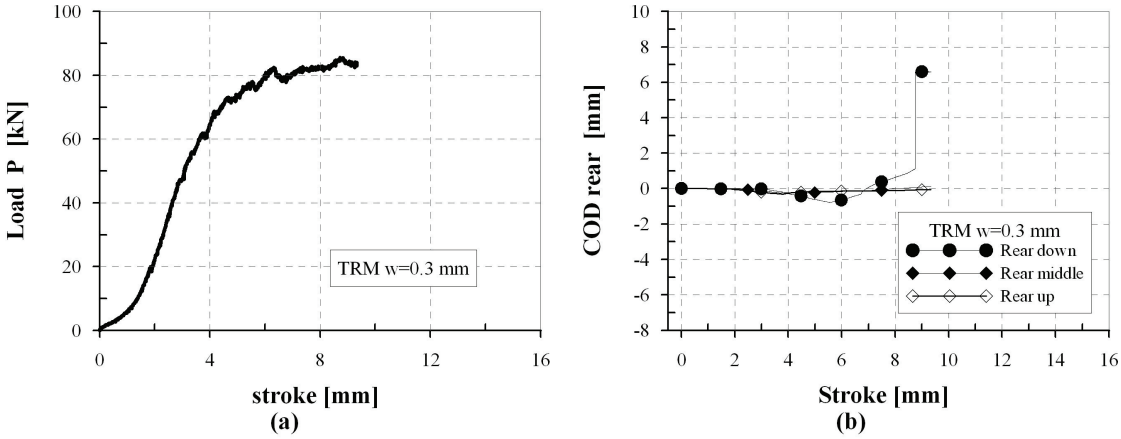

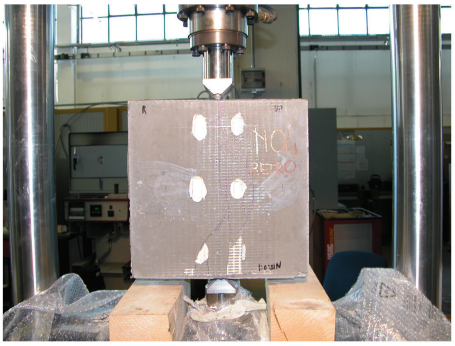

(e)

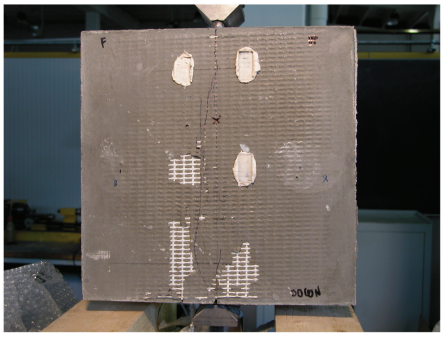

(f)

Figure C.4: TRM w=0.3 mm N01

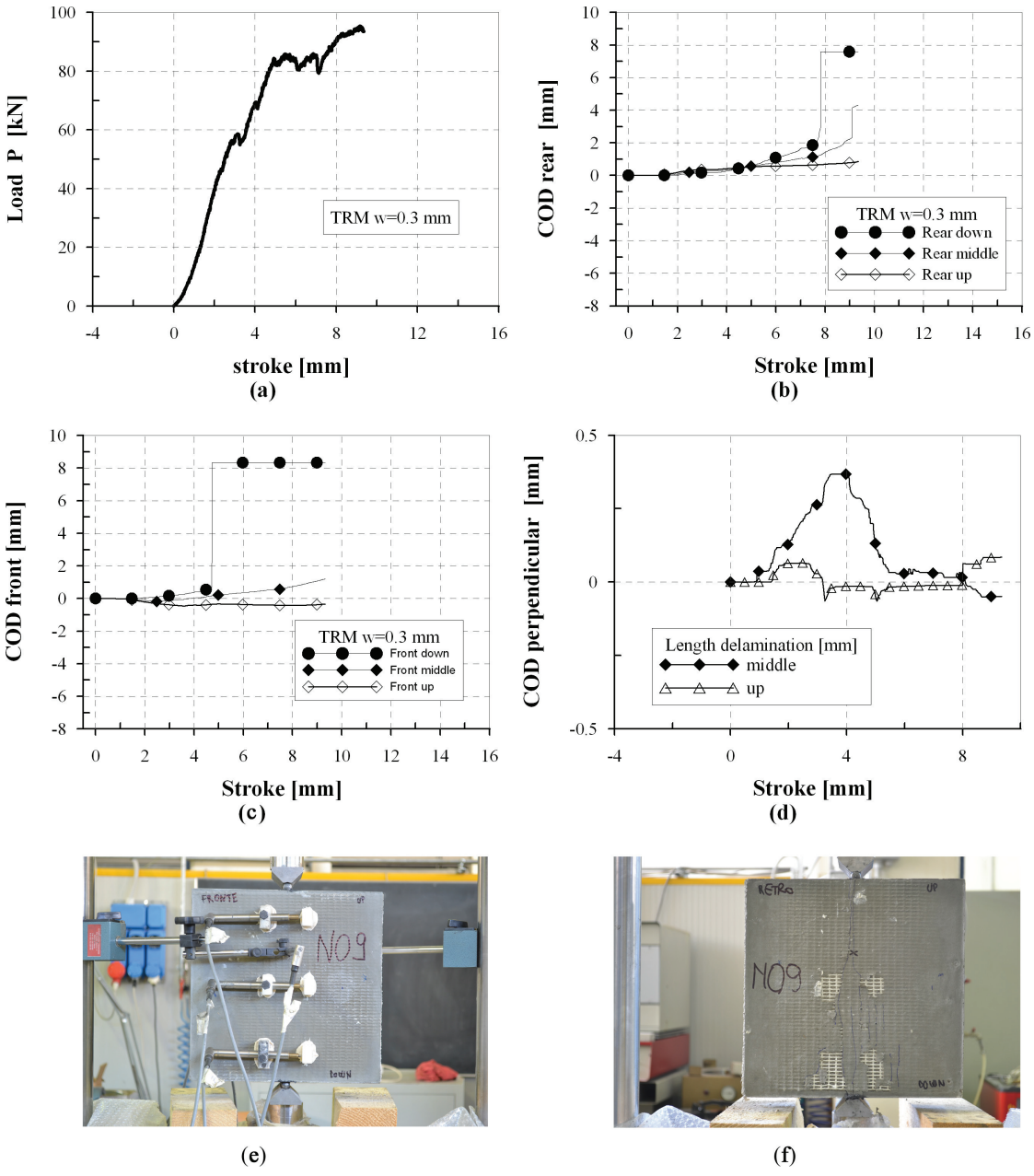

Figure C.5: TRM w=0.3 mm N02

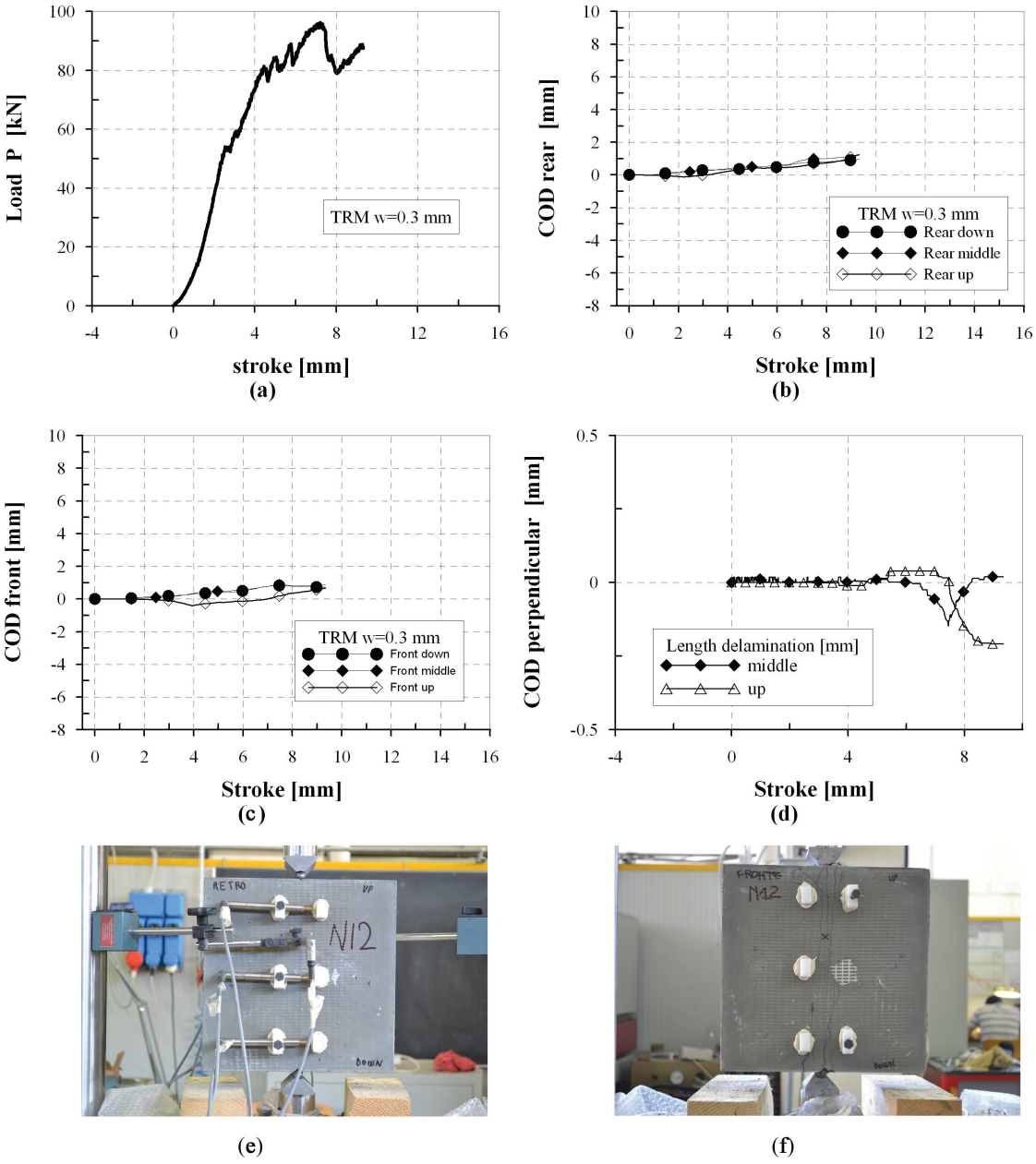

Figure C.6: TRM w=0.3 N03

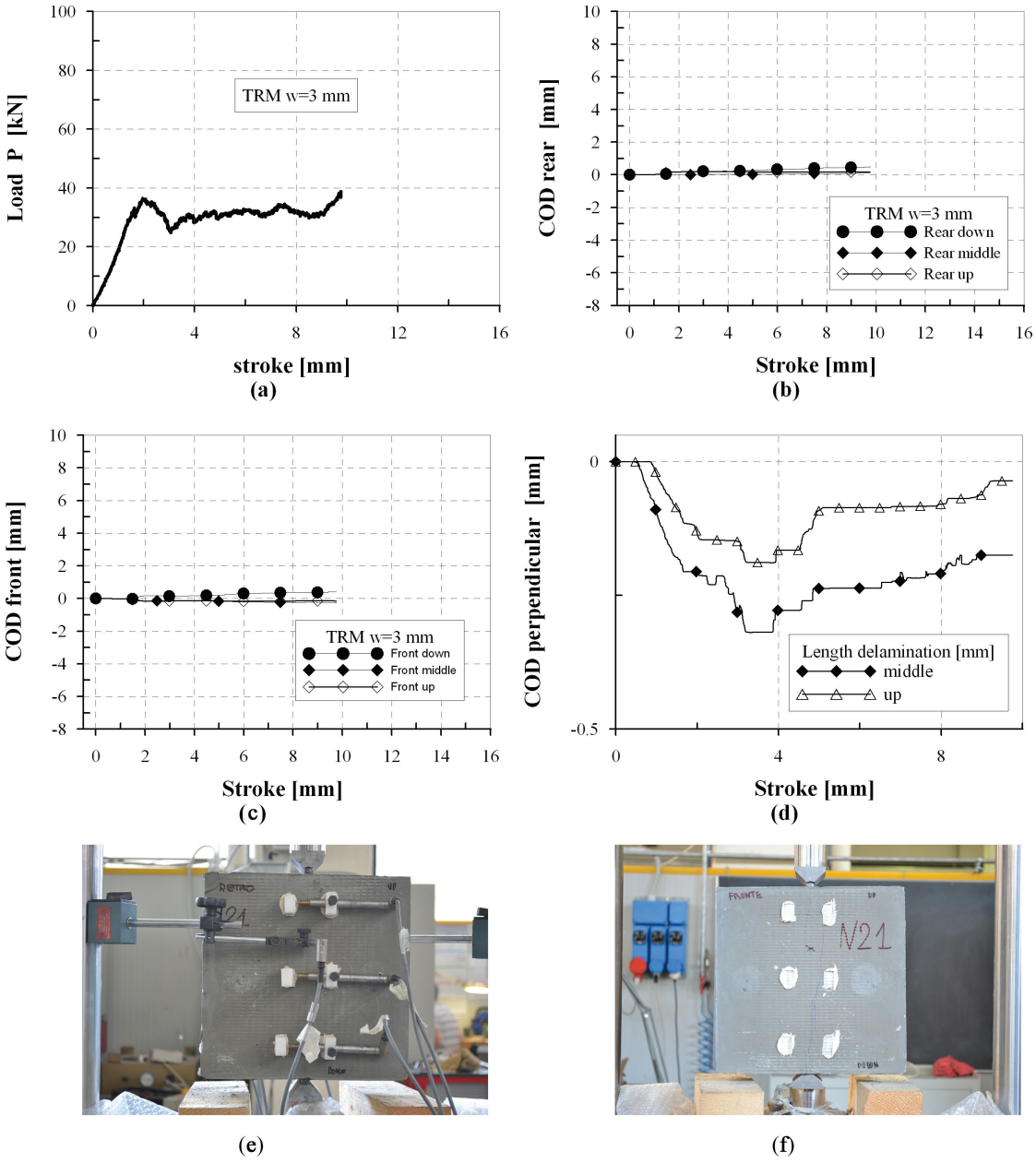

Figure C.7: TRM w=3 mm N01

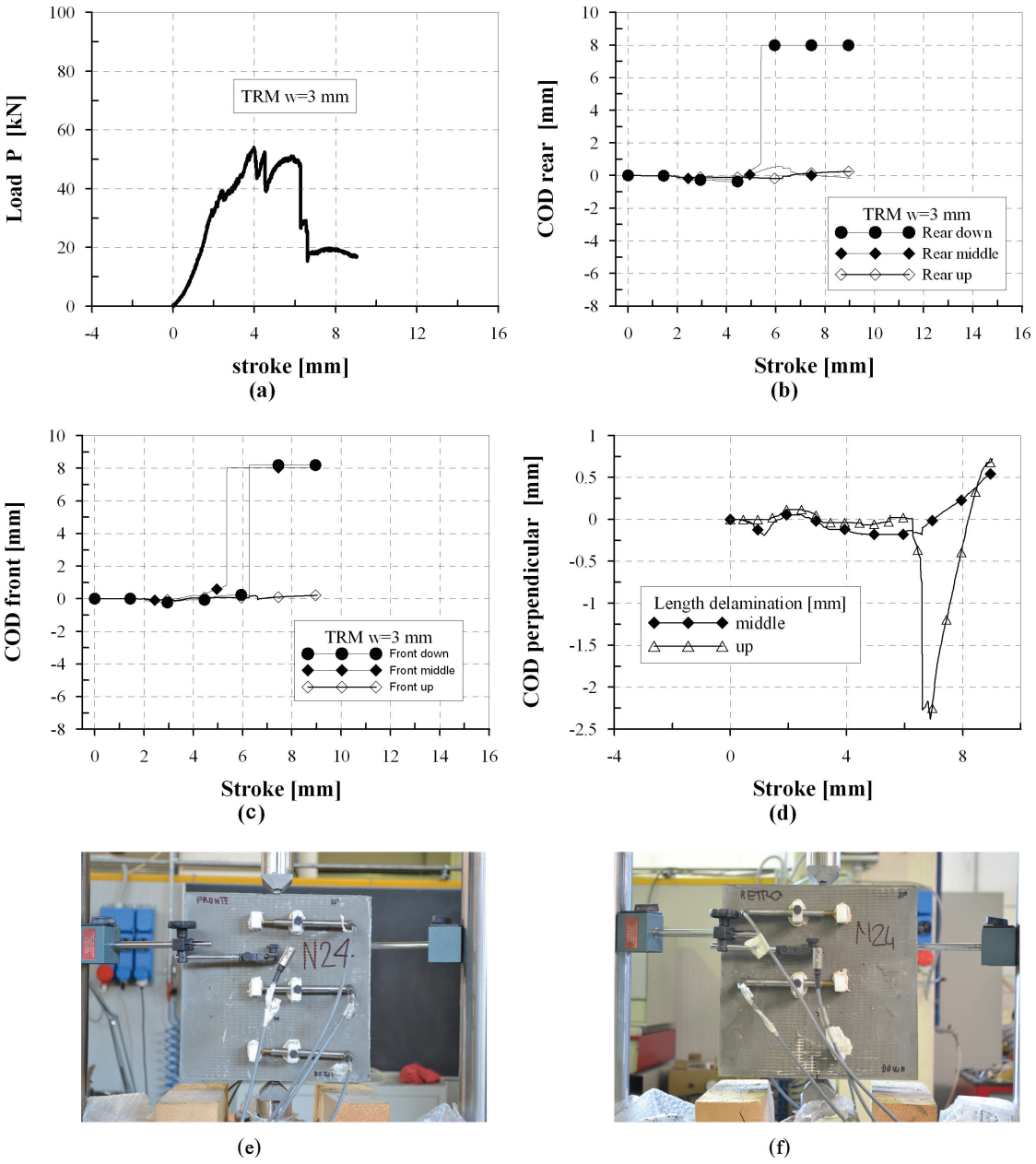

Figure C.8: TRM w=3 mm N02

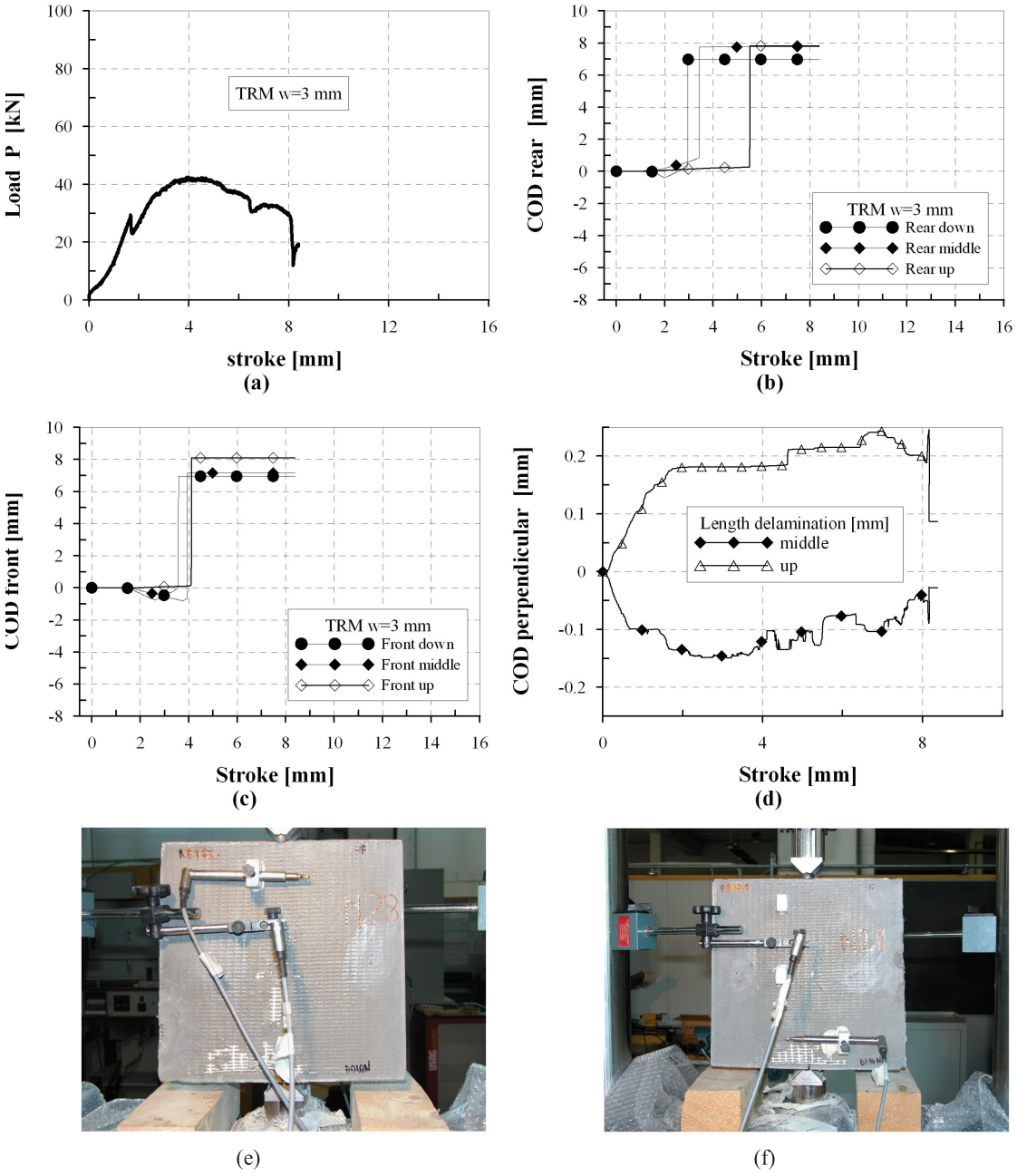

(e)

(f)

Figure C.9: TRM w=3 mm N03

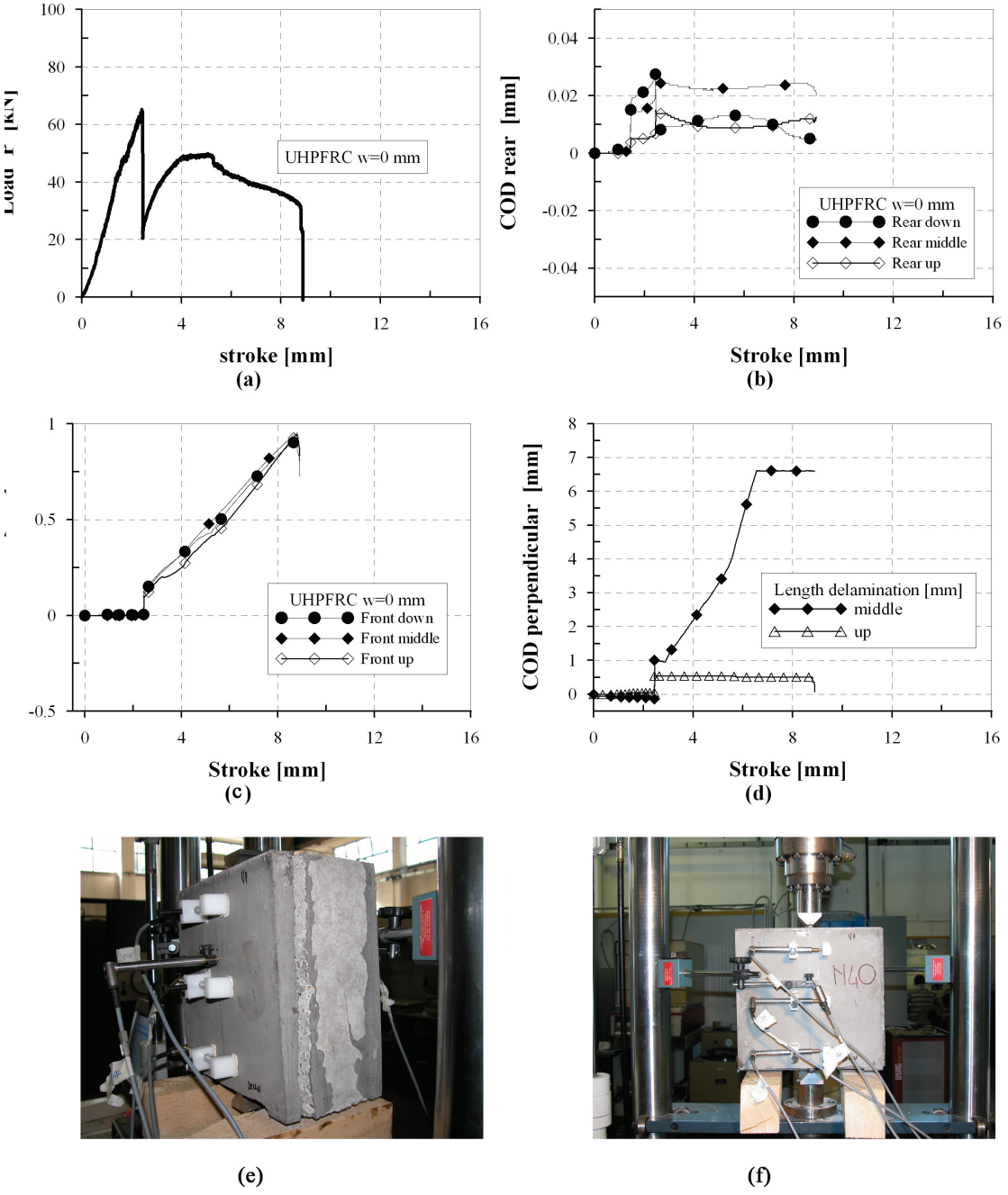

Figure C.10: UHPFRC w=0 mm N01

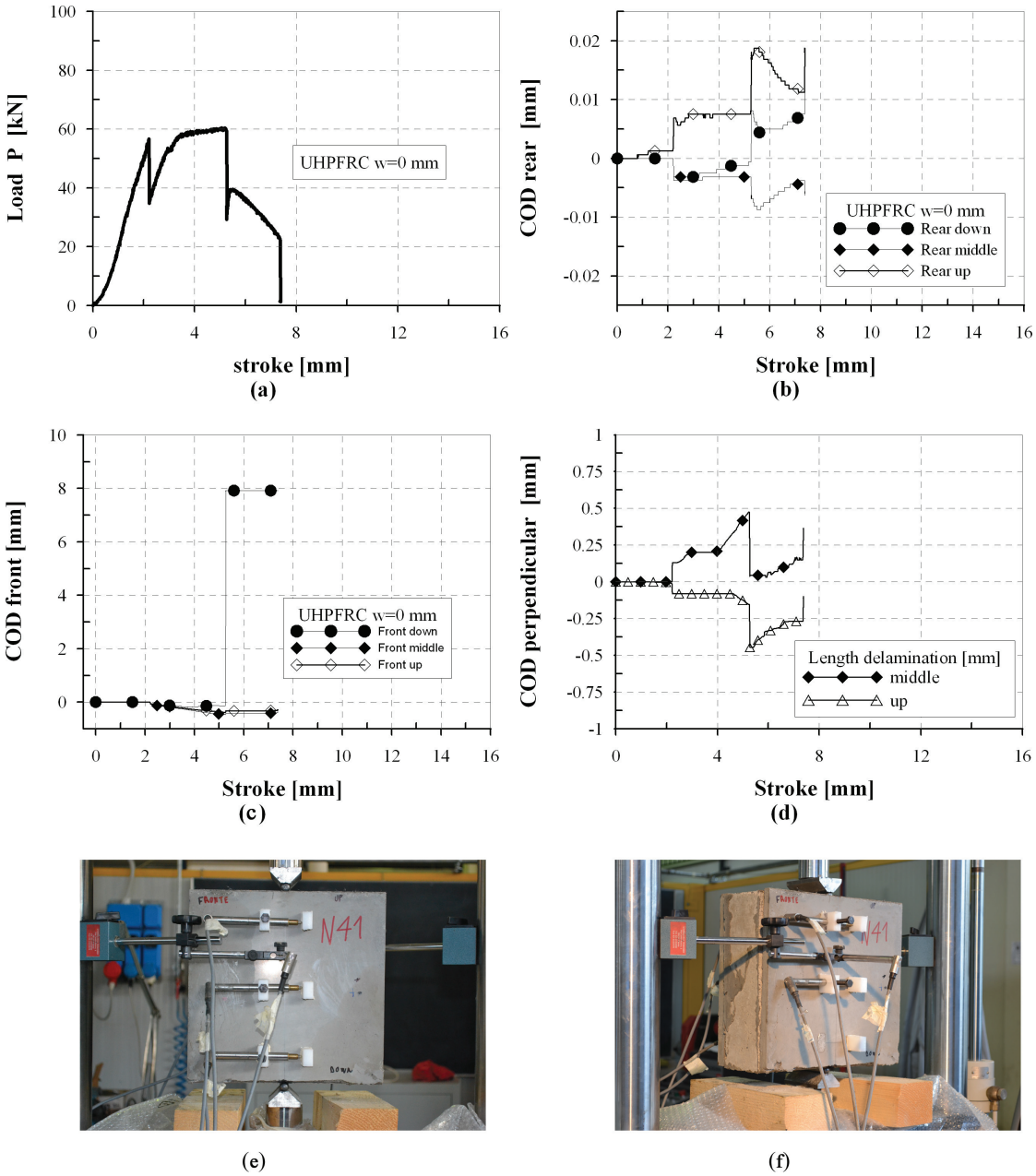

Figure C.11: UHPFRC w=0 mm N02

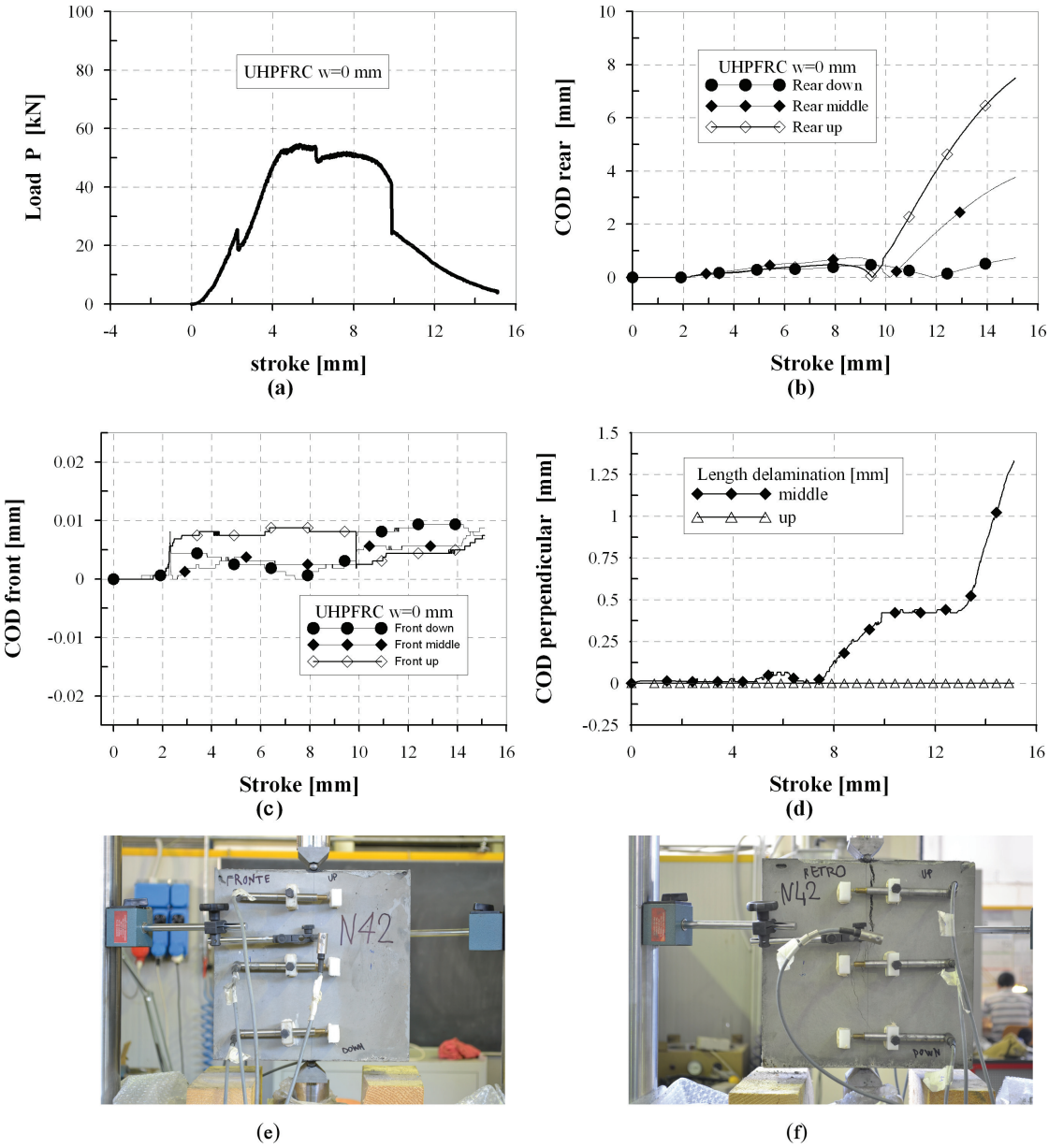

Figure C.12: UHPFRC w=0 mm N03

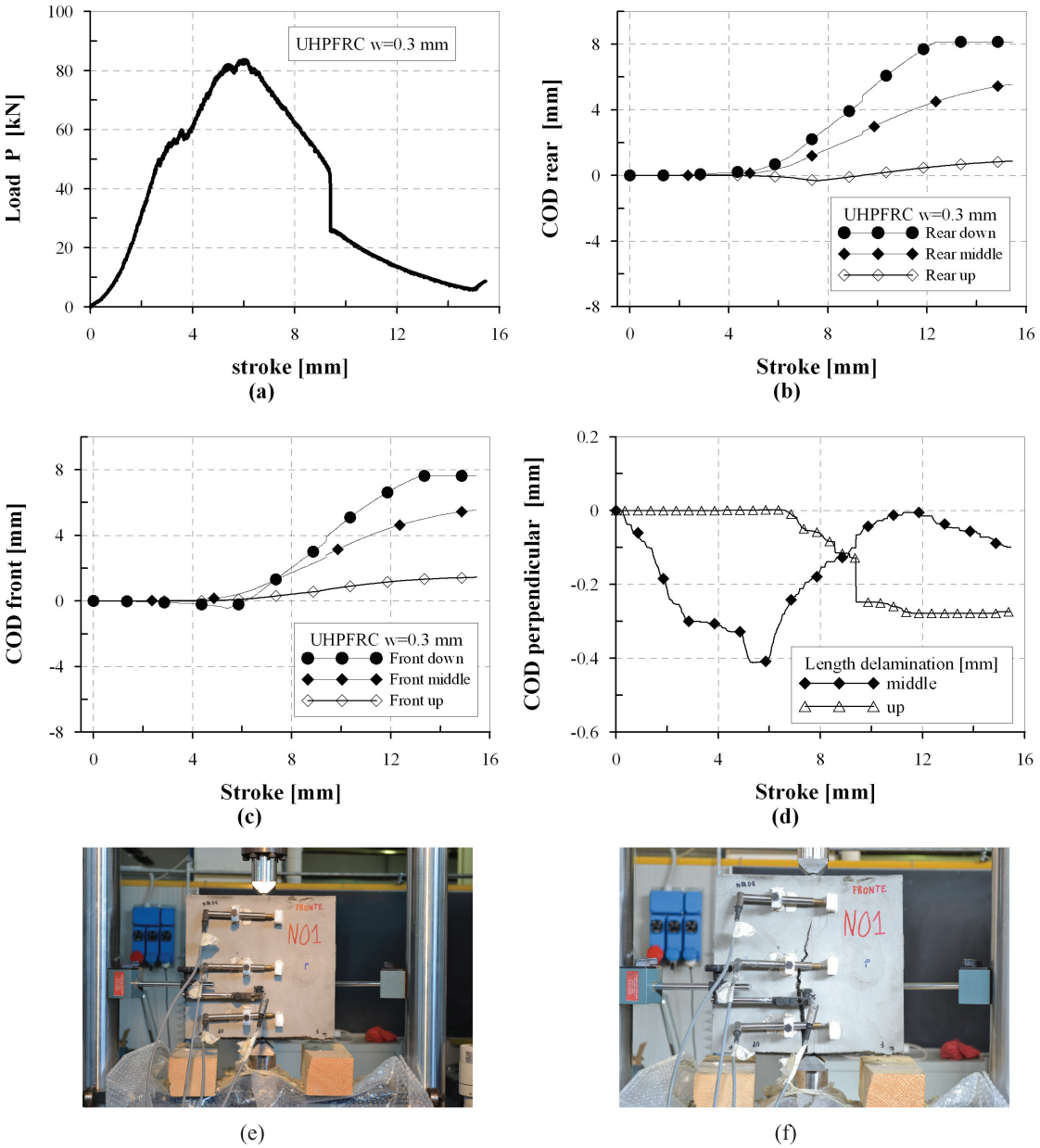

Figure C.13: UHPFRC w=0.3 mm N01

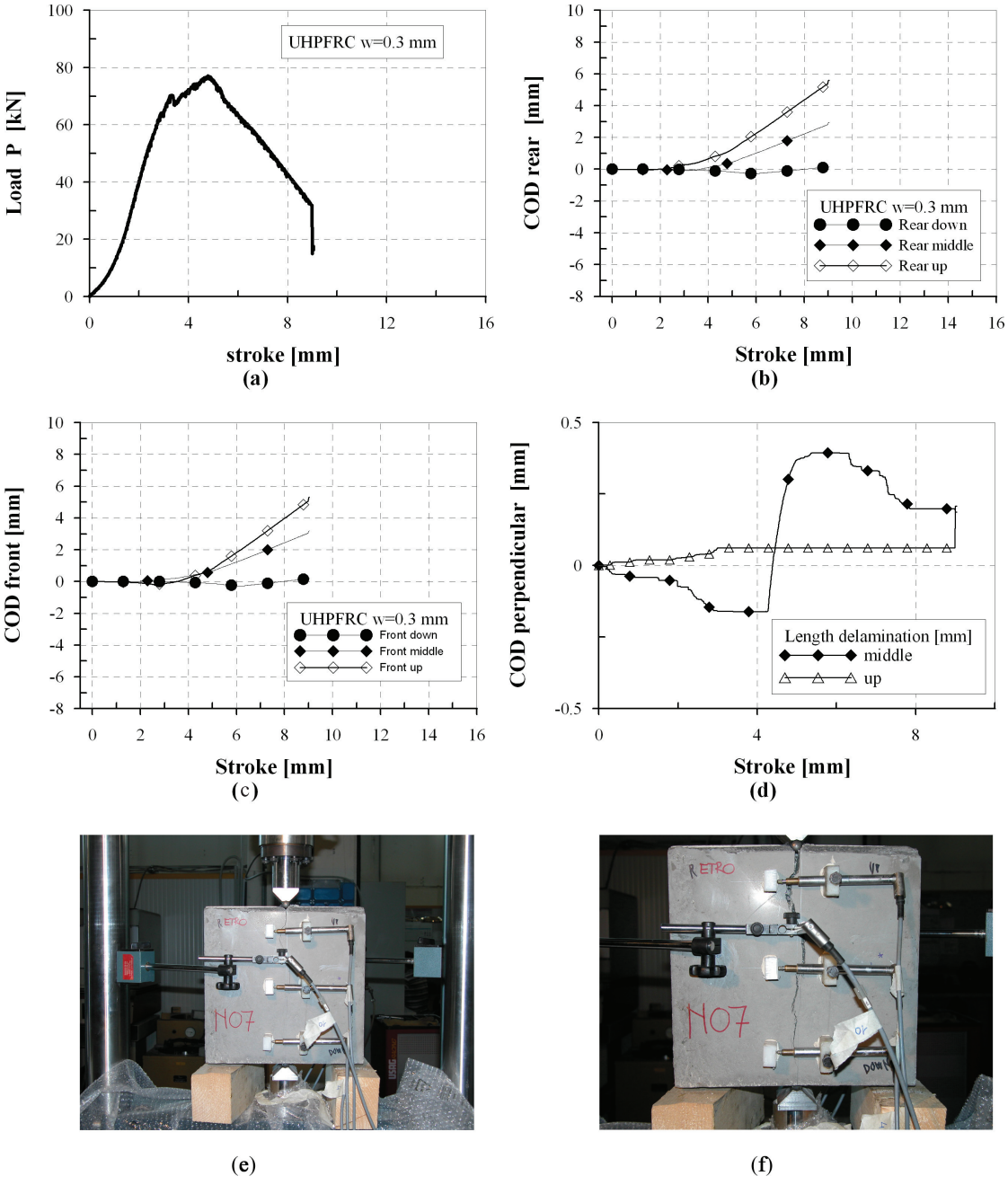

Figure C.14: UHPFRC w=0.3 mm N02

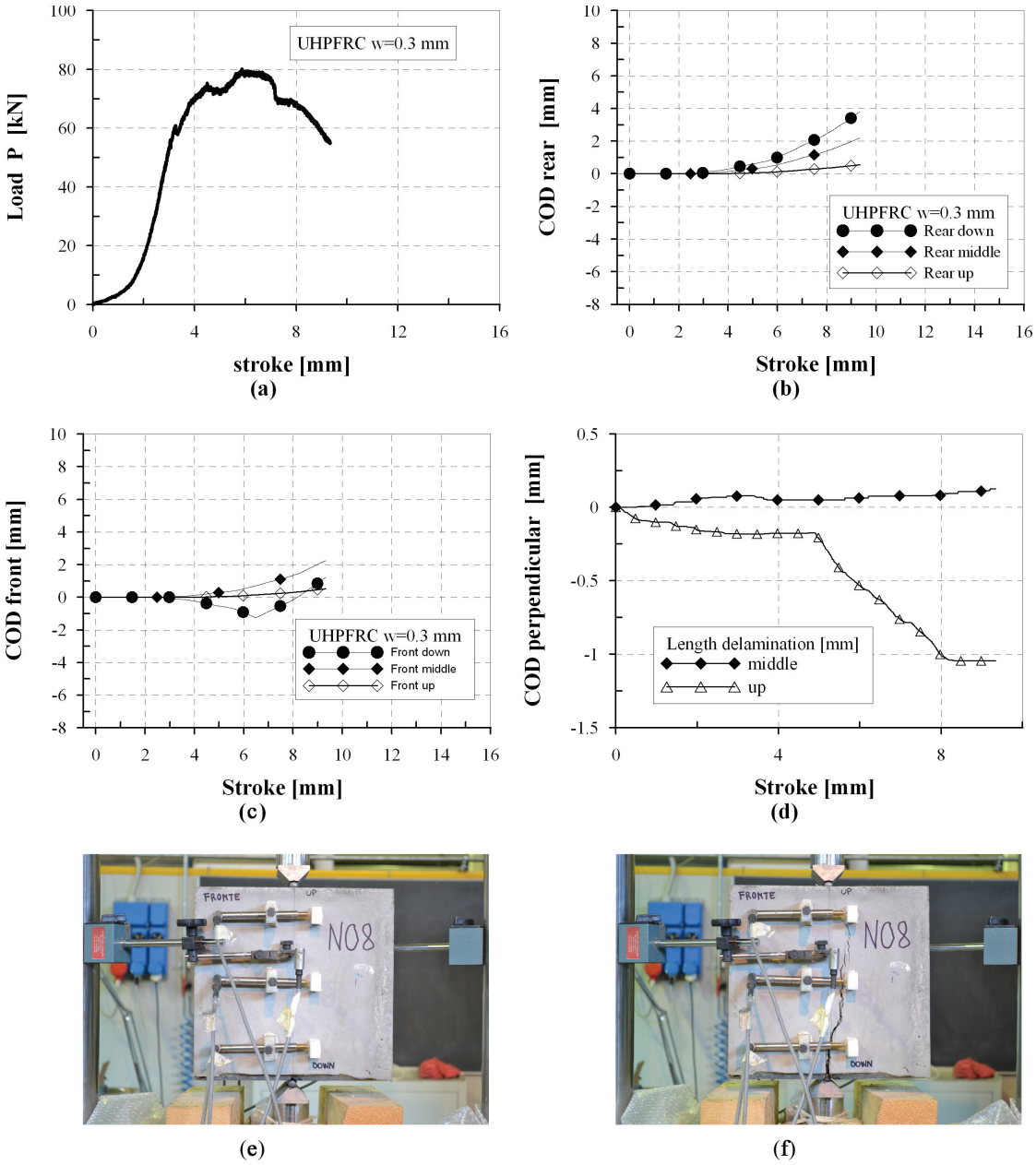

Figure C.15: UHPFRC w=0.3 mm N03

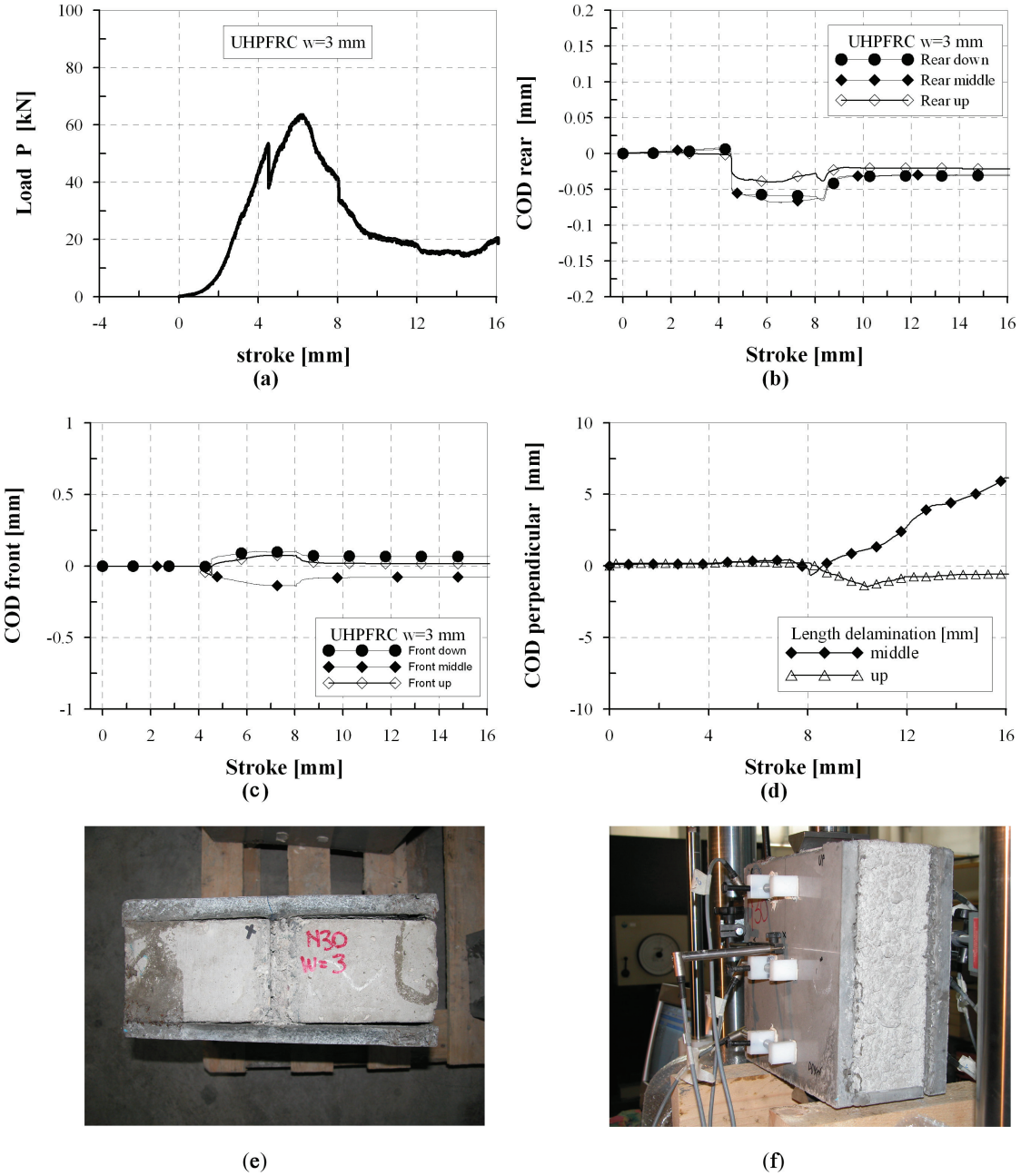

Figure C.16: UHPFRC w=3 mm N01

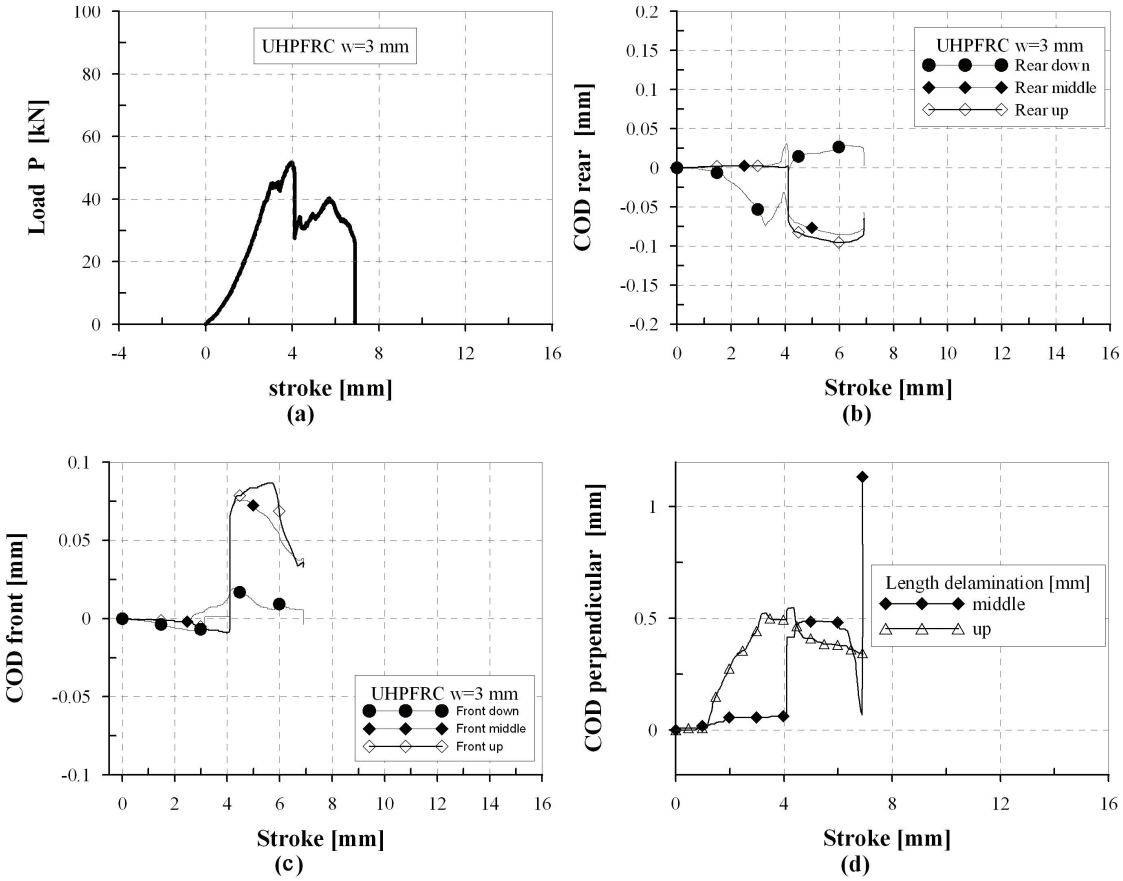

(e) (f)

Figure C.17: UHPFRC w=3 mm N02

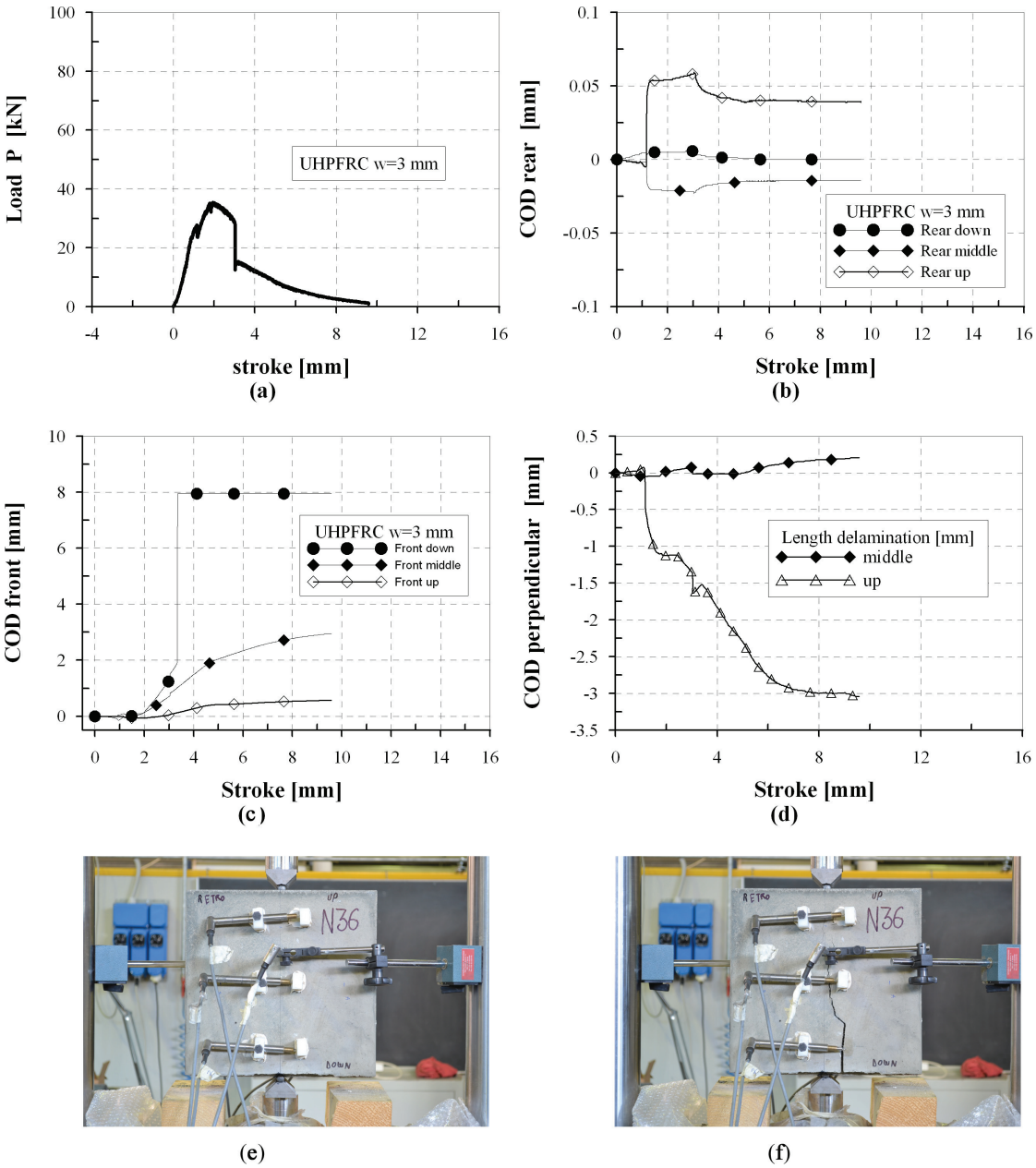

Figure C.18: UHPFRC w=3 mm N03

Appendix D

Compression test

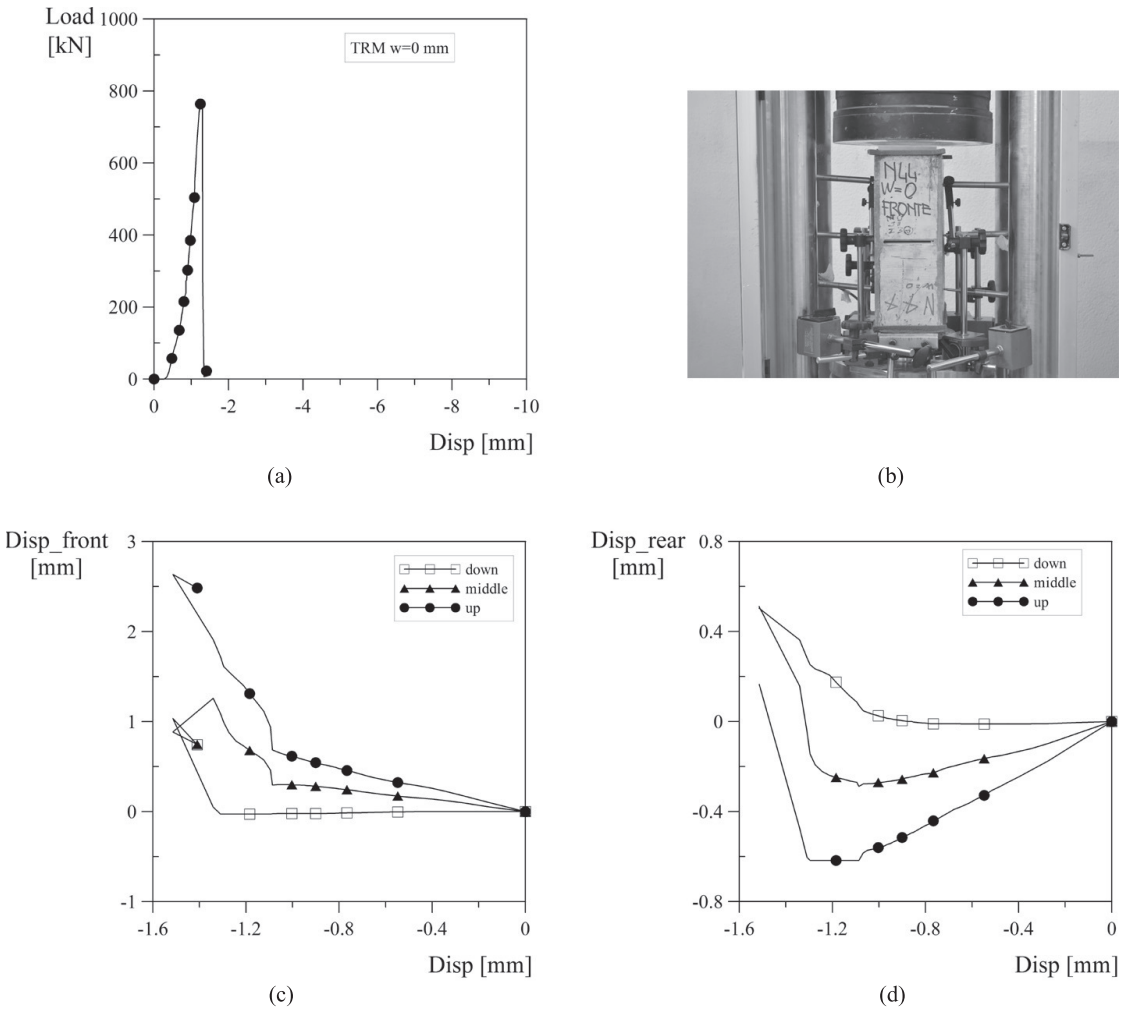

Figure D.1: TRM w=0 mm N01

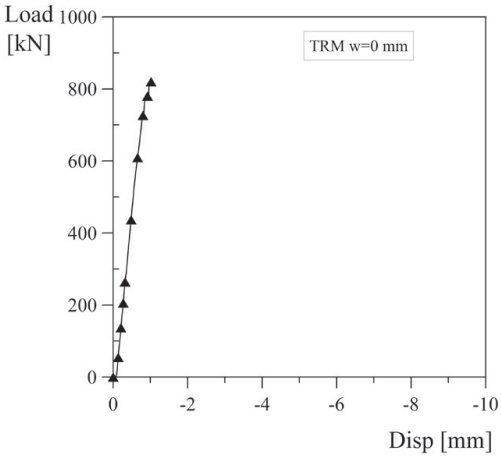

(a)

(b)

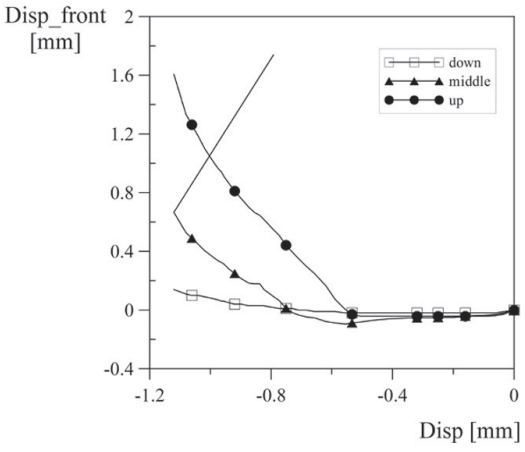

(c)

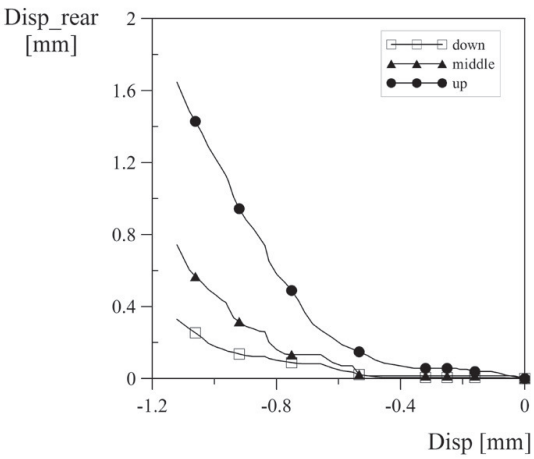

(d)

Figure D.2: TRM w=0 mm N02

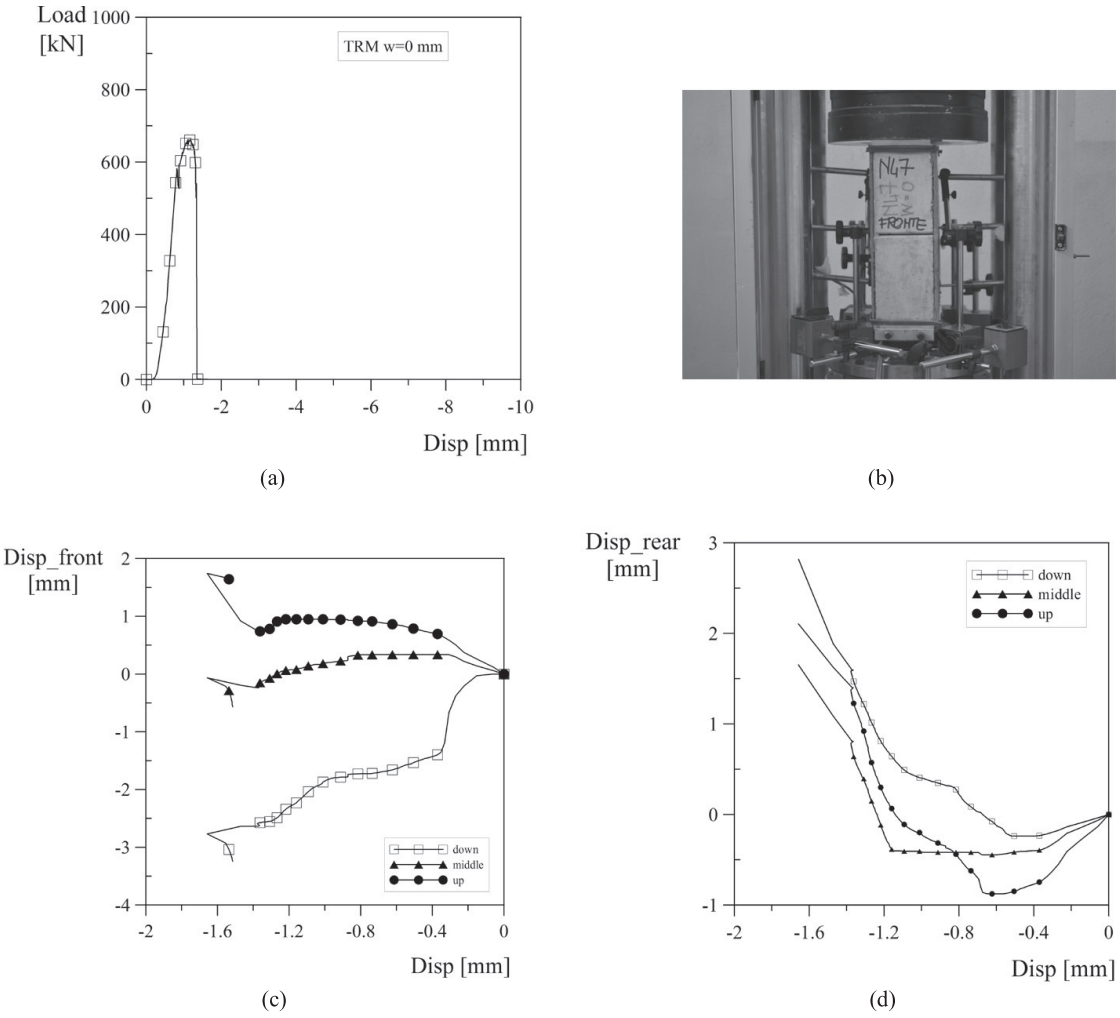

Figure D.3: TRM w=0 mm N03

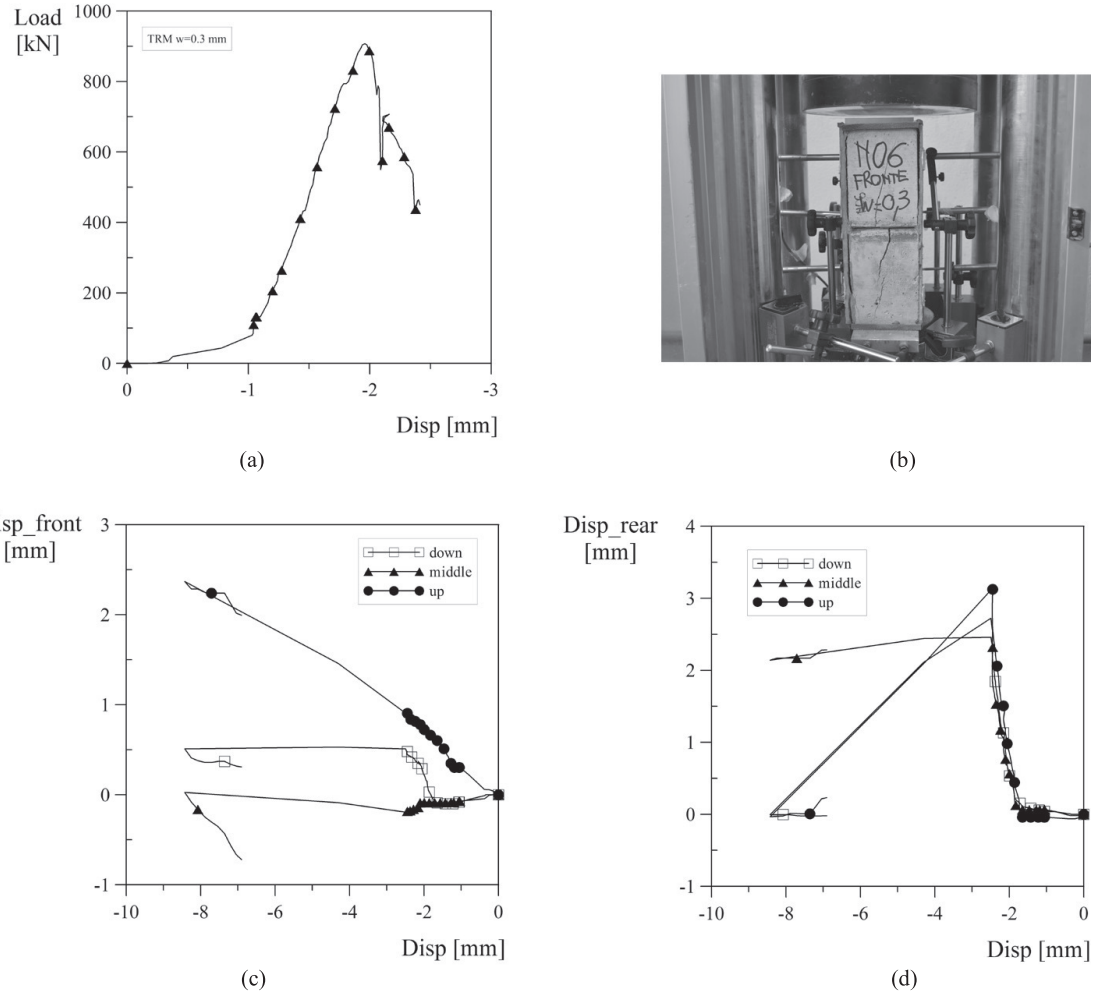

Figure D.4: TRM w=0.3 mm N01

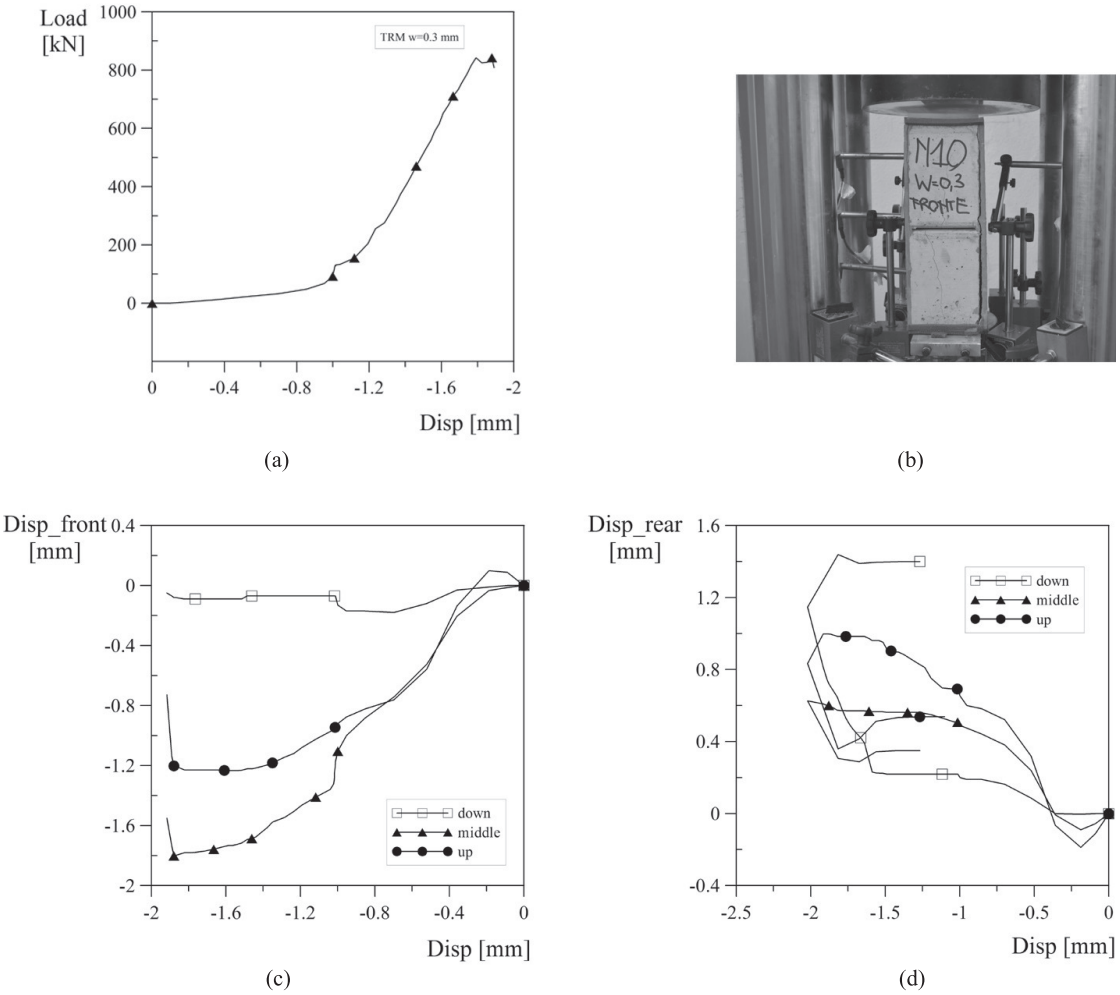

Figure D.5: TRM w=0.3 mm N02

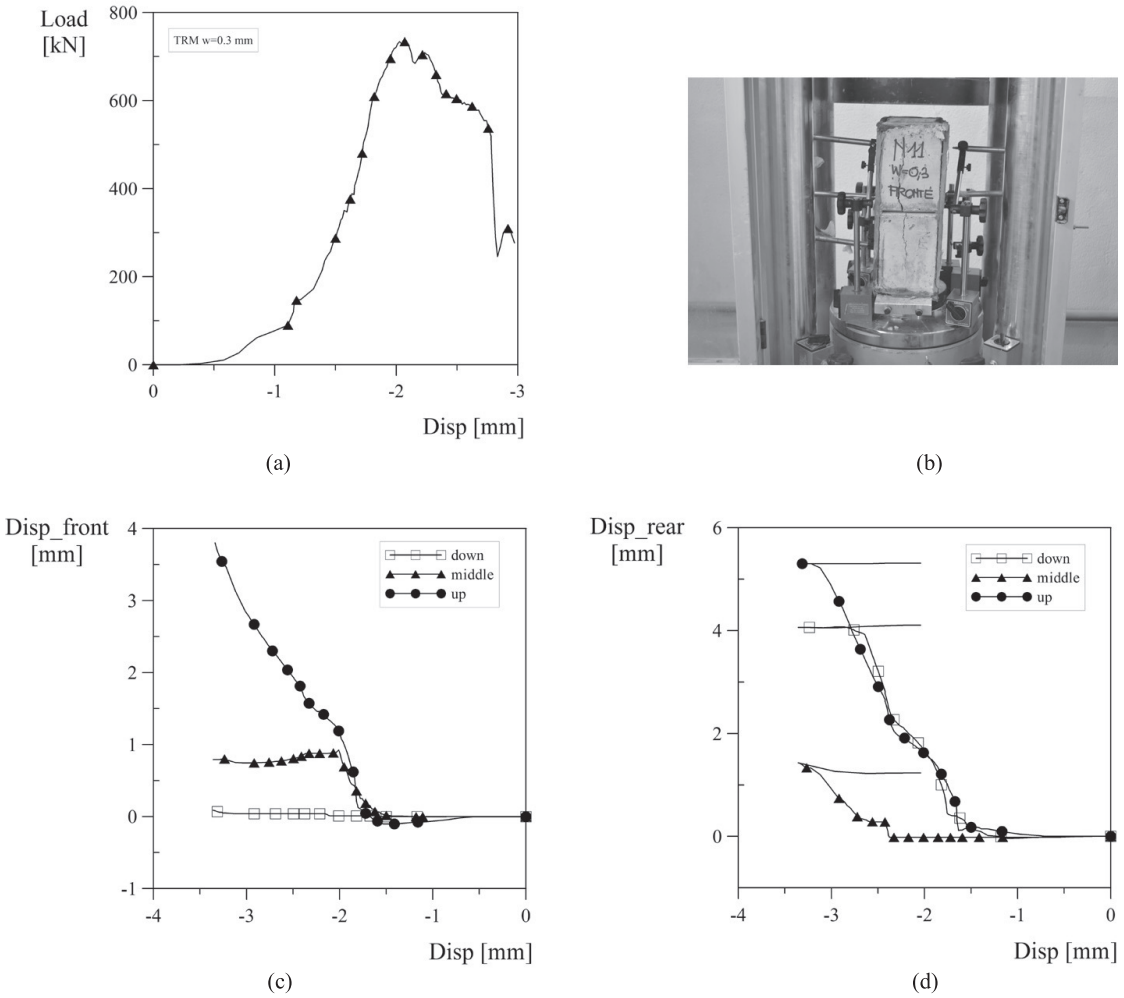

Figure D.6: TRM w=0.3 mm N03

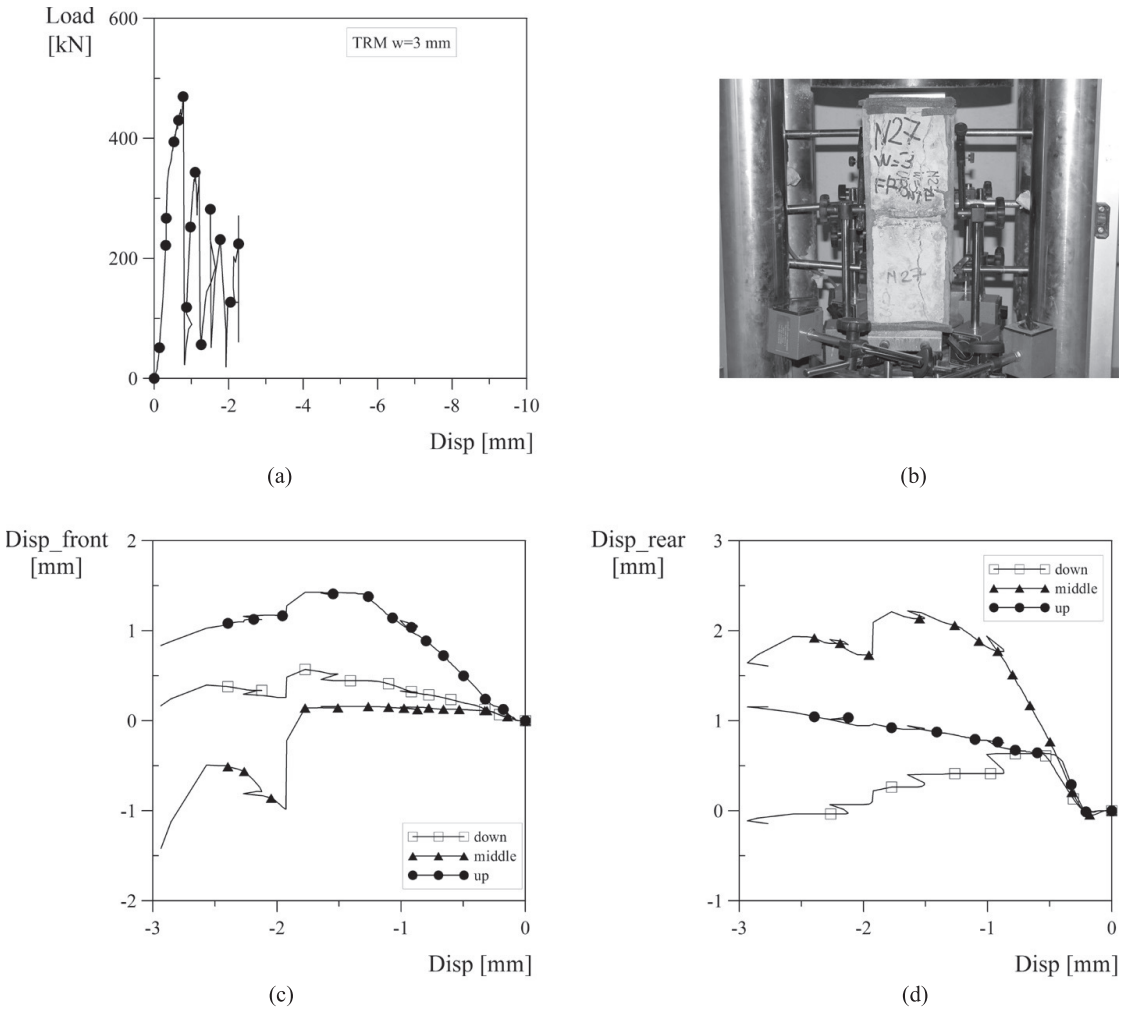

Figure D.7: TRM w=3 mm N01

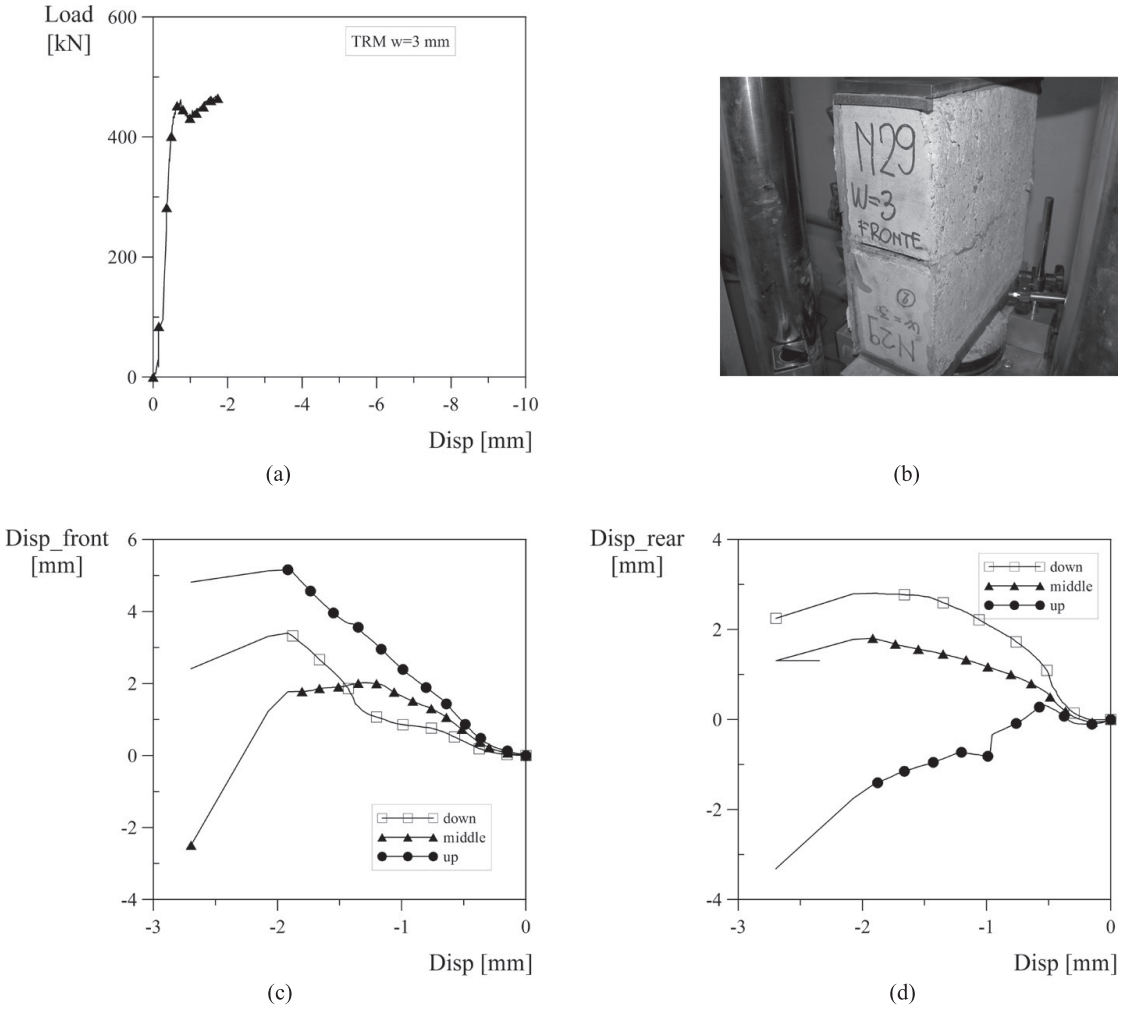

Figure D.8: TRM w=3 mm N02

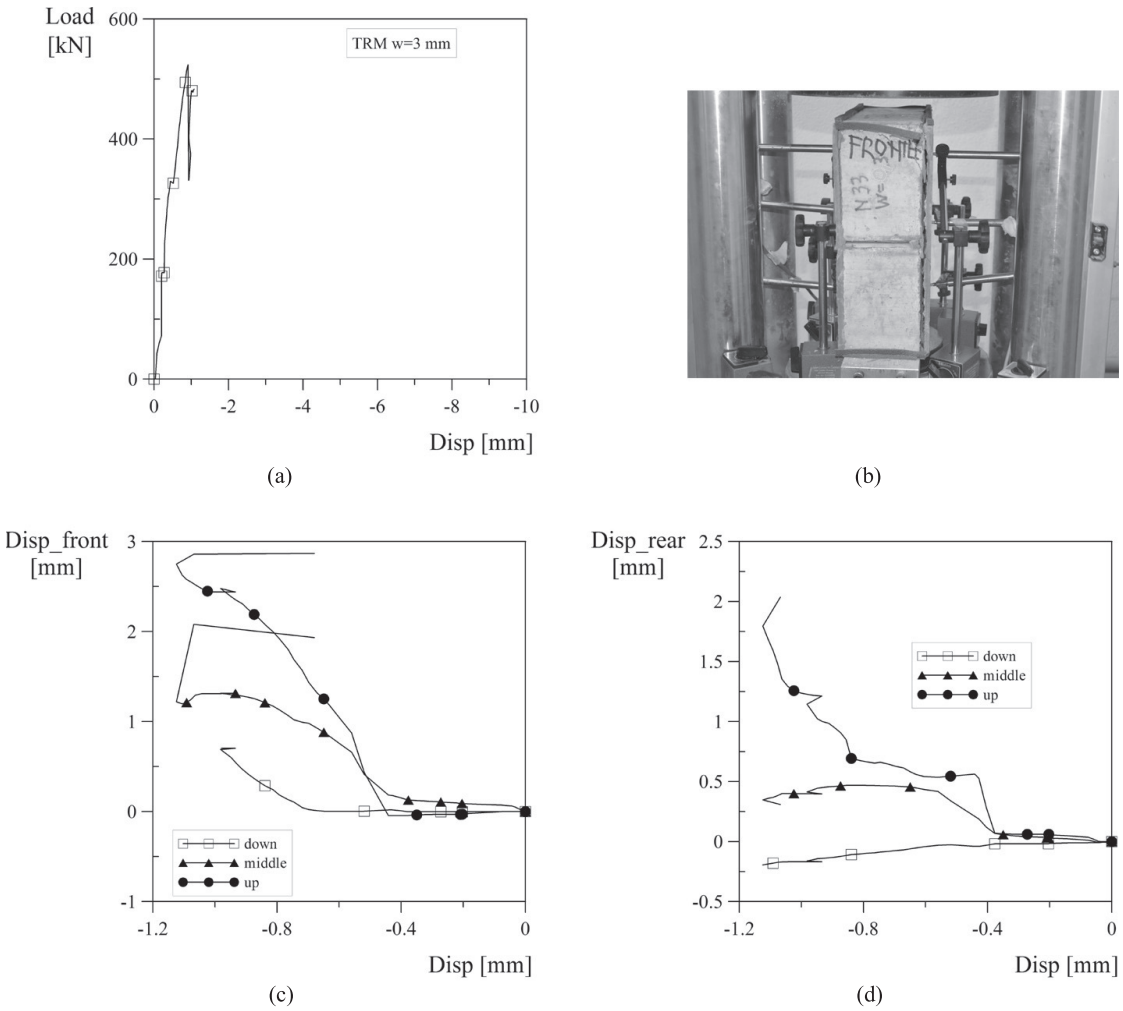

Figure D.9: TRM w=3 mm N03

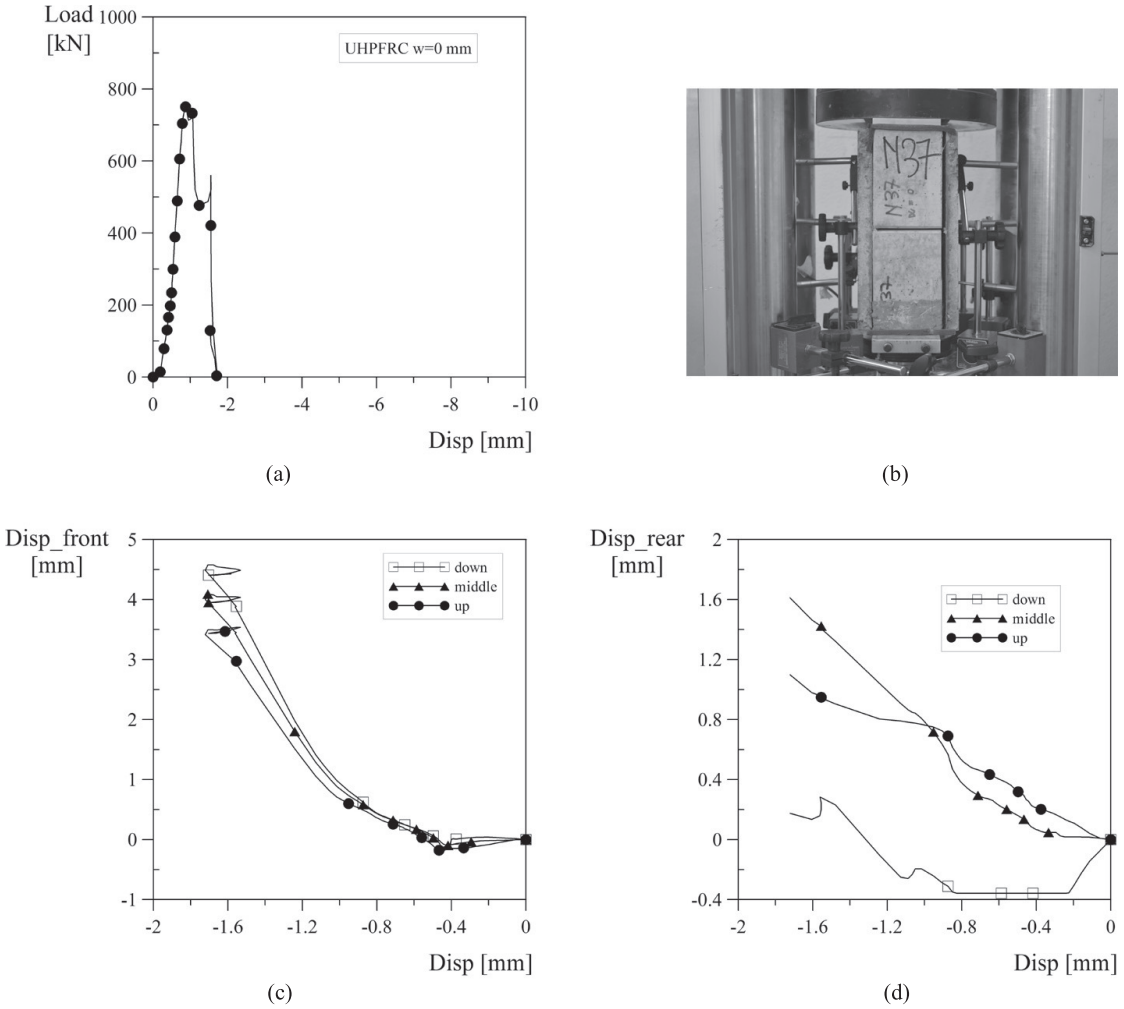

Figure D.10: UHPFRC w=0 mm N01

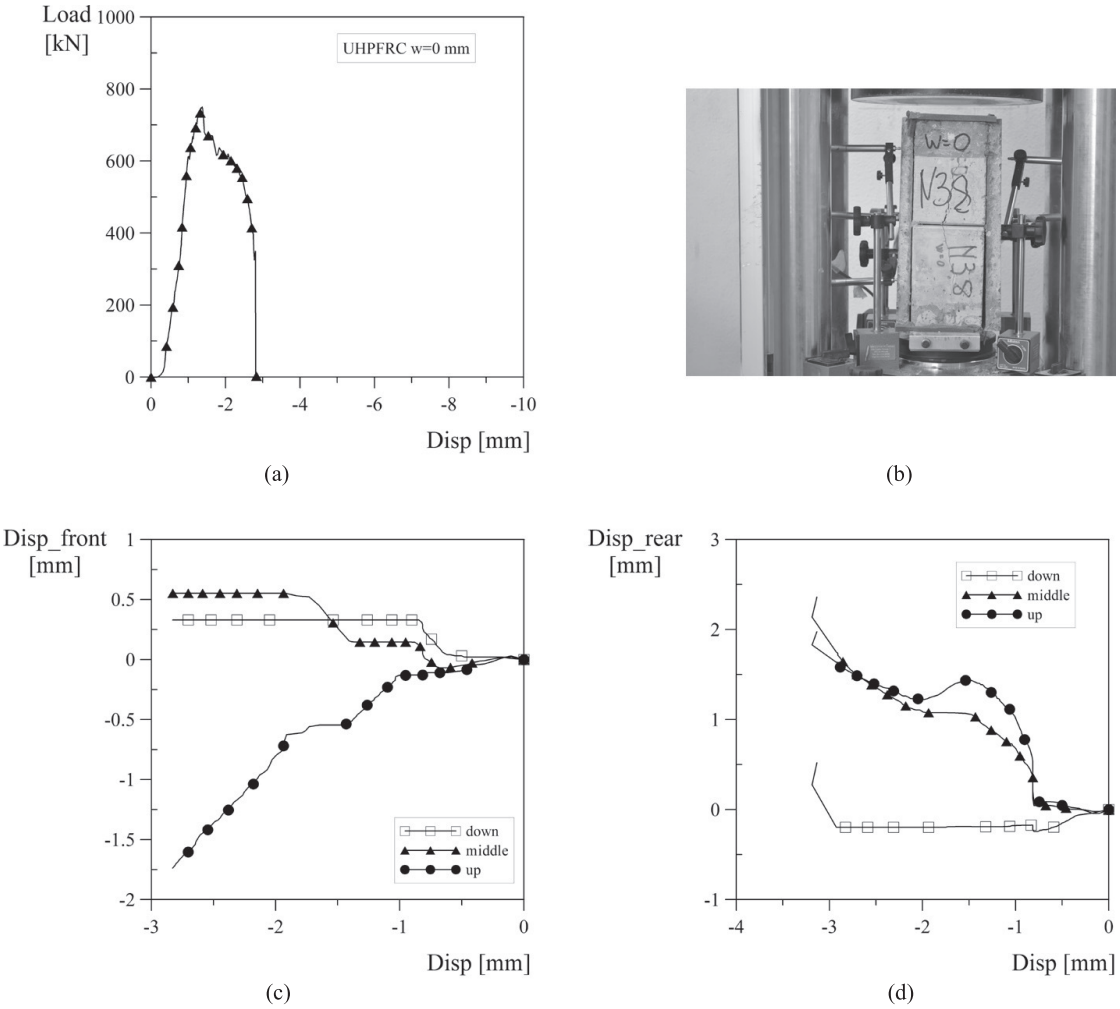

Figure D.11: UHPFRC w=0 mm N02

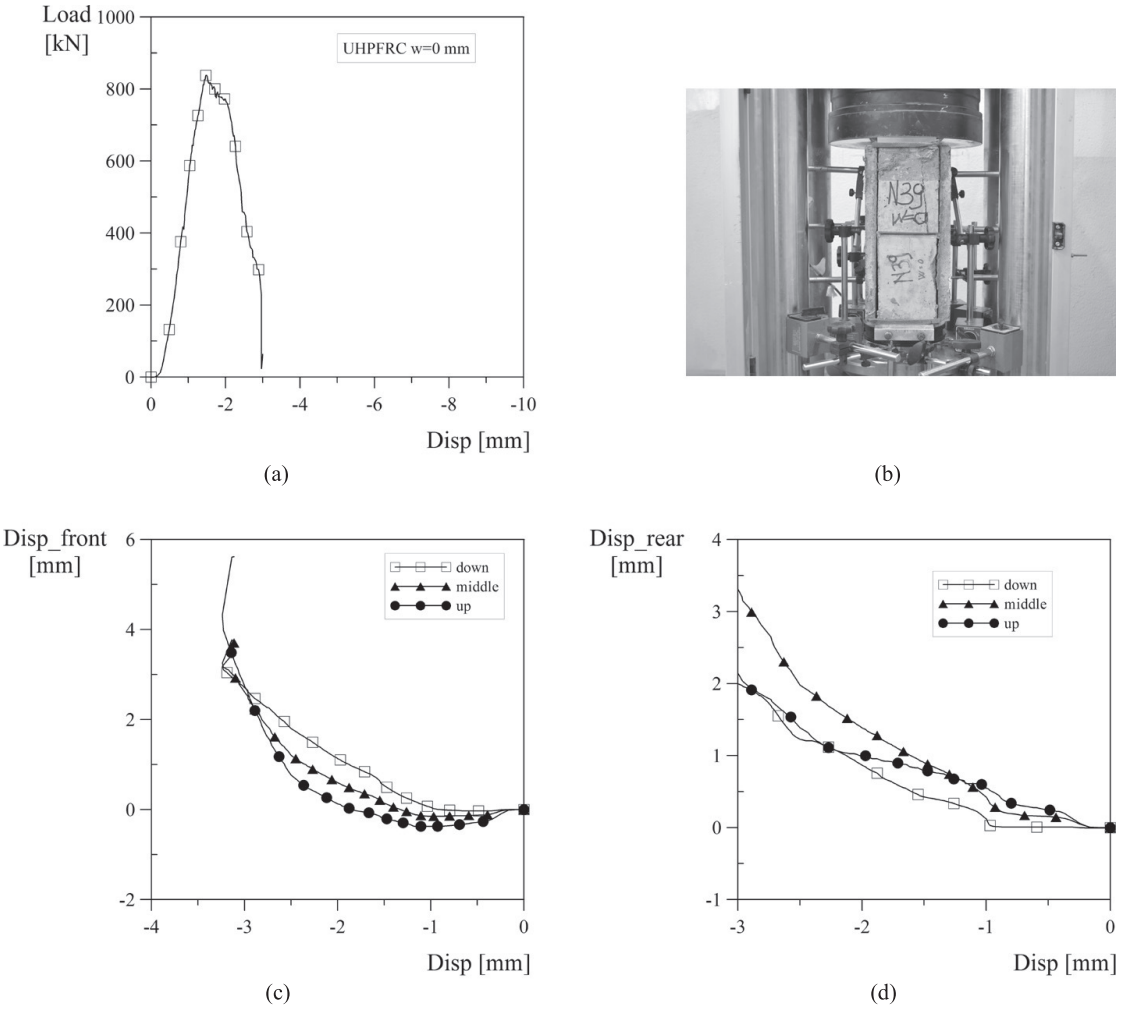

Figure D.12: UHPFRC w=0 mm N03

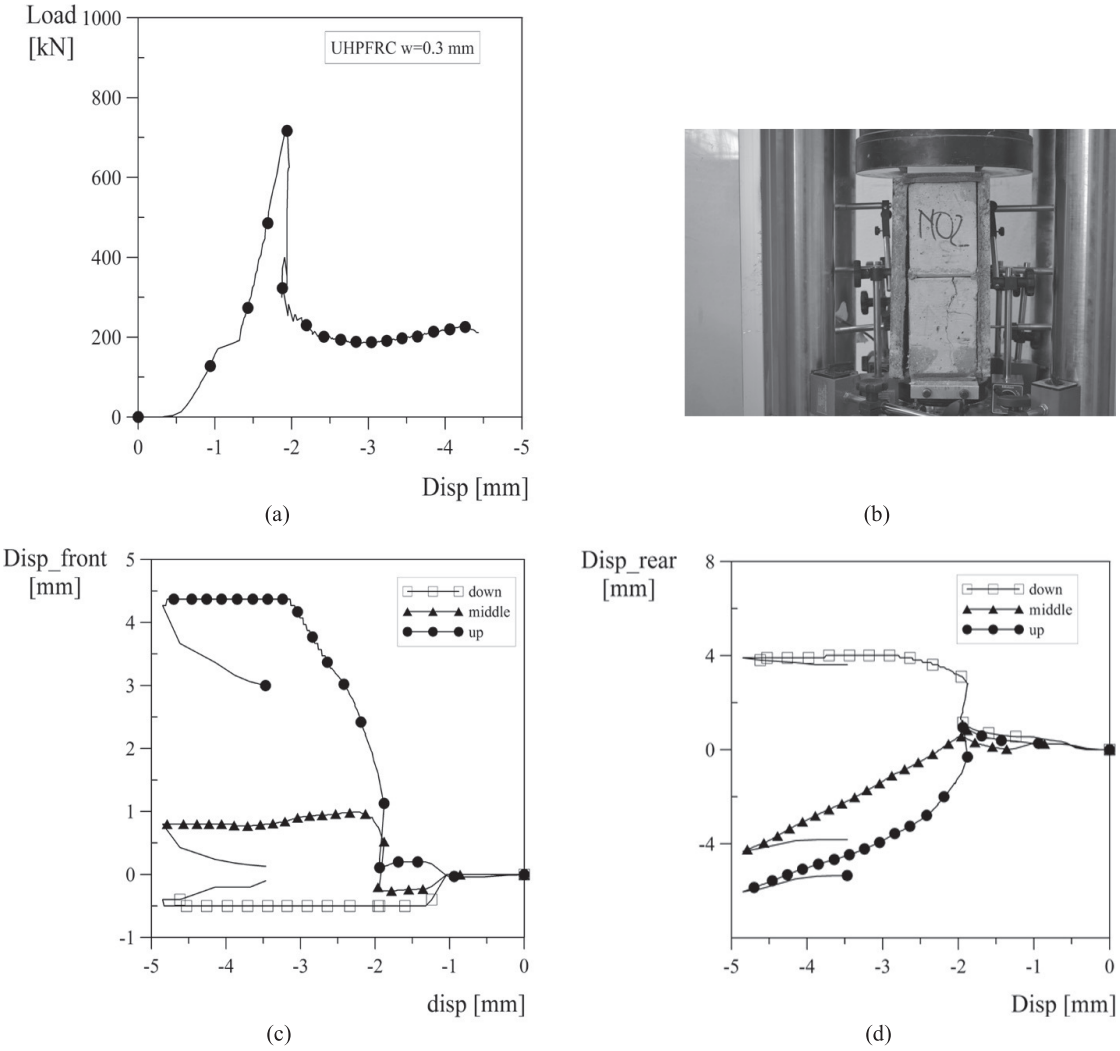

Figure D.13: UHPFRC w=0.3 mm N01

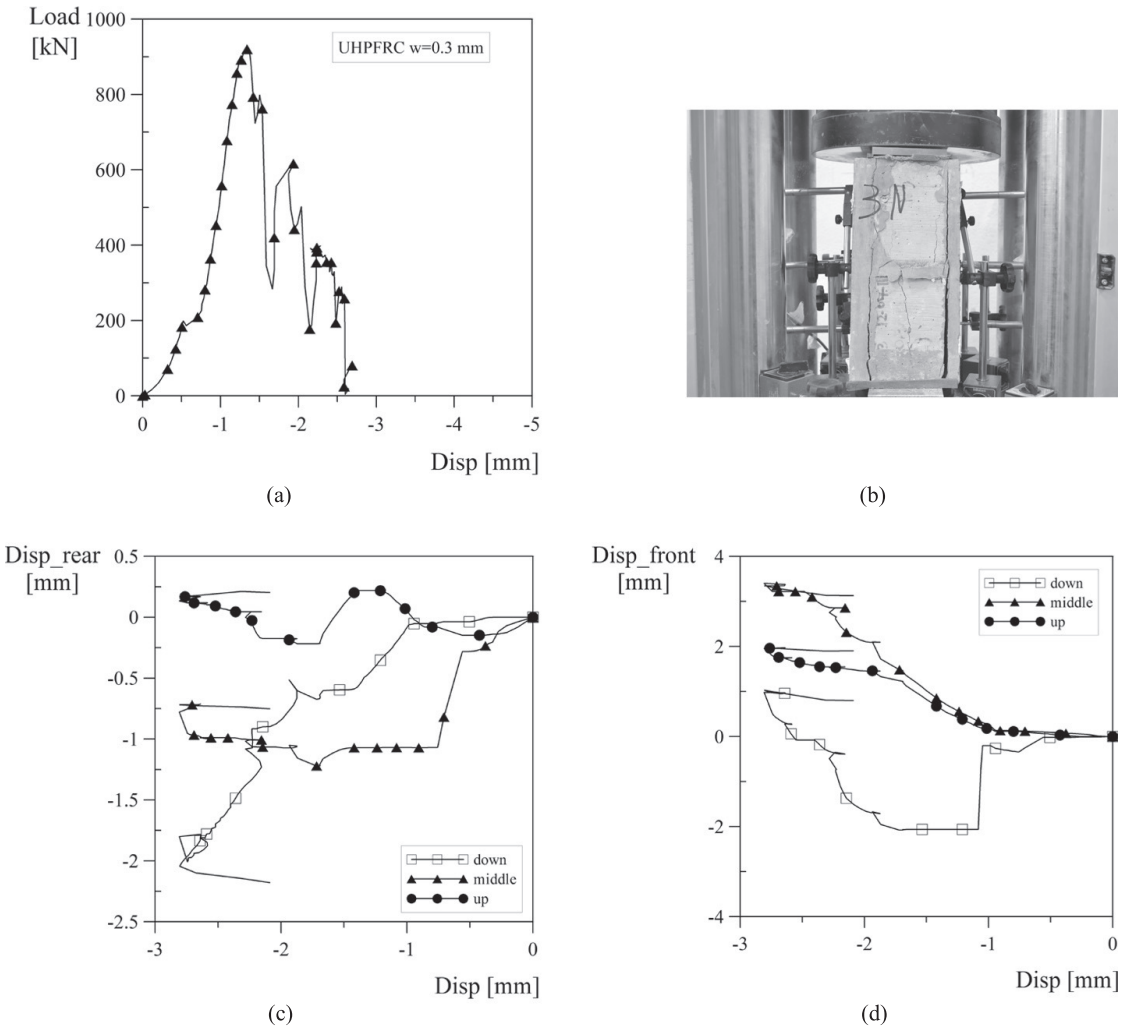

Figure D.14: UHPFRC w=0.3 mm N02

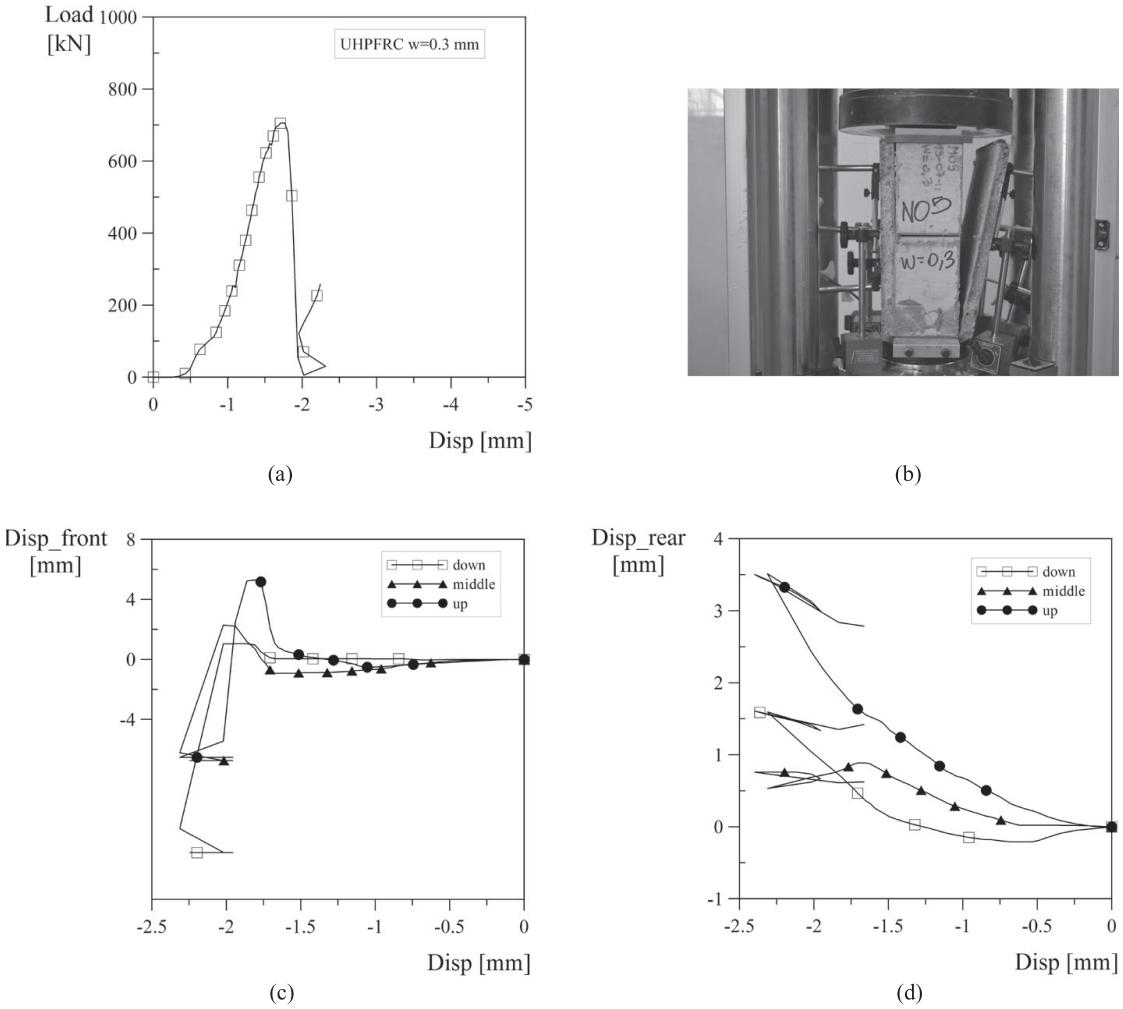

Figure D.15: UHPFRC w=0.3 mm N03

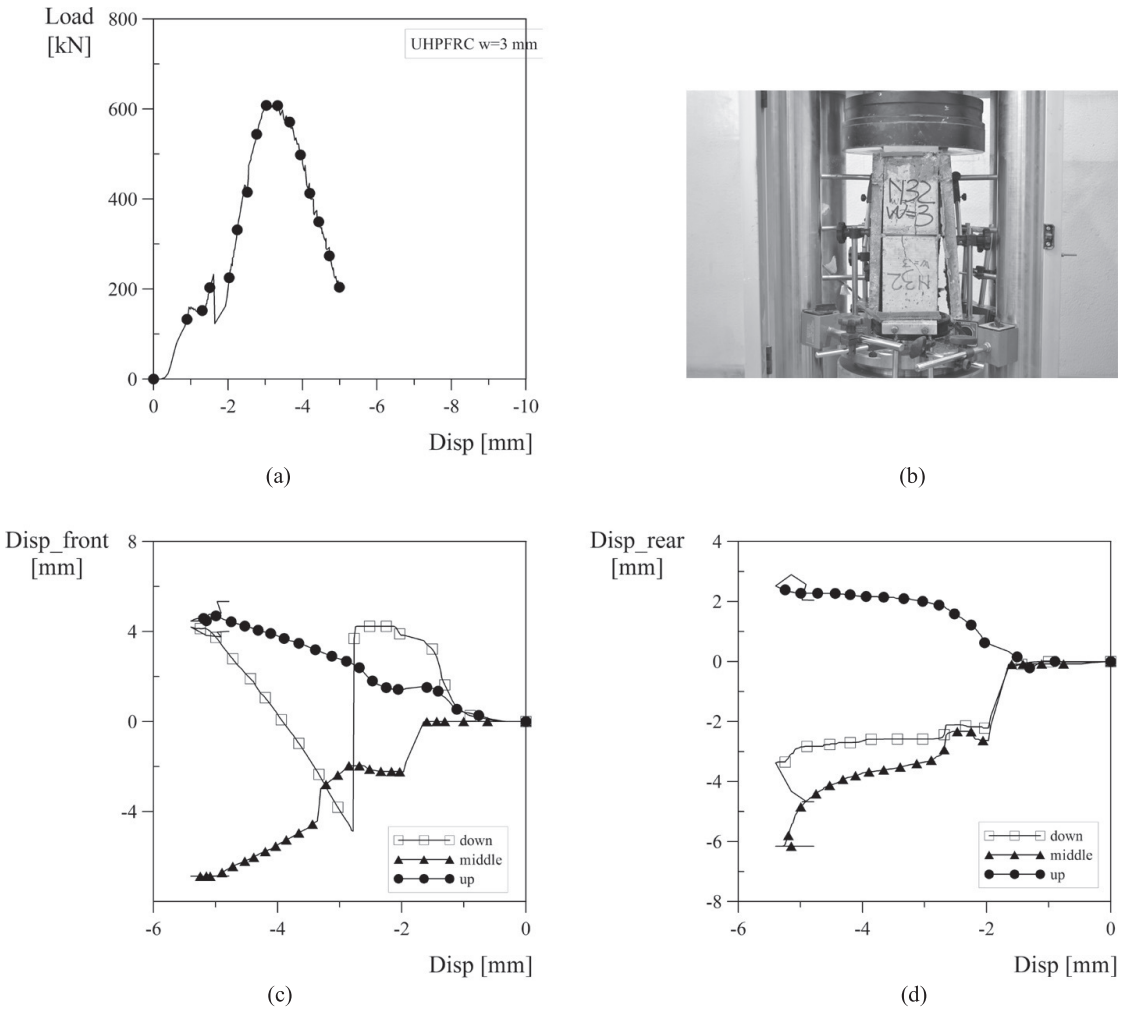

Figure D.16: UHPFRC w=3 mm N01

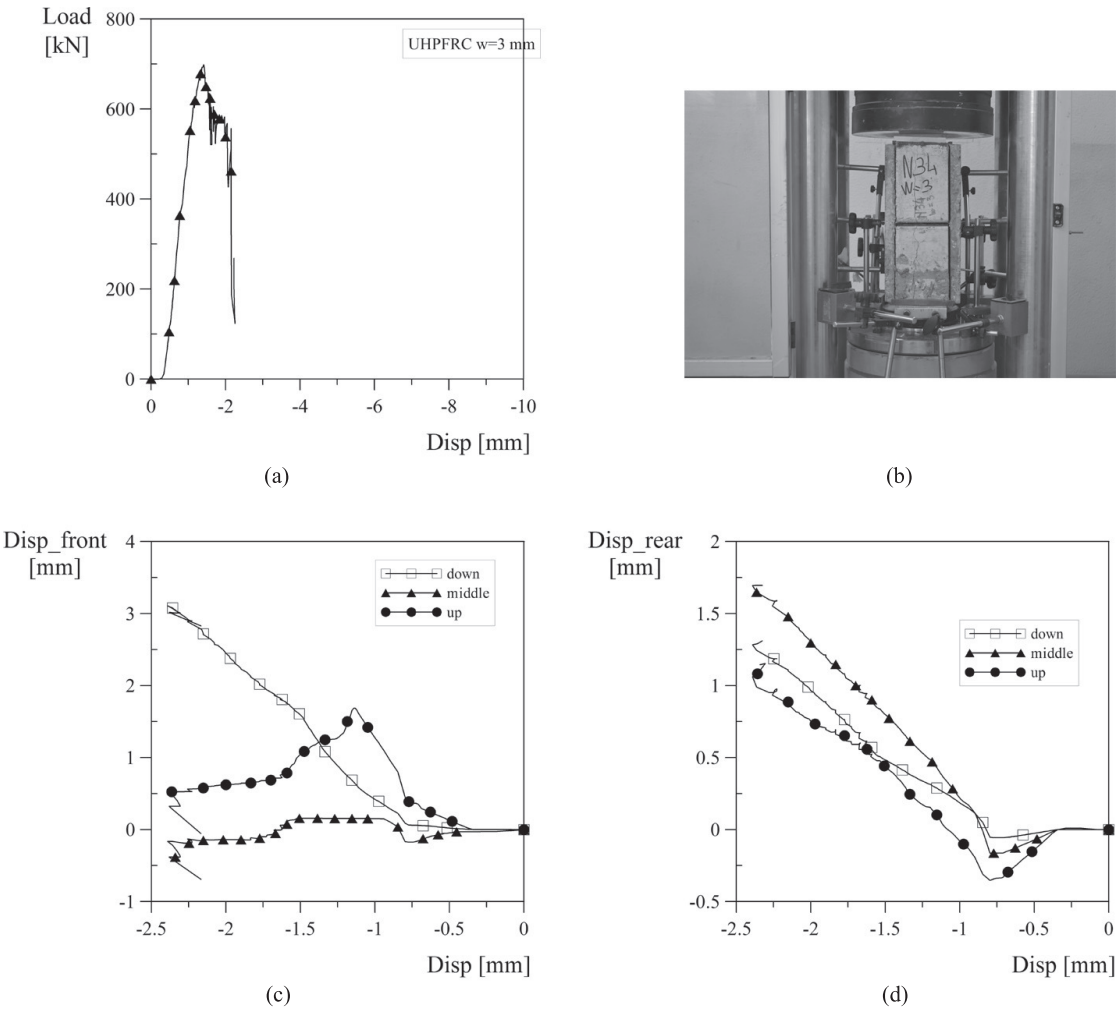

Figure D.17: UHPFRC w=3 mm N02

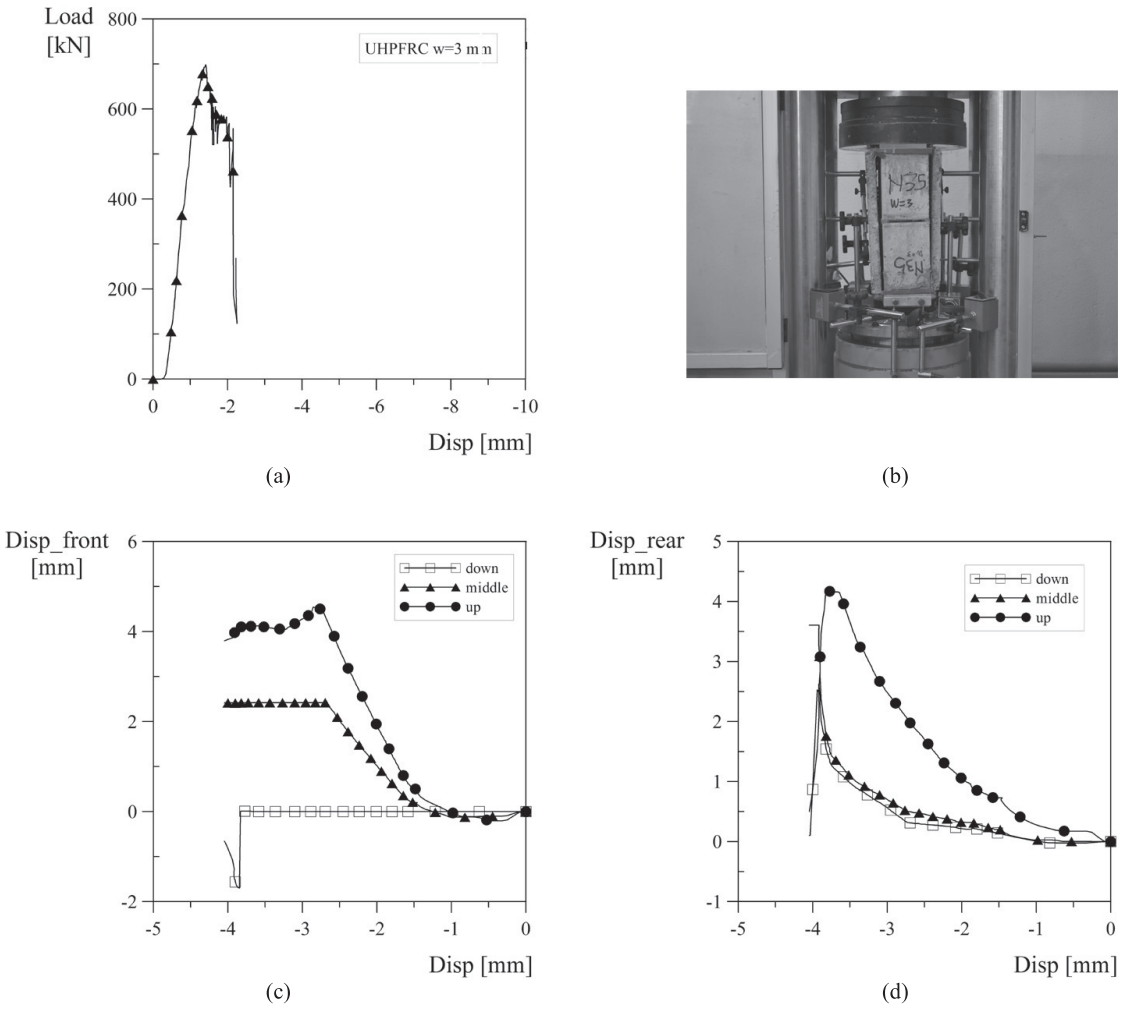

Figure D.18: UHPFRC w=3 mm N03

References

[1] Naaman, A.E. Evaluation of steel fibers for applications in structural concrete. *Proceeding of the Sixth RILEM symposium on Fibre Reinforced Concrete(FRC), BEFIB*, (3):389–400, 2004. (document), 3.10, 3.3.3, 3.11

[2] Wille, K., Kim, D., and Naaman, A. Strain-hardening UHP-FRC with low fiber contents. *Materials and Structures*, 44:583–598, 2011. (document), 3.3.4, 3.16, 3.17, 3.18

[3] Kockritz, U., Hausding,J., Engler, Th., Cherif, Ch. Innovative technology for the manufacture of textile reinforcements for concrete. In W. Brameshuber J. Hegger and N. Will, editors, *ICTRC 2006 - 1st International RILEM Conference on Textile Reinforced Concrete*, pages 3–12. RILEM Publications SARL, 2006. (document), 3.35

[4] Brameshuber, W. *Report 36: Textile Reinforced Concrete - State-of-the-Art Report of RILEM TC 201-TRC*. RILEM reports. RILEM publications, 2006. (document), 2.5, 3.37, 3.4.1, 3.4.4, 3.69, 4.2.2

[5] Banholzer, B. Bond behaviour of multifilament yarn embedded in a cementitiuos matrix. In *In Schrifteneihe Aachener Beitrage zur Bauforschung, Institut fur Bauforschung der RWTH Aachen*, 2004. (document), 3.4.4, 3.4.4, 3.44, 4.2.4

[6] Kruger, M., Reinhardt, H. W., Ficthlscherer, M. Bond behaviour of textile reinforcement in reinforced and prestressed concrete. In *In Otto Graf Journal Vol 12*, pages 33–50, 2001. (document), 3.4.4, 3.47

[7] Hegger, J.,Norbert, Will, Curbach, M., and Jesse, F. Load-bearing behaviour of Textile Reinforced Concrete. Bond cracking behaviour and load-bearing behaviour. *Beton- und Stahlbetonbau*, 99(6):452 – 455, 2004. (document), 3.4.4, 3.51

[8] Contamine, R. and Si Larbi, A. and Hamelin, P. Contribution to direct tensile testing of textile reinforced concrete (TRC) composites. *Materials Science and Engineering A*, 528(29-30):8589 – 8598, 2011. (document), 3.4.4, 3.53

[9] Peled, A., and Bentur, A. Mechanisms of fabric reinforcement of cement matrices. *Beton- und Stahlbetonbau*, 99(6):456–459, 2004. (document), 3.4.4, 3.58

[10] Singla, N. *Experimental and Theoretical Study of Fabric Cement Composites for Retrofitting Masonry Structures*. Arizona State University, 2004. (document), 3.4.4, 3.59

[11] Martinelli E. Nigro E. Paciello S. Faella, C. Shear capacity of masonry walls externally strengthened by a cement-based composite material: An experimental campaign. *Construction and Building Materials*, 24(1):84 – 93, 2010. (document), 3.4.5, 3.62

[12] Larrinaga, P., San-José, J.T., García, D.,Garmendia, L., Díez, J. Experimental Study of the Flexural Behaviour of Low Performance RC Beams Strengthened with Textile Reinforced Mortar. In W. Brameshuber, editor, *International RILEM Conference on Material Science*, pages 235 – 244. RILEM Publications SARL, 2010. (document), 3.4.5, 3.63

[13] Weiland, S., Ortlepp, R., Curbach, M. Strengthening of predeformed slabs with textile reinforced concrete. In *Prooceedings of the second international congress Fédération Internationale du Béton*. RILEM Publications SARL, 2006. (document), 3.4.5, 3.64, 3.65, 3.66

[14] Bruckner, A. and Ortlepp, R. and Curbach, M. Textile reinforced concrete for strengthening in bending and shear. *Materials and Structures/Materiaux et Constructions*, 39(292):741 – 748, 2006. (document), 3.4.5, 3.67, 3.4.5, 3.68

[15] Ortlepp, R., Ortlepp, S., Curbach, M. Stress transfer in the bond joint of subsequently applied textile reinforced concrete strengthening. In R. Felicetti M. di Prisco and G.A. Plizzari, editors, *In 6th International RILEM Symposium on Fibre Reinforced Concretes*, pages 1483 – 1494. RILEM Publications SARL, 2004. (document), 3.4.5, 3.70, 3.4.5, 3.71, 3.72

[16] Al-Jamous, A., Ortlepp, R., Ortlepp,S., Curbach, M. Experimental investigations about construction members strengthened with textile reinforcement. In Brameshuber W. Will N. Hegger, J., editor, *ICTRC'2006 - 1st International RILEM Conference on Textile Reinforced Concrete*, pages 161 – 170. RILEM Publications SARL, 2006. (document), 3.4.5, 3.74, 3.76

[17] Dahl, K. *A Failure Criterion for Normal and High Strength Concrete*. PhD thesis, Danmarks tekniske Hojskole, Lyngby, 1992. (document), 3.4.5, 3.75, 3.4.5

[18] Ferrara, L., Ozyurt, N., di Prisco, M. High mechanical performance of fibre reinforced cementitious composites: the role of casting-flow induced fibre orientation. *Materials and Structures*, 44:109–128, 2011. (document), 3.3.4, 4, 4.1, 4.1, 4.2, 4.3, 4.1, 4.1, 4.5, 4.1

[19] di Prisco, M., Zani, G. Experimental and numerical analysis of advanced cementitious composites for sustainable roof elements. In *In Numerical modelling strategies for sustainable concrete structures*. RILEM Publications SARL, 2012. (document), 4.1, 4.7, 4.1

[20] Pros, A., Díez, P., Molins, C. Model validation of the numerical simulation of the double punch test. In *IV European Conference on Computational Mechanics*, 2010. (document), 5.2, 5.13

[21] Tan, K. H., Hendra, S. S., Chen, S. P. Out of plane behaviour of masonry walls strengthened with fiber reinforced materials: a comparative study. In H. W. Reinhardt and A.E. Naaman, editors, *High Performance Gibre Reinforced Cement Composites (HPFRCC5)*, pages 419 – 426. RILEM pubblications S.A.R.L., 2007. (document), 2.1, 2.1.2, 2.3

[22] Kosmatka, S.H., Kerkhoff, B. and Panarese, W. C. *Design and Control of Concrete Mixtures*. Engineering Bullettin 001, fourteenth edition, 2003. (document), 3.3.2, 3.1

[23] Brockmann, T. Requirements on and properties of mineral based fine grained concrete matrices. In *Textilbeton. 1. Fachkolloquium der Sonderforschungsbereiche*, pages 528–532, 2001. (document), 3.9, 3.10

[24] Banholzer, B., Brockmann, T., and Brameshuber, W. Material and bonding characteristics for dimensioning and modelling of textile reinforced concrete (TRC) elements. *Materials and Structures*, 39:749–763, 2006. 10.1617/s11527-006-9140-x. (document), 3.11, 3.4.2

[25] Brameshuber, W., Brockmann, T. Size effect on mechanical properties of fine grained concrete matrices. *Textile Reinforced Structures, Proceedings of 2nd Colloquium, Dresden (CTRS2)*, pages 161–172, 2003. (document), 3.11, 3.4.2

[26] Papanicolaou, C. G., Triantafillou, T. C., Karlos, K., Papathanasiou, M. Seismic retrofitting of unreinforced masonry structures with TRM. In W. Brameshuber, editor, *ICTRC'2006 - 1st International RILEM Conference on Textile Reinforced Concrete*, pages 341 – 350. RILEM Publications SARL, 2006. 2.1.1, 3.4.5

[27] Papanicolaou, C. G., Triantafillou, T. C., Bournas,D. A., Lontou, V. TRM as strengthening and seismic retrofitting material of concrete structures. In W. Brameshuber J. Hegger and N. Will, editors, *ICTRC'2006 - 1st International RILEM Conference on Textile Reinforced Concrete*, pages 331 – 340. RILEM Publications SARL, 2006. 2.2.1, 2.3, 2.4.2

[28] Meda, A and Rinaldi, Z and Martinola, G and Plizzari, GA. Strengthening of r/c beams with high performance fiber reinforced cementitious composites. *HPFRCC 5 - High performance fiber reinforced cement composites*, 2007. 2.2.2

[29] Martinola, G., Meda, A., Plizzari, G. A. and Rinaldi, Z. Strengthening and repair of rc beams with fiber reinforced concrete. *Cement and Concrete Composites*, 32(9):731 – 739, 2010. 2.2.2

[30] Triantafillou, T. C., Papanicolaou,C. G. Shear strengthening of reinforced concrete members with textile reinforced mortar (TRM) jackets. *Materials and Structures/Materiaux et Constructions*, 39(285):93 – 103, 2006. 2.3, 3.4.5, 3.4.5

[31] Meda, A., Plizzari, G. A., Rinaldi, Z., and Martinola, G. Strengthening of R/C existing columns with high performance fiber reinforced concrete jacket. *2nd Int. conf. on Concrete Repair, Rehabilitation and Retrofitting*, 2008. 2.4.1

[32] Meda, A., Rinaldi, Z., Martinola, G., and Plizzari G.A. An application of high performance fiber reinforced cementitious composites for R/C beams strengthening. *FraMCos-6. 6th Int. conf. on fracture mechanics of concrete and concrete structures*, 2007. 2.5

[33] Powers, T. C. Structure and Physical Properties of Hardened Portland Cement Paste. *Journal of the American Ceramic Society*, 41(1):1–6, 1958. 3.2

[34] Breitenbucher, R. Developments and applications of high-performance concrete. *Materials and Structures*, 31(3):209–215, April 1997. 3.2

[35] Romualdi, J.P. and Batson, G.B. Mechanics of crack arrest in concrete. In *Journal of Engineering Mechanics*, pages 147–168. Proceedings of ASCE, 1963. 3.2

[36] Romualdi, J.P. and Mandel, J.A. Tensile Strength of concrete Affected by Uniformly Distributed and Closely Spaced Short Lengths of wire Reinforcement. *ACI Journal*, 61(3):657–672, June 1964. 3.2

[37] H. Krenchel. *Fibre reinforcement: theoretical and practical investigations of the elasticity and strength of fibre-reinforced materials*. Akademisk forlag, 1964. 3.2

[38] Kelly, A. Reinforcement of structural materials by Long Strong Fibres. *Metallurgical and Materials Transactions B*, 3:2313–2325, 1972. 3.2

[39] Naaman,A.E., Argon, A.S., Moavenzadeh, F. A fracture model for fiber reinforced cementitious materials. *Cement and Concrete Research*, 3(4):397 – 411, 1973. 3.2

[40] Naaman, A. and Reinhardt, H. Proposed classification of HPFRC composites based on their tensile response. *Materials and Structures*, 39:547–555, 2006. 3.2, 3.3.1

[41] Naaman, A. E. Tensile strain-hardening FRC composites: Historical evolution since the 1960. In Christian U. Grosse, editor, *Advances in Construction Materials 2007*, pages 181–202. Springer Berlin Heidelberg, 2007. 3.2, 3.3.1

[42] Naaman, A. E. *A statistical theory of strength for fiber reinforced concrete*. Massachusetts Institute of Technology, 1972. 3.2

[43] di Prisco, M., Plizzari, G., Vandewalle, L. Fibre reinforced concrete: new design perspectives. *Materials and Structures*, 42:1261–1281, 2009. 3.2

[44] di Prisco, M., Ferrara, L., Lamperti, M., Lapolla, S., Magri, A. and Zani, G. Sustainable Roof Elements: A Proposal Offered by Cementitious Composites Technology. *Innovative Materials and Techniques in Concrete Construction*, pages 167–181, 2012. 3.2

[45] van Mier, J.G.M. Cementitious composites with high tensile strength and ductility through hybrid fibres. In *Proc. 6th International RILEM Symposium on Fibre Reinforced Concretes BEFIB 2004*, pages 219–236, 2004. 3.3

[46] Naaman, A. E. Engineered steel fibers with optimal properties for reinforcement of cement composites. *Journal of Advanced Concrete Technology*, 1(3):241–252, 2003. 3.3.3, 3.3.3

[47] CNR DT 204. *Guidelinese for the Design, Construction and Production Control of Fibre Reinforced Concrete Structures*, 2006. 3.3.3

[48] Rossi, P. Ultra high performance fibre reinforced concretes (UHPFRC): An overview. *PRO 15: 5th RILEM Symposium on Fibre-Reinforced Concretes (FRC) - BEFIB' 2000*, 2000. 3.3.5

[49] Colombo, I., Magri, A., Zani, G., Colombo, M., di Prisco, M. Textile reinforced concrete: an experimental investigation on design parameters. *Materials and Structures*, page submitted, 2012. 3.4, 4

[50] CNR DT 200/2004. *Istruzioni per la Progettazione, l'Esecuzione ed il Controllo di Interventi di Consolidamento Statico mediante l'utilizzo di Compositi Fibrorinforzati*, 2004. 3.4.1

[51] Mobasher, B., Peled, A., Pahilajani, J. Pultrusion of fabric reinforced high flyash blended cement composites. In *Proceedings, World Of Coal Ash, April 11-15, 2005, Lexington, KY, USA Pultrusion*, 2005. 3.4.2, 3.4.2, 3.4.3

[52] Brameshuber W., Brockmann T. Textile reinforced ultra high strength concrete. In Holschemacher K. Dehn F. Konig, G., editor, *Ultrahochfester Beton:3. Leipziger Fachtagung Innovationen im Bauwesen, 2003*, pages 153–164, 2003. 3.4.2

[53] Brameshuber W., Brockmann T. Calcium aluminate cement as binder for textile reinforced concrete. In ROYAUME-UNI (2001) (Monographie) Institute of Ceramics, Stoke-on-Trent, editor, *Proc. International conference on calcium aluminate cements, Edinburgh , ROYAUME-UNI 16/07/2001*, pages 659–666, 2001. 3.4.2

[54] Peled, A. and Mobasher, B. Tensile behavior of fabric cement-based composites: Pultruded and cast. *Journal of Materials in Civil Engineering*, 19(4):340 – 348, 2007. 3.4.3

[55] Jesse, F. Load bearing behaviour of filament yarns embedded in cementious matrix. In *PhD thesis, Dresden, Faculty of Civil Engineering, Technische Universitat Dresden*, 2005. 3.4.4

[56] Peled, A. and Yankelevsky, D. and Bentur, A. Bonding and interfacial microstructure in cementitious matrices reinforced by woven fabric. In *Materials Research Society Symposium - Proceedings*, volume 370, pages 549 – 558, Boston, MA, USA, 1995. 3.4.4

[57] Peled, A. and Yankelevsky, D. and Bentur, A. Influences of yarns shape in woven fabric on bonding performance of cementitious composites. pages 192 – 192, 1995. 3.4.4

[58] Peled, A., Bentur, A., and Yankelevsky, D. Effects of Woven Fabric Geometry on the Bonding Performance of Cementitious Composites: Mechanical Performance. *Advanced Cement Based Materials*, 7(1):20 – 27, 1998. 3.4.4

[59] Peled, A. and Yankelevsky, D. and Bentur, A. Microstructural characteristics of cementitious composites reinforced with woven fabrics. *Advances in Cement Research*, 9(36):149 – 155, 1997. 3.4.4

[60] Peled, A. and Bentur, A. Fabric structure and its reinforcing efficiency in textile reinforced cement composites. *Composites Part A: Applied Science and Manufacturing*, 34(2):107 – 118, 2003. 3.4.4, 3.4.5

[61] Peled, A. and Bentur, A. Mechanisms of fabric reinforcement of cement matrices: Effect of fabric geometry and yarn properties. *Beton- und Stahlbetonbau*, 99(6):456 – 459, 2004. 3.4.4

[62] Alva Peled and Arnon Bentur. Geometrical characteristics and efficiency of textile fabrics for reinforcing cement composites. *Cement and Concrete Research*, 30(5):781 – 790, 2000. 3.4.4

[63] Z. Cohen and A. Peled. Controlled telescopic reinforcement system of fabric - cement composites - Durability concerns. *Cement and Concrete Research*, 40(10):1495 – 1506, 2010. 3.4.4, 3.4.4

[64] Hegger, J., Voss, S., Bruckermann, O.,. AR Glass and Carbon Fibers for Textile Reinforced Concrete - A comparison of Efficiency. In *Concrete Soars, Spans and Supports, ACI-Covention, New York*, 2005. 3.4.4

[65] Molter, M. Load bearing capacity and serviceability of textile reinforced bending beams. In *In Proceedings of first colloquium on special research areas 528 and 532, Aachen University*, pages 205–219, 2001. 3.4.4

[66] Hegger, J., Voss, S.,. Textile Reinforced Concrete - Bearing behaviour, design, application. In *Composites in construction 1005- third International conference, Lyon, France*, pages 1139–1146, 2005. 3.4.4

[67] Aveston, J. and Kelly, A. Theory of multiple fracture of fibrous composites. *Journal of Materials Science*, 8:352–362, 1973. 3.4.4

[68] Hegger, J. and Will, N. and Bruckermann, O. and Voss, S. Load-bearing behaviour and simulation of textile reinforced concrete. *Materials and Structures/Materiaux et Constructions*, 39(292):765 – 776, 2006. 3.4.4

[69] Mashima, M. and Hannant, D.J. and Keer, J.G. Tensile properties of polypropylene reinforced cement with different fiber orientations. *ACI Materials Journal*, 87(2):172 – 178, 1990. 3.4.4

[70] Butler, M., Mechtcherine, V., and Hempel, S. Durability of textile reinforced concrete made with AR glass fibre: Effect of the matrix composition. *Materials and Structures/Materiaux et Constructions*, 43(10):1351 – 1368, 2010. 3.4.4

[71] Majumdar, A.J., Laws, V. Glass fibre reinforced cement. In *In BS Professional Books, Oxford*, 1991. 3.4.4

[72] Raupach, M., Orlowsky, J., Buttner, T., Dilthey, U., Schleser, M. Epoxy impregnated textiles in concrete: Load bearing capacity and durability. In W. Brameshuber J. Hegger and N. Will, editors, *ICTRC 2006 1st International RILEM Conference on Textile Reinforced Concrete, RILEM Publications SARL*, pages 77–88, 2006. 3.4.4

[73] Katz, A., Bentur, A. Mechanisms and processes leading to changes in time in the properties of CFRC. *Advanced Cement Based Materials*, 3(1):1 – 13, 1996. 3.4.4

[74] Purnell, P. and Beddows, J. Durability and simulated ageing of new matrix glass fibre reinforced concrete. *Cement and Concrete Composites*, 27(9-10):875 – 884, 2005. 3.4.4

[75] Bonomelli, F., Colombo, M., di Prisco, M., Mazzoleni, L. Textile cementitious composites at high temperatures. In *Proceeding of 2nd Int. Symposium on Ultra High Performance Concrete, March, Kassel (Germany)*, pages 339 –346, 2008. 3.4.4

[76] Butler, M. and Lieboldt, M. and Mechtcherine, V. Application of Textile-Reinforced Concrete (TRC) for structural strengthening and in prefabrication. *Advances in Cement-Based Materials - Proceedings of the International Conference on Advanced Concrete Materials*, pages 127 – 136, 2010. 3.4.5

[77] Mobasher B.-Jain-N. Aldea, C. Cement-based matrix-grid system for masonry rehabilitation. In *ACI spring Convention, New York*, 2005. 3.4.5

[78] Bournas, Dionysios A. and Lontou, Panagiota V. and Papanicolaou, Catherine G. and Triantafillou, Thanasis C. Textile-reinforced mortar versus fiber-reinforced polymer confinement in reinforced concrete columns. *ACI Structural Journal*, 104(6):740 – 748, 2007. 3.4.5

[79] Ortlepp, R., Curbach, M. Bonding behaviour of textile reinforced concrete strengthening. In W. Brameshuber, editor, *In International Workshop High Performance Fiber Reinforced Cement Composites*, pages 505 – 527. RILEM Publications SARL, 2003. 3.4.5

[80] Brameshuber, W. *Proceedings PRO75 Textile Reinforced Concrete- Proceedings of the International RILEM Conference on Material Science (MatSci)*. RILEM Proceedings. RILEM publications, 2010. 3.4.5, 3.4.5

[81] Hegger, J., Feldmann, D., Raupach, M., Feger, C. Sandwich Panels Made of TRC and Discrete and Continuous Connectors. In W. Brameshuber, editor, *International RILEM Conference on Material Science*, pages 381 – 392. RILEM Publications SARL, 2010. 3.4.5

[82] Hegger, J., Brameshuber, W., Will, N. *Proceedings PRO50 Textile Reinforced Concrete-Proceedings of the first International RILEM Symposium*. RILEM Proceedings. RILEM publications, 2006. 3.4.5

[83] Ferrara, L., di Prisco, M., Lamperti, M.G.L. Identification of the stress crack opening behaviour of HPFRCC: the role of flow induced fiber orientation. In *In Fracture Mechanics of Concrete Structures*, pages 1541 – 1550, 2010. 4, 4.1

[84] Farina, C. Elementi sandwich in composito fibrorinforzato ad alte prestazioni con core in schiuma: indagine sperimentale e modellazione teorica del comportamento flessionale. Master's thesis, Politecnico di Milano, 2012. 4.1

[85] pren12350-8: Testing fresh concrete-part 8: self compacting concrete- slum flow test. 4.1

[86] pren12350-8: Testing fresh concrete-part 8: self compacting concrete -v-funnel test. 4.1

[87] pren12350-8: Testing fresh concrete-part 8: self compacting concrete -l-box test. 4.1

[88] pren12350-8: Testing fresh concrete-part 8: self compacting concrete -j-ring test. 4.1

[89] Cnr-dt204 (2006) guidelines for the design, manufacturing and control of sfrc structures (in italian). 4.1, 4.1

[90] UNIEN196. Methods of testing cement - part 1: Determination of strength. 4.2.1

[91] Soranakom, C. and Mobasher, B. Geometrical and mechanical aspects of fabric bonding and pullout in cement composites. *Materials and Structures/Materiaux et Constructions*, 42(6):765 – 777, 2009. 4.2.4

[92] Neville, A. M. *Properties of concrete*. Arizona State University, 1996. 4.2.4

[93] Silva, F., de A., Butler, M., Mechtcherine, V., Zhu, D., Mobasher, B. Strain rate effect on the tensile behaviour of textile-reinforced concrete under static and dynamic loading. *Materials Science and Engineering A*, 528(3):1727 – 1734, 2011. 4.2.4

[94] Orlowsky, J. and Raupach, M. Durability model for ar-glass fibres in textile reinforced concrete. *Materials and Structures*, 41:1225–1233, 2008. 4.2.4

[95] Ehlig,D., Jesse, F., Curbach, M. High Temperature Tests on Textile Reinforced Concrete (TRC) Strain Specimens. In W. Brameshuber, editor, *International RILEM Conference on Material Sciencee*, pages 141 – 151. RILEM Publications SARL, 2010. 4.2.4

[96] di Prisco, M., Lamperti, M.G.L., Lapolla, S. Double edge wedge splitting test: Preliminary results. In *Proceedings of conference FRAMCOS 7, Seogwipo, Jeju, KOREA*, 2010. 5.2, 5.2

[97] Brahwiler, E., Wittmann, F.H. The wedge splitting test, a new method of performing stable fracture mechanics tests. *Engineering Fracture Mechanics*, 35:117 – 125, 1990. 5.2

[98] Chen, Wai F. and Yuan, Robert L. Tensile strength of concrete: Double-punch test. 106(8):1673 – 1693, 1980. 5.2

[99] CEB/FIB. *Model Code*, 2010. 7.2.3

[100] di Prisco M., Scola, M. Technical report: Campagna prove sperimentali Pigazzi Reti. 2009. 7.2.4